

**AMBIENT IONIZATION MASS SPECTROMETRY FOR THE
FORENSIC SCREENING OF PHARMACEUTICALS AND THE
DETERMINATION OF POTENTIAL DRUG CANDIDATES**

A Dissertation
Presented to
The Academic Faculty

by

Leonard Nyadong

In Partial Fulfillment
of the Requirements for the Degree
Doctor of Philosophy in the
School of Chemistry & Biochemistry

Georgia Institute of Technology

December 2009

**AMBIENT IONIZATION MASS SPECTROMETRY FOR THE
FORENSIC SCREENING OF PHARMACEUTICALS AND THE
DETERMINATION OF POTENTIAL DRUG CANDIDATES**

Approved by:

Dr. Facundo M. Fernández, Advisor
School of Chemistry & Biochemistry
Georgia Institute of Technology

Dr. Thomas M. Orlando
School of Chemistry & Biochemistry
Georgia Institute of Technology

Dr. Lawrence A. Bottomley
School of Chemistry & Biochemistry
Georgia Institute of Technology

Dr. Mark R. Prausnitz
School of Chemical & Biomolecular
Engineering
Georgia Institute of Technology

Dr. Boris Mizaikoff
School of Chemistry & Biochemistry
Georgia Institute of Technology

Date Approved: Oct. 30th, 2009

This thesis is dedicated to...

*my mother, Mrs Forwang Prudensia Acha (deceased)
may her soul rest in perfect peace*

ACKNOWLEDGEMENTS

Let me mention that it has taken a whole village and beyond to raise me to this point in life, so undoubtedly I might omit some very deserving persons to whom I owe recognition of their contribution to this milestone accomplishment and to them, I extend my sincere apologies. First and foremost I will like to express my earnest gratitude to my advisor, Dr. Facundo M. Fernández for being such a wonderful mentor, whose mentorship has enabled me to grow as a person and as a scientist. It has been a real privilege for me to have had the opportunity of working under his supervision and I'm overly grateful for his dedication and commitment towards my success. I will like to also thank Dr. Lawrence Bottomley, Dr. Thomas Orlando, Dr. Boris Mizaikoff and Dr. Mark Prausnitz for their advisement and for serving in my committee.

I am grateful to the collaboration provided by Dr. Paul Newton, Dr. Michael Green, Dr. Sergei Kazarian, Dr. Camilla Ricci, Dr. Dallas Mildenhall, Dr. Véronique Gilard, Stéphane Balayssac, Dr. Ajay Banga and Dr. Sameer Late in counterfeit antimalarial drug screening investigations. I also appreciate the assistances of Dr. David Sherrill and Edward Hohenstein for computational calculations and Dr. Julia Kubanek, Dr. May Wang, Dr. Amy Lane, and Dr. Mitchell Parry for DESI MS imaging.

I'll like to thank Sam Mize of the college of science machine shop as well as Richard Berdell and José Fonts in the electronic shop in the school of chemistry and biochemistry for their various machining and electronic assistance respectively. I want to also express appreciation to Dr. Cameron Tyson, Dr. David Collard, Dr. Jean-Luc Brédas, Dr. Leigh Bottomley, Dr. Toby Block, Dr. Robert Braga, Dr. Mary Peek, Dr.

Mostafa El-Sayed, Dr. John Zhang, and Dr. Adegboyega Oyelere for their assistance in facilitating my graduate student experience.

Special thanks goes to all my group member, past and present, for all the insightful discussion and friendship over the past years, which has also enabled me to learn a lot about the world, in no particular order: Mark Kwasnik, Dr. Christina Hampton, Arti Navare, Krystyn Alter-Hall, Carrie Pierce, Glenn Harris, Dr. Manshui Zhu, Kristin Johnson, José Perez, Felicia Yang, Catherine Silvestri, Joe Caramore, Dr. Asiri Galhena and David Rizzo. I also like to thank Selina Tinsley and Kourtnie Robin for their assistance in ordering supplies.

I will like to thank my various professors and mentors who helped to build my foundation in chemistry, Dr. Bruce Averill, Dr. Josepha Foba, Dr. Stanley Ngeyi, Dr. Yong Joseph, George Njino and Tata Augustine. I will also like to thank my friends, all of whom have been a significant part of my support system, Dr. Emmanuel Abatih, Dr. Divine Dugah, Walters Atemnkeng, Chi Celestine, Sebastein Awondo, Dr. Pascal Itambi, Timothy Beng, Roland Njabon, Georges Che, Bassem Hallac, Babajide Olanrewaju, ...

Finally, I will like to thank my family for their unconditional love and support that has helped to make me whom I am today, my mom, Prudensia Forwang, my dad Vincent Forwang and all my siblings. Special thanks go to my cousin, Thomas Ngwa and wife, Rockzeen Ngwa for their love and support over the years, to my in-laws Joshua Cheng, Priscilla Cheng and to all my uncles and aunts. Most importantly, I will like to express earnest gratitude to my wife Odilia Nwanacha for her unwavering love, support and perseverance that has enabled me to reach this milestone goal. I will also like to thank my baby, Lily Nyadong for her timely arrival.

TABLE OF CONTENTS

ACKNOWLEDGEMENTS.....	iv
LIST OF TABLES.....	xiv
LIST OF FIGURES.....	xv
LIST OF SYMBOLS	xxv
LIST OF ABBREVIATIONS.....	xxvii
LIST OF PUBLICATIONS.....	xxxi
SUMMARY	xxxiii
CHAPTER 1. AMBIENT MASS SPECTROMETRY	1
1.1. ABSTRACT	1
1.2. VACUUM IONIZATION TECHNIQUES.....	1
1.3. ATMOSPHERIC PRESSURE IONIZATION TECHNIQUES.....	3
1.4. AMBIENT IONIZATION TECHNIQUES	10
1.4.1. Spray- or Jet-based Desorption/Ionization Techniques: DESI, DeSSI and PESI.....	12
1.4.2. Ambient Gas-, Heat-, Laser-, or Radiofrequency-based Desorption/Electrospray-assisted Ionization Techniques: FD-ESI, EESI, nanoEESI, ND-EESI, UA-EESI, RADIO, ELDI, MALDESI, LAESI, IR-LADESI and LIAD/ESI.....	17
1.4.3. Electric Discharge-, Beta Electron-, or Photon-based Ambient Chemical Ionization Techniques: DART, DAPCI, LD-APCI, DBDI, LTP, PADI, FAPA, BADCI, APTDI, DAPPI.....	22
1.5. CONCLUSIONS.....	27
CHAPTER 2. CONSTRUCTION OF A PROTOTYPE DESI MS ION SOURCE FOR THE RAPID DETERMINATION OF COUNTERFEIT ANTIMALARIAL TABLETS	28
2.1. ABSTRACT	28

2.2. INTRODUCTION	28
2.3. EXPERIMENTAL DETAILS	32
2.3.1. Sample Collection.....	32
2.3.2. Analysis of Physical Appearance and Tablet Packaging.....	33
2.3.3. DESI Ion Source.....	35
2.3.4. DESI MS	37
2.3.5. FTIR Spectroscopic Imaging.....	38
2.4. RESULTS AND DISCUSSION.....	39
2.4.1. Genuine Artesunate.....	40
2.4.2. Counterfeit Artesunate Containing Wrong Active Ingredient(s)	42
2.4.3. Counterfeit Artesunate Containing Insufficient Amount of Active Ingredient	46
2.4.4. Counterfeit Artesunate Containing No Active Ingredient	48
2.5. CONCLUSIONS.....	50
CHAPTER 3. REACTIVE DESI LINEAR ION TRAP MS OF LATEST- GENERATION COUNTERFEIT ANTIMALARIALS VIA NONCOVALENT COMPLEX FORMATION.....	51
3.1. ABSTRACT	51
3.2. INTRODUCTION	51
3.3. EXPERIMENTAL DETAILS	54
3.3.1. Samples and Reagents.....	54
3.3.2. DESI MS and LC-MS	55
3.4. RESULTS AND DISCUSSIONS.....	55
3.4.1. Reagentless vs. Reactive DESI MS of Genuine Artesunate Tablets.....	55
3.4.2. Experimental Variables Affecting Artesunic Acid Ion Yield in Reactive DESI MS.....	60

3.4.3. Reactive DESI MS of Other Artemisinins	62
3.4.4. Rapid Screening of Field-collected Artesunate Tablets by Reactive DESI MS.....	64
3.5. CONCLUSIONS.....	67
CHAPTER 4. DIRECT QUANTITATION OF ACTIVE INGREDIENTS IN SOLID ARTESUNATE ANTIMALARIALS BY NONCOVALENT COMPLEX FORMING DESI MS.....	68
4.1. ABSTRACT	68
4.2. INTRODUCTION	68
4.3. EXPERIMENTAL DETAILS	70
4.3.1. Samples and Reagents.....	70
4.3.2. Synthesis of Isotopically Labeled Internal Standard (IS)	71
4.3.3. Preparation of Standard Artesunate Tablets.....	73
4.3.4. Sample Pretreatment with IS and DESI MS	74
4.4. RESULTS AND DISCUSSIONS.....	75
4.4.1. Reagentless DESI vs. Reactive DESI of IS Treated Artesunate Tablets.....	75
4.4.2. Comparison of Internal Standard Deposition Methods	77
4.4.3. Effect of DESI Geometrical Settings on the Analyte-to-Internal Standard Signal Ratio	81
4.4.4. Effect of Sample Properties on the Analyte-to-Internal Standard Intensity Ratio	82
4.4.5. Calibration and Direct Quantitation of Artesunic Acid in Pharmaceutical Tablets by Reactive DESI MS.....	86
4.5. CONCLUSIONS.....	89
CHAPTER 5. DESI REACTIONS BETWEEN HOST CROWN ETHERS AND THE NEURAMINIDASE INHIBITOR OSELTAMIVIR FOR THE RAPID SCREENING OF TAMIFLU®	90
5.1. ABSTRACT	90

5.2. INTRODUCTION	91
5.3. EXPERIMENTAL DETAILS	92
5.3.1. Reagents and Samples.....	92
5.3.2. Substrates and Samples Preparation	94
5.3.3. DESI MS	94
5.3.4. Computational Calculations	95
5.4. RESULTS AND DISCUSSION.....	96
5.4.1. Effect of Spray Solvent Composition/Substrates on DESI MS Signal	96
5.4.2. Conventional vs. Reactive DESI MS of Oseltamivir Standards	97
5.4.3. Gas Phase Stability of Oseltamivir -Crown Ethers Complexes	103
5.4.4. Solution Phase Selectivity for Oseltamivir by Crown Ethers	107
5.4.5. Samples Preparation/Rapid Qualitative Screening of Field- Collected Samples by Reactive DESI CRM MS.....	109
5.4.6. Effect of Signal Ratio of Oseltamivir-Crown Ether Complexes on DESI Experimental Variables	112
5.4.7. Direct Quantitation of Oseltamivir in Field-Collected Tamiflu Capsules by Reactive DESI MS	113
5.5. CONCLUSIONS.....	115
CHAPTER 6. APPLICATION OF REAGENTLESS AND REACTIVE DESI MS IMAGING TO PHARMACEUTICAL FORENSICS AND DRUG DISCOVERY	116
6.1. ABSTRACT	116
6.2. INTRODUCTION	116
6.3. EXPERIMENTAL DETAILS	118
6.3.1. Samples and Reagents.....	118
6.3.2. DESI Imaging Ion Source	119
6.3.3. DESI MS Imaging of Artesunate Tablets	121

6.3.4. DESI MS Analysis of Bromophycolides and Imaging of Alga Tissue Samples	122
6.3.5. Estimation of the Concentration of Bromophycolides in Surface Patches of Untreated Alga Tissue by Reactive DESI MS	123
6.3.6. Computational Calculations	123
6.4. RESULTS AND DISCUSSION-CASE STUDY 1: REAGENTLESS DESI MS IMAGING OF ARTESUNATE PHARMACEUTICAL TABLETS	124
6.4.1. Reagentless DESI MS Imaging of a Genuine Artesunate Tablet.....	124
6.4.2. Reagentless DESI MS Imaging of a Counterfeit Artesunate Tablet	126
6.5. RESULTS AND DISCUSSION-CASE STUDY 2: DESI MS ANALYSIS OF BROMOPHYCOLIDES AND IMAGING OF ALGA TISSUE	128
6.5.3. Conventional vs. Reactive DESI MS Analysis of Bromophycolides/Gas Phase Structure of Observed Species	128
6.5.4. Direct Reactive DESI MS Profiling of Untreated Alga Tissue Samples	140
6.5.5. Reactive DESI MS Imaging of Untreated Alga Tissue	143
6.6. CONCLUSIONS.....	144
CHAPTER 7. DESORPTION ELECTROSPRAY/METASTABLE-INDUCED IONIZATION (DEMI): A FLEXIBLE MULTIMODE AMBIENT IONIZATION TECHNIQUE	146
7.1. ABSTRACT	146
7.2. INTRODUCTION	147
7.3. EXPERIMENTAL DETAILS	148
7.3.1. Samples and Reagents.....	148
7.3.2. DEMI Ion Source.....	149
7.3.3. Mass Spectrometry	151
7.4. RESULTS AND DISCUSSION.....	152

7.4.1. DEMI Ion Source Operation Modes.....	152
7.4.2. Reagent Ion Generation/Source Optimization	153
7.4.3. Capabilities of Ion Source Operation in the MICI-only Mode	157
7.4.4. Capabilities of Ion Source Operation in the Spray-only Mode	161
7.4.5. Capabilities of Ion Source Operation in the DEMI Mode	162
7.5. CONCLUSIONS.....	170
CHAPTER 8. CONCLUSIONS AND OUTLOOK	171
8.1. ABSTRACT	171
8.2. ACCOMPLISHMENTS-AMBIENT (DESI AND DART) MS INVESTIGATIONS	171
8.3. PROPOSED FUTURE DIRECTIONS.....	174
APPENDIXES – SURVEY OF OTHER TECHNIQUES USED IN COMBINATION WITH AMBIENT MS FOR CHARACTERIZING COUNTERFEIT ARTEMISININ-BASED ANTIMALARIALS	178
APPENDIX A. ASSESSMENT OF HAND-HELD RAMAN INSTRUMENTATION FOR IN SITU SCREENING FOR POTENTIALLY COUNTERFEIT ARTESUNATE ANTIMALARIAL TABLETS BY FT- RAMAN SPECTROSCOPY AND DIRECT IONIZATION MS	179
A.1. ABSTRACT	179
A.2. INTRODUCTION.....	179
A.3. EXPERIMENTAL DETAILS	181
A.3.1. Samples	181
A.3.2. Portable Raman Spectroscopy.....	181
A.3.3. FT-Raman Spectroscopy.....	182
A.3.4. Direct Ionization (DESI and DART) MS.....	182
A.4. RESULTS AND DISCUSSION.....	183
A.4.1. Analysis of Genuine Artesunate and Artemisinin-containing Tablets.....	184

A.4.2. Analysis of Counterfeit Tablets.....	187
A.5. CONCLUSIONS.....	191
APPENDIX B. COMBINING TWO-DIMENSIONAL DIFFUSION-ORDERED NUCLEAR MAGNETIC RESONANCE SPECTROSCOPY, DESI MS AND DART MS FOR THE INTEGRAL INVESTIGATION OF COUNTERFEIT PHARMACEUTICALS	192
B.1. ABSTRACT.....	192
B.2. INTRODUCTION.....	192
B.3. EXPERIMENTAL DETAILS	194
B.3.1. Samples	194
B.3.2. ¹ H and 2D DOSY ¹ H NMR Analysis.....	195
B.3.3. Ambient Ionization (DART and DESI) MS.....	198
B.4. RESULTS AND DISCUSSION	198
B.4.1. Analysis of Genuine Artesunate Tablets.....	199
B.4.2. Analysis of Counterfeit Artesunate Tablets.....	200
B.5. CONCLUSIONS.....	206
APPENDIX C. A COLLABORATIVE EPIDEMIOLOGICAL INVESTIGATION INTO THE CRIMINAL FAKE ARTESUNATE TRADE IN SOUTH EAST ASIA	207
C.1. ABSTRACT.....	207
C.2. INTRODUCTION.....	207
C.3. EXPERIMENTAL DETAILS	209
C.3.1. Samples	209
C.3.2. Palynology.....	209
C.3.3. XRD and IRMS.....	210
C.3.4. LC Diode Array Analysis.....	211
C.3.5. Ambient Ionization (DESI and DART) MS	211

C.4. RESULTS AND DISCUSSION	211
C.4.1. Determination of API(s) in the Samples	212
C.4.2. Palynological and Mineralogical Investigation	212
C.4.3. Interpretation of the Evidence	215
C.5. CONCLUSIONS.....	220
REFERENCES	221
VITA	241

LIST OF TABLES

Table 4.1. Comparison of the reproducibility of the absolute DESI signal vs. the signal intensity ratio of analyte-to-IS for various DESI variables.	82
Table 4.2. Quantitation of artesunic acid in genuine sample by DESI MS compared with the expected amount present in the sample.....	89
Table 5.1. Comparison of the relative stability of oseltamivir-crown ether complexes in the gas phase versus B3LYP-D computations.....	105
Table 5.2. Comparison of the robustness of the absolute DESI signal versus the signal intensity ratio of two different oseltamivir-crown ether complexes. Reactive DESI was performed by interrogating a genuine Tamiflu [®] capsule, pressed into a tablet, with an equimolar concentration (10 μ M) of 18-C-6 and 15-C-5 in neat acetonitrile.....	113
Table 5.3. Quantitation of the amount of oseltamivir in various Tamiflu [®] capsules purchased over the Internet by DESI MS compared with the amount present in each sample determined by HPLC-UV. The standard deviation of the concentrations reported by DESI was calculated from the precision observed for the intensity ratio of the two complexes measured in each mass spectrum obtained across the pellet while its surface was being scanned by the sprayer.....	115
Table 6.1. Binding energies for various bromophycolide-anion complexes obtained from geometry optimizations at the B3LYP-D/6-31+G* level of theory. The intermolecular hydrogen bond lengths are indicated in parenthesis.	137
Table 6.2. Limits of detection ($S/N \geq 3$) for various bromophycolides obtained by monitoring different species by DESI MS in negative ion mode: [a] reagentless DESI, [b] reactive DESI where various anions including Br ⁻ , CF ₃ COO ⁻ and Cl ⁻ were added to the spray solution.[a] = reagentless DESI, [b] = reactive DESI.....	140
Table 7.1. Limit of detection ($S/N \geq 3$) for each of the components in a binary mixture of angiotensin I (0.5 mg/mL) and dibromodibenzosuberone (1 mg/mL) spotted onto glass slides (10 μ L) from a solution in 90:10 MeOH:H ₂ O and analyzed with each of the operation modes after solvent evaporation.	164
Table A.1. Description of the samples studied.....	189
Table B.1. ¹ H NMR data of APIs detected in the artesunate antimalarial samples investigated in this study.....	197
Table B.2. APIs and excipients detected by 2D DOSY ¹ H NMR, DESI and DART MS in 14 different antimalarial formulations.	205

LIST OF FIGURES

Figure 1.1. Schematic of a typical DESI MS set-up showing various experimental set-up variables.....	13
Figure 2.1. Structure of artemisinin and its derivatives.....	29
Figure 2.2. Map of the distribution of fake artesunate as of 2008, compiled by the Wellcome Trust-University of Oxford SE Asian Tropical Medicine Research Program and collaborators. Map taken from Newton, et al. ²⁰⁰	33
Figure 2.3. Hologram type of samples evaluated in this study, (a) genuine Guilin Pharmaceutical artesunate blister pack hologram, (b) Type 4, (c) Type 8, (d) Type 9, (e) Type 11, (f) Type 13. ²³⁶	35
Figure 2.4. Schematic of a custom-built DESI ion source coupled to a commercial linear ion trap (LiT) mass spectrometer.....	36
Figure 2.5. Area impacted by the custom-built DESI sprayer jet for various ion source settings. The spots were obtained by spraying 1 mM Reactive Blue 4 dye onto a white sheet of paper. (a) Impacted area vs. spray duration at a dye solution flow rate of 5 $\mu\text{L min}^{-1}$, (b) impacted area vs. dye solution flow rate (10 s spray duration).....	40
Figure 2.6. Analysis of a genuine Guilin Pharmaceutical Co. Ltd. artesunate tablet by: (a) reagentless DESI MS in positive ion mode, (b) reagentless DESI MS in negative ion mode, (c) Micro-ATR-FTIR imaging showing the distribution of (i) artesunic acid, (ii) avicel and (iii) talc. The size of each image is approximately 64x64 μm^2 . The representative spectra at the location indicated by the arrow are also shown and compared with the reference spectra of (ii) pure avicel and (iii) pure talc.....	41
Figure 2.7. Analysis of a fake artesunate Type 4 (11 KHA 7 7/1 #2) by (a) reagentless DESI MS in positive ion mode, (b) reagentless DESI MS in negative ion mode, (c) Micro-ATR-FTIR imaging showing the distribution of the bands at (i) 1008 cm^{-1} and (ii) 1655 cm^{-1} . The size of each image is approximately 64x64 μm^2 . The representative spectra at the locations indicated by the letters are also shown and compared with the reference spectra of pure talc and pure dipyrone.	43
Figure 2.8. Analysis of a fake artesunate Type 8 (12 PAS P 64/1) by (a) reagentless DESI MS in positive ion mode, (b) reagentless DESI MS in positive ion mode for different x-y positions on the tablet surface, (c) Micro-ATR-FTIR imaging showing the distribution of the band at 1403 cm^{-1} . The size of the image is approximately 64x64 μm^2 . The representative spectrum at the location	

indicated by the arrow is also shown and compared with the reference spectrum of pure calcium carbonate.45

Figure 2.9. Analysis of fake Type 13 (SMRU 40-1) by (a) DESI MS in positive ion mode, (b) Micro-ATR-FTIR imaging showing the distribution of the absorbance of the bands at (i) 1735 cm^{-1} and (ii) 1008 cm^{-1} . The size of each image is approximately $64 \times 64 \mu\text{m}^2$. The representative spectra at the location indicated by the arrows are also shown and compared with the reference spectrum of pure talc.46

Figure 2.10. Analysis of a fake artesunate Type 9 (SMRU 12/2005) by (a) reagentless DESI MS, (b) reactive DESI MS (insert shows the MS/MS spectrum of the peak at m/z 570.3), (c) Micro-ATR-FTIR imaging showing the distribution of the bands at (i) 1008 cm^{-1} , (ii) 1148 cm^{-1} . The size of each image is approximately $64 \times 64 \mu\text{m}^2$. The representative spectra at the location indicated by the letters are also shown and compared with the reference spectrum of talc. M = artesunic acid.48

Figure 2.11. Analysis of a fake artesunate Type 11 (Lao 05/03) by reagentless DESI MS by spraying the sample with a solution of (a) 75:25 $\text{CH}_3\text{CN}:\text{H}_2\text{O}$, (b) 100 % MeOH. The insert in (b) corresponds to the MS/MS spectrum generated from the peak at m/z 365.3 for (i) the sample (Lao 05/03) and (ii) lactose standard.49

Figure 3.1. DESI spectra of a genuine artesunate tablet analyzed in (a) reagentless DESI MS mode, by spraying the tablet with a solution of 75:25 $\text{CH}_3\text{CN}:\text{H}_2\text{O}$ and (b) reactive DESI MS mode by spraying tablets with a solution containing 100 μM of (i) hexylamine (Hex), (ii) dodecylamine (DDA) and (iii) octadecylamine (ODA) in 75:25 $\text{CH}_3\text{CN}:\text{H}_2\text{O}$. A = $\text{C}_4\text{H}_6\text{O}_4$, B = $\text{C}_2\text{H}_4\text{O}_2$. The inserts represent MS/MS spectra of the $[\text{M} + \text{amine} + \text{H}]^+$ ions with m/z 486.3, 570.3 and 654.5 respectively. M = artesunic acid.56

Figure 3.2. Positive ion mode reactive DESI of genuine artesunate tablets at different Hex, DDA and ODA concentrations. The bar graphs represent the intensities of the ions at m/z 486.3, 570.3, 654.5 obtained by spraying 1, 5, 50 and 100 μM solutions of each of the amines dissolved in 75:25 $\text{CH}_3\text{CN}:\text{H}_2\text{O}$58

Figure 3.3. Fragmentation efficiency curves [(sum of fragment intensities)/(total intensities)] for various artesunic acid-alkylammonium complexes. M = artesunic acid.59

Figure 3.4. Intensity dependence of the $[\text{M} + \text{DDA} + \text{H}]^+$ adduct ion (m/z 570.3) with (a) spray solution flow rate; error bars represent the standard deviation for 3 repeat measurements, (b) nebulizer gas flow, (c) spray solution charging voltage. Experiments were performed by spraying a solution of 100 μM dodecylamine in 75:25: $\text{CH}_3\text{CN}:\text{H}_2\text{O}$ onto genuine artesunate tablets. M = artesunic acid.61

Figure 3.5. Reactive DESI spectra of artemisinin-based antimalarials tablets collected in Laos and Kenya with collection codes: (a) Lao 12012, (b) Kenya 07/01, (c) Lao 07/20/2. Spectra were obtained by spraying tablets with a solution containing 100 μM DDA in 75:25 $\text{CH}_3\text{CN}:\text{H}_2\text{O}$. The inserts represent the MS/MS spectra of the ions with at m/z 468.4, 470.4 and 484.4 observed from each spectrum respectively. The peaks at m/z 750.5, 754.5 and 782.6 correspond to the dodecylammonium complexes of dimeric artemisinin, dihydroartemisinin and artemether respectively.	63
Figure 3.6. SRM traces obtained by reactive DESI MS/MS analysis of different genuine artesunate samples. The m/z 570.3 \rightarrow m/z 452.1 transition was used for monitoring the presence of artesunic acid.	65
Figure 3.7. Reactive DESI SRM trace corresponding to the duplicate analysis of last generation counterfeit artesunate samples collected in the Thai Burma border, together with a genuine sample. Sample codes: A: Control, B: Lao 06/04, C: S 35/1, D: S 29, E: S 40/2, F: S 45, G: S 40/1, H: S 47/2, I: S 47/1, J: Genuine (Gen-3). SRM was carried out following reactive DESI MS/MS by monitoring the m/z 570.3 \rightarrow m/z 452.1 transition.	66
Figure 4.1. Reaction scheme for IS synthesis.	71
Figure 4.2. ESI spectra of 1 μM (a) artesunic acid standard, (b) reaction product from IS synthesis. M = artesunic acid.	72
Figure 4.3. (a) Sample pretreatment with IS: (i) pipette deposition of a solution of d_4 -artesunic acid in neat acetonitrile onto the sample surface, (ii) air drying of sample after treatment with IS, and (iii) reactive DESI MS analysis of air-dried samples; (b) DESI MS interface showing various DESI set-up variables.	74
Figure 4.4. DESI spectra of genuine artesunate tablets pretreated with 25 μL , 100 mM solution of IS following analysis in (a) reagentless DESI mode and (b) reactive DESI mode.	76
Figure 4.5. Normalized traces of the ion intensity ratio of the ion at m/z 570 to that at m/z 574 for various internal standard deposition methods at various DESI spray solution flow rates. (a) Spray deposition from a solution of 75:25 $\text{CH}_3\text{CN}:\text{H}_2\text{O}$ (b) Doping of the DESI spray solution with the internal standard.	78
Figure 4.6. Normalized ion intensity traces at various solution flow rates by reactive DESI. (a) Relative intensity of ions at m/z 570 (black trace) and m/z 574 (gray trace), (b) intensity ratio of the ion at m/z 570 to that at m/z 574.	79
Figure 4.7. Normalized ion intensity traces at various nebulizer gas pressures by reactive DESI. (a) Sum of ion intensities generated from the ions at m/z 570 and m/z 574, (b) intensity ratio of the ion at m/z 570 to that at m/z 574.	80

Figure 4.8. Depth profiling of a genuine artesunate tablet treated with a IS: (a) Sum of ion intensities of the ions at m/z 570 and m/z 574. (b) intensity of ions at m/z 570, and m/z 574 respectively, (c) intensity ratio of ion at m/z 570 to that at m/z 574. The intensity values were normalized for each plot.	81
Figure 4.9. Dependence of the m/z 570 to m/z 574 ion intensity ratios following reactive DESI MS analysis of artesunate tablet standards with varying hardness. The intensity ratios were normalized to that of the maximum value.	83
Figure 4.10. Depth profiling of standard artesunate tablets prepared at different hardness values. Samples were treated with 100 μ M d ₄ -artesunic acid followed by DESI MS analysis. Plots show the intensity ratio of the ion at m/z 570 to that at m/z 574 for different DESI spray solution flow rates including: (a) 2 μ L min ⁻¹ , (b) 6 μ L min ⁻¹	84
Figure 4.11. Dependence of the m/z 570 to m/z 574 ion intensity ratios following reactive DESI MS analysis of artesunate tablet standards with varying tablet surface (a) diameter, (b) topology.	86
Figure 4.12. (a) Calibration curve obtained from standard samples prepared at a hardness of 2.4 Kg. The response is plotted as the signal intensity ratio divided by the product of tablet hardness by tablet surface area. (b) Method validation: plot of the amount of artesunic predicted from the calibration curve to the known amount present for a validation sample set. Error bars represent standard deviations for three different tablets. Each sample was probed on four quadrant and the signals averaged.	87
Figure 5.1. Structures of (a) oseltamivir and (b) crown ethers investigated in this study.....	93
Figure 5.2. DESI spectra of oseltamivir phosphate standard (10 μ L, 1mg/mL) deposited onto PTFE surfaces and interrogated with a solution of neat acetonitrile; (a) Full MS spectrum, (b) MS/MS of the precursor ion at m/z 313, (c) MS/MS/MS of the precursor ion at m/z 225. M = oseltamivir, A = 3-pentanol (C ₅ H ₁₂ O), B = ammonia (NH ₃), C = acetamide (C ₂ H ₅ NO).....	98
Figure 5.3. Optimized structure of the protonated oseltamivir molecule from <i>ab initio</i> molecular modeling calculations.....	99
Figure 5.4. Reactive DESI of oseltamivir phosphate standard (10 μ L, 1mg/mL) deposited onto PTFE surfaces and interrogated after solvent evaporation with a solution of 100 μ M of (a) 12-crown-4, (b) 15-crown-5, (c) 18-crown-6 and (d) 2,5 dibenzo-21-crown-7. The inserts represent the corresponding MS/MS spectra of the [M + crown ether + H] ⁺ ions at m/z 489, 533, 577, and 717 respectively. M = oseltamivir, A = 3-pentanol (C ₅ H ₁₂ O).....	100

Figure 5.5. Fragmentation efficiency curves [(sum of fragment intensities)/(total intensities)] for various crown ether-oseltamivir complexes. The fragmentation fraction was normalized to 100%.....	104
Figure 5.6. Complex geometries optimized at the B3LYP-D/6-31G** level of theory: (a) [M + 12-C-4 + H] ⁺ , (b) [M + 15-C-5 + H] ⁺ , (c) [M + 18-C-6 + H] ⁺ , (d) [M + 2,5-DB-21-C-7 + H] ⁺	106
Figure 5.7. (a) Reactive DESI spectra of oseltamivir standards deposited onto PTFE surfaces with various pairs of equimolar concentration (10 μM) of crown ethers (i) 18-C-6 and 2,5-DB-21-C-7, (ii) 18-C-6 and 15-C-5, (iii) 15-C-5 and 12-C-4. (b) Effect of the amount of oseltamivir present on the substrate on the signal ratio of various pairs of oseltamivir-crown ether complexes: (i) 18-C-6 and 2,5-DB-21-C-7, (ii) 15-C-5 and 18-C-6, (iii) 12-C-4 and 15-C-5. The inserts represent the logarithmic plots of the corresponding signal ratio versus the amount of oseltamivir present on the substrate. The signal ratio was normalized to that of the maximum value.	108
Figure 5.8. Effect of increasing the concentration of each crown ether in equimolar solutions of crown ether pairs on the signal intensity ratio from the reactive DESI MS analysis of fixed amounts (10 μL, 1 mg/mL) of oseltamivir deposited onto PTFE substrates. The crown ether pairs investigated include (a) 18-C-6 and 2,5-DB-21-C-7, (b) 18-C-6 and 15-C-5, (c) 15-C-5 and 12-C-4. The signal ratio was normalized to that of the maximum value.	109
Figure 5.9. (i) Sample preparation; (ii) reactive DESI MS. The insert shows the dependence of the reserpine DESI MS signal intensity on pellet hardness. Plotted are the intensities for the observed protonated reserpine species that has been normalized for the pellet hardness.....	110
Figure 5.10. (a) Reactive DESI mass spectra of an oseltamivir phosphate standard (10 μL, 1mg/mL) interrogated with a solution of 100 μM 18-crown-6: (i) Full spectrum, (ii) MS/MS spectrum of the ion at <i>m/z</i> 577, (iii) MS/MS/MS spectrum generated from the ion at <i>m/z</i> 313 (iv) CRM isolation of the oseltamivir fragment at <i>m/z</i> 225 generated by MS/MS/MS. (b) CRM traces obtained by reactive DESI MS analysis of a genuine Tamiflu [®] capsule and capsules purchased over the Internet.....	111
Figure 5.11. Selected ion chromatogram traces obtained by reactive DESI of a genuine versus potentially counterfeit Tamiflu [®] capsules purchased over the Internet. Samples were interrogated with a solution of 10 μM 15-C-5 and 5 μM 18-C-6. The traces correspond to complexes of oseltamivir with 15-C-5 (<i>m/z</i> 533) and 18-C-5 (<i>m/z</i> 577) respectively. Samples were placed in a line on the microscope stage and sequentially exposed to the DESI spray.	114

Figure 6.1. DESI MS imaging set-up. (i) Extended capillary (760 μm i.d. x 33cm), (ii) Prior Scientific microscope stage (iii) off-the-shelf Thorlabs parts, (iv) high performance sprayer.	120
Figure 6.2. (a) Representative DESI spectrum of a genuine artesunate tablet manufactured by Mekophar Pharmaceuticals. (b) DESI MS images of the tablet constructed using the spatial relationship between various spectral features and their intensity, with data acquisition in full-scan MS mode: (i) sodiated artesunic acid (m/z 407.2), (ii) sodiated artesunic acid dimer (m/z 791.2), (iii) sodiated lactose (m/z 365.3) and (iv) sodiated acetaminophen (m/z 174.1). All images are shown in false color scale and pixilated format.	125
Figure 6.3. Representative DESI spectrum of a fake artesunate tablet (collection code, Lao 12060, type 8 fake). (b) DESI MS images of the tablet constructed based on the spatial relationship between various spectral features and their intensity, with data acquisition in full-scan MS mode: (i) sodiated acetaminophen (m/z 174.1), (ii) sodiated acetaminophen dimer (m/z 325.1), (iii) sodiated lactose (m/z 365.3) and (iv) sodiated artesunic acid (m/z 407.2). All images are shown in false color scale and pixilated format.	127
Figure 6.4. Structures of a subset of bromophycolides extracted from the Fijian red alga <i>Callophycus serratus</i> . ²⁷³	128
Figure 6.5. Conventional DESI MS, MS ² , and MS ³ spectra of bromophycolide standards. (a) Full MS of bromophycolide A and (b) corresponding MS ² of m/z 665 precursor (MS ³ of m/z 583 precursor inserted), (c) full MS of bromophycolide B and (d) corresponding MS ² of m/z 665 precursor (MS ³ of m/z 583 precursor inserted), (e) full MS of bromophycolide E and (f) corresponding MS ² of m/z 583 precursor.	129
Figure 6.6. Geometries of (a) bromophycolide A (b) deprotonated bromophycolide A dimer, optimized at the B3LYP/6-31+G* level of theory.	130
Figure 6.7. DESI MS ⁵ spectra of pure bromophycolides, (a) bromophycolide A, (b) bromophycolide B.	132
Figure 6.8. Effect of ion source collision induced dissociation energy in the multipole region for various DC offset voltages on the intensity of various bromophycolide A ionic species including: [bromophycolide A - HBr - H] ⁻ at m/z 583, [bromophycolide A - H] ⁻ at m/z 665 and [2 bromophycolide A - H] ⁻ at m/z 1329. The intensity values were normalized to that of the maximum observed.	133
Figure 6.9. Reactive DESI MS and MS ² spectra of bromophycolide A standards interrogated with spray solutions of various anions in methanol. (a) 100 μM NH ₄ Cl, and (b) corresponding MS ² spectrum of the m/z 701 precursor, (c) 10 μM HBr, and (d) corresponding MS ² spectrum of the m/z 745 precursor, (e) 0.001 %v/v (135 μM) CF ₃ COOH and (f) corresponding MS ² spectrum of the m/z 779 precursor.	135

Figure 6.10. Optimized geometries for: (a) bromophycolide A, and its complexes with (b) Cl ⁻ , (c) Br ⁻ and (d) CF ₃ COO ⁻ optimized at the B3LYP-D/6-31+G* level of theory.	136
Figure 6.11. Effect of Cl ⁻ concentration on the intensity of the [bromophycolide A + Cl] ⁻ and [2 bromophycolide A - H] ⁻ ions. The intensity values were normalized.	138
Figure 6.12. Signal-to-noise ratios observed for various bromophycolide species obtained from the DESI MS analysis of pure bromophycolides standards; spraying with a solution of 100 % MeOH, (i and ii) and spraying with a solution of methanol containing various anions including Cl ⁻ (100 μM), Br ⁻ (10 μM) and CF ₃ COO ⁻ (135 μM) (iii, iv and v) respectively.	139
Figure 6.13. (a) Typical spatially-resolved reactive DESI spectra of <i>C. serratus</i> surface. (b) Representative reactive DESI spectrum from patch-free algal surface prior to and following mechanical damage. Ion clusters centered at 701, 619 and 583 correspond to [bromophycolide A(B) + Cl] ⁻ , [bromophycolide E + Cl] ⁻ and [bromophycolide E - H] ⁻ respectively.	141
Figure 6.14. (a) <i>Callophycus serratus</i> optical image. (b) Representative reactive DESI spectrum of a light-colored patch on the <i>Callophycus serratus</i> surface. (c) Reactive DESI MS image reconstructed for the ion at <i>m/z</i> 701. The ion clusters centered at 701 and 619 represent [bromophycolide A(B) + Cl] ⁻ and [bromophycolide E + Cl] ⁻ respectively.	143
Figure 7.1. Schematic of the DEMI ion source coupled to a quadrupole ion trap mass spectrometer (only inlet shown).	150
Figure 7.2. Pictorial representation of the different DEMI operation modes, and the corresponding ion generation mechanisms believed to be prevalent in each case.	153
Figure 7.3. Mass spectrum showing typical reagent ions for source operation in the MICI and DEMI modes.	154
Figure 7.4. Optimization of the total reactant ion signal for the ion source operating in MICI-only mode (a) as a function of He or N ₂ discharge gas flow rate (corresponding normalized intensity scale on left ordinate). The dotted lines show the effect of He gas flow rate on the ion trap analyzer pressure (scale on the right ordinate) for different source-to-MS inlet distances (<i>D</i> _{AB}). The effect of (b) the glow-discharge voltage, (c) the source-to-MS distance (<i>D</i> _{AB}), (d) the grid voltage and (e) the voltage bias on T-union on the total reactant ion intensity is shown on the bottom plots. For each plot, the total ion signals were normalized to that of the maximum value.	155
Figure 7.5. Mass spectra of powders of some low polarity compounds and their mixture with the source operating in MICI-only mode. (a) dibenzosuberone, (b)	

dibromodibenzosuberone, (c) cholesterol (d) mixture of all three. 2 mg powder of each sample deposited onto a glass slide were aerosolized and transported by the N₂ nebulizer gas from the pneumatic sprayer (with spray solvent off) through the glass capillary. 1 mg of each compound was used to prepare the mixture. The N₂ nebulizer gas temperature and pressure were 14°C (unheated) and 150 psi, respectively. 158

Figure 7.6. Mass spectra of various powdered samples with the source operating in the MICI-only mode. (a) spray dried lactose, (b) powdered chloroquine-containing fake artesunate antimalarial tablet, and (c) powdered Halfan[®] antimalarial tablet containing halofantrine. The pressure of the unheated nebulizer gas was 150 psi. 159

Figure 7.7. Direct ionization mass spectra of a multi-vitamin tablet with the source operating in the MICI-only mode: (a) intact tablet analyzed with the nebulizer gas heated to 83°C, (b) powdered sample deposited on a glass slide and analyzed with the nebulizer gas unheated. 160

Figure 7.8. Left panel: (a) selected ion intensity (m/z 152±0.15) traces obtained from the analysis of an intact acetaminophen tablet with the source operating in the MICI-only mode. Samples were probed with the nebulizer gas from the sprayer (solvent off) heated to various temperatures with an inline heating element. **Right panel:** corresponding mass spectra obtained for the nebulizer gas heated to (b) 54°C, (c) 71°C, and (d) 77°C. 161

Figure 7.9. (a) Typical mass spectrum obtained from the analysis of an acetaminophen tablet with the source operating in spray-only mode, (b) Selected ion intensity traces (m/z 152, 174, 303 and 325) from the analysis of an acetaminophen tablet with the nebulizer gas set to ramp from 14°C – 83°C at a rate of ~ 6.5°C/min with the source operated in spray-only mode. The window width for all selected ion traces was 0.3 m/z . M = acetaminophen. 162

Figure 7.10. Mass spectra of a binary mixture (10 µL, 0.5 mg/mL angiotensin I, 1mg/mL dibromodibenzosuberone, deposited onto a glass slide) analyzed in, (a) MICI-only mode, (b) spray-only mode and (C) DEMI mode. (m/z 1319 = [angiotensin I + Na]⁺). Noted in the upper right corner of each plot is the base peak absolute intensity. 163

Figure 7.11. Mass spectra of a binary mixture (10 µL, 0.5 mg/mL angiotensin I, 1mg/mL dibromodibenzosuberone) deposited onto a glass slide and analyzed with a spray solution composed of 50:50 MeOH:acetone, in (a) spray-only and, (b) DEMI modes. The unheated nebulizer gas pressure was 150 psi and the solvent flow rate was 10 µl/min. 165

Figure 7.12. Mass spectra of an acetaminophen tablet with the source operated in DEMI mode for different solvent flow rates (a) 5 µL/min, (b) 10 µL/min, (c) 15 µL/min and (d) 20 µL/min. The temperature of the nebulizer gas was set to 71°C. 166

Figure 7.13. Selected ion intensity traces (m/z 152, 174, 303, 325 corresponding to $[M+H]^+$, $[M+Na]^+$, $[2M+H]^+$, $[2M+Na]^+$ respectively, where M = acetaminophen) from the analysis of an acetaminophen tablet under different DEMI ion source operating conditions: (a) spray-only mode, while switching the electrospray voltage off and on repeatedly, (b) spray-only mode while switching the glow discharge gas flow off and on repeatedly while maintaining the glow discharge voltage off, and (c) DEMI mode while switching the glow discharge voltage off and on repeatedly. The nebulizer gas was heated to 71°C and the spray solvent flow rate was 12 μ l/min. The window width for all selected ion traces was 0.3 m/z 167

Figure 7.14. Selected ion intensity traces (m/z 152, 174, 303, 325 corresponding to $[M+H]^+$, $[M+Na]^+$, $[2M+H]^+$, $[2M+Na]^+$ respectively, where M = acetaminophen) observed for the infusion of an acetaminophen standard (5 μ M) operating the ion source in the pneumatically-assisted electrospray/chemical ionization mode while switching the glow discharge voltage off and on repeatedly. The solvent flow rate was 12 μ L/min and the nebulizer gas temperature and pressure were 61°C and 150 psi respectively. The window width for all selected ion traces was of 0.3 m/z 168

Figure 7.15. Mass spectra of an artemisinin-containing fake artesunate antimalarial tablet with the source operated in the: (a) MICI-only mode, (b) spray-only mode and (C) DEMI mode. (m/z 265 = $[M - H_2O + H]^+$, m/z 237 = $[M - H_2O - CO + H]^+$, m/z 209 = $[M - H_2O - 2CO + H]^+$; where M = artemisinin). 169

Figure A.1. (a) FT-Raman spectra of genuine (i) Guilin and (ii) Mekophar artesunate tablets, compared with the reference spectrum of artesunic acid. (b) DESI spectra of the genuine Guilin tablet obtained by the (i) reagentless DESI MS and (ii) reactive DESI MS modes. 185

Figure A.2. (a) FT Raman spectra of fake tablet S 40-1 compared with the reference spectra of starch and artemisinin. (b) Corresponding DESI spectra of fake tablet S 40-1: (i) reagentless DESI MS and (ii) reactive DESI MS. 186

Figure A.3. (a) (i) Portable Raman and (ii) FT-Raman spectra of fake tablet LAO BW8 compared with the reference spectra of starch and dypirone. (b) Corresponding reagentless DESI spectra of fake tablet LAO BW8. 187

Figure B.1. Analyses of formulation 4 by: (a) 2D DOSY 1H NMR in DMSO- d_6 with TMPS as internal reference standard, positive ion mode (b) DART MS (C) DESI MS. 199

Figure B.2. Analyses of formulation 2 by: (a) 2D DOSY 1H NMR in DMSO- d_6 with TMPS as internal reference standard (S_{DMSO} represents DMSO satellite signals), positive ion mode (b) DART MS (c) DESI MS. 201

Figure B.3. Analyses of formulation 11 by: (a) 2D DOSY ^1H NMR in DMSO-d_6 with TMPS as internal reference standard (S_{DMSO} represents DMSO satellite signals); and (b) DESI MS in positive ion mode. (C) DESI spectrum of a sucrose standard ($10\ \mu\text{L}$, $1\ \text{mg mL}^{-1}$), (D) DESI spectrum of a lactose standard ($10\ \mu\text{L}$, $1\ \text{mg mL}^{-1}$). Standards were deposited onto PTFE and analyzed after air drying. The inserts in (b), (c) and (d) represent the corresponding DESI MS^2 spectra generated from the ion at m/z 365.3.	203
Figure B.4. Fragment ions observed for the isomeric species: (a) $[\text{lactose} + \text{Na}]^+$ and (b) $[\text{sucrose} + \text{Na}]^+$	204
Figure C.1. Photomicrographs of material found in fake artesunate tablets. (a) Debris, including charcoal fragments. (b) <i>Pinus</i> pollen grain. (c) <i>Juglans</i> pollen grain. (d) <i>Acacia</i> pollen grain with charcoal deposit. (e) <i>Dermatophagoides</i> mite nymph... ..	213
Figure C.2. Plot of $\delta^{13}\text{C}$ and $\delta^{18}\text{O}$ values, in % of carbonate in tablets. Approximate values expected from calcite in different geological environments (pink = igneous; yellow = metamorphosed; green = unaltered) is also plotted. The top right data point represents sample 05/17.....	215
Figure C.3. Counterfeit artesunate samples seized during arrests made after reporting of findings of Operation Jupiter to Chinese government officials... ..	219

LIST OF SYMBOLS

2^3S_1	Helium metastable atom excited to the triplet state
ca.	approximately
Ci	curie
Da	Dalton
He*	Helium metastable atom
$E_c^{50\%}$	Enthalpy of dissociation
eV	electronvolt
IC ₅₀	half maximal inhibitory concentration
i.d.	inner diameter
in.	inches
kcal mol ⁻¹	kilocalorie per mole
kDa	kilodaltons
kV	kilovolt
L/s	liters per second
Liq	Liquid
<i>m/z</i>	mass-to-charge ratio
M _w	molecular weight
MΩ	mega ohms
o.d.	outer diameter
psi	pounds per square inch
rpm	revolutions per minute
w/w	weight/weight

\AA	angstrom
μ	micro
ν	frequency

LIST OF ABBREVIATIONS

ACT	Artemisinin-based Combination Therapy
AGC	Automatic Gain Control
AP	Atmospheric Pressure
APCI	Atmospheric Pressure Chemical Ionization
API	Active Pharmaceutical Ingredient
APIE	Atmospheric Pressure Ion Evaporation
APPI	Atmospheric Pressure Photoionization
ASAP	Pressure Solid Analysis Probe
ATR	Attenuated Total Reflectance
BADCI	Beta electron-Assisted Direct Chemical Ionization
C-G	Corona-to-Glow
CI	Chemical Ionization
CID	Collision-Induced Dissociation
COSY	Correlation Spectroscopy
CRM	Consecutive Reaction Monitoring
DAPCI	Desorption Atmospheric Pressure Chemical Ionization
DAPPI	Desorption Atmospheric Pressure Photoionization
DART	Direct Analysis in Real Time
DBDI	Barrier Discharge Ionization
DEMI	Desorption Electrospray/Metastable-induced Ionization
DESI	Desorption Electrospray Ionization

DeSSI	Desorption Sonic Spray Ionization
DOSY	Diffusion-Ordered Spectroscopy
EASI	Easy Ambient Sonic-spray Ionization
EESI	Extractive Electrospray Ionization
EC	Electron Capture
EI	Electron Ionization
ELDI	Electrospray-assisted Laser Desorption/Ionization
Er:YAG	Erbium-doped Yttrium Aluminium Garnet
ESI	Electrospray Ionization
FAB	Fast Atom Bombardment
FAPA	Flowing Atmospheric Pressure Afterglow
FD	Fused Droplet
FPA	Focal Plane Array
FT	Fourier Transform
G-A	Glow-to-Arc
GC	Gas Chromatography
HMBC	Heteronuclear Multiple Bond Correlation
HPLC	High Pressure Liquid Chromatography
ICR	Ion Cyclotron Resonance
IMS	Ion Mobility Spectrometry
IR	Infrared
IRMS	Isotope Ratio Mass Spectrometry
IS	Internal Standard

LA	Laser Ablation
LC	Liquid Chromatography
LD	Laser Desorption
LIAD	Laser-Induced Acoustic Desorption
LiT	Linear ion Trap
LOD	Limit of Detection
LTP	Low Temperature Plasma
MALDESI	Matrix-Assisted Laser Desorption Electrospray Ionization
MALDI	Matrix-Assisted Laser Desorption Ionization
MICI	Metastable-Induced Chemical Ionization
MS	Mass Spectrometry
MS/MS	Tandem Mass Spectrometry
ND	Neutral Desorption
NMR	Nuclear Magnetic Resonance
OCN	Oscillating Capillary Nebulizer
PADI	Plasma-Assisted Desorption/Ionization
PEEK	Polyaryletheretherketone
PESI	Probe Electrospray Ionization
PTFE	Polytetrafluoroethylene
QCM	Quartz Crystal Microbalance
QiT	Quadrupole ion Trap
QqQ	Triple Quadrupole
Q-TOF	Quadrupole Time-of-Flight

RADIO	Radio-frequency Acoustic Desorption/Ionization
RIT	Rectilinear Ion Trap
RSD	Relative Standard Deviation
SIMS	Secondary Ion Mass Spectrometry
SNR	Signal-to-Noise Ratio
SRM	Selected Reaction Monitoring
SSI	Sonic Spray Ionization
TDI	Thermal Desorption/Ionization
TLC	Thin Layer Chromatography
TOF	Time-of-Flight
TS	Thermospray
UA	Ultrasonically-Assisted
UV	Ultraviolet
XRD	X-Ray Diffraction

LIST OF PUBLICATIONS

CHAPTER 1

Harris GA, Nyadong L, Fernández FM, “Recent Developments in Ambient Ionization Techniques for Analytical Mass Spectrometry”, *Analyst*, **2008**, 133 1297-1301.

CHAPTER 2

Ricci C, Nyadong L, Fernández FM, Newton PN, Kazarian SG, “Combined Fourier-transform Infrared Imaging and Desorption Electrospray-ionization Linear Ion-trap MS for Analysis of Counterfeit Antimalarial Tablets”, *Anal. Bioanal. Chem.*, **2007**, 387, 551-559.

CHAPTER 3

Nyadong L, Green MD, De Jesus VR, Newton PN, Fernández FM, “Reactive Desorption electrospray Ionization Linear Ion Trap MS of Latest-generation Counterfeit Antimalarials via Noncovalent Complex Formation”, *Anal. Chem.*, **2007**, 79, 2150-2157.

CHAPTER 4

Nyadong L, Late S, Green MD, Banga A, Fernández FM, “Direct Quantitation of Active Ingredients in Solid Artesunate Antimalarials by Noncovalent Complex Forming Reactive Desorption Electrospray Ionization Mass Spectrometry”, *J. Am. Soc. Mass Spectrom.*, **2008**, 19, 380-388.

CHAPTER 5

Nyadong L, Hohenstein HG, Johnson K, Sherrill CD, Green MD, Fernández FM, “Desorption Electrospray Ionization Reactions between Host Crown Ethers and the Neuraminidase Inhibitor Oseltamivir for the Rapid Screening of Tamiflu[®]”, *Analyst*, **2008**, 133, 1513-1522.

CHAPTER 6

Nyadong L, Harris GA, Balayssac S, Galhena AS, Malet-Martino M, Martina R, Parry RM, Wang MD, Fernandez FM, Gilard V, “Combining Two-Dimensional Diffusion-Ordered Nuclear Magnetic Resonance Spectroscopy, Imaging Desorption Electrospray Ionization Mass Spectrometry, and Direct Analysis in Real-Time Mass Spectrometry for the Integral Investigation of Counterfeit Pharmaceuticals”, *Anal. Chem.*, **2009**, 81, 4803-4812.

Nyadong L, Hohenstein HG, Galhena A, Lane AL, Kubanek J, Sherrill CD, Fernández FM, “Reactive Desorption Electrospray Ionization Mass Spectrometry (DESI-MS) of Natural Products of a Marine Alga”, *Anal. Bioanal. Chem.*, **2009**, 394, 245-254.

Lane AL, Nyadong L, Galhena AS, Stout EP, Parry RM, Kwasnik M, Wang M, Hay ME, Fernández FM, Kubanek J, “Desorption Electrospray Ionization Mass Spectrometry Reveals Surface-mediated Antifungal Chemical Defense of a Tropical Seaweed”, *PNAS*, **2009**, 106, 7314-7319.

CHAPTER 7

Nyadong L, Galhena AS, Fernández FM, *Anal. Chem.*, “Desorption Electrospray/Metastable-Induced Ionization (DEMI): A Flexible Multimode Ambient Ion Generation Technique”, *Anal. Chem.*, **2009**, 81, 7788-7794.

APPENDIX A

Ricci C, Nyadong L, Yang F, Fernández FM, Brown CD, Newton PN, Kazarian SG, “Assessment of Hand-held Raman Instrumentation for In Situ Screening for Potentially Counterfeit Artesunate Antimalarial Tablets by FT-Raman Spectroscopy and Direct Ionization MS”, *Analytica Chimica Acta*, **2008**, 623, 178-186.

APPENDIX B

Nyadong L, Harris GA, Balayssac S, Galhena AS, Malet-Martino M, Martina R, Parry RM, Wang MD, Fernández FM, Gilard V, “Combining Two-Dimensional Diffusion-Ordered Nuclear Magnetic Resonance Spectroscopy, Imaging Desorption Electrospray Ionization Mass Spectrometry, and Direct Analysis in Real-Time Mass Spectrometry for the Integral Investigation of Counterfeit Pharmaceuticals”, *Anal. Chem.*, **2009**, 81, 4803-4812.

APPENDIX C

Newton PN, Fernández FM, Plancon-Lecadre A, Mildenhall D, Green MD, Ziyong L, Christophel EM, Phanouvong S, Howells S, MacIntosh E, Laurin P, Blum N, Hampton CY, Faure K, Nyadong L, Xoong CWR, Santoso B, Zhiguang W, Newton J, Palmer K, “A Collaborative Epidemiological Investigation into the Criminal Fake Artesunate Trade in South East Asia”, *PLoS Med.*, **2008**, 5, e32.

SUMMARY

The ability of generating ions directly from solid samples, in their native state without the need for sample preparation is rapidly changing the field of mass spectrometry (MS). The key technological innovations enabling these advancements include the development of atmospheric pressure ionization MS interfaces and the introduction of ambient ionization technologies. Pioneered by desorption electrospray ionization (DESI) introduced by Cooks and coworkers in 2004, and followed closely by direct analysis in real time (DART) introduced by Cody *et al.* in 2005, ambient MS methods allow removal of sample size and shape constraints, thereby making many objects amenable to direct MS analysis. The elimination of sample preparation requirements allows rapid analysis times, making such mass spectrometric methodologies more amicable over other techniques where throughput is sought, especially when dealing with the analysis of a large sample set.

The work presented in this thesis is aimed at studying some of the fundamental processes prevailing in ambient mass spectrometry, and the application of these techniques to the detection of molecules of pharmaceutical importance. A review of the state-of-the-art in ambient mass spectrometry is presented in Chapter 1. Chapter 2 presents the first implementation of DESI MS to the chemical fingerprinting of counterfeit drug tablets that mimic the vital anti-malarial artesunate. Chapter 3 presents an investigation of the effect of performing various ion-molecule reactions in the charged liquid droplet/solid sample boundary in DESI and its effect on the selectivity, gas phase stability and the associated analyte ion yields for the determination of artesunate in drug

tablets. Chapter 4 presents the direct quantitation of artesunate in solid antimalarial tablets by DESI MS. Chapter 5 presents the development of a selective and sensitive DESI MS protocol for screening of Tamiflu® quality. Chapter 6 presents an implementation of DESI MS in imaging mode. In Chapter 7, an investigation of the complementarity between DESI and DART is presented, enabling the development of a robust multimode ambient ion source.

CHAPTER 1. AMBIENT MASS SPECTROMETRY

1.1. Abstract

Ambient ionization mass spectrometry provides the ability to record mass spectra on a variety of samples in their native environment, without the need for sample preparation or prepreparation, by generating ions directly from the sample placed outside the instrument. In these methods, analyte desorption/ionization occurs in concert or decoupled resulting in several different permutations culminating in a proliferation of techniques and acronyms. This chapter presents some of the earlier ionization techniques still commonly in use today, underscoring the capabilities provided by ambient MS methods. It also portrays some of the technological advancements leading to the introduction of this new field, and highlights the different ionization approaches and some of their applications since the description of DESI in 2004.¹ The multitude of techniques that have been reported since then are also sorted into various categories based on the physicochemical processes involved in surface sampling and ionization.

1.2. Vacuum Ionization Techniques

In the past, the range of sample types and chemical species amenable to mass spectrometric investigations was greatly limited by the vacuum requirement of the spectrometer's modular components including the ion source, mass analyzer and detector. Common ionization sources, for example for coupling gas chromatography (GC) with MS, include electron ionization (EI)² and chemical ionization (CI)³. In EI, ions are generated from vaporized neutral analytes by interactions with 70 eV electrons resulting

in extensive fragmentation, frequently exploited to obtain structural information. CI usually deposits a lower amount of internal energy than EI, with less fragmentation and simpler spectra where the intact analyte is easily recognized. In CI, the large ratio of reagent gases (e.g methane, ammonia, isobutene) to analyte molecules that interact with the electrons entering the ionization volume, results in dampening of the electron's kinetic energy by preferential ionization of the reagent gas. Reactive species produced by this process interact with gaseous analyte neutral species resulting in protonated analyte ions. The 70 eV energy commonly used to accelerate electrons in EI and CI, results in their de Broglie wavelengths matching the typical bond lengths in organic molecules, maximizing energy transfer to them and allowing efficient ionization/fragmentation.⁴ These techniques have commonly been used in the analysis of low molecular weight volatile organic molecules, but fail terribly when applied to molecules larger than ~700 Da due to the higher number of degrees of freedom.

Vacuum ionization techniques such as secondary ion mass spectrometry (SIMS), vacuum matrix-assisted laser desorption ionization (MALDI), and fast atom bombardment (FAB) have also played a pivotal role for chemical interrogation and for biomolecule characterization. These techniques provide an extension of the range of molecular weights and sample types that can be investigated in vacuum by MS, enabling applications in a wide range of fields including biology, material sciences and geochemistry.⁵⁻⁷ SIMS is probably the most sensitive surface analysis technique and historically has been developed to measure the elemental, isotopic, or molecular composition of surfaces. SIMS is able to detect elements present in parts per billion ranges by sputtering the sample surface with a primary ion beam, and analyzing the

secondary ions generated. MALDI, on the other hand, is a soft ionization technique and has extensively been used for analyzing biomolecules such as peptides, proteins sugars etc. In MALDI, analyte desorption and ionization is triggered by a laser beam that is fired onto the sample, co-crystallized in a matrix. This matrix serves to absorb the laser energy, mitigating fragmentation and facilitating vaporization/ionization of the analyte.⁶ In FAB, the analyte mixed with a non-volatile matrix (e.g glycerol, thioglycerol, 3-nitrobenzylalcohol etc.) is bombarded with a high energy beam of atoms such as argon or xenon, resulting in intact gas phase protonated or deprotonated analyte species in the positive and negative ion modes, respectively.⁸ The generation of intact gas phase ions by FAB makes it a relatively soft ionization technique, however, not as soft when compared to MALDI. One of the main advantages enjoyed by surface chemical interrogation techniques such as SIMS and MALDI is their ability to provide spatially-resolved chemical information, a feature advantageously exploited for chemical imaging applications.⁷

1.3. Atmospheric Pressure Ionization Techniques

Driven by the need to investigate high molecular weight species, and for coupling liquid-phase separation techniques such as liquid chromatography and capillary electrophoresis to mass spectrometry; the introduction of atmospheric pressure ionization (API) techniques was a critical milestones in the progressive implementation of the present-day mass spectrometer. API sources are characterized by operation at atmospheric pressure outside the vacuum system of the mass spectrometer. Technical challenges arise from the fact that interfacing of an API source with a mass analyzer

requires a 10^7 - 10^8 fold pressure reduction for preserving the mean free path of the ions.⁹ In addition, the marriage of liquid chromatography with mass spectrometry (LC-MS) is particularly challenging because of the need to vaporize the LC mobile phase prior to MS analysis in order to prevent overloading of the vacuum system. In order to meet these challenges, two major approaches have been used to couple API ion sources to MS. The first approach includes the sampling of ions from the AP region directly into high vacuum using either a relatively small orifice (10-25 μm) or a very high pumping capacity ($> 100,000$ L/s) section.¹⁰ The second approach, which turns out to be the most preferred and probably the only employed today, uses a multi-stage differential pumping system. In this approach, ions are first drawn into the sampling orifice from AP (760 Torr) into a first chamber where they are pumped down to approximately 1-4 Torr by a rotary pump. Secondly, part of the expanding beam of gas and ions is sampled into a second chamber pumped down to 10^{-3} Torr or less, at which point most of the gases and solvent molecules have been pumped away. Finally, a suitable arrangement of ion optics elements guides the ions to the mass analyzer region.

Historically important approaches for the generation of ions at atmospheric pressure comprise the use of a radioactive metal foil (^{63}Ni) or a plasma initiated by an electrical discharge at the tip of a needle held at high voltage, both of which provide a source of ionizing electrons.¹¹⁻¹³ These ionizing electrons initiate the generation of ions by interactions with nearby gases. Because of the short mean free path between molecules at atmospheric pressure, the initial species quickly undergo ion-molecule reactions with air and other gaseous molecules producing various reactive intermediate ions that readily interact with analyte molecules resulting in atmospheric pressure

chemical ionization (APCI). Application of these approaches for the analysis of condensed phase analytes generally requires heating using a heated gas passing over the sample and/or resistive heating. As such, these techniques are limited to the analysis of relatively low molecular weight species that can be vaporized intact, thereby precluding their application for the analysis of thermally labile, highly polar and high molecular weight compounds. In APCI-MS, vaporized analytes with high gas phase basicities or acidities are preferentially ionized in positive and negative ion modes respectively. Early APCI-MS systems were highly publicized for their ability to rapidly analyze various target analytes in complex matrices without the need for chromatography or sample clean-up. In these systems, selectivity was afforded by tandem MS with typical applications being drugs of abuse and explosives detection.^{14, 15}

Prior sample separation via chromatography is generally beneficial (perhaps necessary) to allow detection of components with lower volatility and/or concentration. The most difficult challenge for generating ions of biomolecules from a liquid inlet system has been the ability to transition these molecules from the liquid to the gas phase without depositing too much internal energy in them to cause degradation. This transition normally occurs at the ion source interface and begins with the generation of uniform-sized droplets from the liquid effluent stream. Solvent molecules can be removed gradually from these droplets to eventually produce gas phase analyte molecules/ions.

The first reported coupling of LC to MS for the analysis of biomolecules was reported by Horning in 1974 through an APCI interface. The effluent stream emanating from the LC column, generally a mixture of a volatile solvent and analyte, is vaporized

using heated nebulizer gas. The vaporized sample then undergoes ionization through ion/molecule reactions with reagent ions present in the area surrounding the APCI needle.^{16, 17}

In 1979, Thomson et al. introduced AP Ion Evaporation (APIE), using a pneumatic nebulizer to create a spray of droplets from a nebulizer approximately 1 cm away from an induction electrode held at 3.5 kV to induce droplet charging.¹⁸ Spectra obtained using this technique showed solvent clusters in high abundance, resulting in poor sensitivity and interferences. The same authors later modified this approach by introducing a heated nebulizer probe coupled to a corona discharge needle, such as in APCI. This technique gave similar spectra and showed similar limitations to APCI.¹⁹

In 1980, Vestal and coworker introduced Thermospray (TS)^{20, 21}, a technique in which an aqueous mobile phase was vaporized as it passed through a heated stainless steel capillary located in a heated ion source with no external field charging to induce ionization. The composition of the spray after exiting the heated capillary was believed to be at least 90 % vapor, the remainder being composed of small droplets containing a statistical imbalance of charges originating from pre-charged solutes in solution. Ions were generated from these droplets after they gradually decreased in size following evaporation of neutral solvent molecules. Because no external field charging was used, this technique suffered from poor sensitivity. Later integration of a discharge needle into the apparatus allowed for the generation of APCI-type spectra. However, it also suffered from poor interday reproducibility with analyte signal intensity exhibiting a strong dependence on solvent composition and flow rate.

Notwithstanding the partial successes of these techniques, the final breakthrough that enabled the facile coupling of LC to MS for widespread routine application for the analysis of biomolecules occurred with the introduction of electrospray ionization (ESI) by Fenn and coworkers²²⁻²⁴ and Aleksandrov and coworkers.^{25,26} In conventional ESI, the first essential step involves the dispersion of a sample solution into a charged aerosol, which undergoes desolvation as droplets migrate into the high vacuum regions of the mass spectrometer. The charged aerosol is generated by application of a potential to the exterior of a capillary, which induces charge separation in the through-flow solution. Charge builds up at the capillary tip, forming a Taylor cone and causing the forcible ejection of a charged droplet. In early experiments, Dole and coworkers in 1968 made use of a concurrent flow of inert gas to facilitate droplet desolvation in the analysis of negative ions of relatively high molecular weight polystyrene.²⁷

With John Fenn's report at a 1988 symposium in San Francisco showing the interfacing of ESI with MS for the analysis of peptides and proteins of molecular weight up to 40 kDa²⁸ (later extended to 180 kDa the following year²²), the golden era of modern mass spectrometry begun. Fenn built on his knowledge of free-jet expansions²⁹ to improve Dole's ESI method. Fenn's approach required a countercurrent flow of N₂ for efficient droplet desolvation, thus eliminating re-solvation of the formed macromolecule ions. Because the electrospray process requires efficient solvent evaporation, typical ESI solutions are prepared by mixing a volatile organic solvent e.g (methanol, acetonitrile) with water and small amounts of a weak organic acid (e.g formic, acetic acid etc). The charged aerosol emanating from the Taylor cone is sampled into the first vacuum stage of a mass spectrometer through a capillary, which is generally heated to facilitate further

solvent evaporation. As the droplets/ions transit through the AP and first evacuated region, they reach the Rayleigh limit where they become unstable undergoing Coulombic explosion to give progeny droplets. This cycle continues until the droplets reach such a size from which desolvated ions are generated following two proposed mechanisms: (1) the ion evaporation model, which suggests that as the droplets reach a certain size, they start emitting ions directly into the gas phase after the repulsion forces on the droplet surface become high enough to break the surface tension¹⁸, or (2) the charge residue model, which proposes that charged droplets undergo evaporation and explosion cycles, resulting in progeny droplets, which finally contain one analyte molecule per droplet on average. Complete evaporation of solvent liberates the analyte carrying the charge initially present in the droplet.²⁷ A large proportion of indirect evidence suggests that smaller ions are liberated into the gas phase by the ion evaporation mechanism while larger ions are formed by the charge residue model.

Operation of the electrospray ion source at low flow rates such as in micro- and nano-ESI to generate much smaller initial droplets results in improved ionization efficiency due to the smaller initial droplet population. Because of spray instabilities observed in conventional ESI experiments, Henion and coworkers introduced pneumatically assisted ESI³⁰ where they used a coaxial flow of an inert gas around the spray capillary to facilitate droplet formation. This has now become the most widely used approach for implementing ESI. A variant of pneumatically-assisted ESI is electrosonic nebulization, which operates a traditional microESI source with a much higher velocity, supersonic nebulizer gas resulting in the preservation of even the weakest non-covalent interactions during the transition to the gas-phase.³¹ The elimination of the

spray voltage used in pneumatically assisted ESI has given rise to a relatively new technique known as sonic spray ionization (SSI),^{32, 33} where gas phase ions can be generated due to the statistical imbalance in the droplet charge distribution.

Other AP ion sources which are also gaining a significant amount of popularity include: atmospheric pressure photoionization (APPI), the atmospheric pressure version of MALDI (AP-MALDI), and atmospheric pressure solid analysis probe (ASAP). In APPI, analytes aerosolized from a nebulizer, are selectively ionized by 10 eV photons emitted by a krypton discharge lamp. The ionization mechanism in APPI depends on the analyte and solvent system used.³⁴⁻³⁶ High ionization efficiencies are usually achieved in the presence of a dopant (e.g toluene) which is directly photoionized generating reactant ions. In positive ion mode, and in the presence of an aprotic solvent (e.g hexane, chloroform), ionization by charge exchange predominates, while in protic solvents (e.g methanol) ionization by proton transfer is the most important pathway. In negative ion mode, compounds with high electron affinity ionize by electron capture or by charge exchange, while compounds with high gas phase acidities ionize by proton transfer.^{35, 36} APPI shows superior performance over ESI and APCI for the analysis of low polarity compounds, thus broadening the range of analytes that can be investigated by MS based techniques. AP-MALDI is similar to vacuum MALDI with the exception that ions are created at atmospheric pressure, resulting in limited sensitivity and mass range. ASAP is a commercial corona discharge-based atmospheric pressure ionization technique that was introduced in 2005 by McEwen *et al.*³⁷ In ASAP a solid sample probe is introduced directly into the corona discharge region of a commercial APCI ion source via a custom

built sample port. Heated N₂ nebulizer gas is used to facilitate vaporization of the sample from which ions are generated by standard APCI processes.³⁸

1.4. Ambient Ionization Techniques

The technological advancements that enabled the establishment of AP ionization techniques eliminated the requirement for samples to be ionized in vacuum, greatly increasing the scope of compounds amenable to MS analysis and increasing the analytical toolbox for the fields of proteomics and metabolomics. However, the need to dissolve, extract and/or filter the sample prior to analysis still remains, limiting throughput and setting limitations on the type, sizes and shape of samples susceptible to MS analysis. Recently introduced ionization techniques operated under ambient conditions aim to address these limitations.

Ambient ionization mass spectrometry allows for the direct analysis of the surface of samples of any size, shape texture/morphology by creating ions in the open air. Whereas in conventional mass spectrometric experiments the sample is generally dissolved prior to analysis, in ambient MS the sample is interrogated in its native state. The importance of this new field is reflected by the explosive appearance of a multitude of new ionization approaches catalyzed by the introduction of DESI¹ in the fall of 2004 and closely followed by DART.³⁹ Ambient ionization techniques can be separated into three major categories based on their associated desorption and/or ionization mechanisms including spray or jet based desorption/ionization techniques; ambient gas-, heat-, laser- and radiofrequency-based desorption/electrospray-assisted ionization techniques, and electric discharge-, beta electron-, photon-based ambient chemical ionization techniques.

Spray- or jet-based desorption/ionization techniques include DESI, desorption sonic spray ionization (DeSSI⁴⁰, also referred to as easy ambient sonic-spray ionization, EASI^{41, 42}) and probe electrospray ionization (PESI).⁴³⁻⁴⁵ Techniques that rely on ambient gas-, heat-, laser- and radiofrequency-based desorption/electrospray-assisted ionization include fused droplet ESI (FD-ESI),⁴⁶ extractive electrospray ionization (EESI),⁴⁷⁻⁵¹ nano EESI (nano-EESI),⁵² neutral desorption sampling extractive electrospray ionization (ND-EESI),⁵³⁻⁵⁵ ultrasonically-assisted EESI (UA-EESI),⁵⁶ radio frequency acoustic desorption/ionization (RADIO),⁵⁷ electrospray-assisted laser desorption/ionization (ELDI),⁵⁸⁻⁶³ matrix-assisted laser desorption electrospray ionization (MALDESI),⁶⁴⁻⁶⁷ laser ablation-electrospray ionization (LAESI),⁶⁸⁻⁷⁰ infrared laser-assisted desorption ESI (IR-LADESI),⁷¹ and laser-induced acoustic desorption/ESI (LIAD/ESI).⁷² Techniques that rely on electric discharge-, beta electron-, photon-based ambient chemical ionization include DART, desorption atmospheric pressure chemical ionization (DAPCI),^{73, 74} laser desorption-atmospheric pressure chemical ionization (LD-APCI),⁷⁵⁻⁷⁷ dielectric barrier discharge ionization (DBDI),^{78, 79} low temperature plasma (LTP),⁸⁰ plasma-assisted desorption/ionization (PADI),⁸¹ flowing atmospheric pressure afterglow (FAPA),^{82, 83} beta electron-assisted direct chemical ionization (BADCI),⁸⁴ atmospheric pressure thermal desorption/ionization (APTDI),⁸⁵ and desorption atmospheric pressure photoionization (DAPPI).⁸⁶⁻⁸⁹

1.4.1. Spray- or Jet-based Desorption/Ionization Techniques: DESI, DeSSI and PESI

These are open-air ionization techniques where a solvent spray is used to effect surface sampling and ionization. A schematic of a typical DESI MS set-up is shown in Figure 1, together with all the experimental set-up variables.

In DESI, a pneumatically assisted ESI source equipped with XYZ translation capabilities (for spray positioning) is placed over the sample to be analyzed. An extended AP ion transfer capillary is used to lead ions from the surface desorption point to the mass spectrometer. The sample is often mounted on a movable stage to facilitate positioning, improving reproducibility and providing imaging capabilities. Similar to ESI, a voltage between 2-8 kV is applied to the emitter. A combination of the high voltage, solvent flow (1.5-10 $\mu\text{L}/\text{min}$), and coaxial flow of high velocity nebulizer gas (100-200 psi) helps to create charged solvent micro-droplets, which are directed to the sample surface creating an elliptical^{90, 91} impact region from which surface chemicals are desorbed.

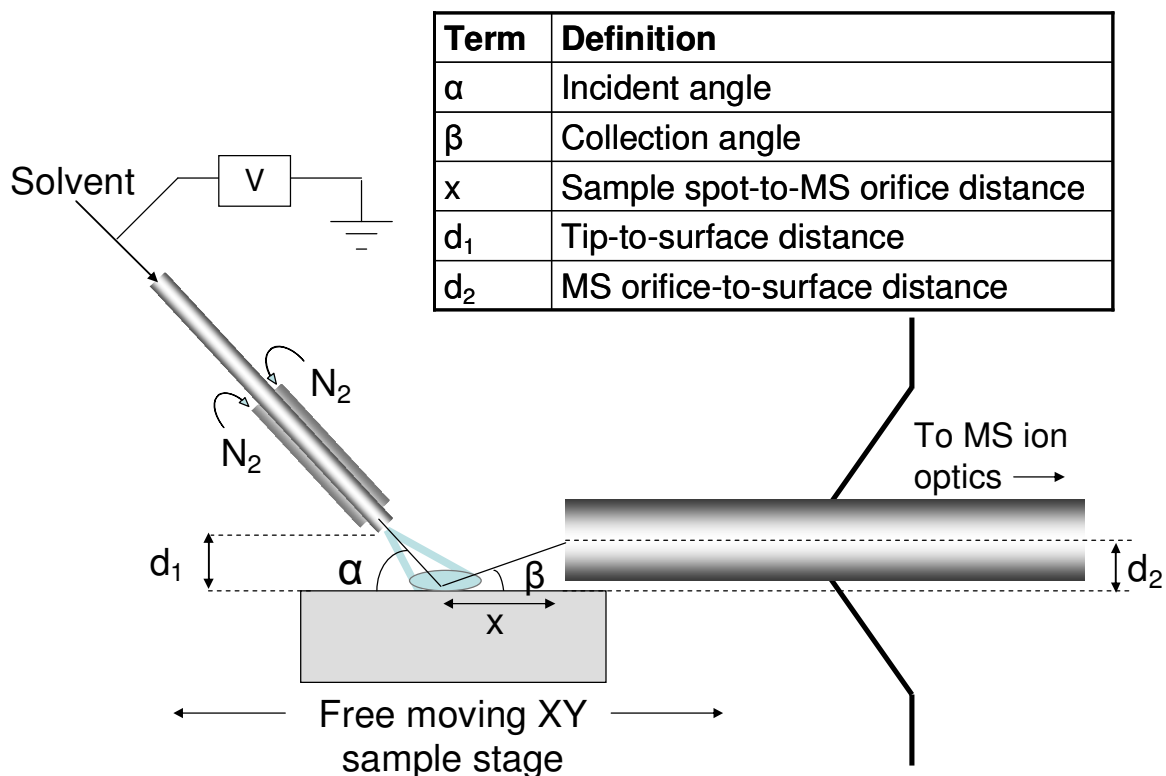


Figure 1.1. Schematic of a typical DESI MS set-up showing various experimental set-up variables.

The most critical variables in DESI are the tip-to-surface distance (d_1), the incident angle (α), the spray solvent composition and the gas flow rate. For analytes present in a compact solid matrix, sensitivity also depends on sample hardness. For dried analytes spots deposited onto hard surfaces, sensitivity also depends on the choice of surface material, which determines the degree of analyte-to-surface interactions and the crystal size. For the same material, sensitivity and signal stability are a function of the surface roughness, with rough surfaces showing better sensitivity than smooth surfaces. The DESI emitter is typically positioned 1–3 mm above the surface to be analyzed, and at an angle of 45–60 degrees relative to it. The spray-to-capillary distance is typically in the 2–3 mm range. The mass spectrometer inlet capillary is usually positioned in close

proximity of the surface (~1 mm), however, Kertesz and coworkers have shown that up to a 5-fold sensitivity improvement can be obtained by positioning the bottom of the sampling capillary beneath the surface plane in what they termed “edge sampling”.⁹² Other DESI MS configurations have also been reported including geometry independent DESI,⁹³ which eliminates sample to sample parameter adjustments, and transmission mode DESI,^{94, 95} implemented for analyzing samples spotted on a mesh.

In DESI, the continuous liquid jet directed onto the sample surface results in a thin solvent film where surface molecules are dynamically extracted. The solvent flow from the spray continuously dislodges the surface film resulting in the generation of analyte-containing secondary droplets, sampled downstream by the mass spectrometer inlet capillary. Ionization occurs following ESI mechanisms.^{24, 96} Further evidence of the similarity of ESI and DESI ionization mechanisms was provided by recent internal energy deposition studies with thermometer molecules.⁹⁷ Several mechanisms were initially proposed for DESI, including droplet pick-up, momentum transfer, and chemical sputtering.^{1, 98} However, recent investigations utilizing Doppler particle sizing analysis provided new insight, supporting the droplet pick-up or ‘splashing’ mechanism, and dismissing momentum transfer effects.⁹⁹ Computational fluid dynamics simulations have also confirmed the prevalence of this mechanism.^{100, 101}

DESI has been implemented in combination with various types of mass spectrometers including linear (LiT), quadrupole (QiT) ion traps,^{1, 102} triple quadrupoles (QqQ),¹⁰³ orbitraps,¹⁰⁴ quadrupole time-of-flights (Q-TOFs),¹⁰⁵ Fourier transform ion cyclotron resonance (FT-ICR),¹⁰⁶ QqQ/LiT,^{107, 108} miniature handheld rectilinear ion traps (RIT),¹⁰⁹ ion mobility spectrometry (IMS)/TOFs,¹¹⁰ and ion mobility/QTOF¹¹¹⁻¹¹³ hybrid

instruments. The numerous literature reports on DESI MS demonstrate its potential as a powerful tool for a wide range of surface-sampling applications including detection of non-volatile pyrolysis products,¹¹⁴ polymers,¹¹⁵ inks,¹¹⁶ various organic compounds,¹¹⁷⁻¹¹⁹ carbohydrates,^{120, 121} peptides,¹¹² semi-volatile organic compounds,¹²² chemical warfare agents,^{122, 123} intact bacteria,¹²⁴⁻¹²⁶ proteins,¹²⁷ tissues,¹²⁸⁻¹³⁰ aerosols,¹³¹ lipids,¹³² amino acids,¹³³ metabolites,^{51, 134-136} pharmaceuticals,^{105, 107, 137-140} drugs of abuse,¹³⁴ explosives,¹⁴¹⁻¹⁴³ agrochemicals,^{142, 144} genuine and counterfeit drugs.^{102, 145-150} Particularly appealing are those experiments taking advantage of the 'reactive' and imaging capabilities of DESI as outlined below.

In reactive DESI MS the spray solvent is doped with an additive, enabling heterogeneous chemical reactions between the reagents in the charged micro-droplets and condensed phase analytes exposed on the sample surface. These reactions are believed to take place in the thin solvent film present on the sample surface or in the secondary droplets as they are transported through the atmospheric sampling capillary of the mass spectrometer. Reactive DESI MS methods enjoy the same high throughput capabilities of conventional DESI, with the added benefits of increased selectivity and/or sensitivity^{102, 136, 146, 147, 151-154}. The high sensitivity afforded by reactive DESI has also been exploited for chemical imaging applications.¹⁵⁵ Recently, direct quantitation by reactive DESI of active ingredients in pharmaceutical formulations, in the presence of an isotopically labeled internal standard has been shown. This approach showed a 6 % precision and 94 % accuracy.¹⁴⁸ Porous tetrafluoroethylene (PTFE) substrates, which show good signal stability, have also been used to demonstrate the quantitative capability of DESI MS for

the analysis of various analytes spotted together with an internal standard, showing good inter-day precision (13 % RSD) and accuracy (± 7 % relative error).^{156, 157}

Chemical imaging with DESI MS is emerging as a powerful tool for determining the two dimensional distribution of various chemical species. It has already been employed in applications such as profiling phospholipids in tissue sections,¹⁵⁸⁻¹⁶² the forensic examination of ink on paper,^{90, 116, 163} investigation of analyte bands on thin-layer chromatography plates,¹⁶⁴ analysis of propranolol in whole mice body sections,¹⁶⁵ active ingredient in pharmaceutical tablets,¹⁴⁵ bromophycolides on alga tissue etc.¹⁶⁶ In DESI imaging the sprayer is kept in a fixed position and a specimen is mounted on an automated sample stage that is programmed to move in a predetermined raster pattern, allowing the DESI spray to probe specific points of the sample surface. Fundamental investigation of the surface scanning and alignment conditions conducted by Van Berkel and colleagues have shown that fixing the DESI source positioning and distances relative to the sample is critical, and that chemical image resolution is enhanced by utilizing unidirectional scanning instead of raster scanning.^{90, 91} The lateral resolution for routine applications is estimated to be less than 500 μm , however for samples with a uniform texture and appropriately strong analyte-to-surface interaction, lateral resolutions approaching 40 μm are achievable by exerting very careful control of operational parameter such as the spray tip-to-surface distance, solvent flow rate and spacing of lane scans.¹⁶⁷

Very similar to DESI is a technique termed desorption sonic spray ionization (DeSSI),⁴⁰ also referred to as EASI,^{41, 42, 168-170} the only difference in terms of implementation being that no voltage is applied to the spray solution, which leads to

inferior sensitivity. It is believed that droplet charging in DeSSI occurs as a result of statistical fluctuations of the charge spatial distributions within the sprayed droplets such as in the SSI mechanism.^{32, 33, 171, 172} The capabilities of DeSSI have been showcased in various applications including the analysis of TLC plates,⁴¹ biodiesel,¹⁶⁸ perfumes,¹⁶⁹ fabric softeners,¹⁷⁰ and has been coupled to membrane introduction MS for the analysis of drug molecules.⁴²

In PESI, a solid needle is used to probe the surface of a wet sample resulting in the pick-up of a small amount of biological fluid (0.35 ± 0.09 pl) by adhesion to the needle tip.⁴⁵ The needle is then actuated to the sampling inlet of the mass spectrometer where an electrospray is initiated by turning on the potential on the needle probe. In the case where the biological fluid dries out before the needle gets to the MS inlet, the sample can be re-dissolved (prior to electrospray initiation) by solvent vapors generated from an auxiliary heated solvent sprayer. PESI has been used in the analysis of biological samples such as mouse brain, urine, mouse liver, salmon eggs, and fruits⁴⁴ and in the ambient molecular imaging of rat brain tissues with 60 μm lateral resolution.¹⁷³

1.4.2. Ambient Gas-, Heat-, Laser-, or Radiofrequency-based Desorption/Electrospray-assisted Ionization Techniques: FD-ESI, EESI, nanoEESI, ND-EESI, UA-EESI, RADIO, ELDI, MALDESI, LAESI, IR-LADESI and LIAD/ESI

These techniques decouple the processes involving analyte desorption and/or transport from the subsequent electrospray-assisted ionization event for the generation of gas phase ions. FD-ESI^{46, 174} introduced by Shiea and coworkers, and essentially the same as EESI⁴⁹, introduced by Cooks et al. have both been shown to be very useful for the

analysis of solution phase analytes in the presence of relatively high salt contents. In these techniques, an analyte solution is nebulized into a fine aerosol and directed towards highly charged micro-droplets emanating from an ESI emitter. This gives progeny analyte-containing droplets following fusion, with subsequent ionization by electrospray processes. Both techniques rely on liquid-liquid extraction for the uptake of analytes into progeny droplets resulting in selectivity being largely dependent on the relative solubility of sample components in the electrospray solvent. Using methanol as ESI solvent, Shiea and coworker were able to obtain good quality spectra of various peptides and protein including cytochrome C in solutions containing up to 10 % w/w NaCl.⁴⁶ The high salt tolerance of the technique has also been showcased in the direct analysis of undiluted urine, milk, serum and polluted waters without sample clean-up by Cooks and coworkers.⁴⁹ Chen and coworkers introduced a variant of EESI termed nanoEESI where a conventional nanoESI emitter is used for the generations of charged solvent droplets, which are then fused with an analyte-containing aerosol.⁵² Zenobi and coworkers have also described a clever variant of EESI, which they termed ND-EESI.^{54, 175} In ND-EESI, analytes are desorbed or aerosolized from a sample using a gentle stream of nitrogen or air to give an analyte-containing gas stream, which is then merged with the normal desolvation gas stream of a pneumatically assisted ESI emitter. Coupling ND-EESI to a hybrid Q-TOF mass spectrometer allowed rapid metabolic fingerprinting of a wide variety of biological samples with detection limits as low as 10 femtograms/cm².⁵³ Other applications of ND-EESI include the rapid analysis of fruits for maturation⁴⁷ manipulation of the charge state of biopolymers,⁴⁸ in-vivo fingerprinting of nonvolatile compounds in breath,⁵⁰ sampling on living tissues including human skin, plant tissues,⁵³

analysis of perfumes,¹⁷⁶⁻¹⁷⁸ and coupling to a hybrid Q/IMS/TOF instrument for the rapid analysis of drugs.⁵⁵

UA-EESI and RADIO use ultrasonic volatilization for decoupling analyte desorption from subsequent electrospray-assisted ionization. In UA-EESI a small sample droplet (~3 μL) is deposited on an ultrasonic transducer and nebulized into an aerosol. In RADIO, an analyte solution (1 μL) is deposited onto a quartz crystal microbalance (QCM) and immediately aerosolized by radiofrequency actuation. The sample aerosol generated is entrained by charged droplets from an ESI emitter resulting in the extraction and ionization of sample constituents. UA-EESI has been coupled to a hybrid QTOF mass spectrometer and has been successfully applied to the detection of melamine in various food matrices including raw milk, wheat gluten, and milk powder.⁵⁶ RADIO has been coupled to a hybrid LiT/FTICR mass spectrometer for the analysis of some model peptides, including melittin and ubiquitin.⁵⁷

A few different laser-based techniques have been reported. These decouple surface sampling by laser desorption/ablation from the subsequent electrospray-assisted ionization for the generation of ions from various samples in the open air including ELDI, LAESI, MALDESI, and IRLADESI. In ELDI, first reported by Shiea and coworkers,⁶² a 337 nm N_2 laser operating at 20 μJ per shot is used to ablate samples placed underneath an electrospray plume. The ablated material is then captured by the charged micro-droplets with subsequent ionization by ESI processes, leading to the observation of multiply charged species such as peptides and proteins. ELDI has been employed for the characterization of various chemicals on the surface of different solids including paintings, compact discs, drug tablets, tissue samples,^{60, 62} identification of

organic compounds separated on TLC plates,⁶¹ characterization of the polar components of crude oil, analysis of amber and humic substances,⁵⁹ continuously monitoring the state of ongoing chemical reactions,⁵⁸ detection of intact multiply-charged proteins (up to 66 kDa) and tryptic digests.^{62, 63, 179} In-situ chemical reactions between reagents that are incorporated into the electrospray solvent and laser ablated analyte species have also been implemented within this technique and referred to as reactive ELDI.¹⁸⁰

MALDESI is a hybrid ionization technique very similar to ELDI (both use UV lasers) with the only difference being the use of an organic acid matrix in the former, which affords increased sensitivity and is believed to extend the limit of detection and molecular weight range of ELDI.^{64, 66} Analysis of peptides and proteins by MALDESI results in the generation of multiply charged species suggesting ESI to be the predominant mechanism for ion generation.^{64, 65} An infrared laser has also been used for MALDESI for the direct top-down characterization of carbohydrates, proteins and lipids.¹⁸¹ A variant of this technique referred to as liquid MALDESI (Liq-MALDESI) has also been reported where ions are generated by laser ablation of a liquid sample that is deposited onto a stainless steel target and biased up to 3 kV. In this case multiply charged ions of peptides and proteins are generated from the liquid sample directly without any secondary ionization.⁶⁷ The liquid sample is reported to act as a macroscopic charged droplet similar to those generated by electrospray ionization, resulting in the generation of multiply charged ions.

LAESI and IR-LADESI employ electrospray-like ionization of entrapped material ablated and/or desorbed from a surface by an IR laser source. The penetration of the IR lasers used in these techniques is several orders of magnitude larger than the UV lasers

used in ELDI or MALDESI, resulting in the removal of larger amounts of material from the sample surface. Nemes and Vertes developed LAESI by sampling the ablation plume formed by an Er:YAG laser with the spray from an ESI emitter.⁶⁹ The implementation of the laser source at a 90° angle respect to the sample surface is believed to preferentially contribute to sample ablation.⁶⁹ Femtomolar-level detection limits for proteins, lipids, and metabolites were attained.⁶⁹ LAESI has been used for two dimensional imaging and depth profiling applications^{68, 70} and is the only ambient MS techniques with demonstrated capabilities for 3D chemical imaging.¹⁸² The Murray group developed a similar technique termed IR-LADESI for the direct analysis of biological fluids and pharmaceuticals.⁷¹ In this case, the laser was positioned at 45° with respect to the sample surface, and lower pulse energies were used, resulting in both ablation and desorption of surface neutrals.⁷¹ The mechanisms of both LAESI and IR-LADESI are probably similar, where the material ablated from the surface interacts with ESI droplets, in a dynamic solid–liquid extraction-like process. It has been postulated that in IR-LADESI, small, more volatile materials are directly desorbed as free molecules, and incorporated directly into ESI droplets.

In LIAD/ESI, a sample solution deposited on a metal foil is irradiated in transmission mode with a Nd:YAG IR laser that creates acoustic waves, which propagate through the foil, enabling thermally-assisted sample desorption. The analytes then interact with the charged droplets from an ESI emitter to give single and multiply charged ions following ESI processes. LIAD/ESI has been used for the analysis of small organic and large biological compounds including amino acids, peptides, and proteins.⁷²

1.4.3. Electric Discharge-, Beta Electron-, or Photon-based Ambient Chemical Ionization Techniques: DART, DAPCI, LD-APCI, DBDI, LTP, PADI, FAPA, BADCI, APTDI, DAPPI

This group of techniques takes advantage of ion-molecule reactions to effect ionization of desorbed analyte from various samples. DART is a commercial ambient ionization technique that was introduced by Cody et al in 2005.^{39, 183} In DART, a glow discharge sustained by the continuous flow of He gas results in the generation of electronically excited (metastable) He atoms (2^3S_1 , 19.82 eV) with lifetimes of up to 8000 s.¹⁸⁴ The gas stream carrying these metastables is heated (to facilitate thermal desorption of analytes) before exiting the ionization source where Penning ionization occurs to eventually generate protonated water clusters. In positive ion mode, the protonated water clusters serve as proton transfer reagents for chemical ionization of analytes desorbed from samples placed directly within the ionization region. Under appropriate conditions, oxygen radical ($O_2^{+\bullet}$) and nitric oxide (NO^+) cations can also be generated by Penning ionization both of which are dependent on the source-to-mass spectrometer distance, the grid potential and/or addition of various charge exchange reagent in the sampling region. These modify the chemistry of the reactive ionization region resulting in analyte ionization by charge exchange, hydride abstraction, or/and oxidation reactions.^{39, 183, 185} In negative ionization mode ionization occurs predominantly by electron capture (EC), dissociative EC, proton transfer, and anion attachment.^{38, 186} Ion transmission efficiency within the DART ionization region has been shown to dependent on complex coupled fluid dynamic, heat transfer and electrostatic phenomena, which are determined by sample placement considerations.¹⁸⁷ Ion transmission has also been shown

to improve by about two orders of magnitude when the DART ion source is coupled to the mass spectrometer through a commercial VAPUR® interface, which acts as an gas/ion separator.¹⁸⁸ Because of its commercial nature, DART has enjoyed a significant amount of popularity and its potential has been demonstrated for several applications including the analysis of whole bacterial cells,¹⁸⁹ planar chromatography plates,¹⁹⁰ flavors and fragrances,^{191, 192} reaction product monitoring,¹⁹³ self-assembled monolayers,¹⁸⁵ contaminated pet food,¹⁹⁴ drinking water,¹⁹⁵ writing ink,¹⁹⁶ in-vivo hydrocarbon analysis,¹⁹⁷ counterfeit drugs,^{145, 150, 198-200} authentication of olive oils,²⁰¹ urine samples for drugs of abuse²⁰² and for quantitative analysis of drugs in biological matrices.¹⁸⁸ Very similar to DART is the technique referred to as FAPA,^{82, 83} introduced by Hieftje and coworkers. The major difference reported between DART and FAPA is the fact that DART operates within a corona-to-glow transition (C-G) discharge regime, whereas FAPA operates via a glow-to-arc transition (G-A) discharge.²⁰³ Some applications of FAPA include the direct detection of volatile organic compounds,⁸² tea leaves, coffee beans, pharmaceutical tablets⁸³ and for elemental analysis.²⁰⁴ Laser ablation had also been used to decouple analyte desorption from FAPA ionization for the ambient chemical imaging of pharmaceutical tablets.²⁰⁵

DAPCI, originally introduced by Cooks and coworkers in 2005, uses toluene as the reagent gas in a modified DESI sprayer where the spray capillary is replaced with a sharp stainless steel needle to generate a corona discharge.²⁰⁶ DAPCI has been observed to show superior performance for ionizing compounds of moderate to low polarity than DESI¹³⁹, and is preferred in cases where the sample surfaces may be damaged by the application of DESI solvent spray.⁷⁴ In DAPCI, the plasma generated by the electrical

discharge interacts directly with the sample enabling direct surface sampling/ionization by APCI processes, unlike in DART, which employs a non-contact plasma physically separated from the ionization region. DAPCI has also been implemented without the use of carrier gases. Instead, ambient air, with about 60 % relative humidity, was used as a reagent to generate primary ions.^{207, 208} Applications of DAPCI include the trace detection of pharmaceuticals, molecular markers of meat spoilage, impurities, explosives, herbicides, chemical warfare agent simulants, illicit drugs, peptides and tea products.^{73, 74, 139, 207, 208} Doping the carrier gas with chemical reagents such as ammonia can also enable gas phase ion/molecule reactions improving the sensitivity of the technique.⁷³

In an earlier technique referred to as LD-APCI, laser desorption has been coupled to APCI using a corona discharge in ambient air. LD-APCI was initially implemented to probe the gas-phase neutral molecule population generated by the AP-MALDI. The source utilizes a laser pulse to desorb molecules from a stainless steel target followed by chemical ionization via reagent ions produced by a corona discharge. The technique has been shown to provide up to three orders of magnitude improvement in the AP-MALDI signal.^{75, 209} LD-APCI has been used for various applications including the analysis of compounds separated by TLC,²¹⁰ peptides from aqueous solution,⁷⁵ and proteins separated on polyacrylamide gels.^{76, 77}

DBDI, LTP and PADI are electric discharge-based ionization techniques which differ from DAPCI, DART and FAPA in that they use an alternating voltage to drive the electrical discharge. In DBDI a low temperature, dielectric barrier discharge is created between a hollow stainless steel needle (discharge electrode) and a dielectric barrier material (glass). The AC voltage that initiates the discharge is applied between the

discharge electrode and a copper sheath electrode holding the dielectric barrier material. In DBDI, the dielectric barrier material also serves as the sample plate. The discharge is sustained by the flow of He gas through the hollow discharge electrode to generate metastable helium atoms and fast electrons, which serve to induce desorption and ionization of analytes. DBDI has been used for the analysis of amino acids⁷⁹ and explosives.⁷⁸ LTP is very similar to DBDI, the only difference being that in LTP the dielectric barrier discharge is created between a grounded stainless steel electrode and a glass tube surrounding it. The discharge gas (He, Ar, N₂ or air) flows through a small gap between these two electrodes. The counter electrode consists of a copper tape surrounding the outside of the glass tube. This design allows the low temperature plasma to be projected away from the probe, enabling the direct analysis of a broader range of sample types than DBDI. LTP has been used for the analysis of explosives on PTFE substrates, cocaine on human skin, active ingredients in pharmaceutical tablets, toxic and therapeutic compounds in complex biological samples,⁸⁰ and recently for the detection and quantitation of melamine in milk.²¹¹ PADI employs a radiofrequency driven non-thermal atmospheric glow discharge in helium, to probe the surface of various samples.⁸¹ The plasma normally extends up to 10 mm away from the probe tip and can be brought into direct contact with the sample to effect desorption/ionization of various surface chemicals. PADI has been used for applications in the analysis of pharmaceuticals tablets, tobacco and garlic.⁸¹

BADCI is a technique recently introduced by Fernández and coworkers where thermally assisted analyte desorption is followed by chemical ionization under atmospheric pressure. The unique feature in BADCI is that the reactions leading to the

formation of CI reagent ions are initiated by beta electrons emitted from a low activity (~10 μCi) ^{63}Ni probe eliminating the need for high voltages within the ionization region. BADCI has been used for the direct analysis of pharmaceutical tablets.⁸⁴

Direct thermal ionization of condensed phase species in the ambient environment was first reported by Cooks and coworkers in a technique referred to as APTDI. This technique has been shown to be very useful for the analysis of inorganic and organic salts including ionic liquids.⁸⁵ In APTDI, a sample is placed in a tube and heated, resulting in the breakdown of the strong ionic interactions, followed by sublimation of one or both of its counter ions. The flow of N_2 carrier gas through the tube helps to transfer the sublimated counter ions to the mass spectrometer for detection. Doping the carrier with various protic solvents such as methanol has been shown to enable chemical ionization of vaporized neutrals by gas phase protonation.⁸⁵

In DAPPI a heated nebulizer microchip is used to deliver a hot jet of vaporized solvent (e.g toluene) to facilitate the thermally-assisted desorption of analytes from various surfaces. A krypton discharge UV lamp emitting 10 eV photons and positioned ~10 mm above the sample spot then effects the ionization of vaporized neutrals following similar mechanisms such as in APPI.⁸⁶⁻⁸⁹ One of the major advantages of DAPPI is its superior performance for the analysis of low polarity compounds compared to DESI.⁸⁶ Together with applications in the analysis of low polarity compounds,⁸⁶ DAPPI has also been employed in the analysis of illicit drugs.^{88, 89}

1.5. Conclusions

The introduction of ambient MS methods has triggered a renewed interest in the field of analytical mass spectrometry due to the removal of some of the bottlenecks present in AP ionization techniques. Ambient mass spectrometry preserves spatial chemical information, avoids dilution and maximizes sensitivity. The breadth of this new field is reflected by the explosive appearance of a multitude of new ionization approaches, which continue to provide unprecedented capabilities such as rapid quantitative screening, high throughput imaging, and direct in vivo analysis.

CHAPTER 2. CONSTRUCTION OF A PROTOTYPE DESI MS ION SOURCE FOR THE RAPID DETERMINATION OF COUNTERFEIT ANTIMALARIAL TABLETS

2.1. Abstract

This chapter presents the implementation of DESI MS for the rapid characterization of counterfeit artesunate antimalarial tablets. Proof-of-concept results on coupling a custom-built DESI ion source interfaced to a linear ion trap (LiT) mass spectrometer for the routine characterization of counterfeit artesunate tablets collected in South East Asia are presented. The results are complemented and validated using attenuated total reflectance Fourier transform infrared (ATR-FTIR) spectroscopic imaging analysis enabling the facile typing of samples based on their chemical fingerprints.

2.2. Introduction

Malaria is a life threatening parasitic disease transmitted by *Anopheles* mosquitoes. It is a risk for some 40 % of the world's population, and claims over one million lives each year.^{212, 213} To date, there are no effective vaccines to prevent malaria in humans and, as such, prevention and treatment has depended on potent antimalarial drugs including chloroquine, sulfadoxine-pyrimethamine etc. Unfortunately, in many areas all of these have become ineffective, due to development of drug resistance.²¹⁴ The current increase in drug resistance to malaria treatments not only threatens the life of any individual who travels to malaria-endemic areas, but also damages the economies of

tropical countries, which are a major market for goods and services.²¹⁵ The most effective treatment therapies, especially for the multidrug resistant *Plasmodium falciparum* malaria parasite strain, are based on semi-synthetic artemisinin derivatives (depicted in Figure 2.1); the most common one being artesunic acid (artesunate). Artemisinin is a sesquiterpene lactone isolated from the Chinese herbal plant *Artemisia annua*, which is then converted into various semi-synthetic derivatives to improve solubility and

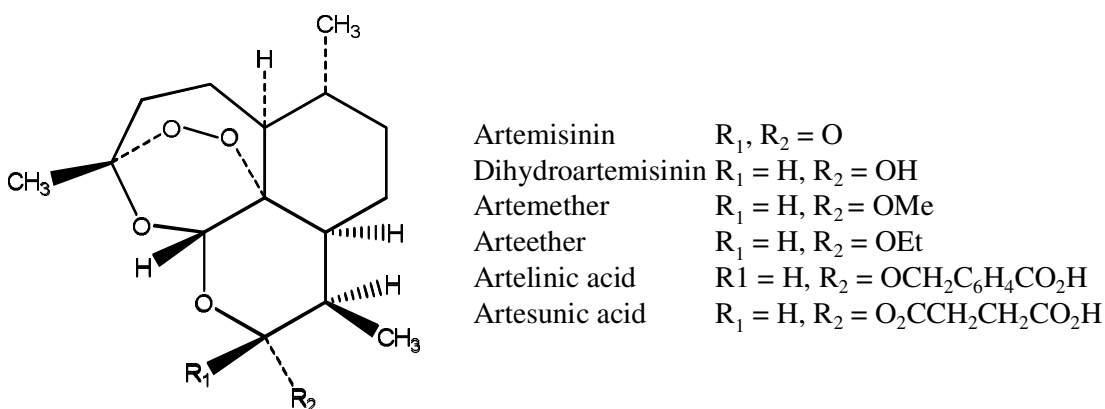


Figure 2.1. Structure of artemisinin and its derivatives.

bioavailability. Artemisinins contain an endoperoxide linkage in their structure believed to be responsible for their antiparasitic activity by causing free radical damage to the parasitic membrane systems.²¹⁶ With malaria being one of the principal health problems in developing countries, and antimalarial drugs representing a large sector of the pharmaceutical market, these drugs have been increasingly targeted by counterfeiters.

Counterfeit drugs are pharmaceutical products, which are deliberately and fraudulently mislabeled with respect to their identity and/or source. This includes products, which contain wrong active pharmaceutical ingredient(s) (APIs), insufficient

quantities of the API(s), no API(s), and/or false packaging. Basically, a counterfeit drug is produced with the intent of deceiving the customer and should be differentiated from a substandard drug, which is simply a drug produced by the genuine manufacturer, but that does not meet the quality standards set for it. Counterfeit antimalarials have been particularly detected in SE Asia and Africa, as malaria is one of the principal health problems in those areas.^{198, 200, 217-220} Since 1998 an “epidemic” of multiple types of counterfeit artesunate tablets has occurred in mainland SE Asia. Ad hoc surveys conducted since 2000 in Myanmar, Lao People’s Democratic Republic (Lao PDR, Laos), Cambodia, Vietnam, and along the Thai-Myanmar border suggested that 33-53% of bought artesunate was counterfeit, containing either no or subtherapeutic quantities of artesunate.^{200, 217, 218, 220-223} In SE and East Asia there are at least 16 manufacturers of artemisinin and its derivatives and millions of tablets are produced each year both for consumption in Asia and export to Africa. Of these manufacturers, one major producer of artesunate, Guilin Pharmaceutical Co. Ltd. (Guilin, Guangxi autonomous region, China), has been particularly targeted by counterfeiters resulting in 16 different types of fakes so far.²⁰⁰

The consumption of fake antimalarial medicines is believed to have resulted in more deaths than have been documented^{220, 224} as various evidence suggests that the production of counterfeit antimalarials is on an industrial scale.²⁰⁰ One example is a case where one health care organization in SE Asia purchased 100,000 artesunate tablets, all of which were later shown to be counterfeit.²¹⁸ In another related example, an alliance between Belgian and Chinese authorities resulted in the interception of 57,000 packs of counterfeit halofantrine capsules (another antimalarial) en route from China to Nigeria.²²⁵

Conventional antimalarial tablet analysis is generally carried out via liquid chromatography with optical or mass spectrometric detection.^{222, 226, 227} Although these methods offer comprehensive information on sample composition, they suffer from throughputs of a few samples per hour. Since artesunate tablets are manufactured in the millions in Asia and Europe, exploring new approaches for antimalarial tablet screening is central to rapidly ensuring the quality of the genuine product and for the early detection of fakes.

In this study, a prototype DESI ion source was constructed and tested for the routine rapid chemical fingerprinting of various types of counterfeit artesunate antimalarial tablets. The DESI MS results were complemented and validated using attenuated total reflectance Fourier transform infrared (ATR-FTIR) spectroscopic imaging. FTIR spectroscopic imaging has been shown to be a versatile tool in pharmaceutical analysis with a broad range of applications, ranging from the characterization of drug formulations to the elucidation of kinetic processes in drug delivery.^{149, 228-235} ATR-FTIR is also advantageous for the analysis of pharmaceutical tablets because the analysis is non-destructive, therefore requiring no sample preparation.

In FT-IR imaging, infrared spectra are acquired at different areas on a sample in a grid pattern, and the variation of the intensity of a specific absorption band that represents a particular component can be plotted as a map to obtain an image that corresponds to the 2 dimensional distribution of that component in the sample. Conventionally, this is achieved by performing a point-by-point mapping with an aperture and a computer-controlled motorized stage, making it a very time-consuming process. With the introduction of the focal plane array (FPA) detector, images based on the distribution of

IR absorption bands can be collected within a matter of a few minutes or even seconds with up to 4 μm lateral resolution.²³⁰

In this study, the combined potential of DESI MS and ATR-FTIR as orthogonal and complementary tools for rapidly screening and characterizing counterfeit antimalarial tablets is evaluated.

2.3. Experimental Details

2.3.1. Sample Collection

Sample collection for the present study and for the routine chemical characterization of artesunate samples by DESI MS in various studies was coordinated by Dr. Paul N. Newton. Since 1998, sixteen different types of fake artesunate samples have been cataloged as shown in the next section. Counterfeit and genuine artesunate tablets were collected in a wide area of SE Asia encompassing Laos, Myanmar, Vietnam, Cambodia, and along the Thai-Myanmar border. Figure 2.2 shows a map of the distribution of fake artesunate in relation to the fake packaging type. As a proof-of-concept, a total of six samples constituting six different packaging types were evaluated in this study. These included a genuine sample and five counterfeit samples with the following collection codes: 11 KHA P 7/1 #2 (Type 4), 12 PAS P 64/1 (Type 8), S 12/2005 (Type 9), Lao 05/03 (Type 11) and S 40-1 (Type 13).



Figure 2.2. Map of the distribution of fake artesunate as of 2008, compiled by the Wellcome Trust-University of Oxford SE Asian Tropical Medicine Research Program and collaborators. Map taken from Newton, et al.²⁰⁰

2.3.2. Analysis of Physical Appearance and Tablet Packaging

The manufacturer of the most commonly counterfeited artesunate antimalarials; Guilin Pharmaceutical Co. Ltd. first developed a hologram as a security measure in response to the first type ('Type 1') of counterfeit artesunate circulated, which had no hologram attached. As a result, any 'Guilin Pharmaceutical Co. Ltd' artesunate

circulating without a blister pack hologram is almost certainly counterfeit or expired. Thereafter, a total of sixteen different hologram types, which mimic the genuine packaging used by Guilin (Figure 2.3.a) have been found in Southeast Asia with counterfeit stickers or holograms, and there are probably more types circulating.

The physical appearance, text on packets, leaflet inserts and blisterpacks were examined by Paul Laurin of the Royal Canadian Mounted Police Forensic Laboratory Services, National Anti-Counterfeiting Bureau in Ottawa, Ontario, Canada.

For these analyses, tablets are compared with known genuine Guilin Pharmaceutical Co. Ltd artesunate obtained directly from the company. Packets, leaflets and blisterpacks are examined with an x6 hand lens, x100 stereo microscope and a handheld UV (375nm) light source and then electronically scanned. Batch numbers, expiration and manufacture dates, the color, clarity and text of printing on the blisterpack, packet and leaflet (when present) are documented. Guilin Pharmaceuticals Co. Ltd. then provides information about the validity of batch numbers.

Figure 2.3 shows blister pack holograms for the samples analyzed in this study with the counterfeit holograms showing a range in sophistication with the most common feature being the misalignment of the blocks forming the circular border of the Guilin logo. The different counterfeit holograms show various specific features including: Type 4, which is a good hologram copy but lacks microscopic 'Guilin Pharma' legend and has 'Tablet' printed on blisterpack (Figure 2.3.b), Type 8, which has a poor sticker with shoulder plateau on mountain with abbreviations of 'MFG', 'EXP' in capital letters (Figure 2.3.c), Type 9, which is a good hologram with 'Guilin Pharma' legend in correct font (Figure 2.3.d), Type 11, which has a sticker similar to Types 8 but mountain outline

differs and also has abbreviations of ‘MFG’, ‘EXP’ in capital letters (Figure 2.3.e) and Type 13, which has a hologram, with similar mountain outline to Types 4 but with different pictograms and outer circle with no ‘Guilin Pharma’ legend (Figure 2.3.f). For a full description of all fake packaging identified, see Figure S-1 from Newton, et al.²⁰⁰

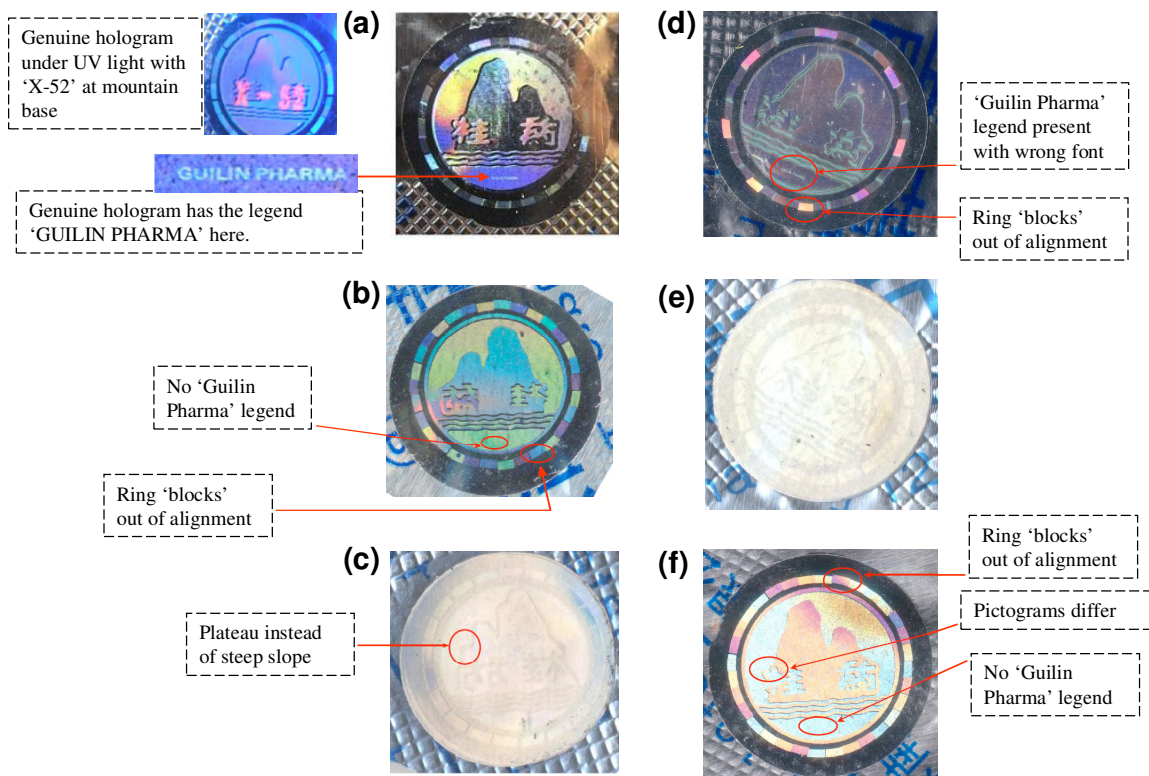


Figure 2.3. Hologram type of samples evaluated in this study, (a) genuine Guilin Pharmaceutical artesunate blister pack hologram, (b) Type 4, (c) Type 8, (d) Type 9, (e) Type 11, (f) Type 13.²³⁶

2.3.3. DESI Ion Source

The custom-built DESI ion source consisted of a movable sample stage and a high performance sprayer based on the oscillating capillary nebulizer (OCN) concept (Figure 2.4). The OCN produces primary droplets with a small mean diameter and narrow size distribution compared to conventional pneumatic nebulizers, thus potentially

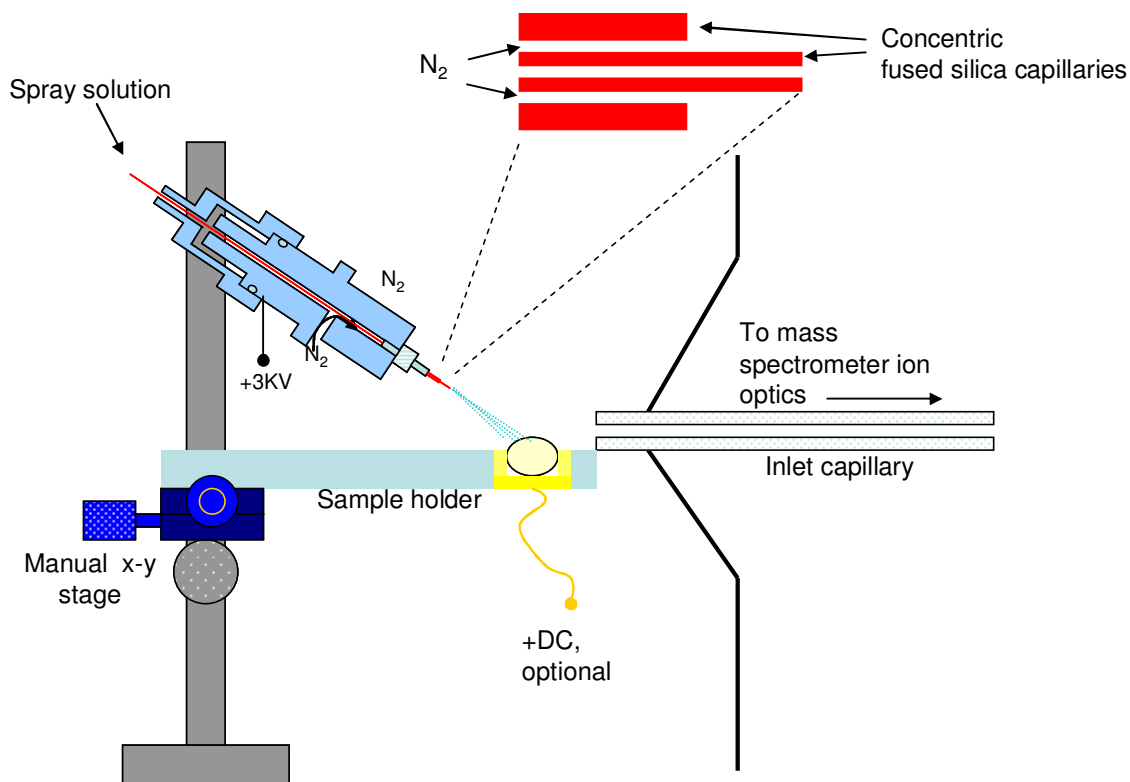


Figure 2.4. Schematic of a custom-built DESI ion source coupled to a commercial linear ion trap (LiT) mass spectrometer.

maximizing surface desorption/ionization.²³⁷

The spray emitter consisted of a 18.2 cm long inner spray capillary (147 μm o.d., 50 μm i.d.) surrounded by an outer nebulizer gas capillary (358 μm o.d., 250 μm i.d.), both made from polyimide-coated, fused silica tubing (Polymicro Technologies, Phoenix AZ). The inner capillary was offset from the outer capillary by 0.2 mm, which gave the most stable spray conditions. This distance can be manually adjusted by screwing the two pieces that conform the sprayer body, thus changing their position with respect to each other. The inner capillary is fixed to the proximal piece of the sprayer, and the outer capillary is fixed to the distal piece. Samples are held in a cylindrical brass hollow tablet holder (9.3 mm i.d., 3.5 cm deep), which is mounted at the distal end of a 10.2 cm-long

laminated carbon fiber piece, which is affixed to a manual x-y translational stage. The sprayer tip, from where charged microdroplets are emitted, is positioned at 5-6 mm from the mass spectrometer capillary inlet, and 1-2 mm away from the surface of the mounted tablet, at an angle of 55°. The collection angle was approximately 0°. The sample holder is mounted on a system of rods and clamps affixed to the bench where the mass spectrometer is placed. The nebulizer gas consists of nitrogen. The spray solution is normally biased via an external high voltage power supply (SRS PS350, Sunnyvale CA), which is placed in electrical contact with the spray solution through one of the ports of a T union. The DESI spray mixture is usually delivered to a second port of this T union by a 500 µL glass syringe (Hamilton Company, Reno, NV). The third port of the T union is connected to the DESI sprayer by a short piece of 127 µm i.d. PTFE tubing.

2.3.4. DESI MS

All reagents were used as purchased, without additional purification. HPLC grade acetonitrile (Fisher, Hampton NH), dodecylamine (DDA) (Sigma-Aldrich, St. Louis MO) was used for “reactive” DESI (See details in Chapter 3) experiments. Ultrapure water (18.2 MΩ cm⁻¹) was obtained from a Nanopore purification unit (Barnstead, San Jose CA).

DESI MS experiments were performed by coupling the DESI ion source to an LTQ linear ion trap mass spectrometer (Thermo Finnigan, San Jose, CA). Dr. Charlene Bayer and Dr. Victor de Jesus in the Georgia Tech Research Institute provided access and training on the use of this instrument. “Reagentless” DESI MS was performed by spraying samples using a solution of 75:25 CH₃CN:H₂O unless stated otherwise, at a flow

rate of $5 \mu\text{L min}^{-1}$. The spray was pneumatically assisted by a coaxial spray of N_2 gas at a flow rate of 0.3 L min^{-1} . The spray solution was electrically charged to $\pm 3 \text{ kV}$, depending on the ionization mode used. For all experiments, the mass spectrometer was auto-tuned for optimum detection of analytes of interest. Data was acquired *via* the Xcalibur software interface set to collect spectra in automatic gain mode for a maximum ion trap injection time of 200 ms, and 2 micro-scans per spectrum. The capillary temperature was set to 300°C . Tablets were mounted on an x-y stage and exposed to the DESI jet for 6 s, resulting in a maximum sample throughput of approximately $6 \text{ samples min}^{-1}$, if the time taken to place a tablet in the sample holder is taken into account. Artesunate analysis by LC-MS requires approximately one hour per sample, if the time required by the sample preparation steps are included in the calculation.²²² For this study, several points on the tablet surface were sampled in order to obtain an accurate picture of the components present. In addition to reagentless DESI, one of the samples (S 12/2005, Type 9) was also analyzed by “reactive” DESI MS by spraying the sample with a solution containing $100 \mu\text{M}$ dodecylamine in 75:25 $\text{CH}_3\text{CN}:\text{H}_2\text{O}$, to further verify the identity of its constituent(s).

2.3.5. FTIR Spectroscopic Imaging

FTIR imaging experiments were performed by Dr. Camilla Ricci, a postdoctoral associate with Dr. Sergei Kazarian in the Department of Chemical Engineering in Imperial College, London. For these experiments, an FPA detector (Santa Barbara, USA) comprising 16384 pixels arranged in a 128x128-grid format was used to measure FTIR spectra with a spectrometer operating in continuous scan mode. Spectra were collected with 8 cm^{-1} spectral resolution in the $4000\text{-}900 \text{ cm}^{-1}$ range using 32 scans. The chemical

images were obtained by attributing a color to each pixel according to the absorbance of a spectral band characteristic of a given compound. In the micro ATR configuration, the spectrometer and the FPA detector were coupled to an infrared microscope with a 20x cassegrainian objective and a Ge ATR crystal. The total area imaged was 64x64 μm^2 .

2.4. Results and Discussion

The short sampling time requirement for high-throughput analysis of pharmaceutical tablets by DESI MS allows only the first layer of the sample to be probed by the DESI spray. For the analysis of counterfeit pharmaceutical, which in most cases are highly inhomogeneous (due to poor manufacturing practices) the spray impact area is a very important parameter as it determines the surface chemical information content that can be captured as the DESI spray plume bounces off the sample surface. The surface information content is expected to increase with the size of the impact area. Figure 2.5 shows the effect of the two most important variables that affect the impact area including the spray duration and the solvent flow rate. The impact area is observed to increase with time at a fixed solvent flow rate (Figures 2.5.a). It also increases with the solvent flow rate for any given spray duration (Figure 2.5.b). Flow rates below $5 \mu\text{L min}^{-1}$ produced a very small spray impact area. This could lead to a DESI spectrum that is less representative of the whole sample. As such a solvent flow rate of $5 \mu\text{L min}^{-1}$ was chosen for all experiments which resulted in the best sensitivity with an appreciably large spray impact area to give a good representative spectrum for single spot rapid throughput analysis. However, for this study several different spots were probed for each sample in order to get a detailed representation of the surface chemical information content.

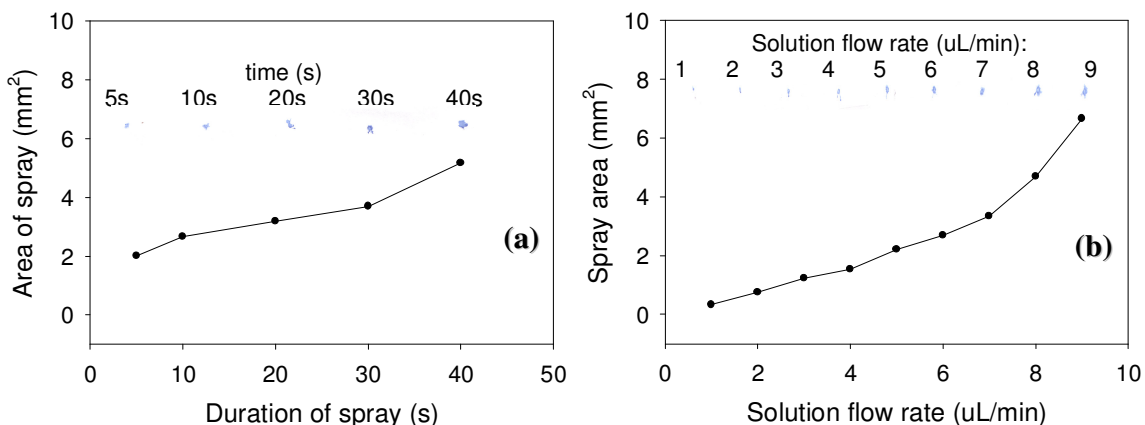


Figure 2.5. Area impacted by the custom-built DESI sprayer jet for various ion source settings. The spots were obtained by spraying 1 mM Reactive Blue 4 dye onto a white sheet of paper. (a) Impacted area vs. spray duration at a dye solution flow rate of $5 \mu\text{L min}^{-1}$, (b) impacted area vs. dye solution flow rate (10 s spray duration).

Analysis of each of the representative samples in this proof-of-concept study by packaging analysis, DESI MS and ATR-FTIR imaging resulted in the classification of the samples in each of the categories of genuine and counterfeit drugs definition. This included (A) Genuine, (B) products with wrong active ingredient(s), (C) insufficient quantities of the AI(s) and (D) no AI(s), as discussed below.

2.4.6. Genuine Artesunate

DESI MS experiments for all samples were performed by spraying a 75:25 $\text{CH}_3\text{CN}:\text{H}_2\text{O}$ solution onto the tablets. This solvent composition was chosen based on preliminary experiments, which indicated that solvent mixtures with higher aqueous content resulted in significant wetting of the tablets with time and higher background in the low m/z region. The positive ion mode DESI spectrum of a genuine Guilin Pharmaceutical Co. Ltd artesunate tablet (50 mg artesunate per tablet) is shown in Figure 2.6.a. The spectrum shows peaks corresponding to monomeric and dimeric artesunic acid adducts and their fragment ions. The formation of Na^+ and K^+ adducts was favored over

the protonated precursor, with peaks at m/z 407.2 and 423.3 respectively. A peak at m/z 790.8 corresponding to the sodiated artesunic acid dimer ($[2 \text{ artesunic acid} + \text{Na}]^+$) was also observed. The peak at m/z 261.2 corresponds to a sodiated fragment of artesunic acid ($[\text{artesunic acid} - \text{C}_4\text{H}_6\text{O}_4 - \text{CO} + \text{Na}]^+$), which originates from in-source fragmentation. Figure 2.6.b shows the negative ion mode DESI spectrum of a genuine artesunate antimalarial tablet. Peaks corresponding to the deprotonated analyte monomer and dimer were observed at m/z 383.2 ($[\text{artesunic acid} - \text{H}]^-$) and m/z 767.7 ($[2 \text{ artesunic acid} - \text{H}]^-$), respectively. Various artesunic acid fragment ions were also observed in negative ion mode, including peaks at m/z 283.5 and m/z 255.5 due to $\text{C}_4\text{H}_4\text{O}_3$ and $\text{C}_4\text{H}_4\text{O}_3 + \text{CO}$ losses from the deprotonated monomer respectively. The peak at m/z 725.2 corresponding to a loss of $\text{C}_2\text{H}_2\text{O}$ from $[2 \text{ artesunic acid} - \text{H}]^-$ was also observed.

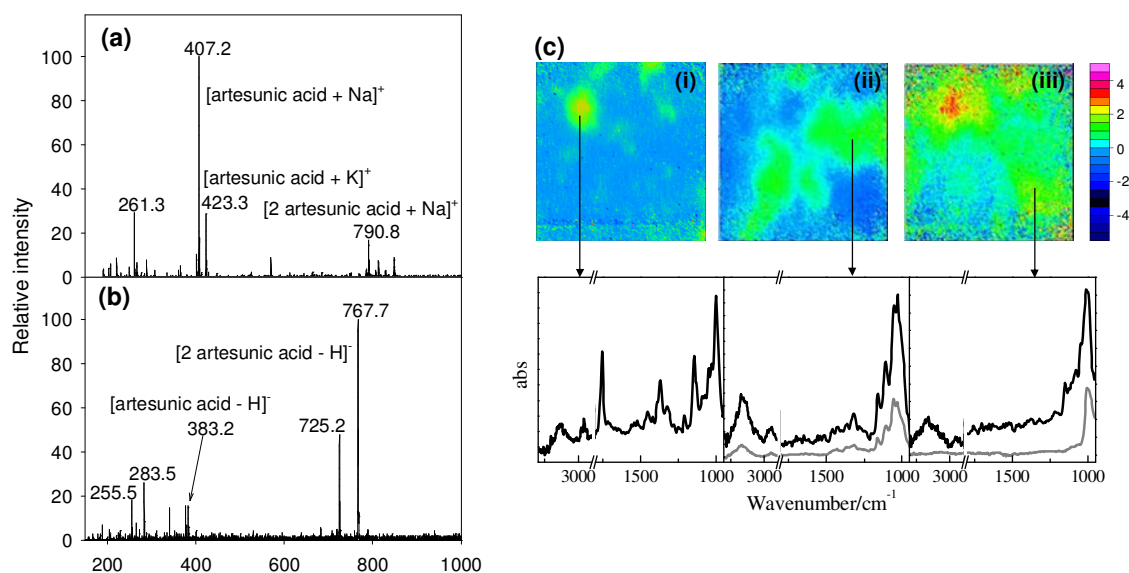


Figure 2.6. Analysis of a genuine Guilin Pharmaceutical Co. Ltd. artesunate tablet by: (a) reagentless DESI MS in positive ion mode, (b) reagentless DESI MS in negative ion mode, (c) Micro-ATR-FTIR imaging showing the distribution of (i) artesunic acid, (ii) avicel and (iii) talc. The size of each image is approximately $64 \times 64 \mu\text{m}^2$. The representative spectra at the location indicated by the arrow are also shown and compared with the reference spectra of (ii) pure avicel and (iii) pure talc.

Analysis of a genuine artesunate tablet by ART-FTIR imaging is shown in Figure 2.6.c. Artesunate shows a strong $\nu(\text{C}=\text{O})$ band at ca. 1750 cm^{-1} , which was used to generate the chemical image representative of the distribution of this drug in the imaged area (Figure 2.6.c.i). For this sample, the presence of a total of four bands within spectral region investigated, at 1030 , 1055 , 1100 , and 1160 cm^{-1} , suggests the presence of avicel, a common excipient used to enhance or control tablet dissolution.²³⁸ The integrated absorbance of the band at 1055 cm^{-1} was used to plot the distribution of this excipient (avicel Figure 2.6.c.ii). The genuine sample also shows a characteristic band at 1003 cm^{-1} , corresponding to the main vibrational mode of talc (Si-O stretching), which was used to create the distribution of this excipient in the imaged area (Figure 2.6.iii). The collected images show that the active ingredient (artesunate) domains in avicel and talc can easily be identified by use of FTIR imaging, unlike in ordinary optical microscopy. In addition to verifying the presence of the correct active ingredient, ATR-FTIR imaging also detected the presence of various excipients including avicel and talc in the genuine Guilin Pharmaceutical Co. Ltd artesunate tablet thereby complementing the DESI MS results.

2.4.7. Counterfeit Artesunate Containing Wrong Active Ingredient(s)

Three of the samples evaluated in this study contained various wrong active ingredient(s) with a range in sophistication including samples containing an analgesic (11 KHA P 7/1 #2, Type 4), no longer efficacious antimalarials (12 PAS P 64/1, Type 8) and the correct active ingredient precursor (detected in S 40-1, Type 13) as presented below.

Results from the analysis of the counterfeit sample 11 KHA P 7/1 #2 (Type 4) are shown in Figure 2.7. Analysis of this sample by DESI MS in positive ion mode shows a peak at m/z 218.2 corresponding to the methylaminoantipyrine proton adduct, a dipyron fragment with the elemental formula ($C_{12}H_{16}N_3O$, Figure 2.7.a). This assignment was verified by DESI MS analysis in negative ion mode, which showed a peak at m/z 310.3 corresponding to deprotonated dipyron (Figure 2.7.b). No artesunate was detected in this sample, as is evident from the absence of the m/z 407.2 peak in the positive ion mode DESI spectrum.

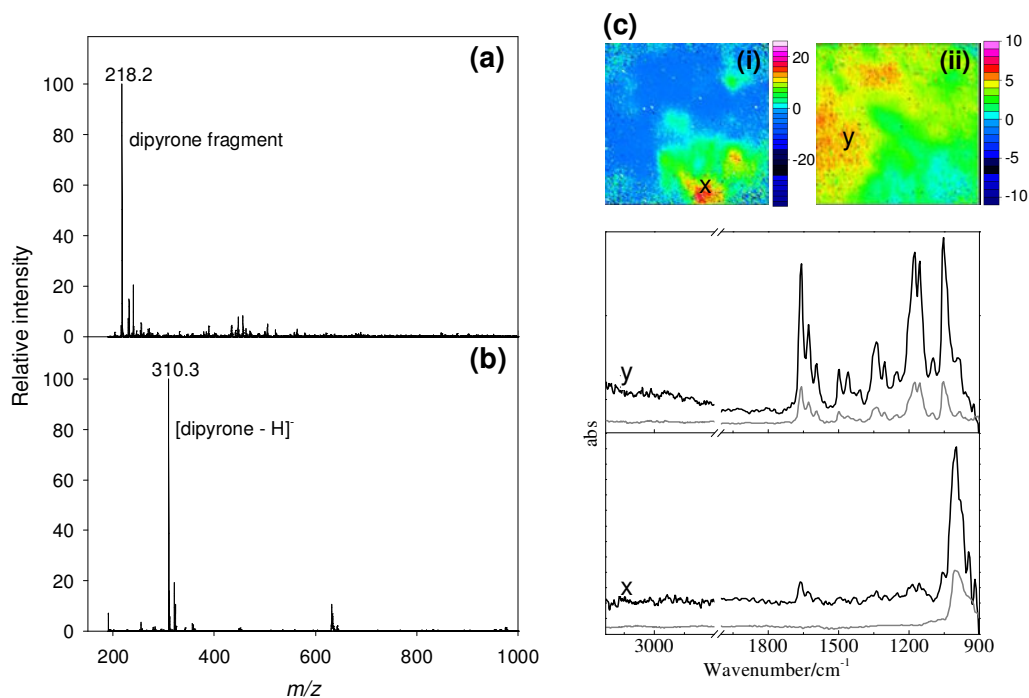


Figure 2.7. Analysis of a fake artesunate Type 4 (11 KHA 7 7/1 #2) by (a) reagentless DESI MS in positive ion mode, (b) reagentless DESI MS in negative ion mode, (c) Micro-ATR-FTIR imaging showing the distribution of the bands at (i) 1008 cm^{-1} and (ii) 1655 cm^{-1} . The size of each image is approximately $64 \times 64\ \mu\text{m}^2$. The representative spectra at the locations indicated by the letters are also shown and compared with the reference spectra of pure talc and pure dipyron.

Analysis of the sample 11 KHA P 7/1 #2 by ATR FTIR imaging is shown in Figure 2.7.c. The analysis shows a strong band at 1008 cm^{-1} corresponding to the presence of talc, with the integrated abundance of this band over the imaged area used to obtain its distribution in the sample (Figure 2.7.c.i). The sample also showed a strong band at 1655 cm^{-1} corresponding to the presence of dipyron and its distribution obtained by plotting the integrated abundance of this band over the imaged area (Figure 2.7.c.ii). Artesunate was not detected in this sample by ATR-FTIR imaging. The presence of dipyron and the absence of artesunate in this sample was consistent with the results obtained by DESI MS analysis. Dipyron is a nonsteroidal anti-inflammatory drug that is used as a powerful painkiller and antipyretic. It has been associated with adverse effects, such as agranulocytosis, and is banned in some countries.²⁰⁰ Administration of this drug might temporarily mitigate some symptoms of malaria, but it does not cure the disease.

Results from the analysis of the sample 12 PAS P 64/1 (Type 8) is shown in Figure 2.8. DESI MS analysis of this sample shows two major peaks, at m/z 249.2 and 311.2 corresponding to protonated pyrimethamine and sulfadoxine, respectively (Figure 2.8.a). By probing different spots on the surface of this sample with the DESI spray plume, different m/z 249.1-to- m/z 311.2 peak intensity ratios were observed suggesting inhomogeneities in the composition of the sample (Figure 2.8.b). Artesunic acid was not detected in this sample by DESI MS analysis. Pyrimethamine-sulfadoxine, detected in this sample is an antimalarial, which is no longer efficacious in SE Asia.

FTIR analysis of the sample 12 PAS P 64/1 shows only one strong band at 1403 cm^{-1} assigned to the asymmetric stretching mode (ν_3) of the carbonate ion. The abundance of this band was used to obtain an image of the distribution of carbonate in the

sample by ATR-FTIR imaging (Figure 2.8.c). No active ingredient was detected in this sample by ATR-FTIR imaging; however, the detection of the carbonate excipient complements the DESI MS results. The inability of detecting pyrimethamine-sulfadoxine in this sample by FTIR is probably because of the large carbonate signal.

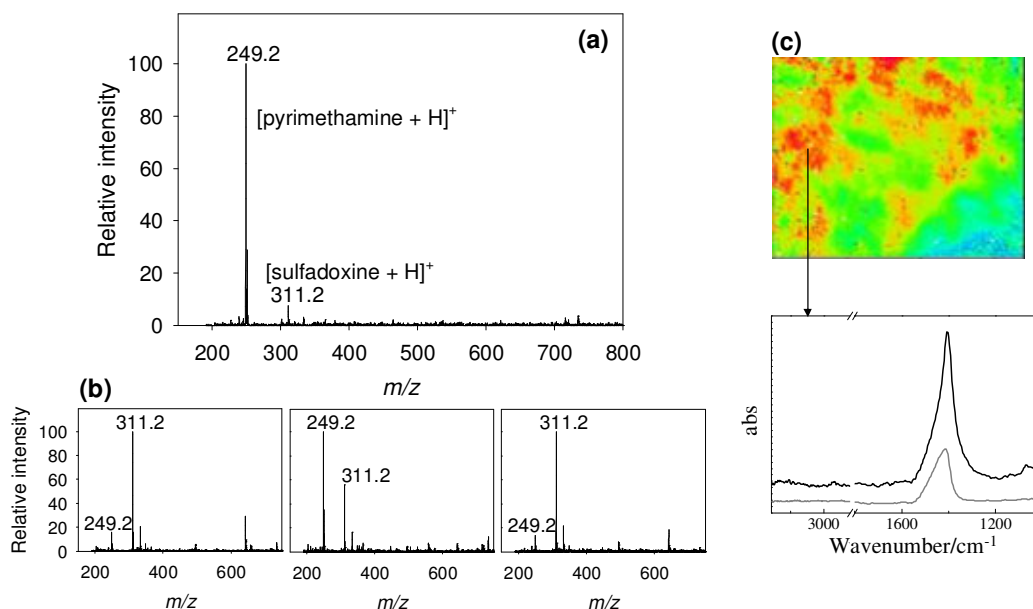


Figure 2.8. Analysis of a fake artesunate Type 8 (12 PAS P 64/1) by (a) reagentless DESI MS in positive ion mode, (b) reagentless DESI MS in positive ion mode for different x-y positions on the tablet surface, (c) Micro-ATR-FTIR imaging showing the distribution of the band at 1403 cm^{-1} . The size of the image is approximately $64 \times 64\ \mu\text{m}^2$. The representative spectrum at the location indicated by the arrow is also shown and compared with the reference spectrum of pure calcium carbonate.

DESI MS analysis of the sample S 40/1 (Type 13) shows peaks at m/z 305.1 and 587.3 corresponding to sodiated artemisinin monomer and dimer respectively (Figure 2.9.a). The characteristic artesunate precursor ion peak at m/z 407.2 was not observed by DESI MS analysis of this sample. These results were validated and complemented by ATR-FTIR imaging analysis (Figure 2.9.b). FTIR analysis of the

sample S 40/1 shows a sharp band at 1735 cm^{-1} which corresponds to the characteristic δ -lactone carbonyl $\nu(\text{C}=\text{O})$ vibration mode of artemisinin, the artesunate precursor.²³⁹ The abundance of the band at 1735 was then integrated over the imaged area to obtain a distribution of artemisinin on the surface of the sample. The FTIR data also shows a sharp band at 1008 cm^{-1} corresponding to talc whose distribution is shown in Figure 2.9.b.ii. Artesunate was not detected in this sample by ATR-FTIR. Artemisinin has a low bioavailability than artesunate, because of its poor water solubility, and is therefore less effective in antimalarial treatments. Its use especially in very small doses can easily facilitate the emergence of artemisinin based antimalarial drug resistance.

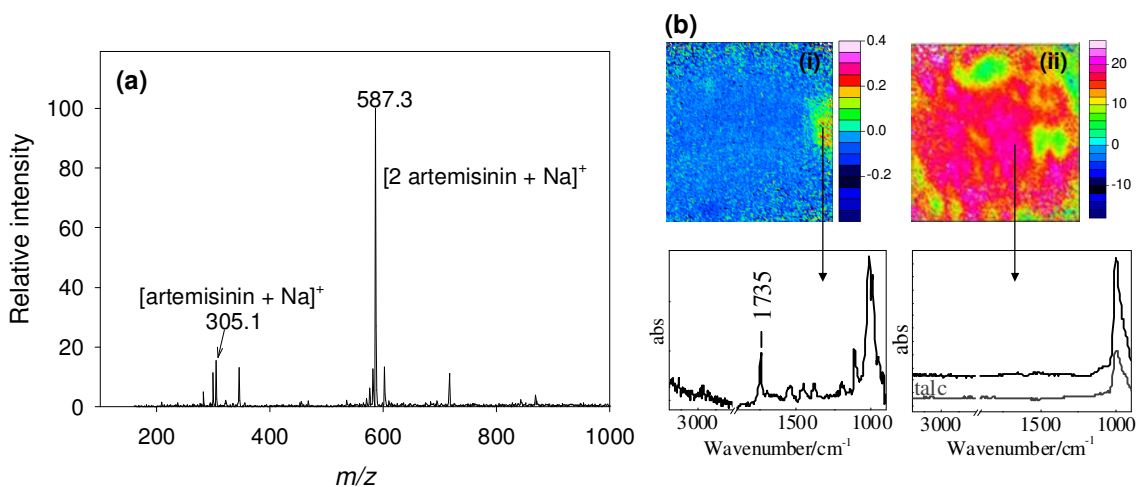


Figure 2.9. Analysis of fake Type 13 (SMRU 40-1) by (a) DESI MS in positive ion mode, (b) Micro-ATR-FTIR imaging showing the distribution of the absorbance of the bands at (i) 1735 cm^{-1} and (ii) 1008 cm^{-1} . The size of each image is approximately $64 \times 64\ \mu\text{m}^2$. The representative spectra at the location indicated by the arrows are also shown and compared with the reference spectrum of pure talc.

2.4.8. Counterfeit Artesunate Containing Insufficient Amount of Active Ingredient

The sample S 12/2009 (Type 9) constitutes an example of a fake artesunate sample containing insufficient amounts of active ingredient, which was previously

determined by HPLC to contain 10 mg artesunate per tablet instead of the usual 50 mg per tablet.¹⁹⁸ Figure 2.10 shows results from the analysis of this sample by DESI MS and ATR-FTIR imaging. Analysis of this sample by DESI MS shows a peak at m/z 152.1 identified as protonated acetaminophen (Figure 2.10.a). The characteristic artesunate ion precursor peak at m/z 407.2 was not detected under these conditions (i.e spraying with a solution of 75:25 $\text{CH}_3\text{CN}:\text{H}_2\text{O}$). DESI analysis of this sample was then evaluated using an alternative, higher sensitivity “reactive” DESI approach by the addition of dodecylamine into the DESI spray solvent. Primary amines have been shown to form stable noncovalent complexes with artemisinins during electrospray ionization.²⁴⁰ Thus, in reactive DESI mode, DDA dissolved in the charged spray microdroplets reacts directly with artesunate molecules exposed on the tablet surface. Analysis of this sample by reactive DESI shows a peak at m/z 570.3 assigned as the proton-bound noncovalent artesunic acid complex with dodecylamine ($[\text{artesunic acid} + \text{DDA} + \text{H}]^+$), (Figure 2.10.b). This peak assignment was verified by DESI MS/MS analysis, which gives the protonated amine (m/z 186.2) and protonated artesunic acid (m/z 385.3) species as the major peaks in the spectrum through a charge competition process (Insert Figure 2.10.b). A peak at m/z 337.1 corresponding to the species $[\text{acetaminophen} + \text{DDA} + \text{H}]^+$ was also observed in the reactive DESI spectrum. The implications of the long-term administration of low doses of artesunate could genetically select artesunate-resistant parasite strains, rendering this last-resource antimalarial medicine ineffective.

Complementary analysis of the sample S 12/2005 (Type 9) by ATR-FTIR shows two major bands, one sharp band at 1008 cm^{-1} ascribed to the presence of talc with its

abundance integrated over the imaged area to give its distribution as shown in Figure 2.10.c.i. There is a second band at 970 cm^{-1} , which suggests the use of ducting powder as excipient. The ATR-FTIR image shown in Figure 2.10.c.ii, is obtained from plotting the abundance over the imaged area for the band at 1148 cm^{-1} corresponds to the distribution of an unidentified species. No artesunate was detected in this tablet by FTIR.

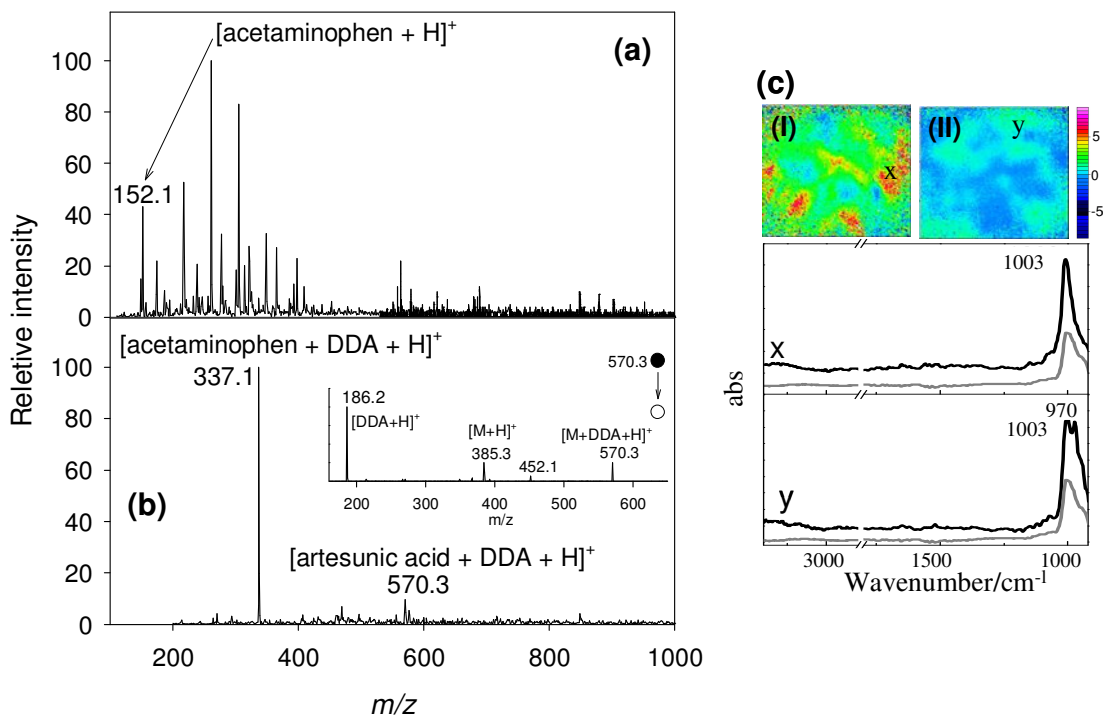


Figure 2.10. Analysis of a fake artesunate Type 9 (SMRU 12/2005) by (a) reagentless DESI MS, (b) reactive DESI MS (insert shows the MS/MS spectrum of the peak at m/z 570.3), (c) Micro-ATR-FTIR imaging showing the distribution of the bands at (i) 1008 cm^{-1} , (ii) 1148 cm^{-1} . The size of each image is approximately $64 \times 64\ \mu\text{m}^2$. The representative spectra at the location indicated by the letters are also shown and compared with the reference spectrum of talc. M = artesunic acid.

2.4.9. Counterfeit Artesunate Containing No Active Ingredient

The sample Lao 05/03 (Type 11) constitutes an example of a sample which contains no active ingredient. This sample was analyzed exclusively by DESI MS using

various spray solvent systems. DESI MS analysis of this sample by spraying the sample with a solution of 75:25 CH₃CN:H₂O resulted in a very noisy spectrum showing peaks at *m/z* 303.5 and 707.2 at the detection limit (Figure 2.11.a).

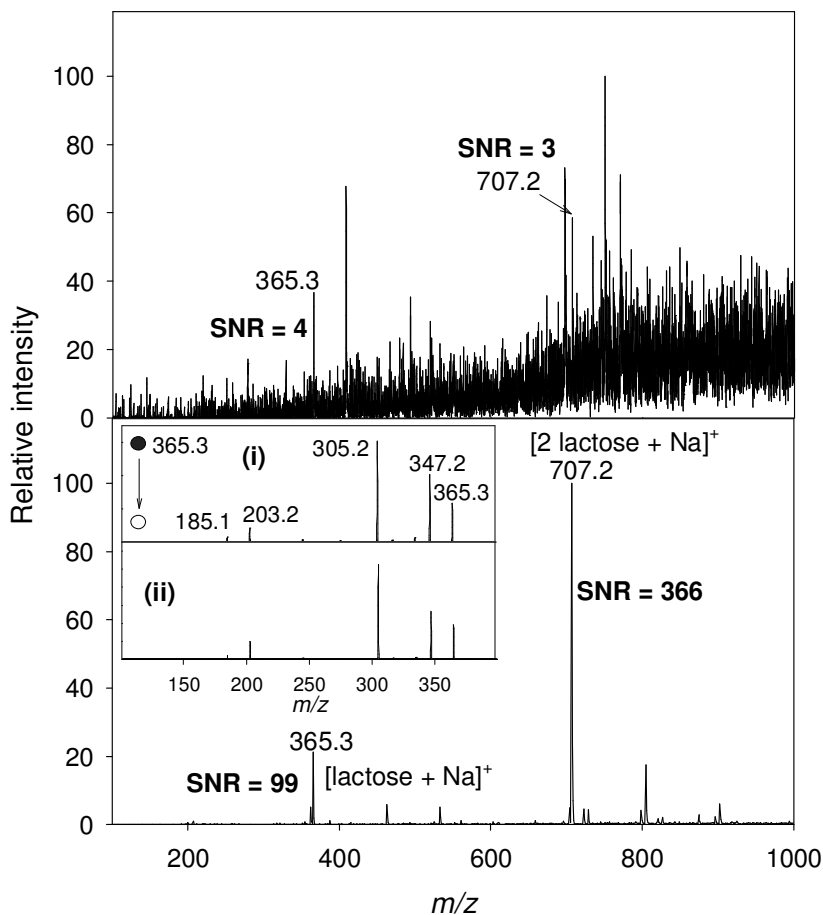


Figure 2.11. Analysis of a fake artesunate Type 11 (Lao 05/03) by reagentless DESI MS by spraying the sample with a solution of (a) 75:25 CH₃CN:H₂O, (b) 100 % MeOH. The insert in (b) corresponds to the MS/MS spectrum generated from the peak at *m/z* 365.3 for (i) the sample (Lao 05/03) and (ii) lactose standard.

Because DESI, relies on the solubility of the analyte in the spray solution various solvent compositions containing decreasing proportions of water were accessed for the analysis of this sample resulting in a spray solvent composed of 100 % MeOH giving the

best signal with the corresponding spectrum shown in Figure 2.11.b. The spectrum shows intense peaks at m/z 303.5 (SNR = 99) and 707.2 (SNR = 366), which were assigned as sodiated lactose monomer and dimer respectively. This assignment was verified by DESI MS/MS analysis of this sample (Figure 2.11.i.) against a lactose standard (Figure 2.11.b.ii). No active ingredient was detected in this sample by both reagentless and reactive DESI MS.

2.5. Conclusions

This initial study demonstrated the capabilities of DESI MS for the rapid qualitative screening of antimalarial artesunate tablets for their facile typing as either counterfeits, which contain wrong active ingredient(s), insufficient amounts of the active ingredient(s) or no active ingredient(s). The dependence of the analyte solubility in DESI on the spray solvent composition can be advantageously exploited to allow efficient sampling of surface chemicals. The ability to also detect various tablet excipient components by ATR-FTIR imaging in a non-destructive manner complemented the high sensitivity provided by DESI MS for reliable routine drug quality analysis applications.

CHAPTER 3. REACTIVE DESI LINEAR ION TRAP MS OF LATEST-GENERATION COUNTERFEIT ANTIMALARIALS VIA NONCOVALENT COMPLEX FORMATION

3.1. Abstract

Presented in this chapter is a detailed characterization of a reactive DESI MS approach for application in the screening of artemisinin-based antimalarial tablets. The method is based on the formation of stable noncovalent complexes between linear alkylamines dissolved in the DESI spray solvent and artemisinins exposed on the tablet surface. Depending on the amine type and concentration, a sensitivity gain of up to 170x can be obtained, in comparison to reagentless DESI, without compromising throughput. Evidence from the analysis of a broad range of different artemisinins and tandem MS experiments indicated that complex formation in reactive DESI occurred by hydrogen bonding between the primary amine hydrogens and the ether-like moieties within the artemisinin lactone ring. The selectivity for the detection of artemisinins can be improved by operating the mass spectrometer in the selected reactions monitoring (SRM) mode. The combined selectivity and sensitivity improvement provided by this approach afford a robust screening tool for the efficient determination of artemisinin-based antimalarial tablets for drug quality control applications.

3.2. Introduction

The 2006 appearance of a new type of artesunate counterfeit (Type 9), containing subtherapeutic amounts of active ingredient spurred great concern following its

detection.¹⁹⁸ This was mainly because its widespread circulation could quickly excite the natural selection and spread of artemisinin-resistant parasites, ridding the world of effective treatment options for multidrug resistant *falciparum* malaria. It has been hypothesized that the administration of artemisinins as monotherapies, even at their proper dosage, could also result in drug resistance. As such, the World Health Organization (WHO) now recommends their administration as combination therapies.

Combination therapies with antimalarial medicines are based on the simultaneous use of two or more blood schizonticidal drugs with independent modes of action and different biochemical targets in the parasite. Artemisinin-based combination drugs (ACTs), base their success on the synergistic or additive potential of two or more active ingredients, to improve therapeutic efficacy and delay the development of resistance to the individual components of the combination. For instance, the probability of a parasite arising that is resistant simultaneously to two drugs with unrelated modes of action is the product of the per parasite mutation frequencies multiplied by the total number of parasites exposed to drugs. For example if the probability of a parasite being resistant to drug A is one in 10^6 and to drug B is one in 10^6 then the probability that a parasite will be simultaneously resistant to both is one in 10^{12} , representing a million-fold reduction in probability.²⁴¹

Artesunate is a crucial component of ACTs, and is still commonly used inappropriately as monotherapy outside of national malaria programs.²⁰⁰ The initial detection of artesunate monotherapy counterfeits containing small amount of active ingredient, was hypothesized to have been an “innovation” introduced by the counterfeiters in an attempt to deceive the colorimetric authentication tests used in the

field. Therefore, the exploration of new approaches for antimalarial tablet screening is central to rapidly ensuring the quality of the genuine product, and for the early detection of fakes artemisinin-based monotherapies or combination therapies that may contain small amounts of active ingredient.

In Chapter 2 a reagentless DESI MS protocol was investigated for the rapid screening of antimalarial tablets, which enabled the distinction between different types of fakes. This method, however, was not able to determine counterfeits which contain insufficient amounts of active ingredient. This was partly because artesunate undergoes appreciable in-source fragmentation, which lowers the sensitivity, limiting its detection in such counterfeits.

One of the potential avenues to mitigate in-source artesunate fragmentation during DESI MS is to exploit DESI modalities that take advantage of selective solution phase chemistry. Cooks et al. first reported that, if the DESI spray is doped with selective chemical reagents, it is possible to perform ion/molecule reactions between the charged microdroplets and an analyte exposed on a solid sample surface.²⁴² In most cases, this results in improved sensitivity due to increase ion evaporation rates and/or reduced fragmentation. Because reactive DESI enjoys the same sample throughput as conventional DESI, it is particularly well suited for the forensic analysis of counterfeit drugs, with the added benefit of increased specificity and sensitivity.

In this Chapter an extensive characterization of a highly sensitive reactive DESI MS method for the rapid screening of antimalarial tablets, enabling the determination of subtherapeutic counterfeits is presented. The method makes use of the reaction between primary alkylamines and artemisinins, forming proton-bound non-covalent complexes.

This study also provides valuable insight on the ion generation processes occurring during the collision of reactive charged microdroplets with the solid sample surface.

3.3. Experimental Details

3.3.1. Samples and Reagents

All reagents were used without additional purification. HPLC grade acetonitrile (Fisher, Hampton NH), dodecylamine (DDA), hexylamine (Hex) and octadecylamine (ODA) (Sigma-Aldrich, St. Louis MO) were used for reactive DESI MS experiments. Ultrapure water ($18.2 \text{ M}\Omega \text{ cm}^{-1}$) was obtained from a Nanopure purification unit (Barnstead, San Jose CA). Genuine artesunate tablets manufactured by Guilin Pharmaceutical Co. Ltd. (50 mg per average 250 mg tablet, Guilin, Guangxi, PR China) were used for all characterization and optimization studies. Preliminary assessment of the authenticity of samples by packaging inspection was performed following the procedure described in section 2.3.2. The following collection code samples: S 35/1 (Type 9), S 29 (Type 9), S 40/2 (Type 13), S 45 (Type 9), S 40/1 (Type 13), S 47/2 (Type 14), S 47/1 (Type 14), Lao 06/04 (Type 10) and Lao 12012 (Type 6) were evaluated in this study (see Figure 2.2 for sample collection location). The samples were all labeled on their blister packs to contain 50 mg of artesunate per tablet. Two additional samples: Kenya 07/01 (Collected in Kenya) and Lao 07/20/2 (collected in Laos), which were labeled on their blister packs as dihydroartemisinin and artemether tablets respectively, were also evaluated in this study. Tablets were stored at 4°C until analysis.

3.3.2. DESI MS and LC-MS

The DESI set-up described in section 2.3.3 was interfaced to a LiT mass spectrometer (Thermo Finnigan, San Jose CA) and operated using similar settings and experimental conditions as described in section 2.3.4. Reagentless DESI experiments were performed by spraying samples with a solution of 75:25 CH₃CN:H₂O. 100 μM amine was added to the above spray solution for reactive DESI MS experiments unless stated otherwise. For each amine, the mass spectrometer was auto tuned in order to obtain maximum signal intensity for their corresponding protonated amine-artemisinin-based noncovalent complex. DESI MS/MS experiments were collected at a normalized collision energy of 10%. Suspected drug samples were also analyzed by LC-MS, following the sample preparation method described by Hall *et al.*²²² and the LC conditions described by Orтели *et al.*²⁴³

3.4. Results and Discussions

3.4.3. Reagentless vs. Reactive DESI MS of Genuine Artesunate Tablets

Figure 3.1.a shows the positive ion mode reagentless DESI spectrum of a genuine artesunate tablet. In this mode of operation, the overall sensitivity was low, primarily because the ionic signal due to artesunic acid species was spread into various channels with the major peaks in the spectrum corresponding to sodiated monomeric and dimeric artesunic acid adducts, and their fragment ions.

Corresponding reactive DESI spectra obtained by spraying genuine tablets successively with spray solutions containing 100 μM of each of the various alkylamine evaluated including Hex, DDA, and ODA are shown in Figure 3.1.b. For each of the

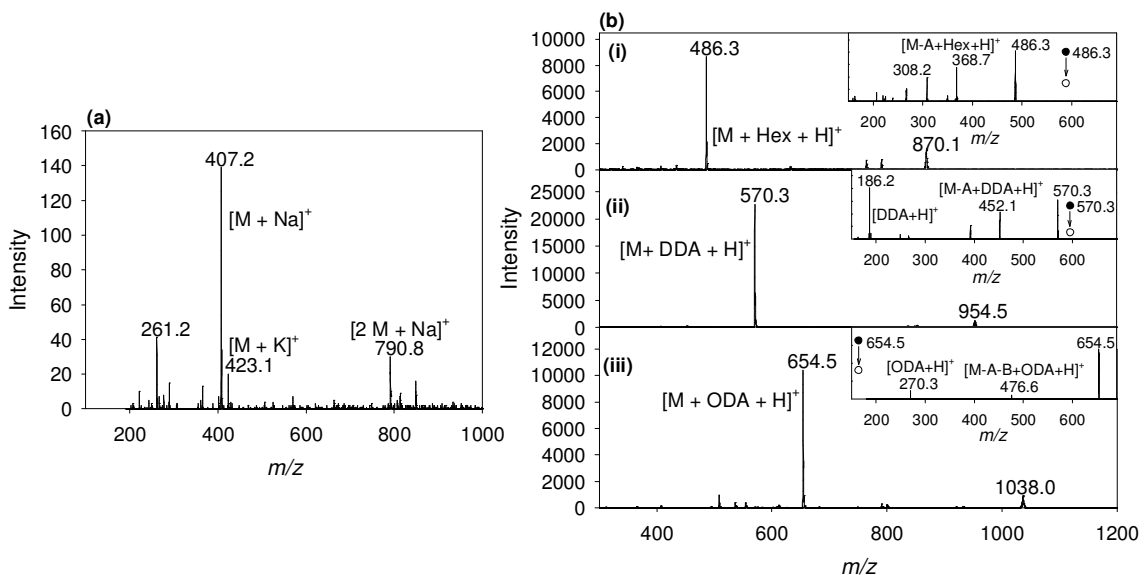


Figure 3.1. DESI spectra of a genuine artesunate tablet analyzed in (a) reagentless DESI MS mode, by spraying the tablet with a solution of 75:25 CH₃CN:H₂O and (b) reactive DESI MS mode by spraying tablets with a solution containing 100 μM of (i) hexylamine (Hex), (ii) dodecylamine (DDA) and (iii) octadecylamine (ODA) in 75:25 CH₃CN:H₂O. A = C₄H₆O₄, B = C₂H₄O₂. The inserts represent MS/MS spectra of the [M + amine + H]⁺ ions with *m/z* 486.3, 570.3 and 654.5 respectively. M = artesunic acid.

alkylamines, the base peak corresponding to a 1:1 artesunic acid-alkylammonium noncovalent complex ion was observed. Analysis with Hex presented a very intense peak at *m/z* 486.3 corresponding to the species [M + Hex + H]⁺, followed by a less intense peak at *m/z* 870.1 assigned as [2 M + Hex + H]⁺ (Figure 3.1.b.i). In Figure 3.1.b.ii, the peaks at *m/z* 570.3 and 954.5 correspond to the species [M + DDA+H]⁺ and [2 M + DDA + H]⁺ respectively. Similar results were observed for ODA, with peaks at *m/z* 654.5 and *m/z* 1038.0 (Figure 3.1.b.iii). The relative intensity of the [2 M + amine + H]⁺ signal with respect to [M + amine + H]⁺ was found to be dependent on the chain length of the amine used, decreasing with an increase in amine chain length from C6 to C12. This is probably due to increased steric hindrance for dimerization, with

increased amine length. A further increase in chain length from C12 to C18, produced insignificant changes in the relative intensity of the dimeric complex ion.

The generation of noncovalent complex ions by reactive DESI arises by cationization from ion-molecule reactions between alkylammonium ions in the spray solution and analyte molecules on the tablet surface. The observed bunching of the analyte signal intensity into a single peak is due to the relatively strong interaction between alkylammonium ions and electron-rich moieties in the artesunic acid molecule. The inserts in Figure 3.1.b depict the DESI MS/MS spectra of each of the three artesunic acid-alkylammonium complexes. Following ion activation, the artesunic acid side chain ($C_4H_6O_4$) was readily lost from the complex ions, forming different fragments. It appears as though the interaction energy in the complexes was high enough so that the internal energy imparted in the MS/MS experiment was sufficient to cause fragmentation of the artesunic acid butanedioic side chain without loss of the amine ligand.²⁴⁴ Some fragment ions retained the alkylamine ligand, indicating that the amine-artesunic acid complex is not formed by interaction with the side chain carbonyl groups, but with the ether or endoperoxide moieties of the sesquiterpene lactone ring system. Other artemisinins including artemisinin, dihydroartemisinin and artemether, which contain different side chains from that in artesunic acid were also observed to form complexes with alkylamines (*vide infra*) thus reinforcing this hypothesis.

A very large signal intensity gain follows droplet pickup and complexation of artesunic acid by alkylammonium ions. This highly improved analyte signal can be attributed to two effects: first, the localization of the positive charge of the complex at the alkylamine nitrogen atom results in minimum or no fragmentation of analyte molecules

by in-source collision-induced dissociation (CID). Secondly, the addition of a positively charged, hydrophobic alkylamine ligand enhances the ion evaporation process after artesunic acid pick-up by the DESI spray droplets. Overall, the signal gain with respect to the intensity of the $[M + Na]^+$ ion observed in reagentless DESI mode was above 60x, 170x, and 70x for Hex, DDA and ODA respectively. Interestingly, a lower signal gain was observed for ODA (Figure 3.1.b.iii) than for DDA (Figure 3.1.b.ii), probably due to increased ionization suppression caused by the more hydrophobic $[ODA + H]^+$ ions.

The noncovalent complex signal intensity was found to increase with the concentration of amine in the spray solvent. Figure 3.2 shows the effect of different

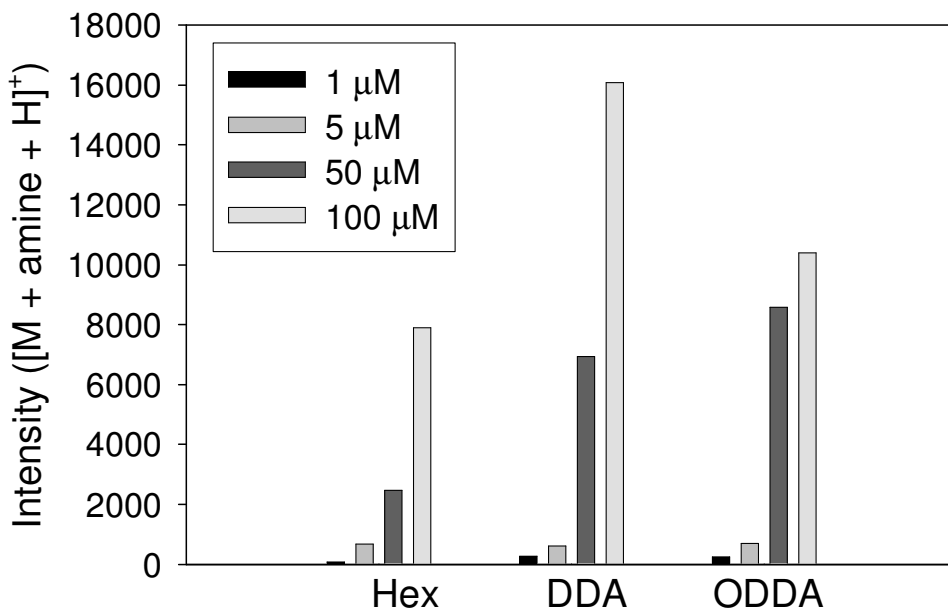


Figure 3.2. Positive ion mode reactive DESI of genuine artesunate tablets at different Hex, DDA and ODA concentrations. The bar graphs represent the intensities of the ions at m/z 486.3, 570.3, 654.5 obtained by spraying 1, 5, 50 and 100 μ M solutions of each of the amines dissolved in 75:25 $CH_3CN:H_2O$.

alkylamine concentrations on the reactive DESI ion yield. A signal plateau was obtained at lower concentrations of more hydrophobic alkylamines, suggesting that artesunic acid complexation efficiency is related to the activity of alkylamine molecules on the DESI droplet surface. This observation supports the hypothesis that reactive DESI of artesunic acid could proceed via a pickup mechanism where heterogeneous reactions between alkylamines on the droplet surface and artesunic acid molecules on the tablet are responsible for initial artesunic acid desorption, followed by noncovalent complex formation. Computational fluid dynamic simulations have confirmed the droplet pick-up mechanism in DESI.^{100, 101}

The gas-phase stability of the artesunic acid-alkylammonium complexes was also investigated. Figure 3.3 presents the fragmentation efficiency curves²⁴⁵ for the different

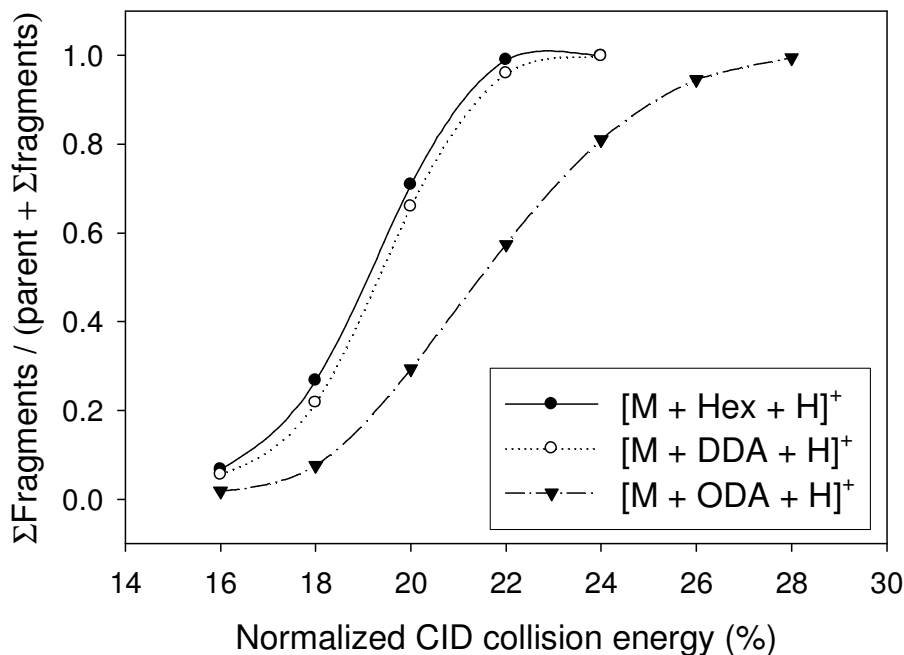


Figure 3.3. Fragmentation efficiency curves [(sum of fragment intensities)/(total intensities)] for various artesunic acid-alkylammonium complexes. M = artesunic acid.

complexes studied. The results suggest that the stability of these complexes increases in the order, $[M + \text{Hex} + \text{H}]^+ < [M + \text{DDA} + \text{H}]^+ \ll [M + \text{ODA} + \text{H}]^+$, following the increase in chain length of the amine ligand, consistently with the trends in basicity of alkylamines in the gas phase.²⁴⁶ Stabilization of the conjugate base (alkylammonium) increases with the alkyl chain length, leading to an increase in stability of the complex.

3.4.4. Experimental Variables Affecting Artesunic Acid Ion Yield in Reactive DESI MS

The effects of various experimental variables on the artesunic acid-alkylammonium complex ion yield, including solution flow rate, nebulizer gas flow rate, and spray voltage, were investigated using genuine artesunate antimalarial tablets. Dodecylamine was chosen for all optimization studies based on the higher intensity of its $[M + \text{amine} + \text{H}]^+$ complex ion compared to those of the other amines. The intensity of the artesunic acid-alkylammonium complex ion was found to rapidly increase with solution flow rate, reaching a maximum between 5 and 6 $\mu\text{l min}^{-1}$, followed by a rapid decrease (Figure 3.4.a). Chen *et al.* have also observed a similar change in DESI response with spray solution flow rate,¹⁴⁰ but with the maximum response shifted to higher rates. This could be assigned to differences in the tablet hardness and/or wettability of the pharmaceutical tablets investigated here. A flow rate of 5 $\mu\text{L min}^{-1}$ was used for all our subsequent experiments.

Figure 3.4.b shows the dependence of the artesunic acid-alkylammonium complex ion yield on the nebulizer gas flow, which was found to increase with an increase in the nebulizer gas velocity. This increase suggests that an increasing amount of material is desorbed or ablated from the tablet surface as absolute droplet velocity increases, or that

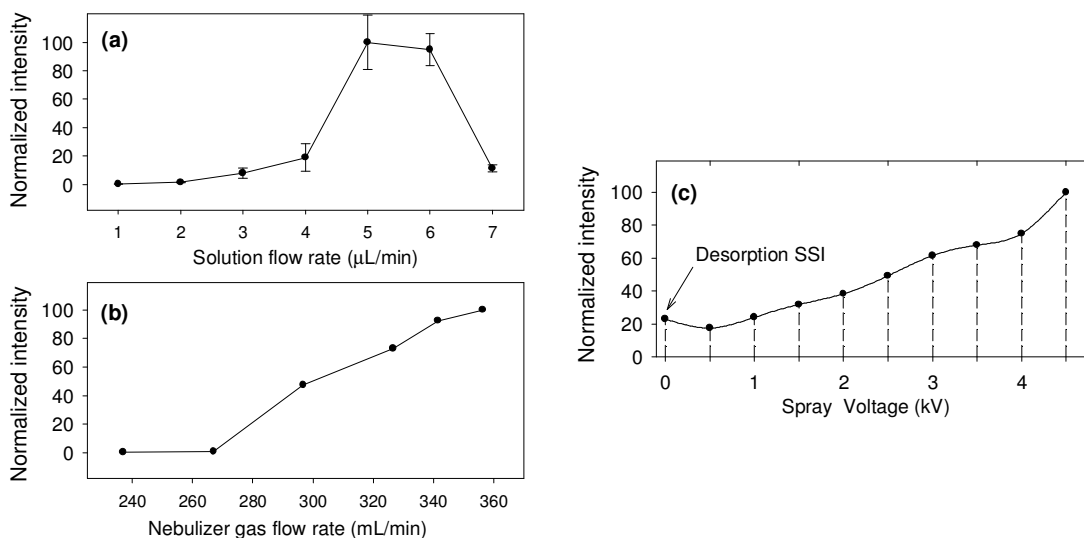


Figure 3.4. Intensity dependence of the $[M + DDA + H]^+$ adduct ion (m/z 570.3) with (a) spray solution flow rate; error bars represent the standard deviation for 3 repeat measurements, (b) nebulizer gas flow, (c) spray solution charging voltage. Experiments were performed by spraying a solution of 100 μ M dodecylamine in 75:25:CH₃CN:H₂O onto genuine artesunate tablets. M = artesunic acid.

faster droplets have a different takeoff trajectory, which improves droplet/ion collection efficiency.¹⁰⁰ A nebulizer gas velocity of 356 mL min⁻¹ was adopted for all experiments. Higher nebulizer gas velocities typically resulted in visible damage to the tablet surface, and were thus avoided.

The artesunic acid-alkylammonium complex ion yield was also observed to increase with solution spray voltage over the entire range investigated (0 - 4.5 kV, Figure 3.4.c). This general increase in ionic current with voltage can be attributed to an increasing number of charges on the droplet surface, probably caused by the increased rate of solvent oxidation processes induced at higher spray charging potentials. Venter *et al.* have also shown reports on the effect of the DESI signal at varying spray voltage, where it was observed that the average charge state, and amount of desorbed melittin

increased with increasing voltage. This also suggests that pH changes within the DESI charged droplets occur when the spray voltage is increased, and that these changes affect the amount and nature of the desorbed ions. Interestingly is the fact that the artesunic acid-alkylammonium complex ion signal was observed even in the absence of charging voltage (Figure 3.4.c). Chen *et al.* have previously reported this phenomenon for conventional DESI,¹⁴⁰ where they assigned this behavior to a sonic spray-type mechanism,³³ which forms the basis of Desorption Sonic Spray Ionization (DeSSI).⁴⁰

3.4.5. Reactive DESI MS of Other Artemisinins

The optimized reactive DESI MS protocol was then evaluated for the analysis of other artemisinins. The samples evaluated included a counterfeit artesunate sample with collection code Lao 12012 (previously determined to contain artemisinin, Figure 3.5.a), and two other samples with collection code Kenya 07/01 (Figure 3.5.b) and Lao 07/20/2 (Figure 3.5.c), indicated on their blister packs to contain dihydroartemisinin and artemether respectively. Reactive DESI MS analysis of each of these samples showed intense peaks at m/z 468.4, 470.4 and 484.4 assigned as 1:1 dodecylammonium complexes of the various artemisinins including artemisinin, dihydroartemisinin and artemether respectively. These assignments were verified by DESI MS/MS analysis as shown by the inserts in each of the spectra. For each complex MS/MS generated predominantly the product ion peak at m/z 186.2 corresponding to the dodecylammonium ion following the neutral loss of the artemisinin present in each of the sample. For dihydroartemisinin and artemether, peaks corresponding to a loss of their respective

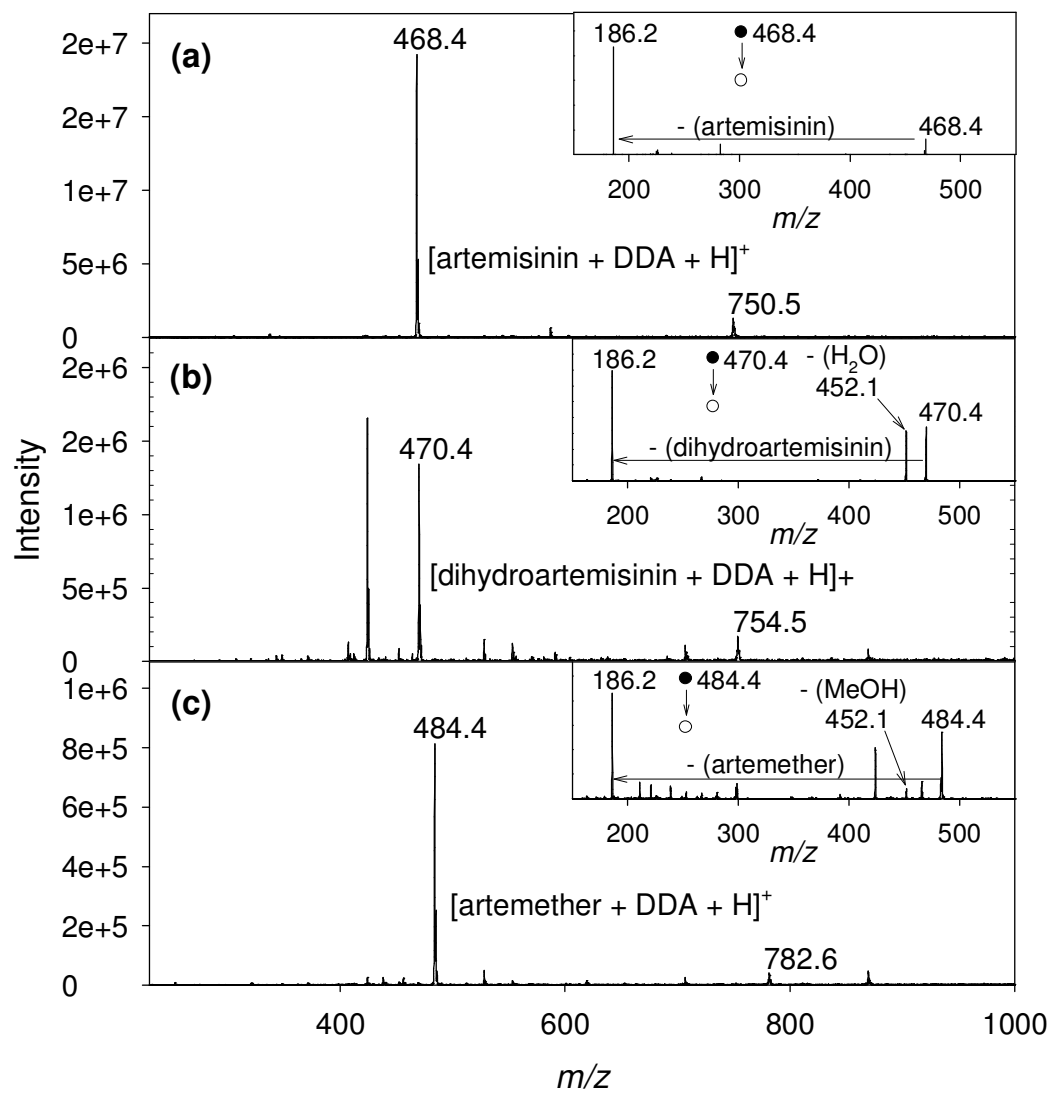


Figure 3.5. Reactive DESI spectra of artemisinin-based antimalarials tablets collected in Laos and Kenya with collection codes: (a) Lao 12012, (b) Kenya 07/01, (c) Lao 07/20/2. Spectra were obtained by spraying tablets with a solution containing 100 μM DDA in 75:25 $\text{CH}_3\text{CN}:\text{H}_2\text{O}$. The inserts represent the MS/MS spectra of the ions with at m/z 468.4, 470.4 and 484.4 observed from each spectrum respectively. The peaks at m/z 750.5, 754.5 and 782.6 correspond to the dodecylammonium complexes of dimeric artemisinin, dihydroartemisinin and artemether respectively.

water and methanol side chains from the complex (occurring without loss of the dodecylamine ligand) were also observed. This further verified that the interaction between alkylamine and artemisinins occur within the endoperoxide moieties of the ring

system. The ability to selectively and sensitively identify each of these artemisinins indicates the utility of reactive DESI as a powerful approach for the reliable analysis of the whole spectrum of artemisinins.

3.4.6. Rapid Screening of Field-collected Artesunate Tablets by Reactive DESI MS

The performance of the reactive DESI MS methodology was then evaluated for applications in the rapid screening of various artesunate samples collected in the field. First, reactive DESI MS/MS analysis in the selected reaction monitoring (SRM) mode was performed on two genuine artesunate samples manufactured by Guilin Pharmaceutical (samples codes “Gen-1”, and “Gen-2”), and on a genuine tablet from a different manufacturer, Mekophar (Hanoi, Vietnam), with sample code “Gen-3”. The SRM analysis was performed by monitoring the characteristic m/z 570.3 ($[M + DDA + H]^+$) \rightarrow m/z 452.1 ($[M - C_2H_4O_2 + DDA + H]^+$) transition, which provided an additional level of selectivity. Repeated analyses were performed by manually positioning the sample holder, so that the sample would be exposed to the DESI spray, and removing it after approximately 50s. Despite the manual sample positioning method used, the SRM traces indicated a relatively good reproducibility (Figure 3.6). The between-run relative standard deviations observed for the “Gen-1”, “Gen-2” and “Gen-3” samples were 17%, 7% and 10%, respectively. Different batches of the Guilin Pharmaceutical product (Gen-1, and Gen-2) showed similar relative intensities in the SRM traces with a difference in the mean intensities of 8.4%. DESI SRM analysis of the genuine Mekophar sample (Gen-3, stated to contain 50 mg of artesunate per average 320 mg tablet) resulted in a lower average signal (34%). This difference could be attributed to

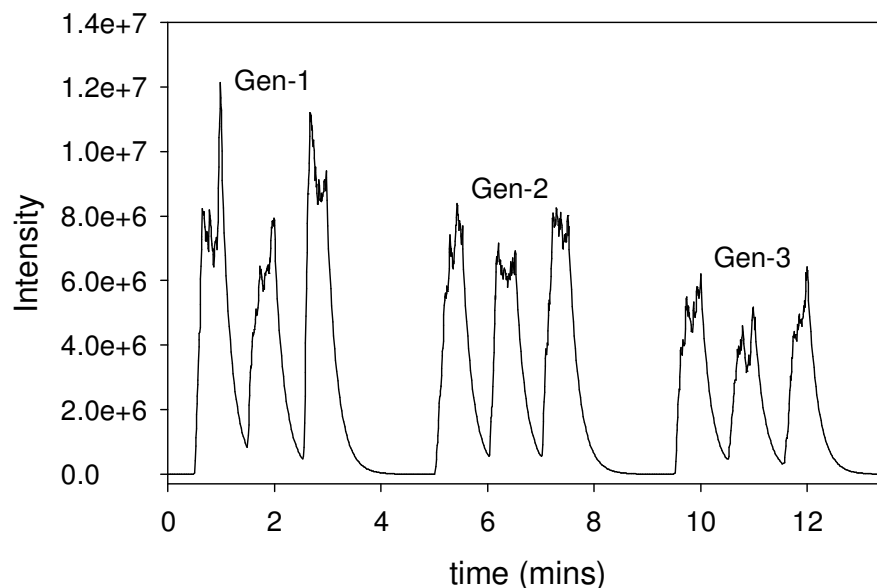


Figure 3.6. SRM traces obtained by reactive DESI MS/MS analysis of different genuine artesunate samples. The m/z 570.3 \rightarrow m/z 452.1 transition was used for monitoring the presence of artesunic acid.

the different hardness, surface morphology and/or the lower concentration of artesunic acid in this tablet, compared to the previously tested tablets.

With the objective of determining if, artesunic acid could be detected or not at the expected levels, reactive DESI MS and MS/MS in SRM mode was applied to various suspicious artesunate tablet. The samples were collected on the Thai/Burma border and on the Lao PDR/China border (collection codes: Lao 06/04, S 35/1, S 29, S 40/2, S 45, S 40/1, S 47/2 and S 47/1). A genuine sample (sample code Gen-3) collected in the same area was also included in the analysis as a positive control. A Type 8 counterfeit artesunate tablet (sample code 12 PAS P 64/1), collected in a previous survey and which did not contain detectable amounts of artesunic acid (as verified by LC experiments), was used as a negative control. The DESI SRM trace generated from screening each of the indicated tablets in duplicate is shown in Figure 3.7. Minute background signals could be

observed for most of the counterfeits, which were comparable to that of the negative control, except for sample S 47/1 (note the y-axis break in Figure 3.7). This suggests the absence of artesunic acid in detectable amounts in all the counterfeits except for sample S 47/1. The large signal deviation for the duplicate measurements for sample S47/1 comes from the low levels of artesunic acid on the surface of this sample which is quickly consumed by the high velocity of the DESI jet after the first exposure of the sample. Although the reactive DESI method presented in this study doesn't allow direct

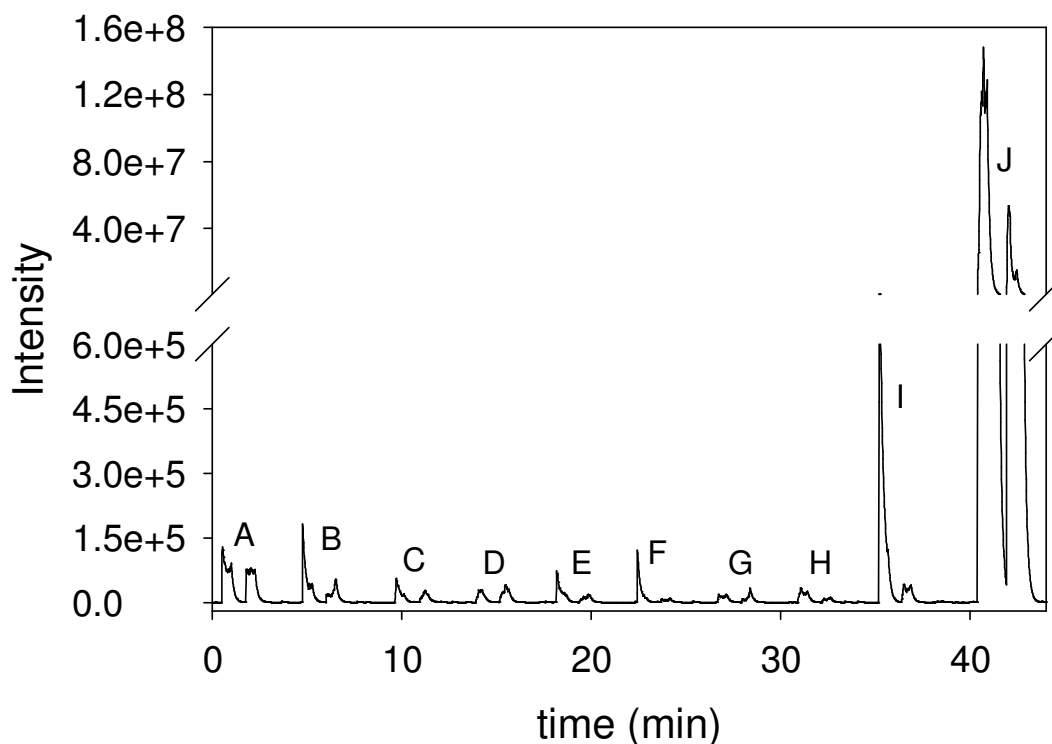


Figure 3.7. Reactive DESI SRM trace corresponding to the duplicate analysis of last generation counterfeit artesunate samples collected in the Thai Burma border, together with a genuine sample. Sample codes: A: Control, B: Lao 06/04, C: S 35/1, D: S 29, E: S 40/2, F: S 45, G: S 40/1, H: S 47/2, I: S 47/1, J: Genuine (Gen-3). SRM was carried out following reactive DESI MS/MS by monitoring the m/z 570.3 \rightarrow m/z 452.1 transition.

quantitation (the subject of investigations in Chapter 4), inspection of the observed signal intensity for sample S 47/1 with respect to the signal observed for Gen-3 clearly indicated that the amount of artesunate in this sample was substandard. The difference in hardness of this tablet did not appear to be sufficient to explain the observed difference in signal intensity. Subsequently, the exterior of this tablet was scraped with a scalpel, and subjected to LC-MS analysis, together with material from the tablet bulk. Although artesunic acid was not detected in the bulk of this sample, triplicate analysis of the tablet surface scrapings indicated the presence of artesunic acid at a level of 4.5 ng mg^{-1} . This very small amount of artesunic acid on the surface of this tablet could have been introduced onto this particular fake as a residue left over from the press used to prepare other tablets with higher amounts of artesunic acid. Clearly, for this particular sample DESI screening produced information that would not have been obtainable using the conventional analysis protocol.

3.5. Conclusions

This study demonstrated the capability of reactive DESI as an effective high throughput approach for screening antimalarial tablets. This method is highly suited for the verification of the quality of the large number of artemisinin-based antimalarial dosage units distributed worldwide by governmental, non-governmental, and commercial organizations, and for the early detection of counterfeits containing artesunate. From the mechanistic point of view, it was observed that the ion generation processes in alkylamine-mediated reactive DESI are affected predominantly by the amine surface droplet activity.

CHAPTER 4. DIRECT QUANTITATION OF ACTIVE INGREDIENTS IN SOLID ARTESUNATE ANTIMALARIALS BY NONCOVALENT COMPLEX FORMING DESI MS

4.1. Abstract

In this Chapter, a rapid throughput approach for the direct quantitation of active ingredients in solid artesunate antimalarial formulations by reactive DESI MS is presented. The applicability of DESI MS for direct quantitative analysis of solid pharmaceutical tablets is complicated by the dependence of the DESI signal on various geometrical settings and morphological sample properties. The signal dependence on geometrical settings was circumvented following synthesis of an internal standard (IS) and the development of a controlled IS deposition method for sample pretreatment prior to reactive DESI MS analysis. Following the homogenous dispersion of the IS on the sample surface using this deposition protocol, the analyte-to-internal standard signal ratio was observed to be largely independent of all DESI variables. However, the signal ratio still showed some dependence on sample properties notably, the sample hardness. By using a correction scheme this dependence was also circumvented enabling the application of this methodology for the direct quantitation of field-collected artesunate tablets with a 6% (n=4) precision and 94% accuracy.

4.2. Introduction

The development of methodologies that allow the quantitative determination of physiologically active analytes in complex matrices is an ongoing trend in analytical and

biological mass spectrometry. This chapter presents discussions on the capabilities of DESI MS for the rapid quantitative analysis of pharmaceutical tablets for the determination of substandard and subtherapeutic counterfeit medications.

Although DESI MS has been shown to be a powerful tool for the qualitative analysis of a broad range of analytes and sample types,²⁴⁷ its applicability for direct quantitative analysis remains limited. This being largely because of the dependence of the DESI signal on various experimental parameters (see Figure 1.1) including the spray tip-to-surface distance (d_1), sample-to-spectrometer orifice distance (x), MS orifice-to-surface distance (d_2), spray incident angle (α) and collection angle (β). Fixed-geometry DESI probes, might somewhat mitigate this problem.⁹³⁻⁹⁵ However, in the case of pharmaceutical tablets there is an additional dependence of the DESI signal on sample properties such as hardness and sample shape, the latter influencing α and β . Cooks and co-workers first suggested that the use of an isotopically labeled internal standard (IS) to circumvent these limitations in order to enable quantitative applications by DESI MS. They demonstrated this capability in a proof-of-concept application in the quantitation of phenylalanine that was codeposited with IS from solution onto glass substrates.¹ Similar proof-of-concept studies have also been shown for the quantitative analysis of pharmaceuticals compounds spiked in various matrices including diluted urine and porcine brain lipid extracts.^{156, 157} The application of DESI MS for quantitative analysis of agrochemicals in foodstuff extracts has also been reported.¹⁴⁴

In this Chapter, the applicability of DESI MS for the direct quantitative analysis of artesunate in solid pharmaceutical formulations is explored by leveraging the advantages provided by the reactive DESI MS protocol presented in Chapter 3. Due to

the challenge posed by the incorporation of a controlled, well-dispersed amount of IS into a solid tablet, several deposition methods were explored and compared for the development of a quantitative analytical tool for the direct sampling of solid antimalarial formulations. The large dependence of the DESI signal intensity with various experimental variables and sample properties was overcome by the homogeneous deposition and co-crystallization of a deuterated IS on the tablet surface enabling direct quantitative determination. The DESI MS results were validated using liquid chromatography.

4.3. Experimental Details

4.3.1. Samples and Reagents

All reagents were used as received. HPLC grade acetonitrile (Fisher, Hampton, NH) and dodecylamine (DDA, Sigma-Aldrich, St. Louis, MO) were used for DESI and reactive DESI experiments. Ultrapure water ($18.2 \text{ M}\Omega \text{ cm}^{-1}$) was obtained from a Nanopure purification unit (Barnstead, San Jose, CA). Genuine artesunate tablets manufactured by Mekophar Chemical Pharmaceutical Joint-Stock Co. (Ho Chi Minh City, Vietnam), stated to contain 50 mg of artesunate per tablet with an average total tablet weight of 320 mg, were used for all characterization and optimization studies. A previously reported LC procedure¹⁹⁸ was used to predetermine the amount of artesunic acid in these samples. Dihydroartemisinin (AApin Chemicals Ltd, UK), d₄-succinic anhydride, triethylamine, tetrahydrofuran, acetic acid, anhydrous sodium sulfate, ethylacetate and hexane (Sigma-Aldrich, St. Louis, MO) were used in the synthesis of d₄-artesunic acid. Cab-o-sil, talc, magnesium stearate (Acros Organics, Morris Plains, NJ),

microcrystalline cellulose (Mallinckrodt Baker Inc., Phillipsburg, NJ), croscarmellose sodium, and spray-dried lactose (FMC Corp., Newark, DE) were used as excipients for the preparation of artesunate tablet standards. Artesunic acid (M) was purchased from AApin Chemicals Ltd. All genuine and standard artesunate tablet samples were stored at 4°C until analyzed.

4.3.2. Synthesis of Isotopically Labeled Internal Standard (IS)

The IS, d₄-artesunic acid, was synthesized by the base catalyzed esterification of dihydroartemisinin with d₄-succinic anhydride according to the scheme shown in Figure 4.1. A previously reported procedure^{248, 249} for the synthesis of artesunic acid was followed with some modifications, using dihydroartemisinin as the starting material. In a typical synthetic procedure, 250 mg of dihydroartemisinin were stirred for 2 minutes in 5 mL of tetrahydrofuran (THF). 125 mg of d₄-succinic anhydride and 500 µL of triethylamine were then added to the reaction flask and stirred for 3 hours at room temperature. At the end of the reaction, 20 mL of cold water, previously adjusted to pH4.0 using dilute acetic acid, was added to the mixture, and the pH finally adjusted to

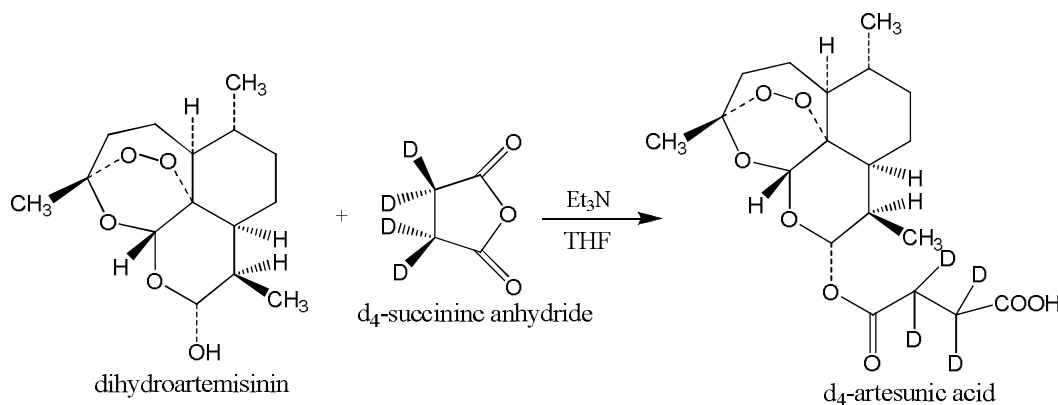


Figure 4.1. Reaction scheme for IS synthesis.

4.0. Product extraction was performed on ice using three separate 20 mL portions of 60:40 ethylacetate:hexane. The extract was washed with three 10 mL portions of chilled water previously adjusted to pH 4.0 and then dried over anhydrous sodium sulfate. The solvent was then evaporated in a Rotavap (30° C) to an estimated final volume of 5 mL, after which the solvent was swapped by 3 separate additions and evaporations of 10 mL portions of hexane. The solvent volume was then reduced to 3 mL, and left to evaporate to dryness in a hood at ambient temperatures. The crude product was purified by recrystallization in hexane. Purity was assessed by electrospray ionization MS of a 50:50 CH₃CN:H₂O solution containing 1 μM of the product in 100 μM DDA. Compared to similar analysis of an artesunic acid standard, which showed a peak at *m/z* 570 corresponding to [M + DDA + H]⁺ (Figure 4.2.a), the ESI spectrum of the reaction

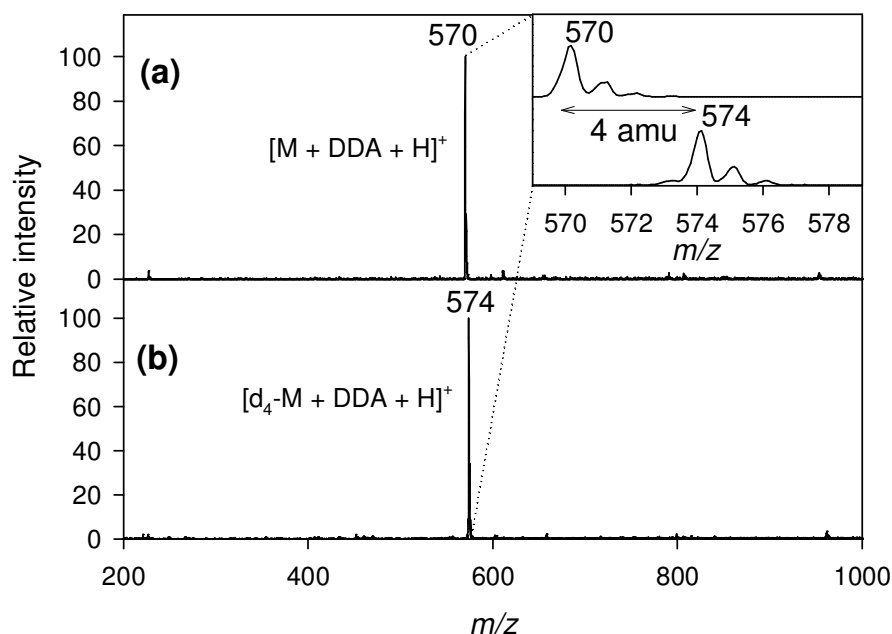


Figure 4.2. ESI spectra of 1 μM (a) artesunic acid standard, (b) reaction product from IS synthesis. M = artesunic acid.

product also showed predominantly a single peak at m/z 574 corresponding to $[d_4\text{-M} + \text{DDA} + \text{H}]^+$ (Figure 4.2.b). The detection of just one peak in the former indicates a high purity of the reaction product, which also showed the expected 4 mass unit shift relative to M (Insert Figure 4.2.a).

4.3.3. Preparation of Standard Artesunate Tablets

Standard artesunate tablets were prepared in collaboration with Dr. Sameer Late and Ajay Banga in the Department of Pharmaceutical Sciences, Mercer University. Artesunate tablet standards were composed of three major constituents: excipient mixture A, spray dried lactose, and artesunic acid. Excipient mixture A was composed of 69% microcrystalline cellulose, 1% fumed silicon dioxide (cab-o-sil), 5% talc, 20% croscarmellose sodium and 5% magnesium stearate. This mixture was prepared as follows: microcrystalline cellulose, cab-o-sil, and croscarmellose sodium were passed through a 20 mesh sieve and mixed together in a zip-lock bag for 5 minutes. Talc and magnesium stearate were also passed through the 20 mesh sieve, added to this bag and mixed with the other components for 2 minutes. Prior to tablet pressing, spray dried lactose, and artesunic acid were also passed through a 20 mesh sieve and mixed with excipient A in a zip-lock bag for 3 minutes. Tablets were composed of 20% excipient A, and variable amounts of artesunic acid and spray dried lactose to obtain tablets with variable properties such as hardness, amount of active ingredient, diameter, and shape. Tablets were pressed using a B2 rotary tablet press (Globe Pharma, New Brunswick, NJ) at 60 rpm. Tablet hardness was measured using a Monsanto hardness tester (Tab-Machines Ltd., Bombay, India).

4.3.4. Sample Pretreatment with IS and DESI MS

For quantitation purposes, all samples were treated with 25 μL of 100 mM IS in neat acetonitrile, unless stated otherwise. The IS solution was kept in a -80°C freezer at all times, and placed on ice during use to minimize evaporation. The preferred IS spiking method consisted of addition of the IS solution by pipette deposition, creating a thin solution film on the surface of the samples (Figure 4.3). The thin film then diffuses into the sample at a rate that was observed to be dependent on the tablet porosity. Samples were allowed to air dry at room temperature before analysis. This procedure is further discussed and compared to other IS deposition approaches in the Results section.

DESI MS was performed using the DESI ion source described in section 2.3.3, using settings similar as those described in section 2.3.4. The ion source was coupled to an LCQ DECA XP+ quadrupolar ion trap mass spectrometer (Thermo Finnigan, San Jose, CA), which auto tuned for optimum detection of the ion of interest. Reagentless

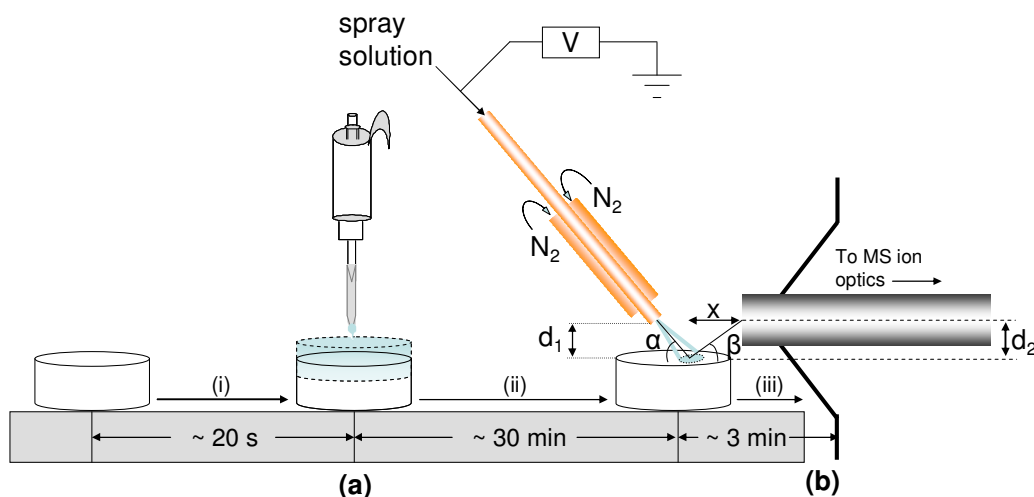


Figure 4.3. (a) Sample pretreatment with IS: (i) pipette deposition of a solution of d_4 -artesunic acid in neat acetonitrile onto the sample surface, (ii) air drying of sample after treatment with IS, and (iii) reactive DESI MS analysis of air-dried samples; (b) DESI MS interface showing various DESI set-up variables.

DESI MS was performed by spraying samples with a solution of 75:25 CH₃CN:H₂O. This solvent mixture was doped with 100 μM dodecylamine for reactive DESI experiments. For all experiments, the spray solution flow rate was set to 2 μLmin⁻¹ unless stated otherwise. Except for initial comparative investigations, all experiments were performed by reactive DESI. The mass spectrometer was set to acquire data in full scan mode via the Xcalibur software (version 2.0, Thermo Finnigan). The ion transfer capillary was set to 300°C. The instrument was set to collect spectra in automatic gain mode for an ion trap injection time of 200 ms at 2 microscans spectrum⁻¹. All DESI characterization experiments were performed using genuine artesunate tablets. The assessment of the effect of sample properties on the DESI signal, and the development of a calibration method were done using artesunate tablet standards with the same surface geometry as the genuine samples.

4.4. Results and Discussions

4.4.5. *Reagentless DESI vs. Reactive DESI of IS Treated Artesunate Tablets*

Figure 4.4 shows results of the initial investigation of the type of ionic species generated by reagentless and reactive DESI of IS treated artesunate tablets. Samples were pretreated with IS following the pipette deposition procedure depicted in Figure 4.3. Analysis by reagentless DESI MS shows peaks corresponding to various sodiated analyte and IS monomeric and dimeric species at m/z 407, 411, 791, 795 and 799 including a few fragment peaks (Figure 4.4.a). The spread of the analyte ion signal into various channels and the observed variation of relative intensity of the different adducts in-between experiments made it complicated to choose an ion peak for quantitative analysis. Similar

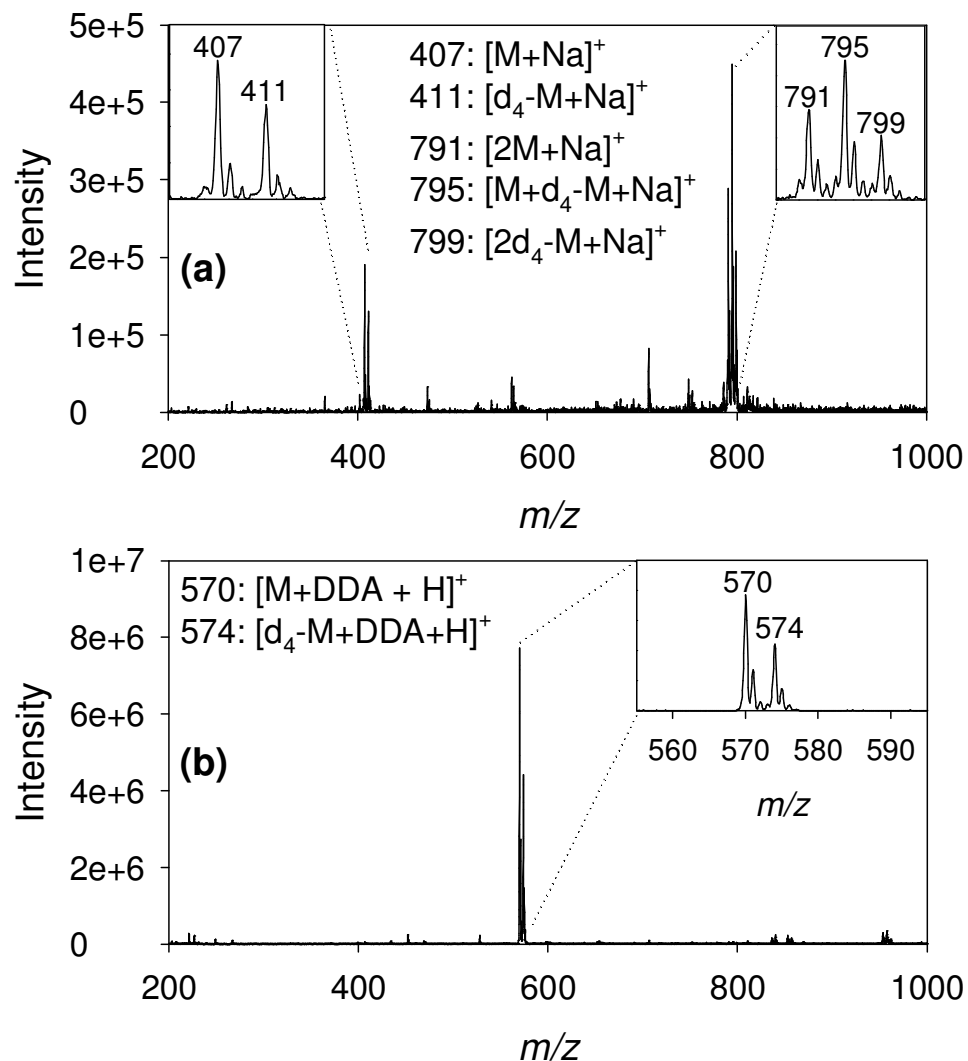


Figure 4.4. DESI spectra of genuine artesunate tablets pretreated with 25 μ L, 100 mM solution of IS following analysis in (a) reagentless DESI mode and (b) reactive DESI mode.

analysis of the IS treated genuine artesunate tablet by reactive DESI showed predominantly one peak for the analyte and one for the IS with close to two orders of magnitude improvement in signal intensity compared to reagentless DESI (Figure 4.4.b). The simplicity of the reactive DESI spectrum together with the improved sensitivity resulted in an easy choice of analyte ion signal for further quantitative analysis. As such all subsequent experiments were performed by reactive DESI MS.

4.4.6. Comparison of Internal Standard Deposition Methods

Various methods were explored for the pretreatment of sample with IS following quantitative investigations by DESI MS including: (i) pneumatically-assisted electrospray deposition, (ii) addition of IS directly into the DESI spray solution and, (iii) pipette deposition of neat acetonitrile IS solution. The performance of each of these deposition methods was assessed by evaluating the temporal stability of the signal intensity ratio of the ion at m/z 570 to that at m/z 574 at different spray solution flow rates and positions across the sample surface.

Nebulizer assisted electrospray deposition of IS resulted in a very unstable signal intensity ratio (Figure 4.5.a). The ratio rises very rapidly with time, suggesting that this deposition method results in a very thin coat of IS on the sample surface, but not sufficient interdispersion with the tablet surface material. This thin layer is quickly depleted by the DESI jet with the depletion rate increasing with spray flow rate. To obtain a uniform coat of material on the sample surface, this approach required very careful control of various variables including the nebulizer gas flow rate, the spray tip-to-sample surface distance, and the elimination of any air draft currents in the room where the sample was being processed. Because of these difficulties, it was quickly realized that it would be tricky to reproduce the amount of IS deposited on different samples, which would translate into a poor day-to-day reproducibility.

Addition of a small amount of IS to the reactive DESI spray solution also resulted in an unstable signal intensity ratio (Figure 4.5.b), with instabilities becoming more prominent at higher flow rates. Because the reactive DESI spray probes the same spot on the sample in this scenario, this spot becomes progressively contaminated by the IS

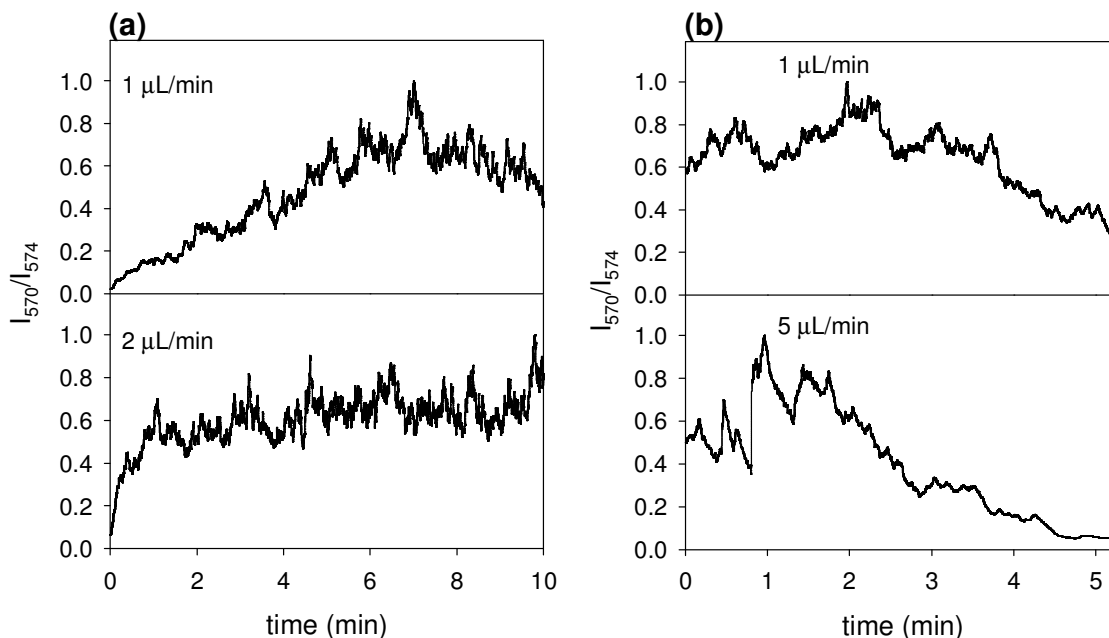


Figure 4.5. Normalized traces of the ion intensity ratio of the ion at m/z 570 to that at m/z 574 for various internal standard deposition methods at various DESI spray solution flow rates. (a) Spray deposition from a solution of 75:25 CH₃CN:H₂O (b) Doping of the DESI spray solution with the internal standard.

contained in the spray, which results in a decreasing analyte-to-IS signal ratio with time.

The method of choice adopted for these studies involved the pipette deposition of the IS dissolved in neat acetonitrile (Figure 4.3). After application of the IS, the acetonitrile solution flows across the sample surface forming a homogenous liquid thin film, which is then observed to diffuse into the sample. This process requires an estimated 20 seconds for a genuine artesunate tablet. No significant disintegration of the tablets was observed during this process. After deposition, the samples are allowed to air dry at room temperature. For consistency across tablets of different hardness, 30 minutes were allowed for this step, which doesn't necessarily decrease throughput significantly as several samples could be dried in parallel. Following IS deposition, 4 spots on the tablet surface were probed by reactive DESI, one on each tablet quadrant. Reactive DESI

analysis of four surface spots required an estimated 3 minutes per tablet with a manual x-y stage.

Reactive DESI analysis of samples spiked by this deposition method at various solvent flow rates ranging from 1-3 $\mu\text{L min}^{-1}$ resulted in analyte and IS ionic signals which basically tracked each other (Figure 4.6.a), resulting in a highly stable signal intensity ratio (Figure 4.6.b). Similar analysis at various nebulizer gas pressures from 100-200 psi resulted in an unstable time trace when the analyte and IS signal intensities were summed (Figure 4.7.a), but produced a stable signal intensity ratio at all nebulizer gas flow rates investigated (Figure 4.7.b). The intensity ratio was also found to be largely stable for different positions across the sample surface, with a relative standard deviation of 7.9% (n=5) which suggests a homogenous distribution of IS over the surface of the

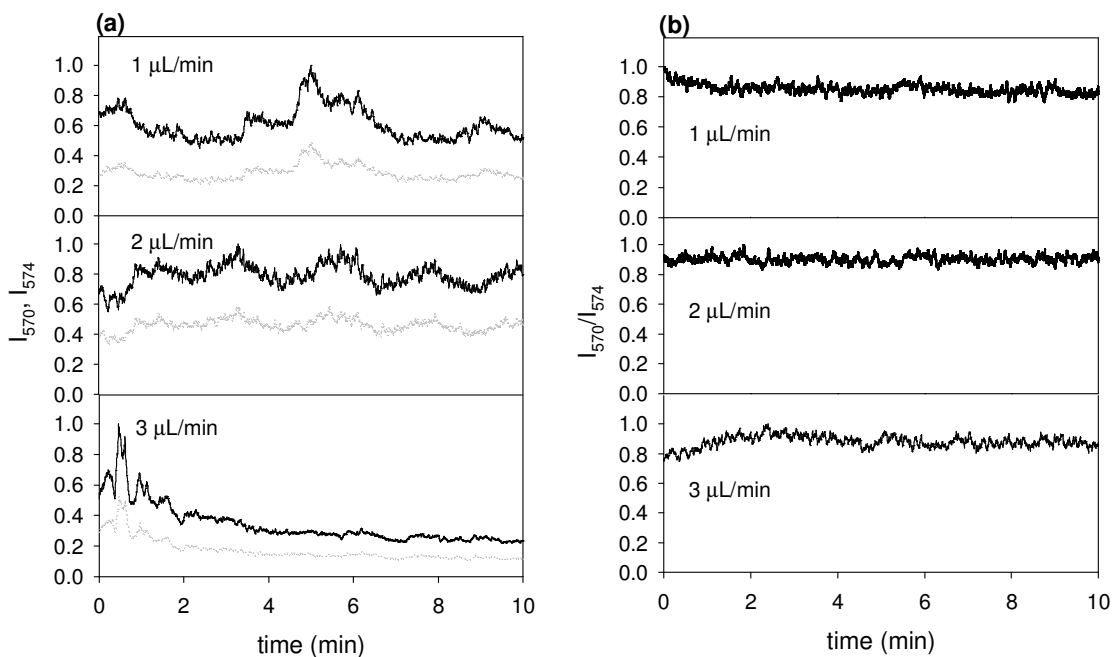


Figure 4.6. Normalized ion intensity traces at various solution flow rates by reactive DESI. (a) Relative intensity of ions at m/z 570 (black trace) and m/z 574 (gray trace), (b) intensity ratio of the ion at m/z 570 to that at m/z 574.

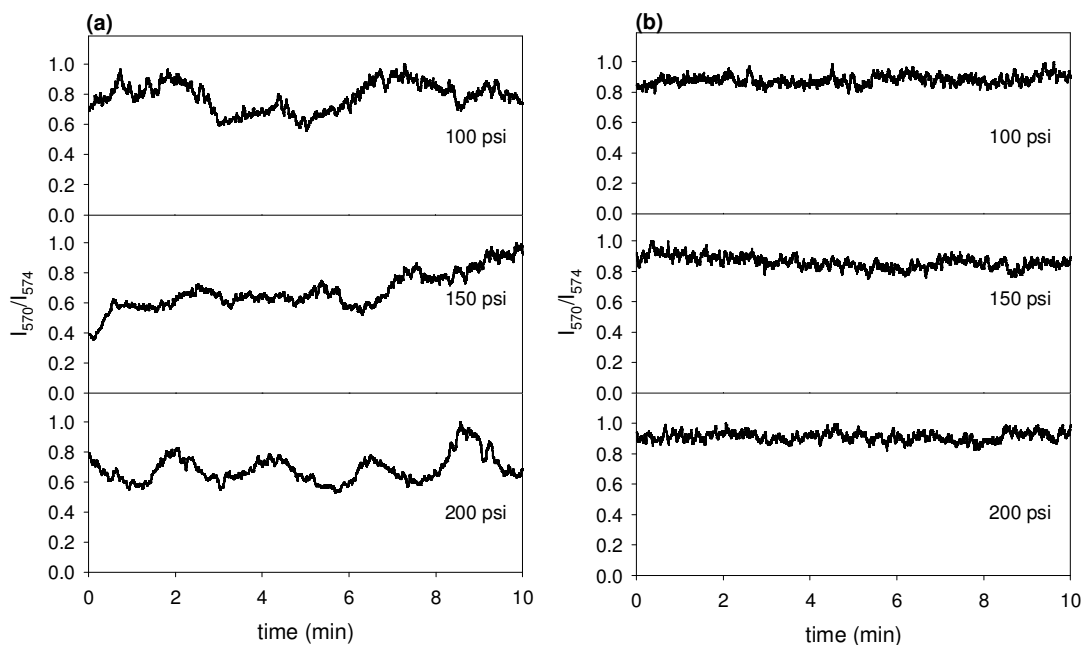


Figure 4.7. Normalized ion intensity traces at various nebulizer gas pressures by reactive DESI. (a) Sum of ion intensities generated from the ions at m/z 570 and m/z 574, (b) intensity ratio of the ion at m/z 570 to that at m/z 574.

sample. This ratio was also largely stable for a wide range of DESI spray flow rate and nebulizer gas pressures, with relative standard deviations of 5.1% ($n=7$) and 5.0% ($n=6$) respectively, as shown in Table 1. Depth profiling of a genuine artesunate sample treated with IS following the pipette deposition protocol showed a stable analyte-to-IS signal intensity ratio when the same spot on the sample was interrogated with the reactive DESI jet for up to 60 min. This resulted in a crater of approximately 0.3 mm in depth (Figure 4.8). This suggests a minimum penetration of the IS up to this depth. All subsequent experiments were performed by this IS deposition method at a DESI spray solution flow rate of $2 \mu\text{L min}^{-1}$ and a nebulizer gas pressure of 110 psi.

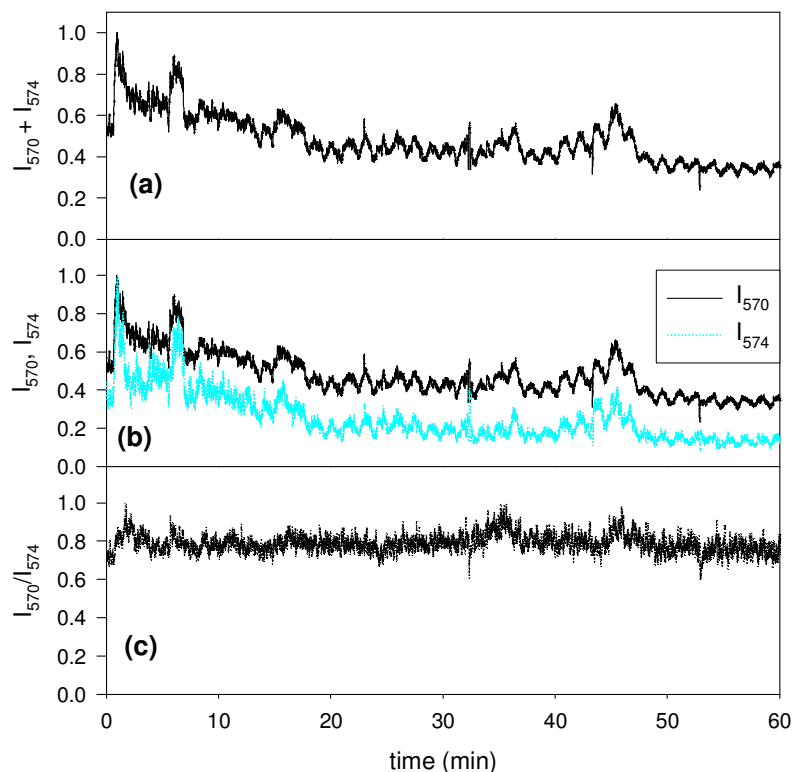


Figure 4.8. Depth profiling of a genuine artesunate tablet treated with a IS: (a) Sum of ion intensities of the ions at m/z 570 and m/z 574. (b) intensity of ions at m/z 570, and m/z 574 respectively, (c) intensity ratio of ion at m/z 570 to that at m/z 574. The intensity values were normalized for each plot.

4.4.7. Effect of DESI Geometrical Settings on the Analyte-to-Internal Standard Signal Ratio

Summarized in Table 1 below are results of the effect of the various experimental and DESI set-up variables including d_1 , d_2 , x , α , β on the analyte-to-IS signal intensity ratio in comparison to the absolute signal, as stated by their relative standard deviation. For the variables α and β , the relative standard deviations observed for the normalized signal intensity ratio were 11.4% ($n=6$) and 6.4% ($n=7$), as opposed to 82.1% and 72.6% respectively when the absolute signals were monitored. For the variables d_1 , d_2 and x , the observed relative standard deviations were 10.6% ($n=6$), 7.8% ($n=4$), and 8.8% ($n=6$) for

Table 4.1. Comparison of the reproducibility of the absolute DESI signal vs. the signal intensity ratio of analyte-to-IS for various DESI variables.

DESI Variable	RSD (%)	
	$I_{570} + I_{574}$	I_{570}/I_{574}
Solution flow rate	29.9	5.1
Nebulizer gas pressure	83.4	5.0
Tip-to-surface distance (d_1)	33.6	10.6
Spectrometer orifice-to-surface distance (d_2)	46.4	7.8
Sample-to-spectrometer orifice distance (x)	66.8	8.8
Spray incident angle (α)	82.1	11.4
Collection angle (β)	72.6	6.4

the signal intensity ratio as opposed to 33.6%, 46.4% and 66.8% respectively for the absolute signal. These results show lower relative standard deviations when the analyte-to-IS signal intensity ratio was monitored compared to the sum of the absolute signals corresponding to the analyte and IS. This indicates a significant independence of the analyte-to-IS intensity ratio for all DESI spray condition and geometrical parameters, and suggests the potential of this approach for the direct quantitative analysis of active ingredients in solid pharmaceutical tablets.

4.4.8. Effect of Sample Properties on the Analyte-to-Internal Standard Intensity Ratio

In Chapter 3, it was observed that the DESI signal shows appreciable dependence on various sample properties including hardness, surface morphology etc. Because of these dependencies, an investigation of the effect of each of these variables on the reactive DESI analyte-to-IS signal ratio is imperative in order to establish conditions under which robust quantitative results can be obtained.

Figure 4.9 shows the effect of sample hardness on the analyte-to-IS signal intensity ratio for artesunate tablet standards containing three different amounts of the active ingredient. All samples were treated with identical amounts of IS and analyzed by reactive DESI at a spray solution flow rate of $2 \mu\text{L min}^{-1}$. An almost linear decrease in signal intensity ratio was observed for hardness values below 5 kg. For harder tablets, the signal ratio becomes relatively constant, and depends on the analyte concentration. The IS solution was observed to percolates into the sample at a rate that depended on the sample porosity. Because the sample porosity increases with decreasing hardness, the IS percolates deeper and faster into the body of softer samples. The end result of this is a more “dilute” superficial IS zone for softer tablets resulting in a larger m/z 570 to m/z 574 signal intensity ratio following reactive DESI analysis. For samples prepared with hardness values larger than 5 kg, the results shown in Figure 4.9 suggest a quasi-constant

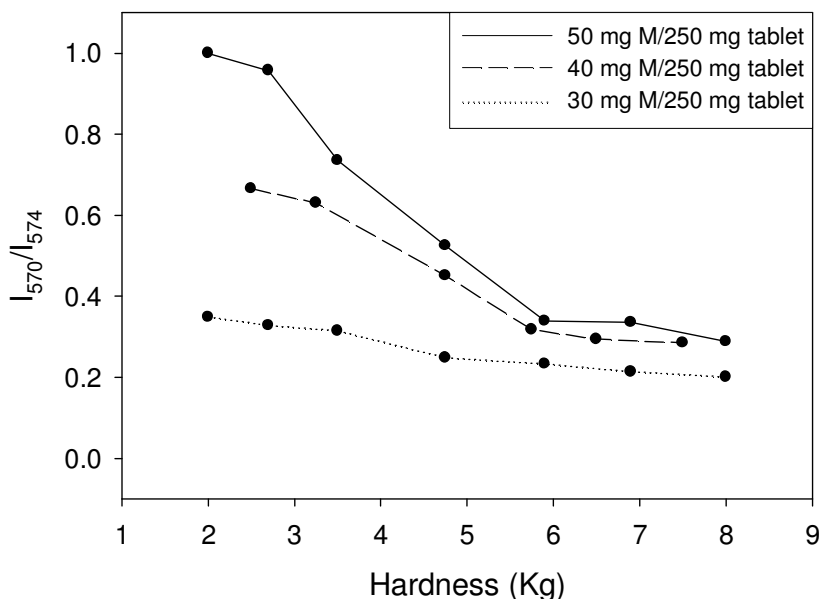


Figure 4.9. Dependence of the m/z 570 to m/z 574 ion intensity ratios following reactive DESI MS analysis of artesunate tablet standards with varying hardness. The intensity ratios were normalized to that of the maximum value.

degree of percolation of the IS into the tablet body. In this case, the rate of evaporative loss of the IS solution solvent is larger than the percolation rate, which determines the amount of material migrating into the tablet.

To further examine the distribution of the IS into the tablet sample, depth profiling analysis was performed at two different spray solvent rates (2 and $6 \mu\text{L min}^{-1}$) for samples prepared at three different hardness values (2.7 , 5.9 , and 8.0 kg , Figure 4.10). At $2 \mu\text{L min}^{-1}$ the analyte-to-IS signal ratio was stable, with relative standard deviations below 10% for all hardness values investigated. This indicated a homogenous distribution of the IS within the outermost tablet layers probed at this flow rate (Figure 4.10.a). Significant disintegration of the sample surface was not observed in this case. However, when the flow rate was increased to $6 \mu\text{L min}^{-1}$, the analyte-to-IS signal ratio was

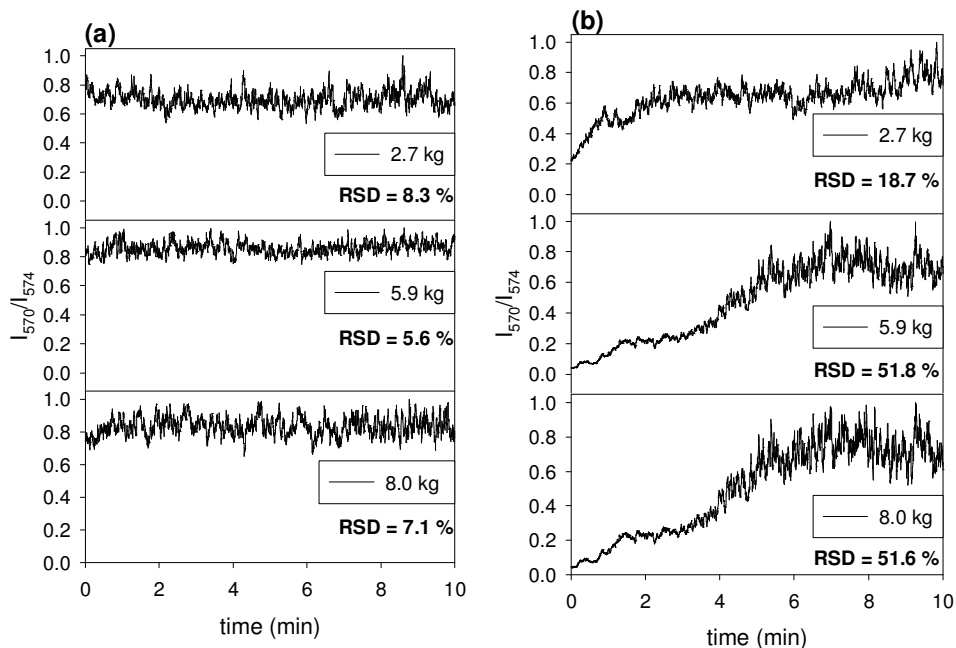


Figure 4.10. Depth profiling of standard artesunate tablets prepared at different hardness values. Samples were treated with $100 \mu\text{M}$ d_4 -artesunic acid followed by DESI MS analysis. Plots show the intensity ratio of the ion at m/z 570 to that at m/z 574 for different DESI spray solution flow rates including: (a) $2 \mu\text{L min}^{-1}$, (b) $6 \mu\text{L min}^{-1}$.

observed to gradually increase over time (Figure 4.10.b). This validates our hypothesis that a gradient of the IS is established within the tablet surface. Tablets with different hardness showed a different temporal evolution of the analyte-to-IS signal ratio due to differences in the rate at which the spray ablates the surface. To ensure optimum dissolution properties, and optimum dosage and absorption, pharmaceutical tablets are usually prepared with hardness lower than 5 kg. This means that the relative hardness of samples and standard must be used as a correction factor for performing quantitative DESI MS.

Quantitative analysis via pipette deposition of an IS solution requires that all samples be treated with the same amount of IS per unit tablet area. It was thus also necessary to evaluate the change in analyte-to-IS signal intensity ratio as a function of the surface area treated with IS. Figure 4.11.a shows results obtained from the reactive DESI analysis of duplicate tablets at two different diameters (9 and 11 mm) treated with identical amount of IS. The results indicate that the analyte-to-IS signal intensity ratio increases with increasing tablet diameter. The average intensity ratio of analyte-to-IS observed for 9 mm and 11 mm diameter, tablets containing 50 mg artesunic acid per 250 mg tablets were 4.5 and 7.7 respectively. Because in both cases the analyte solution is completely dispersed over the whole tablet surface, a lower amount of IS percolated per unit surface area when the tablet diameter was increased.

In addition to tablet diameter, the effect of tablet shape on the analyte-to-IS signal intensity ratio was investigated. Standard tablets of the same diameter, which had flat and convex topology were treated with identical amounts of IS solution and analyzed by reactive DESI. The results showed a negligible change in analyte-to-IS signal intensity

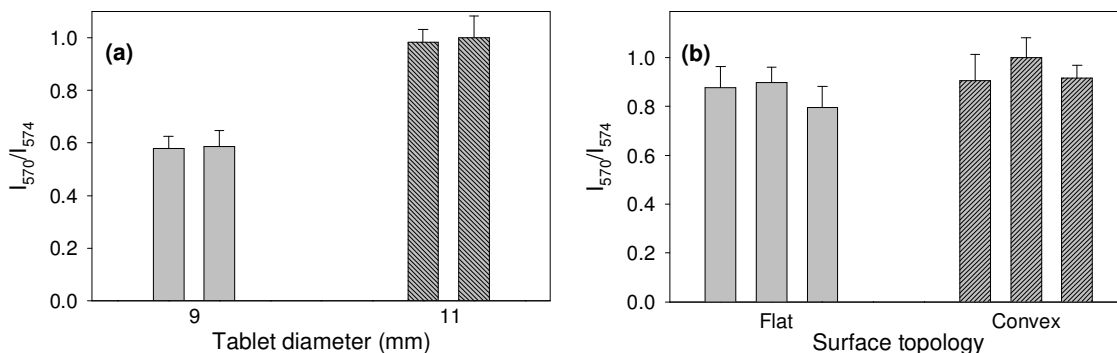


Figure 4.11. Dependence of the m/z 570 to m/z 574 ion intensity ratios following reactive DESI MS analysis of artesunate tablet standards with varying tablet surface (a) diameter, (b) topology.

ratio with convex tablets showing slightly higher ratios compared to flat ones (Figure 4.11.b). The observed average percentage increase in the intensity ratio was 9.9 %. This is probably due to the larger surface area of the convex sample which results in a lower amount of IS per surface area, and thus a higher analyte-to-IS signal intensity ratio.

4.4.9. Calibration and Direct Quantitation of Artesunic Acid in Pharmaceutical Tablets by Reactive DESI MS

The large independence of the analyte-to-IS signal intensity ratio observed for all DESI variables promises applicability of reactive DESI for direct quantitative screening. As a first step in establishing the quantitative capabilities of the approach proposed here, a calibration curve for the prediction of unknown samples was generated. This was done using 250 mg tablet standards with varying artesunic acid amounts, prepared at a hardness close to that of genuine samples (2.4 ± 0.2 kg), with a flat surface shape, and diameters of 9 mm (area=63.6 mm²). Three replicate tablets were prepared at each level of the active ingredient in the range 0.02-0.32 mg artesunic acid mg⁻¹ tablet. The

calibration curve showed good linearity over the investigated concentration range with a correlation coefficient of 0.9985 (Figure 4.12.a). The limit of detection defined as the analyte concentration giving a signal equal to the blank signal plus three standard deviations was calculated from the calibration curve to be equal to 0.018 mg artesunic acid mg^{-1} tablet (4.5 mg artesunic acid /250 mg tablet). A set of test samples, with amounts of artesunic acid that fell in the calibration curve range, was prepared for

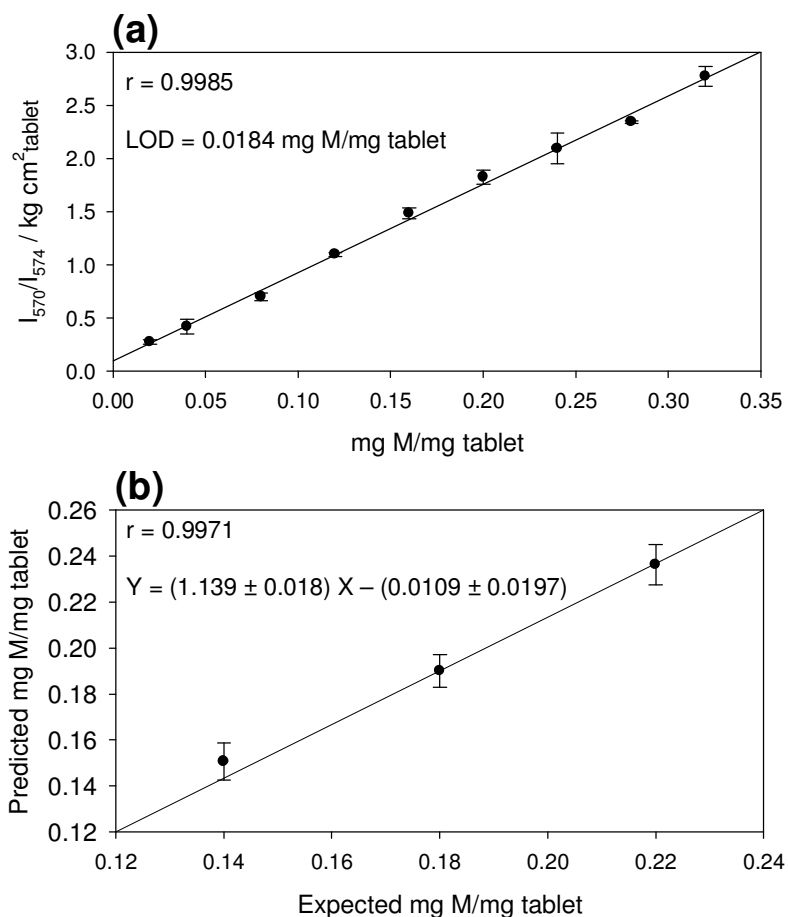


Figure 4.12. (a) Calibration curve obtained from standard samples prepared at a hardness of 2.4 Kg. The response is plotted as the signal intensity ratio divided by the product of tablet hardness by tablet surface area. (b) Method validation: plot of the amount of artesunic predicted from the calibration curve to the known amount present for a validation sample set. Error bars represent standard deviations for three different tablets. Each sample was probed on four quadrant and the signals averaged.

validation purposes. Results showed a good correspondence between the expected and the predicted amounts of artesunic acid present in the validation sample set, with a correlation coefficient of 0.9971, and y-intercept and slope values of 0.0109 ± 0.0197 and 1.139 ± 0.108 respectively (Figure 4.12.b). These results validate the applicability of this quantitative DESI MS approach to samples with known (or constant) hardness, surface area, and shape, such as those encountered in a quality control laboratory setting.

A more challenging application of this DESI approach is the quantitation of active ingredients in samples with hardness not exactly matched to the calibration standards. This would be the case, for example, of drugs suspected of being counterfeit which are collected in the field for further off-field forensic analysis. The performance of the proposed quantitative approach was assessed using three different artesunate tablet samples from Mekophar pharmaceutical collected in the field. The samples had a measured hardness of 2.7 ± 0.2 kg and diameter of 10.1 mm. The samples were treated with IS solution and analyzed by reactive DESI against a calibration curve created with standard tablets. The calibration sample set had a hardness of 2.4 ± 0.2 kg and diameter of 9 mm. Table 2 summarizes the results of these analyses. An average relative standard deviation of 6% was obtained for the predicted amount of artesunic acid present in the three samples, which compares relatively well with the 2% observed for HPLC analysis. Comparison of the predicted amount of artesunic acid to the amount determined by HPLC showed significant deviations (35% on average) if uncorrected by tablet hardness and surface area. Upon normalization of the sample DESI analyte-to-IS signal ratio by the tablet hardness and surface area, and comparison to the 50 mg/tablet standard, the difference between the artesunic acid amount determined by DESI and the expected

Table 4.2. Quantitation of artesunic acid in genuine sample by DESI MS compared with the expected amount present in the sample.

Sample	Artesunic acid (mg tablet ⁻¹)		
	Predicted with no correction	Predicted with correction	HPLC
Tablet 1	73 ± 4	58 ± 3	53 ± 2
Tablet 2	73 ± 5	58 ± 4	56 ± 2
Tablet 3	68 ± 4	53 ± 3	50 ± 2

amount was reduced to 6% on average. This is a clear indication that the sample physical properties play a critical role in quantitative analysis by DESI. When corrected, the average accuracy obtained by reactive DESI MS quantitation can be considered sufficient for determining active ingredient content with a good degree of accuracy (94%) which is acceptable for a high throughput pharmaceutical screening assay such as this.

4.5. Conclusions

This study demonstrated the capability of reactive DESI MS as a high throughput quantitative approach for the direct screening of antimalarial tablets. The controlled deposition of an internal standard enables to perform quantitative measurements independent of the DESI set-up variables. The method shows a precision of 6% (n=4) and an accuracy of 94% which is largely acceptable for the *rapid* quantitation of active ingredients in drug tablets. Sample hardness and surface area are important factors to be taken into account when implementing this method. Although correction schemes to take into account, tablet hardness and shape are feasible it is preferable that whenever possible, the calibration sample set has the same characteristics as the unknowns.

**CHAPTER 5. DESI REACTIONS BETWEEN HOST CROWN
ETHERS AND THE NEURAMINIDASE INHIBITOR
OSELTAMIVIR FOR THE RAPID SCREENING OF TAMIFLU[®]**

5.1. Abstract

This chapter presents an extension of the application of DESI MS to the development of a rapid screening method for other popular drugs, which are also being counterfeited. This is the case for Tamiflu[®], which contains oseltamivir as the active ingredient. Oseltamivir is an orally active neuraminidase inhibitor antiviral commonly administered as treatment for the avian influenza and swine flu. The high cost and demand of this drug around the world has made it a target for counterfeiters requiring the development of rapid and sensitive tools for Tamiflu[®] authentication. In this study, competitive host-guest chemistry on a DESI MS platform is presented as the basis for a rapid and quantitative screening method for assessing the quality of Tamiflu[®] capsules. The method is based on the selective recognition of oseltamivir by crown ethers added to the DESI spray solvent. Crown ethers with various ring sizes were evaluated, all being observed to form stable host-guest complexes with oseltamivir. Competitive experiments with various pairs of crown ethers were used to assess their relative binding selectivities for oseltamivir. The abundance ratio of the formed complexes was observed to be dependent on the amount of analyte present on the surface of the sample, and independent of DESI geometric factors. These competitive reactions were then successfully tested as a means for the rapid quantitation of oseltamivir in field-collected Tamiflu capsules by reactive DESI MS without the need for an internal standard.

5.2. Introduction

The 20th century witnessed three influenza outbreaks, with the most devastating occurring during the 1918-1920 period, believed to be responsible for an estimated 20-50 million deaths. The recent outbreaks of the avian influenza, H5N1 and the pandemic swine influenza, H1N1 have rapidly increased the demand for neuraminidase inhibitor antivirals, with stockpiling leading to shortage of supply. With Tamiflu[®] being the leading orally-active antiviral in the market,²⁵⁰ its high cost and demand quickly made it a preferred target for drug counterfeiters. Reports of counterfeit Tamiflu[®] capsules, which were shown to not contain oseltamivir, but vitamin C, have already appeared.²⁵¹ Current pandemic preparedness plans rely on strategies for influenza control based on the wide distribution of effective medication. Thus, reports of counterfeit Tamiflu[®] have led to an urgent need for rapid and sensitive authentication tools to ensure the quality of the drugs available to the public and healthcare authorities.

The quality of Tamiflu[®] capsules has been previously assessed using standard drug testing methods based on high performance liquid chromatography (HPLC),²⁵² thin layer chromatography combined with disintegration assay²⁵³ and colorimetric authentication tests for field drug quality screening.²⁵⁴ However, chromatographic methods suffer from low sample throughput, and many TLC or colorimetric tests are meant only to provide a pass/fail response, but are not designed to unequivocally identify unknowns or for failsafe selectivity. In this study, crown ether host-guest chemistry in a reactive DESI MS platform is being explored as an alternative approach for the rapid, sensitive and selective detection of oseltamivir in pharmaceutical preparations. The formation of a specific noncovalent complex, coupled with consecutive reaction

monitoring (CRM) mode; where an oseltamivir fragment generated by an MS/MS/MS experiment is monitored, ensures the highest degree of selectivity. This is useful in qualitative pass/fail forensic experiments where the presence or absence of the correct active ingredient is assessed.

In order to gain more insight of the products formed during reactive DESI, the relative gas phase stability of crown ether-oseltamivir complexes was studied via *ab initio* calculations and breakdown curve experiments. Taking advantage of competitive reactions between two crown ethers with different affinities for oseltamivir, a linear relationship was obtained between the logarithmic ionic signal intensity ratio and the amount of oseltamivir present or deposited on a solid substrate, enabling the acquisition of rapid semi-quantitative results without the need for an internal standard.

5.3. Experimental Details

5.3.1. Reagents and Samples

All reagents were used as acquired. High purity HPLC grade methanol and acetonitrile, 99.9⁺% (Honeywell Burdick & Jackson, Muskegon, MI) were used for DESI and reactive DESI experiments. Ultrapure water (18.2 MΩ cm⁻¹) was obtained from a Nanopure purification unit (Barnstead, San Jose, CA). The crown ether hosts: 12-crown-4 (12-C-4), 15-crown-5 (15-C-5) (Alfa Aesar, Ward Hill, MA), 18-crown-6 (18-C-6) (TCI America, Portland, OR) and 2,5-dibenzo-21-crown-7 (2,5-DB-21-C-7) (Acros Organics, Morris Plains, NJ) were used for reactive DESI experiments. Genuine Tamiflu[®] capsules stated to contain 75 mg oseltamivir free base per capsule (166±4 mg ea.) and pharmaceutical grade oseltamivir phosphate, used for characterization and optimization

studies were a generous donation from Roche Pharmaceuticals. Depicted in Figure 5.1 are the structures of oseltamivir (Figure 5.1.a) and the crown ethers evaluated in this study (Figure 5.1.b). The excipients mixture described in section 4.3.3 was used in preparing reserpine (Sigma Aldrich Corp., St. Louis, MO) tablets for hardness optimization studies. Tamiflu[®] samples were purchased over the Internet according to the collection protocol described by Green *et al.*²⁵⁴ All the samples were in capsule form and stated to contain 75 mg of oseltamivir free base per capsule. Quantitative DESI MS measurements were validated by HPLC analysis of the same samples. HPLC analysis was performed by Dr. Michael Green in the Division of Parasitic Diseases, Center for Disease Control and Prevention (CDC), using the method described by Green *et al.*²⁵⁴ All samples were stored at 4°C until analyzed.

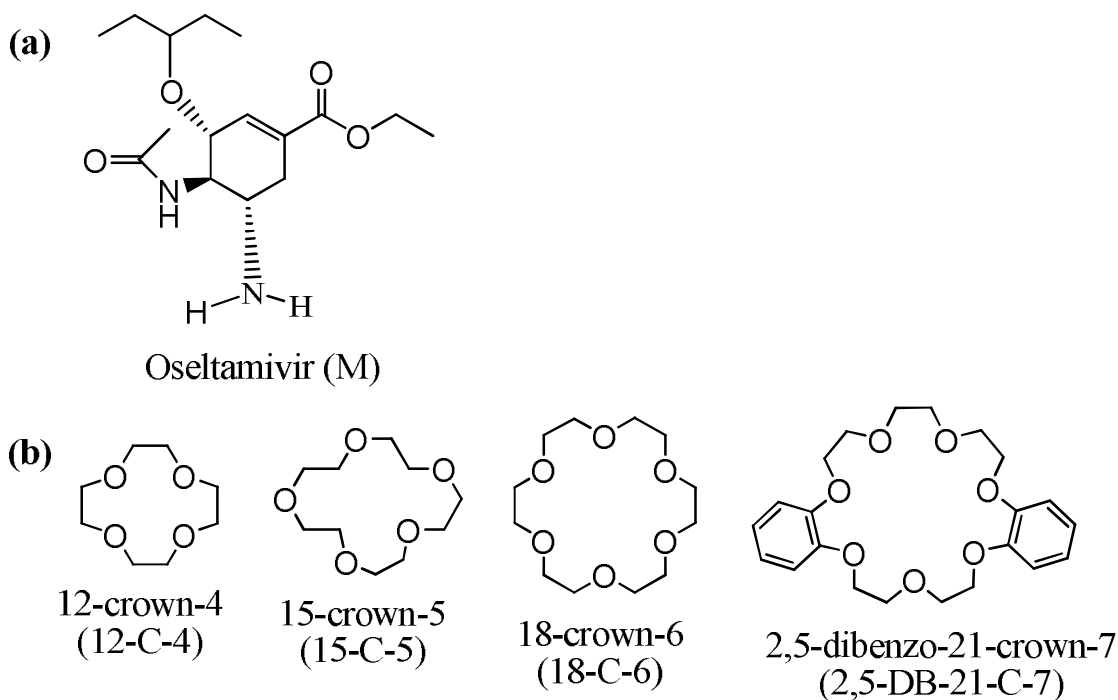


Figure 5.1. Structures of (a) oseltamivir and (b) crown ethers investigated in this study.

5.3.2. Substrates and Samples Preparation

Polytetrafluoroethylene (PTFE) substrates were prepared by cutting a PTFE rod (McMaster-Carr, Atlanta, GA) into 2.6 mm thick, 9.6 mm diameter discs. Disc surfaces were finished by rubbing on 220C grit sand paper (Norton Abrasives, Worcester, MA). PTFE discs were then sonicated in acetone, rinsed extensively in acetonitrile, and allowed to air dry prior to use. Glass substrates were made in an in-house glass shop by cutting a glass rod into 3.9 mm thick, 9.1 mm diameter discs with one of their surfaces etched. These were cleaned by the same procedure as with the PTFE substrates. Unless stated otherwise, glass or PTFE substrates were spotted with 10 μ L of 1 mg/mL of an oseltamivir phosphate standard solution and allowed to air dry prior to analysis. The diameter of sample spots on the PTFE surface was 4.6 ± 0.3 mm and on the glass surfaces 9.1 ± 0 mm. Tamiflu[®] capsules were pressed using a KBr press (Int. Crystal Labs., Garfield, NJ) in 7 mm dyes at a hardness of 73 ± 7 kg/m² unless stated otherwise.

5.3.3. DESI MS

A custom-built DESI ion source with imaging capabilities, described in section 6.3.2, was interfaced to an LCQ DECA XP+ QiT MS (Thermo Finnigan, San Joss CA), and used for all experiments. The ion source and mass spectrometer were operated using settings similar to those described in section 2.3.3 and 4.3.4 respectively. Briefly, the ion source consisted of a motorized stage (Prior Scientific, Rockland, MA) for sample positioning and high performance sprayer mounted on an XYZ manual translation stage (Thorlabs, Newton, NJ) for spray positioning. The spray solvent flow rate was set to 5 μ L/min and was biased to +3 kV for all experiments.

The standard LCQ ion transfer capillary was replaced by an extended version (762 μm i.d., 1588 μm o.d., Small Parts Inc., Miramar, FL). All experiments were performed in positive ion mode. Data were acquired via the Xcalibur software (version 2.0, Thermo Finnigan) for a total acquisition time of 15 s unless stated otherwise. All experiments were performed using high purity acetonitrile (99.9+%) as the spray solvent unless stated otherwise. Initial characterization experiments were performed by adding 100 μM of each of the crown ethers investigated to the DESI spray solvent. For competitive reactive DESI experiments, equimolar concentrations of various crown ether pairs were utilized. Mass spectral data were collected on 4 different spots (one on each quadrant) of the sample and averaged. A 10 μM 15-crown-5 and 5 μM 18-crown-6 solution was used for oseltamivir quantitation.

5.3.4. Computational Calculations

Computational calculations were performed by Edward Hohenstein, a graduate student in Dr. Sherrill's group in the School of Chemistry and Biochemistry, Georgia Institute of Technology. Binding energies for complexes of oseltamivir with 12-crown-4, 15-crown-5, 18-crown-6, and 2,5-dibenzo-21-crown-7 were computed at the B3LYP-D/6-311++G** level of theory,²⁵⁵ where the “-D” denotes the inclusion of empirical terms to account for the dispersion interactions neglected by the B3LYP functional.²⁵⁶ The counterpoise correction scheme of Boys and Bernardi was applied in the computation of binding energies.²⁵⁷ Complex geometries were fully optimized at the B3LYP-D/6-31G** level of theory while including the empirical dispersion correction.

The proton affinities were computed at the B3LYP-D/6-31G** level of theory. Computations were performed using PS13,²⁵⁸ Q-CHEM²⁵⁹ and Jaguar.²⁶⁰

5.4. Results and Discussion

5.4.5. *Effect of Spray Solvent Composition/Substrates on DESI MS Signal*

The development of any DESI MS methodology requires considerations on several factors including spray solvent composition and flow rate, choice of substrate material, and solvent used to deposit the analyte. Particularly important in this study was the choice of the DESI spray solvent. Exploratory experiments were performed with various solvents containing 100 μ M 18-crown-6 to probe oseltamivir standards deposited onto PTFE substrates. It was observed that solvent mixtures containing water or methanol, regardless of their proportion, resulted in the formation of competitive crown ether complexes with ubiquitous metal cations such as Na^+ and K^+ . Crown ethers are well known to form stable complexes with these alkali metal ions, which survive in the gas phase.²⁶¹ Na^+ and K^+ compete with oseltamivir for the formation of crown ether complexes, limiting the amount of reagent available for reaction with the analyte, potentially reducing the analyte signal, and complicating the mass spectrum. Neat, high purity acetonitrile (99.9+%) was chosen as the spray solvent of choice due its negligible alkali metal ion content. Acetonitrile is also know to coordinate metal cations including Na^+ and K^+ ,^{262, 263} thus its use as reactive DESI spray solvent may assist in sequestering these cations. This potentially allows effective reactivity of the crown ether with the analyte. Because of its aprotic nature, acetonitrile is also supposed to cause minimum interference with the hydrogen bonding interactions between the crown ether hosts and

analyte.²⁶⁴ In terms of the sample deposition substrate, PTFE discs were observed to show negligible signal for crown ether-alkali metal complexes. This was not the case for etched glass substrates. This was possibly due to the metal ions intrinsically present in glass compositions. As such, all following characterization experiments were performed using PTFE surfaces and neat acetonitrile as the DESI spray solvent.

5.4.6. Conventional vs. Reactive DESI MS of Oseltamivir Standards

Preliminary investigations involved performing the analysis of oseltamivir phosphate standards in the conventional (i.e reagentless) DESI MS mode, for subsequent comparison with reactive DESI MS experiments. Figure 5.2.a shows results from this analysis. It was observed that the analyte ion signal was spread into a variety of channels corresponding to various oseltamivir species with the most abundant being the protonated monomer at m/z 313. The peak at m/z 625 corresponds to the proton-bound dimer. Various oseltamivir fragment ions generated by in-source decay, can also be observed in the spectrum. The peak at m/z 225 corresponds to the loss of the 3-pentanol side chain (A) to give the $[M-A+H]^+$ species, while the peak at m/z 208 corresponds to the loss of the 3-pentanol side chain and ammonia (B) thus giving the species $[M-A-B+H]^+$. An ion at m/z 166 corresponding to the loss of 3-pentanol and acetamide (C) to give the species $[M-A-C+H]^+$ was also detected. The observation of these fragment ions generated by in-source decay suggests a certain lability of the protonated monomer. Fragment ion connectivity was further investigated by performing MS/MS and MS/MS/MS analyses by collision-induced dissociation (CID). MS/MS analysis of the protonated oseltamivir monomer (m/z 313) generated predominantly the ion at m/z 225 (Figure 5.2.b). Minute

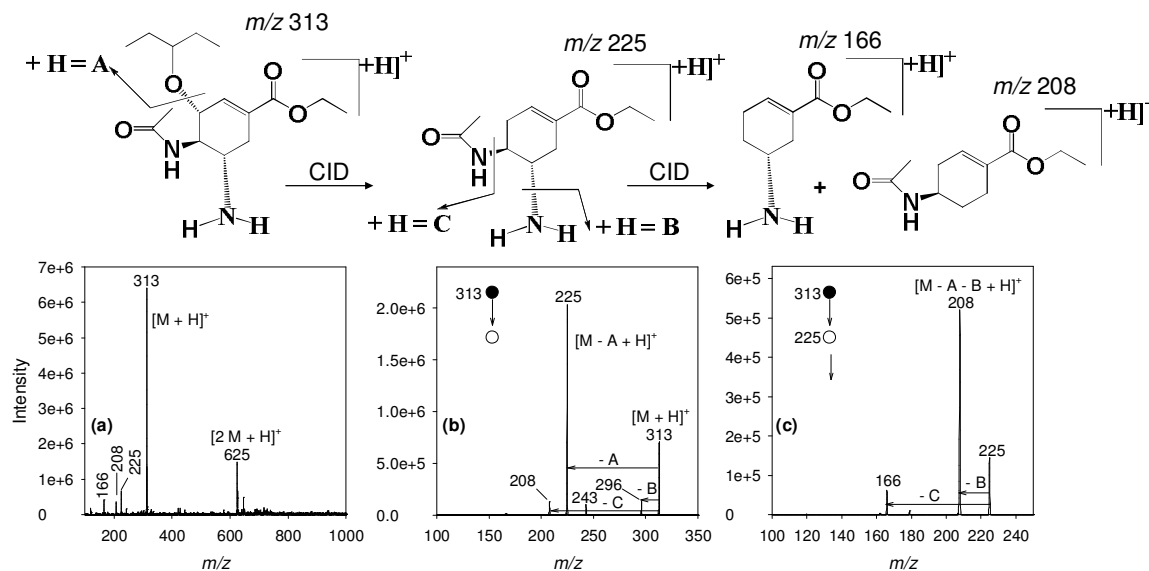


Figure 5.2. DESI spectra of oseltamivir phosphate standard (10 μ L, 1mg/mL) deposited onto PTFE surfaces and interrogated with a solution of neat acetonitrile; (a) Full MS spectrum, (b) MS/MS of the precursor ion at m/z 313, (c) MS/MS/MS of the precursor ion at m/z 225. M = oseltamivir, A = 3-pentanol ($C_5H_{12}O$), B = ammonia (NH_3), C = acetamide (C_2H_5NO).

peaks at m/z 296 (loss of ammonia) and m/z 208 can also be seen in this spectrum. MS/MS/MS analysis on the fragment ion at m/z 225 resulted in signals at m/z 208 and m/z 166, which correspond to the losses of ammonia and acetamide respectively (Figure 5.2.c). The formation of the ions at m/z 208 and 166 from their precursor (m/z 225) is a competitive reaction, indicating that the charge in the protonated oseltamivir monomer probably shuttles between the primary amine and acetamide side chains. This assertion was also suggested by the B3LYP-D/6-31G** optimized structures of the protonated oseltamivir molecule where an intramolecular hydrogen bond was observed to bridge the primary amine nitrogen and the oxygen of the acetamide side chain (Figure 5.3). The greater abundance of the ion at m/z 208 observed in the MS/MS/MS spectrum is probably due to the greater leaving group lability of ammonia compared to acetamide.

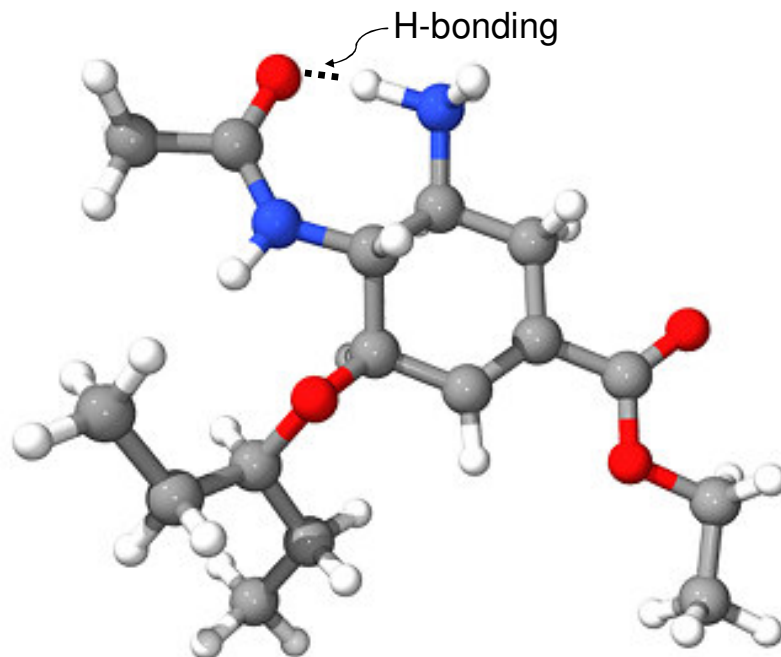


Figure 5.3. Optimized structure of the protonated oseltamivir molecule from *ab initio* molecular modeling calculations.

The spread of the analyte signal intensities due to in-source fragmentation and formation of dimer species in reagentless DESI complicates the mass spectrum and potentially result in insufficient sensitivity for detecting oseltamivir. Furthermore, because the active ingredients in pharmaceutical formulations are embedded in an excipient mixture, the matrix components could compete with the analyte for charge, potentially reducing the analyte signal. These complications were circumvented by performing the experiments in the reactive DESI MS mode where crown ethers were added to the spray solvent to serve as selective recognition agents for analyte signal enhancement. Various crown ethers including 12-C-4, 15-C-5, 18-C-6 and 2,5-DB-21-C-7 (Figure 5.1.b) were assessed for the detection of oseltamivir by reactive DESI MS. Figure 5.4 shows spectra obtained by probing oseltamivir phosphate standards deposited onto PTFE surfaces with spray solutions containing 100 μM of crown ethers in neat

acetonitrile. All crown ethers investigated generated exclusively 1:1 complexes with oseltamivir and were the predominant species. Figure 5.4.a shows the spectrum obtained when 12-C-4 was added to the spray solvent as host. A peak at m/z 489 is evident in the spectrum corresponding to the species $[M+(12-C-4)+H]^+$. In Figure 5.4.b, the crown ether 15-C-5 was employed as host, and a peak at m/z 533 corresponding to a protonated

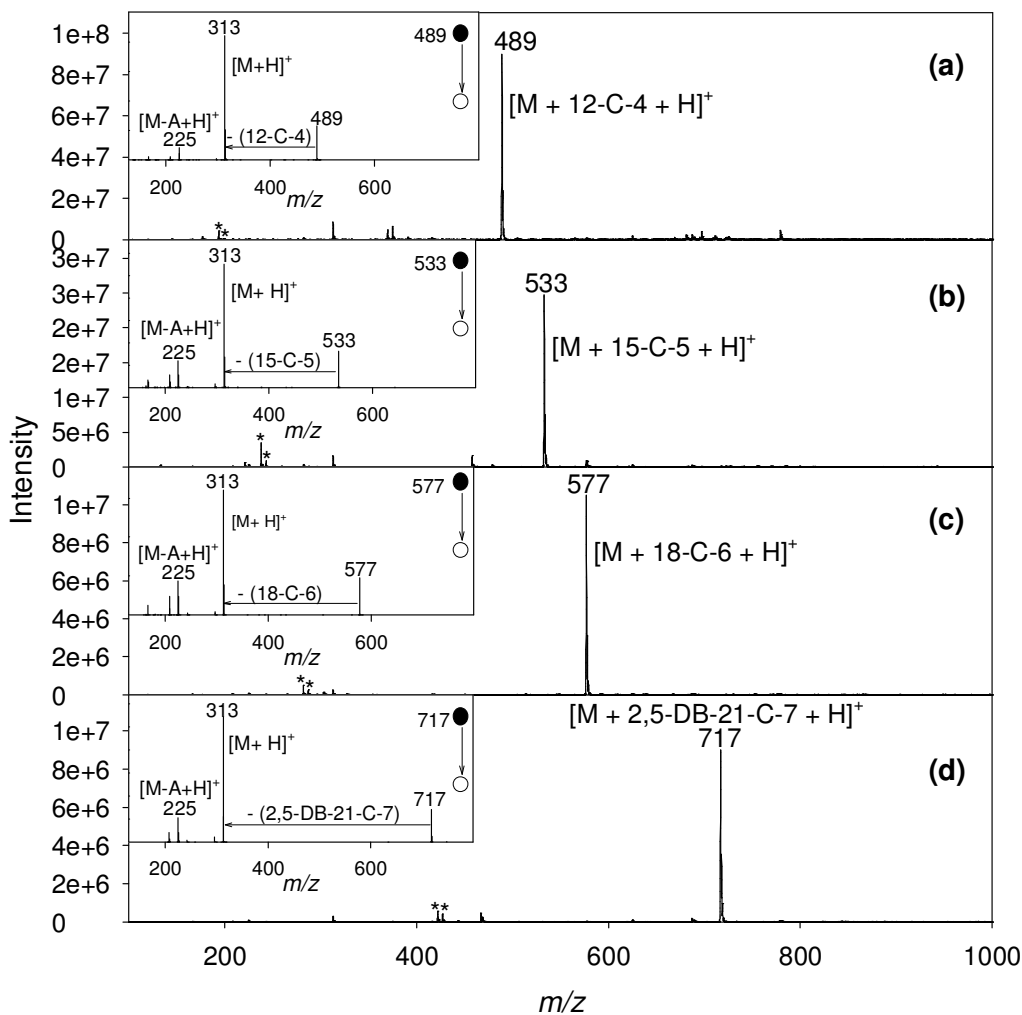


Figure 5.4. Reactive DESI of oseltamivir phosphate standard (10 μ L, 1mg/mL) deposited onto PTFE surfaces and interrogated after solvent evaporation with a solution of 100 μ M of (a) 12-crown-4, (b) 15-crown-5, (c) 18-crown-6 and (d) 2,5 dibenzo-21-crown-7. The inserts represent the corresponding MS/MS spectra of the $[M + \text{crown ether} + H]^+$ ions at m/z 489, 533, 577, and 717 respectively. M = oseltamivir, A = 3-pentanol ($C_5H_{12}O$).

1:1 complex between this host and oseltamivir was observed. With 18-C-6 as host, an ion at m/z 577 generated by reactive DESI was also detected (Figure 5.4.c). This ion corresponds to the species $[M+(18-C-6)+H]^+$. Figure 5.4.d shows the reactive DESI spectrum where 2,5-DB-21-C-7 was employed as host. A peak at m/z 717 corresponding to the species $[M+(2,5-DB-21-C-7)+H]^+$ was observed. Some low abundance signals (indicated by an asterisk) were also observed, assigned as complexes of the corresponding crown ethers with NH_4^+ and Na^+ . These signals originate from impurities present in the spray solvent or the reagents used, or from small amounts of dust in the ambient lab environment. The signal for the ammonium complex could also be due to decomposition of the spray solvent. However, these signals are very minute and largely negligible.

The formation of complexes between oseltamivir and crown ethers occurs by hydrogen bonding interactions between the protonated oseltamivir primary amine moiety and hydrogen bond acceptors in the crown ethers. As previously discussed, the charge in the protonated oseltamivir species seems to shuttle between the primary amine and acetamide side chains. However, complex formation with crown ether leads to localization of the charge on the primary amine group. This assertion was supported by B3LYP-D/6-31G** optimized structures of the protonated oseltamivir-crown ether complexes, where the charging proton was observed to be closer to the primary amine side chain than to the acetamide side chain. Localization of the positive charge on the amine leads to an overall improvement in the stability of the analyte, and reduced in-source CID fragmentation. Also, complex formation results in an increase in the number of degrees of freedom for the molecule, also decreasing fragmentation rates. In addition,

the formation of oseltamivir-crown ether complexes appears to increase their surface activity; increasing ion yields, and allowing an improved sensitivity for oseltamivir detection. The increased ion yields may also be due to the tendency of the crown ether to strongly localize the charge on the complex, inhibiting oseltamivir deprotonation in solution. These two combined effects are evident from the higher signals observed in the reactive DESI spectra, when compared to reagentless DESI. Sensitivity gains of 14x, 3.9x, 1.6x and 1.4 x were observed respect to reagentless DESI when 12-C-4, 15-C-5, 18-C-6 and 2,5-DB-21-C-7 were used as reactive DESI reagents, respectively. For these four reagents, the S/N gains observed were 10x, 13x, 10x and 13x, resulting in detection limits of 0.3, 0.2, 0.3 and 0.2 mg oseltamivir/capsule respectively. The observed detection limit for reagentless DESI was 3.3 mg/capsule.

The inserts in Figure 5.4.(a-d) show the tandem MS spectra for each of the $[M+\text{crown ether}+\text{H}]^+$ precursor ions. Following ion activation, the neutral crown ether is readily lost from the complex generating predominantly the protonated analyte species. The charge stays exclusively with the analyte in this case due to its higher proton affinity compared to all crown ethers investigated (see Table 5.1). The peak at m/z 225 corresponding to an oseltamivir fragment was also observed. However, no peaks corresponding to oseltamivir fragment species were observed in the full scan reactive DESI spectra. This indicates that the interaction of oseltamivir with the assayed crown ethers is sufficiently strong to form stable gas phase complexes which survive transport through the mass spectrometer atmospheric pressure interface and can only be dissociated following activation in the ion trap.

5.4.7. Gas Phase Stability of Oseltamivir -Crown Ethers Complexes

The analysis of binding selectivities to determine which crown ether most selectively binds oseltamivir provides valuable information for quantitative applications, which require the detection of this molecule in an excipient matrix. It is well known that binding selectivities are largely determined by the relative thermodynamic stability of complexes formed between crown ethers and various guest molecules.²⁶⁵ Energy resolved collision induced dissociation was used to establish the relative dissociation energies of oseltamivir with various crown ethers. CID was performed for 2.5 ms. Short activation times, typically below 10 ms are known to result in a linear relationship between the threshold activation voltage and the minimum dissociation energies of complexes.^{266, 267} Longer activation times may allow ions with a small excess of internal energy to decay. Fragmentation efficiency curve analysis of each of these complexes was performed on the same day to minimize any effects caused by instrumental variation.²⁶⁷ Figure 5.5 shows the obtained fragmentation efficiency curves. The $E_c^{50\%}$ values, which represent the activation energy at which half of the isolated complex has been dissociated, are presented in Table 5.1. It is well known that compounds with more degrees of freedom (DOF), require more energy to break a bond within the same time frame. As such, the $E_c^{50\%}$ values were also corrected for DOF differences with the oseltamivir-12-C-4 complex, chosen as reference.^{267, 268} These values are presented in parenthesis in Table 5.1. The binding energies for each of these complexes obtained from B3LYP-D/6-311++G** computations together with the proton affinities²⁶⁹ and cavity size²⁴⁴ for each of the crown ethers are also presented in Table 5.1.

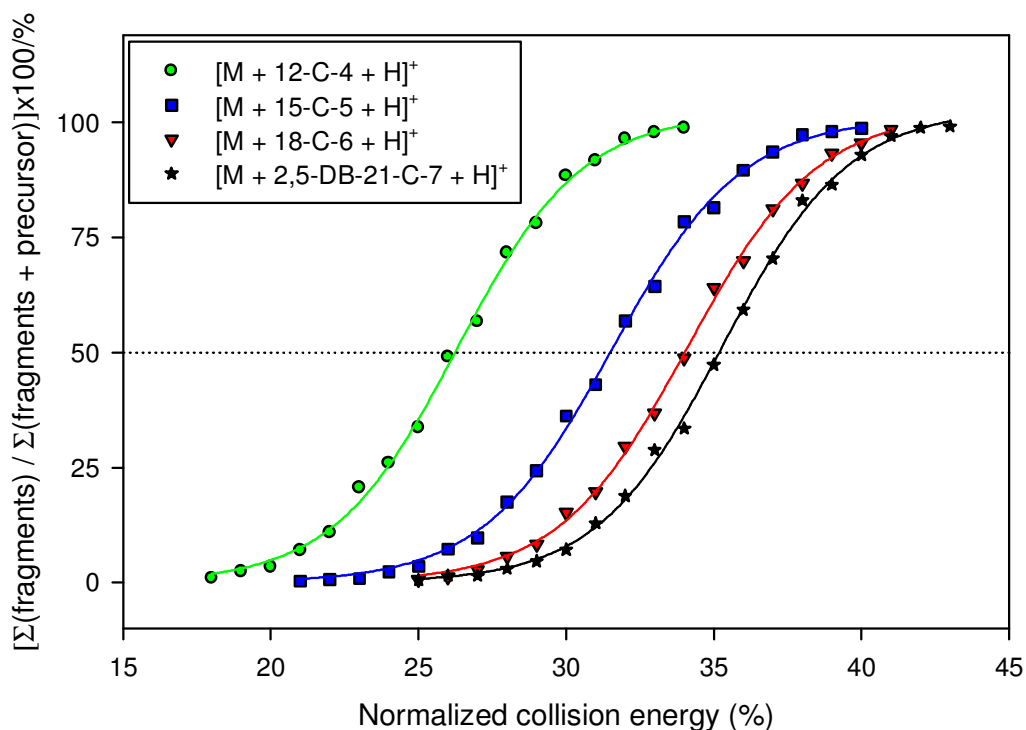


Figure 5.5. Fragmentation efficiency curves $[(\text{sum of fragment intensities})/(\text{total intensities})]$ for various crown ether-oseltamivir complexes. The fragmentation fraction was normalized to 100%.

From the fragmentation efficiency curve results, it was observed that the gas phase stability of the oseltamivir crown ether complexes increases in the order $[\text{M}+(12\text{-C-4})+\text{H}]^+ \ll [\text{M}+(15\text{-C-5})+\text{H}]^+ \ll [\text{M}+(18\text{-C-6})+\text{H}]^+ < [\text{M}+(2,5\text{-DB-21-C-7})+\text{H}]^+$. The retention of charge on the oseltamivir molecule after activation indicates that the analyte has a higher proton affinity compared to all the crown ethers investigated. Quantum-mechanical computations of the proton affinity of oseltamivir performed in this study verified this assertion (Table 5.1). It is also well known that, the larger the differences in the proton affinity of the interacting species, the longer the hydrogen bond length, the weaker the formed hydrogen bond, and the more unstable the formed complex.^{264, 267} The relative gas phase stabilities of the protonated oseltamivir-crown ether complexes are consistent with this trend.

Table 5.1. Comparison of the relative stability of oseltamivir-crown ether complexes in the gas phase versus B3LYP-D computations.

Complex c	Radius ^[c]	PA ^[d]	Δ PA ^[e]	DESI MS		Theory
				$E_c^{50\%}$ ^[a]	R ² ^[b]	Binding energy/ kcalmol ⁻¹
[M + 12-C-4 + H] ⁺	0.6-0.75	220.83	31.6	26.4±1.6 (26.4±1.6)	0.9985	49.63
[M + 15-C-5 + H] ⁺	0.86-0.92	224.95	27.48	31.5±1.4 (34.4±1.5)	0.9988	58.52
[M + 16-C-6 + H] ⁺	1.34-1.43	227.45	24.98	34.0±1.4 (40.2±1.7)	0.9988	77.04
[M + 2,5-DB-21-C-7 + H] ⁺	1.68-2.12	245.74	6.69	35.2±1.3 (48.5±1.8)	0.9990	67.98

^aActivation energy where half of the complex is dissociated (%). $E_c^{50\%}$ values corrected for the degrees of freedom are given in parenthesis. ^bCorrelation coefficient of fitting curves. ^cCavity size of crown ethers (Å). ^dProton affinity (PA) of various crown ethers (kcalmol⁻¹); the value for [M + 2,5-DB-21-C-7 + H]⁺ was computed at the at the B3LYP-D/6-311++G** level of theory. ^e Δ PA computed as PA(oseltamivir) - PA(host). The proton affinity for oseltamivir computed at the B3LYP-D/6-311++G** level of theory was 252.43 kcal mol⁻¹

The binding energy trends determined by fragmentation efficiency curves were also observed in the computed B3LYP-D/6-311++G** binding energies, with the exception of the 2,5-DB-21C-7 complex, where density functional theory predicted a relatively lower binding compared to 18-C-6. In Figure 5.6, the optimized structures of the oseltamivir crown ether complexes are presented. It is observed that for the 12-C-4 and 15-C-5 complexes, the crown ethers do not bind with the amine strongly enough to break the intramolecular hydrogen bond. In the case of 12-C-4, two of the oxygen atoms interact directly with the protonated amine, while the other two have a bifurcated interaction with two of the amine hydrogen atoms. Similar behavior is observed for the 15-C-5 complex; however, there are now three oxygen atoms on the crown ether in a bifurcated configuration. The increase in binding energy, seen in Table 5.1, from the 12-C-4 to the 15-C-5 complex is caused by the interaction of an additional oxygen atom with the amine as well as the increased dispersion from the larger crown ether. The binding of 18-C-6 with protonated oseltamivir is significantly stronger because the interaction between the crown ether and the amine is energetically favorable to an extent that allows the intramolecular hydrogen bond to be broken. From its geometry

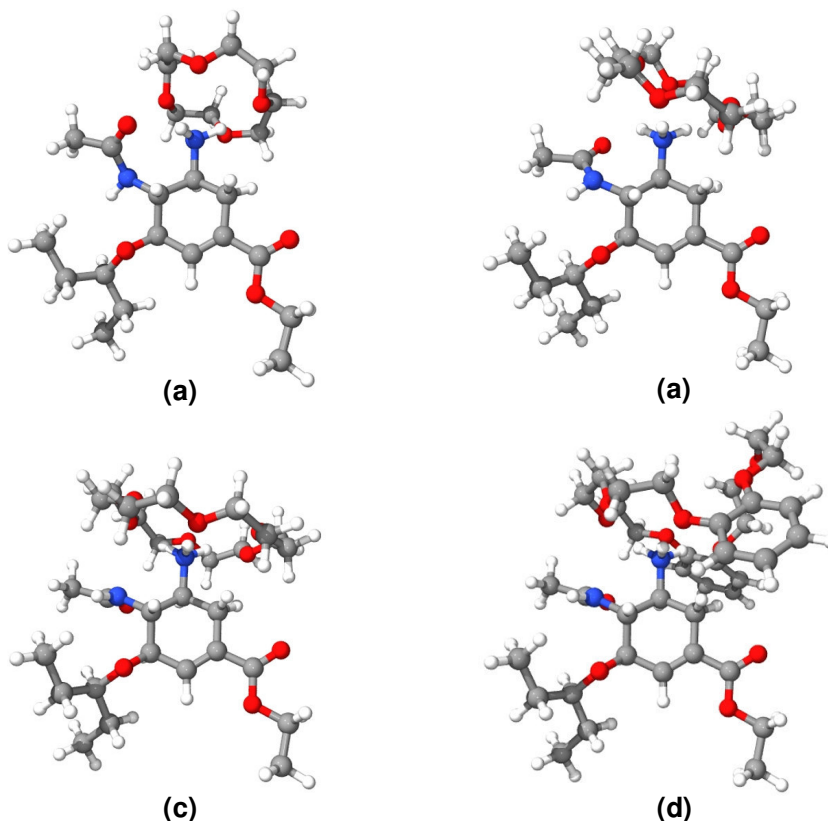


Figure 5.6. Complex geometries optimized at the B3LYP-D/6-31G** level of theory: (a) $[M + 12\text{-C-4} + \text{H}]^+$, (b) $[M + 15\text{-C-5} + \text{H}]^+$, (c) $[M + 18\text{-C-6} + \text{H}]^+$, (d) $[M + 2,5\text{-DB-21-C-7} + \text{H}]^+$.

(Figure 5.6.c), it is observed that the symmetry of 18-C-6 is such that three of its oxygen atoms have a direct interaction with a hydrogen atom in the amine group. The remaining three oxygen atoms have bifurcated interactions with the amine group. The 2,5-DB-21-C-7 complex is predicted to bind less strongly than the 18-C-6 complex. While the cavity in the 18-C-6 molecule is the optimum size for interactions with the protonated oseltamivir molecule, the 2,5-DB-21-C-7 molecule is somewhat larger than the optimum for the ideal interactions to occur. Here three oxygen atoms can interact directly with the protonated amine, while two others are in bifurcated configurations. Of the remaining two oxygen atoms, one shows some longer-range interactions with the

amine, while the other is pointed away from it. Although the trends in the binding energies and predicted cavity sizes do not agree completely with the experimental stabilities with respect to the ordering of the 2,5-DB-21-C-7 complex, the fragmentation efficiency curve results are in good agreement with ΔPA values (Table 5.1).

5.4.8. Solution Phase Selectivity for Oseltamivir by Crown Ethers

Although gas phase stabilities can offer insight into solution phase selectivity, this may not always be the case, as hydration shell displacement also plays a significant role. In this sense, solution phase selectivities are often determined by performing competitive experiments, which were performed by adding two crown ether hosts at a time to the DESI spray solvent. Figure 5.7.a shows results for these competitive experiments indicating that the relative selectivity for oseltamivir was 2,5-DB-21-C-7 > 18-C-6 >> 15-C-5 >> 12-C-4 . This trend was further verified by performing experiments where variable amounts of oseltamivir were deposited on the PTFE substrate. Decreasing the surface concentration of analyte with respect to the amount of crown ether sprayed should favor even more the formation of the more thermodynamically stable complex leading to an increase in the signal intensity ratio as observed in Figures 5.7.b.(i-ii). Additionally, experiments were performed where the concentration of the equimolar mixture of crown ethers sprayed was increased, while the amount of oseltamivir on the surface was kept constant Figure 5.8.(a-c). The results obtained by both approaches were consistent, supporting the aforementioned stability order. Moreover, the trend observed for the solution phase stabilities followed the trend observed in gas-phase studies. A log-log plot of the signal intensity ratio versus the surface concentration results in a linear

curve (inserts Figures 5.7.b.(i-ii)). The logarithmic transformation applied to the spectral data, results in a method with intermediate sensitivity ($\Delta\text{response}/\Delta\log([\text{oseltamivir}])$).

This approach, however, could still have potential for determining oseltamivir content.

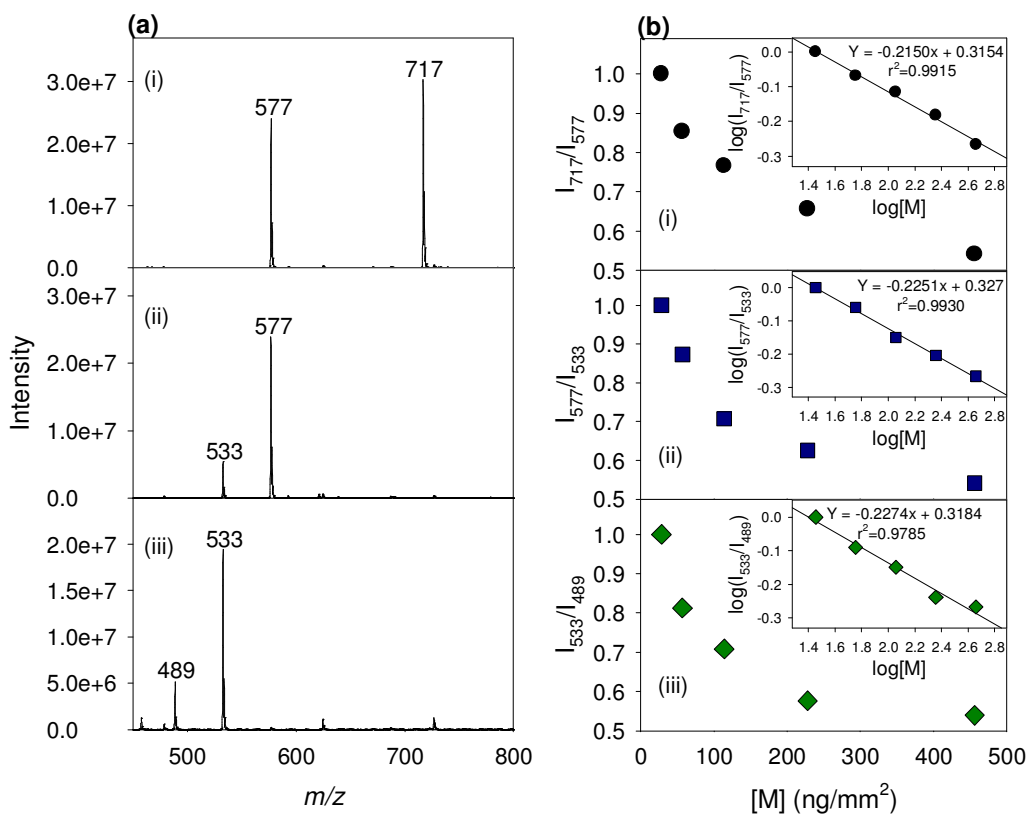


Figure 5.7. (a) Reactive DESI spectra of oseltamivir standards deposited onto PTFE surfaces with various pairs of equimolar concentration (10 μM) of crown ethers (i) 18-C-6 and 2,5-DB-21-C-7, (ii) 18-C-6 and 15-C-5, (iii) 15-C-5 and 12-C-4. (b) Effect of the amount of oseltamivir present on the substrate on the signal ratio of various pairs of oseltamivir-crown ether complexes: (i) 18-C-6 and 2,5-DB-21-C-7, (ii) 15-C-5 and 18-C-6, (iii) 12-C-4 and 15-C-5. The inserts represent the logarithmic plots of the corresponding signal ratio versus the amount of oseltamivir present on the substrate. The signal ratio was normalized to that of the maximum value.

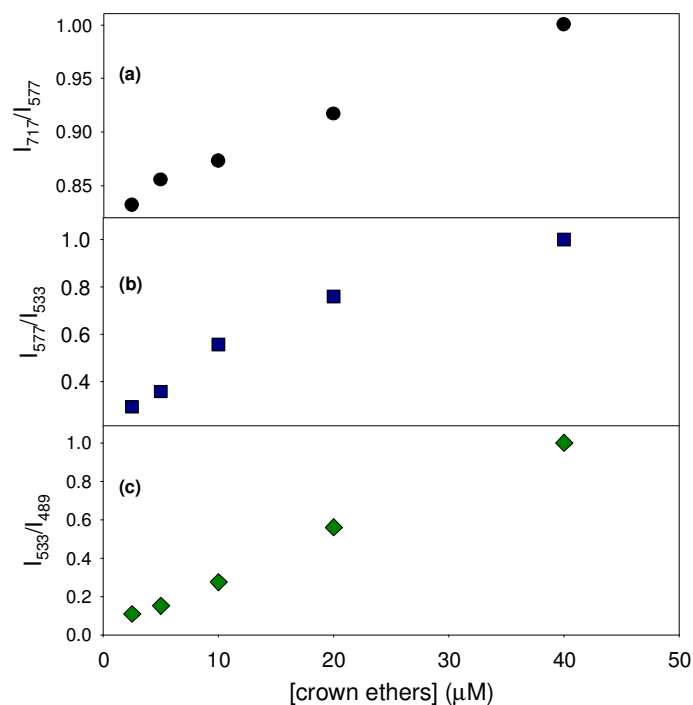


Figure 5.8. Effect of increasing the concentration of each crown ether in equimolar solutions of crown ether pairs on the signal intensity ratio from the reactive DESI MS analysis of fixed amounts (10 μ L, 1 mg/mL) of oseltamivir deposited onto PTFE substrates. The crown ether pairs investigated include (a) 18-C-6 and 2,5-DB-21-C-7, (b) 18-C-6 and 15-C-5, (c) 15-C-5 and 12-C-4. The signal ratio was normalized to that of the maximum value.

5.4.9. Samples Preparation/Rapid Qualitative Screening of Field-Collected Samples by Reactive DESI CRM MS

DESI involves a microscopic dissolution/extraction step between the liquid thin film on the surface and the solid sample. A compromise optimum thus exists for substrate surface hardness, which determines (a) the mass transport rates to the film and (b) the proper droplet scattering angles for maximum secondary droplet sampling efficiency. The hardness optimum was determined by the analysis of reserpine-containing tablets, prepared in a standard excipient mixture at varying hardness using a commercial KBr press (Figure 5.9.i). An optimum tablet hardness of 73 ± 7 kg/m² (insert Figure 5.9) was

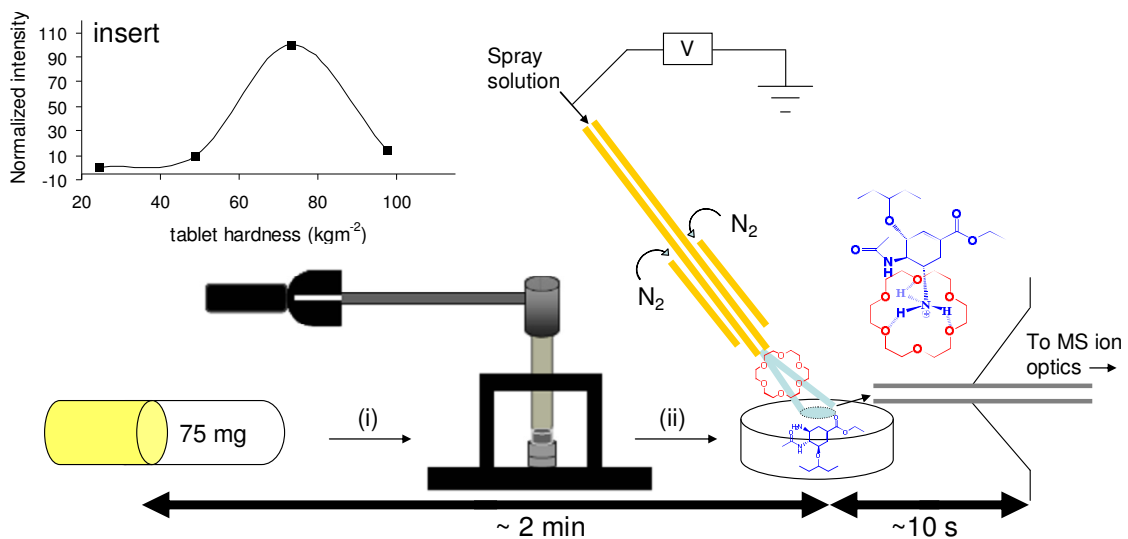


Figure 5.9. (i) Sample preparation; (ii) reactive DESI MS. The insert shows the dependence of the reserpine DESI MS signal intensity on pellet hardness. Plotted are the intensities for the observed protonated reserpine species that has been normalized for the pellet hardness.

determined and was adopted for preparation of all field-collected samples for subsequent reactive DESI MS experiments (Figure 5.9.ii). The error in the hardness measurement was based on the accuracy associated with reading the scale of the KBr press. In practical terms, an estimated 2 min/pellet are required for the preparation of samples. The prying of the capsule was the limiting factor in the sample preparation protocol, but the speed of carrying out this step improves with practice.

Results on the implementation of the reactive DESI protocol for the qualitative screening of potentially counterfeit tablets purchased over the Internet are shown in Figure 5.10. Selectivity was enhanced by using the consecutive reaction monitoring (CRM) mode of the ion trap instrument. Figure 5.10.a shows the steps involved in CRM for oseltamivir detection by reactive DESI. This starts with the

selective recognition of the analyte, leading to complexation to generate an ion at m/z 577 (Figure 5.10.a.i). MS/MS analysis of this complex lead to the neutral loss of the crown ether, with the charge resting on the analyte to give an ion at m/z 313 corresponding to the intact protonated oseltamivir molecule as the major peak in the spectrum

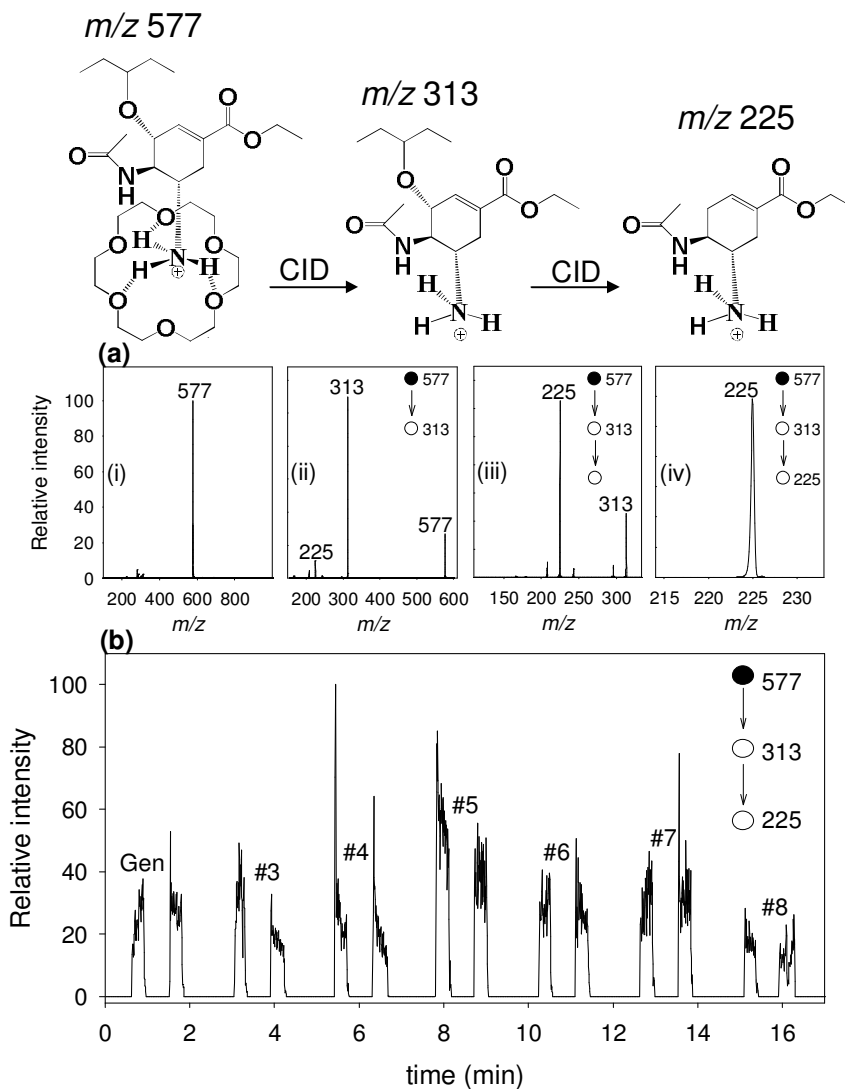


Figure 5.10. (a) Reactive DESI mass spectra of an oseltamivir phosphate standard (10 μ L, 1mg/mL) interrogated with a solution of 100 μ M 18-crown-6: (i) Full spectrum, (ii) MS/MS spectrum of the ion at m/z 577, (iii) MS/MS/MS spectrum generated from the ion at m/z 313 (iv) CRM isolation of the oseltamivir fragment at m/z 225 generated by MS/MS/MS. (b) CRM traces obtained by reactive DESI MS analysis of a genuine Tamiflu[®] capsule and capsules purchased over the Internet.

(Figure 5.10.a.ii). The high abundance of this ion and the fact that it corresponds to the intact analyte was advantageously exploited for further fragmentation to afford an additional level of selectivity. Fragmenting this ion (m/z 313) by MS/MS/MS generates a protonated oseltamivir fragment at m/z 225 as the predominant species (Figure 5.10.a.iii). This ion is generated from the neutral loss of the 3-pentanol side chain from its precursor. The oseltamivir fragment ion (m/z 225) can then be isolated (Figure 5.10.a.iv). Setting the mass spectrometer to monitor the ion at m/z 225 generated by the transition $577 \rightarrow 313 \rightarrow 225$ provides a highly selective approach for screening for the presence of oseltamivir in the capsules. Results on the implementation of this approach are shown in Figure 5.10.b. Samples were secured on the motorized stage and each sample was analyzed in duplicate by the sequential positioning, on and away from the DESI spray plume using the sample stage joystick. All samples were observed to contain oseltamivir as shown by the CRM traces (Figure 5.10.b), with relatively good reproducibility. The competitive complexation of oseltamivir using a pair of crown ethers was then assessed as a means for the direct quantitation of the amount of active ingredient in these samples by reactive DESI MS.

5.4.10. Effect of Signal Ratio of Oseltamivir-Crown Ether Complexes on DESI Experimental Variables

In Chapter 4, it was shown that the dependencies of the DESI signal on various experimental variables and sample properties could be removed by addition of an isotopically labeled internal standard to the sample allowing rapid quantitative analysis by DESI MS. However, the need for an internal standard limits the widespread

applicability of this method. Here the effect of the various DESI variables on the distribution ratio of oseltamivir-crown ether complexes was investigated by spraying sample using two different crown ethers. This was done by interrogating genuine Tamiflu[®] capsules pressed into pellets with a spray solution containing an equimolar mixture of 18-C-6 and 15-C-5. The results are presented in Table 5.2. A lower relative standard deviation for the distribution ratio compared to the sum of absolute signal for the complexes was observed for all the variables investigated indicating its applicability for direct quantitative analysis.

Table 5.2. Comparison of the robustness of the absolute DESI signal versus the signal intensity ratio of two different oseltamivir-crown ether complexes. Reactive DESI was performed by interrogating a genuine Tamiflu[®] capsule, pressed into a tablet, with an equimolar concentration (10 μ M) of 18-C-6 and 15-C-5 in neat acetonitrile.

DESI variable	RSD (%)	
	$I_{577} + I_{533}$	I_{577}/I_{533}
Solution flow rate (5-10 μ Lmin ⁻¹)	36.5	15.0
Nebulizer gas pressure (50-250 psi)	40.5	7.9
d_1 (1-6mm)	138.2	9.3
d_2 (0.8-1.5 mm)	81.7	8.1
x (2-7 mm)	30.1	10.3
α (50°-90°)	46.0	8.3

5.4.11. Direct Quantitation of Oseltamivir in Field-Collected Tamiflu Capsules by Reactive DESI MS

The quantitative capability of this reactive DESI MS approach was assessed by evaluating its performance for predicting the amount of active ingredient present in Tamiflu[®] samples collected over the Internet. Predictions were based on measuring the response ratio in comparison to that of a genuine oseltamivir pellets used as external

standards. Figure 5.11 shows the selected ion intensity trace for the protonated oseltamivir crown ether complexes generated from this analysis. The predicted amounts of oseltamivir in each sample were then compared with the amount predicted by HPLC with diode array detection.²⁵⁴ The results from these analyses are summarized in Table 5.3 showing that similar results are obtained by both techniques, with an average accuracy of 91%. Overall, these results indicate that this reactive DESI methodology shows potential as a rapid, sensitive and semi-quantitative pharmaceutical quality assessment tool for screening Tamiflu[®] capsules.

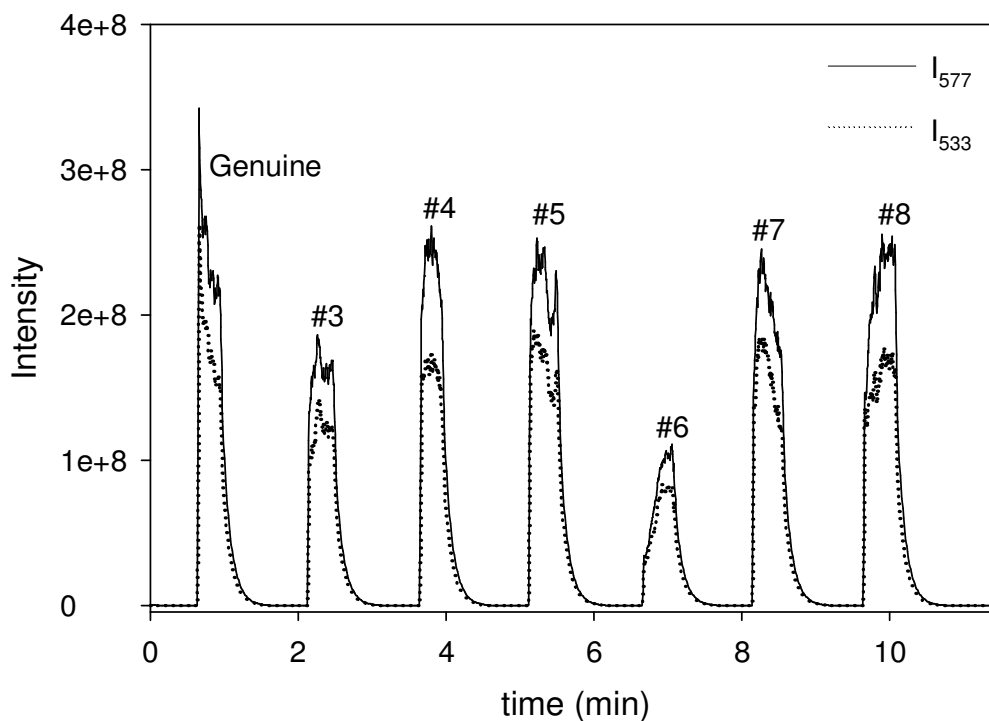


Figure 5.11. Selected ion chromatogram traces obtained by reactive DESI of a genuine versus potentially counterfeit Tamiflu[®] capsules purchased over the Internet. Samples were interrogated with a solution of 10 μM 15-C-5 and 5 μM 18-C-6. The traces correspond to complexes of oseltamivir with 15-C-5 (m/z 533) and 18-C-5 (m/z 577) respectively. Samples were placed in a line on the microscope stage and sequentially exposed to the DESI spray.

Table 5.3. Quantitation of the amount of oseltamivir in various Tamiflu[®] capsules purchased over the Internet by DESI MS compared with the amount present in each sample determined by HPLC-UV. The standard deviation of the concentrations reported by DESI was calculated from the precision observed for the intensity ratio of the two complexes measured in each mass spectrum obtained across the pellet while its surface was being scanned by the sprayer.

Sample code	mg oseltamivir capsule ⁻¹	
	DESI MS	HPLC UV
#3	84±6	72±1
#4	69±4	66±2
#5	79±7	72±3
#6	82±10	73±1
#7	76±8	74±2
#8	68±6	72±0

5.5. Conclusions

This study demonstrated the capabilities of molecular recognition via host-guest complexation reactions by DESI MS as a rapid, highly selective and sensitive method for screening the quality of Tamiflu[®] samples. Various crown ether hosts including 12-crown-4, 15-crown-5, 18-crown-6 and 2,5-dibenzo-21-crown-7 were assessed as selective chemical agents for the recognition of oseltamivir (guest). The formed host-guest complexes were held together predominantly by hydrogen bonding interactions. Solution and gas-phase studies and *ab initio* molecular modelling calculations indicated that, the stability of the gas phase complexes increased in the order: $[M + 12\text{-crown-4} + H]^+ \ll [M + 15\text{-crown-5} + H]^+ \ll [M + 18\text{-crown-6} + H]^+ < [M + 2,5\text{-dibenzo-21-crown-7} + H]^+$. Quantitative predictions using mixtures of crown ethers in the spray solution were 91% accurate when compared to HPLC determinations.

CHAPTER 6. APPLICATION OF REAGENTLESS AND REACTIVE DESI MS IMAGING TO PHARMACEUTICAL FORENSICS AND DRUG DISCOVERY

6.1. Abstract

This chapter presents the implementation of DESI MS in imaging mode for the specific and sensitive determination of the two-dimensional distribution of analytes present on various surfaces. Its capabilities are showcased in the analysis of artesunate pharmaceutical drug tablets for anticounterfeiting and drug quality control applications and for the determination of secondary metabolites directly from the surface of alga tissues in order to shed some light on antimicrobial defense mechanisms.

6.2. Introduction

Molecular imaging using MS allows correlations to be drawn between the chemical identity of each analyte and its spatial distribution at or near the sample surface. In this chapter, an implementation of DESI MS in imaging mode is presented with its utility demonstrated in two different applications.

The first application involves utilization of the optimized reagentless DESI MS protocol presented in Chapter 2 for the determination of the distribution of various components observed in artesunate pharmaceutical tablets for drug quality control and anticounterfeiting applications. Techniques that have become popular for imaging pharmaceutical tablets include Raman spectroscopy²⁷⁰ and attenuated total reflectance Fourier transform infrared (ATR-FIR) spectroscopy.¹⁴⁹ These techniques allow both

spatial and chemical information to be obtained simultaneously, however they are limited by their intrinsic low specificity based on their recognition of specific functional groups. Chemical imaging using DESI MS takes advantage of the exquisite high specificity provided by MS detection for the visualization of the distribution of chemicals, directly from an intact surface without the need for chemical labeling or prior chemical treatment. Because of the less than ideal conditions under which counterfeit drugs are expected to be manufactured, fake tablets could be unevenly mixed to some degree. This would be reflected as an inhomogeneous color distribution in its DESI MS image. Sample properties such as the hardness-dependent dissolution profiles are also contributing factors that influence ion yields in DESI,¹⁴⁸ and these conditions would be directly reflected by DESI molecular images in a spatially resolved fashion. In the case of genuine samples, the information on the spatial distribution and homogeneity of different chemical species on a tablet surface is extremely valuable for drug quality control. For instance, some antimalarial therapies recommend that the tablets be split to optimize the dosage and/or reduce the upfront cost to the patient. Under these circumstances, an inhomogeneous distribution of the API would result in an incorrect dosage being administered.

The second application of DESI MS imaging presented here involves the development of a reactive DESI MS imaging protocol for the determination of the distribution of bromophycolide natural products. Bromophycolides are diterpene benzoate macrolides presented by the Fijian red alga, *Callophycus serratus*. Twenty different bromophycolide natural products including bromophycolides (A-I) and debromophycolide A have thus far been isolated from this alga, the most abundant ones

being bromophycolide A and B.²⁷¹⁻²⁷³ Except for debromophycolide A, which contains no bromine, all other bromophycolides identified from this alga contain 2-3 bromine atoms. The presence of bromines has been shown to be vital for their moderate anticancer and antimicrobial activities providing them with the potential for pharmaceutical drug candidacy.²⁷¹ Furthermore, bromophycolides have also been observed to be very effective antifungal agents, especially against the marine pathogenic fungus *Lindra thalassiae*, with IC₅₀ values at or below whole tissue natural concentrations.¹⁶⁶ As such, bromophycolides have been implicated in anti-microbial chemical defense; however, the chemical defense mechanisms are not yet completely understood. Here a reactive DESI MS protocol for molecular imaging of bromophycolides on the surface of *C. serratus* tissues is developed with the aim of shedding some more light into the processes involved in the chemical defense mechanisms used by this and other algal species. This investigation is supplemented with an assessment of the factors that influence sensitivity for the detection of bromophycolides by DESI MS. In order to gain more insight on the species formed during reactive DESI, the relative gas phase stabilities of different bromophycolide complexes were compared via ab initio computational calculations.

6.3. Experimental Details

6.3.1. Samples and Reagents

All reagents were used as received without additional purification. High purity HPLC grade methanol 99.9+% (Honeywell Burdick & Jackson, Muskegon, MI, USA) was used for all reagentless DESI MS experiments. Ammonium chloride (Sigma-Aldrich, St. Louis, MO), hydrobromic acid (Mallinckrodt Baker Inc., Phillipsburg, NJ) and

trifluoroacetic acid (Fisher Scientific, Fair Lawn, NJ) solutions in methanol were used for reactive DESI MS experiments. A genuine artesunate tablet (Mekophar Chemical Pharmaceuticals Joint-Stock Co., Ho Chi Minh City, Vietnam) and a counterfeit tablet (collection code Lao 12060, Type 8 fake) investigated in the first imaging application were collected in Southern Laos. In the second study, pure bromophycolides A, B and E were isolated from the Fijian red alga, *Callophycus serratus* following previously reported procedures.^{271, 272} Algal samples were collected in February 2008 off Yanuca Island in Beqa Lagoon, Fiji (18° 23' 57" S, 177° 57' 59" E). Samples were preserved in 10 % v/v formalin:sea water and stored at room temperature. Samples were rinsed in ultrapure water and allowed to air dry prior to analysis.

6.3.2. DESI Imaging Ion Source

The DESI imaging ion source consisting of a joystick and software-controlled motorized microscope XY stage (Prior Scientific, Rockland, MA) and a high-performance sprayer (Figure 6.1). The sprayer, affixed to a post was fitted with a high precision rotation mount (Thorlabs, Newton, NJ) for manual adjustment of the spray impact angle. The aforementioned post was attached to a MicroBlock 3-axis positioner (Thorlabs, Newton, NJ) for manual adjustment of the emitter position in the XYZ coordinates with respect to the capillary inlet. This sprayer holder assembly was mounted on a breadboard. The microscope stage on which samples were held was mounted onto a heavy-duty lab jack (Thorlabs, Newton NJ) for manual adjustment of the sample position in the z-axis. The lab jack-microscope stage assembly was also affixed to the breadboard. For DESI MS imaging of pharmaceutical tablets, samples were held in place using two

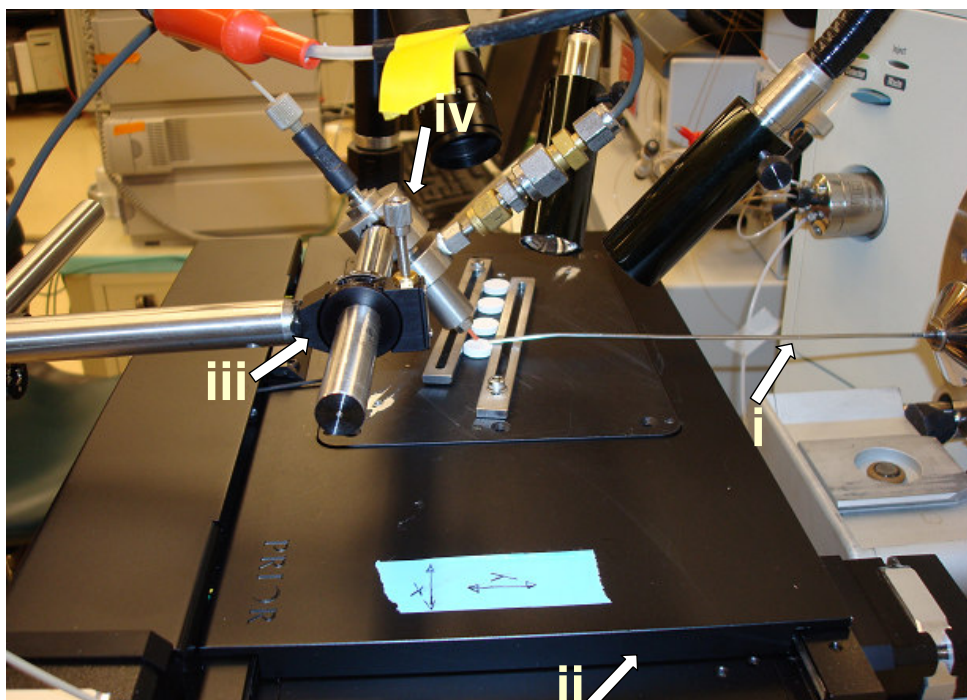


Figure 6.1. DESI MS imaging set-up. (i) Extended capillary (760 μm i.d. x 33cm), (ii) Prior Scientific microscope stage (iii) off-the-shelf Thorlabs parts, (iv) high performance sprayer.

Al sample holders (110x10x3 mm) mounted on the sample plate of the microscope stage. Alga tissue samples were affixed to glass slides using double sided tape for DESI MS and imaging of bromophycolides and alga tissues. The DESI geometrical settings were similar to those described in section 2.3.3. The DESI ion source was coupled to an LCQ Deca XP+ quadrupole ion trap mass spectrometer (Thermo Finnigan, San Jose CA) operated using the *Xcalibur* version 2.0 software. The standard ion transfer capillary was replaced by an extended version (762 μm i.d., 1588 μm o.d., Small Parts Inc., Miramar, FL). The capillary-scattered droplet collection angle was $\sim 10^\circ$. Samples were positioned for DESI analysis so that the atmospheric sampling capillary of the mass spectrometer was ~ 0.5 mm from the sample surface. A CCD camera (JAI Inc., San Jose, CA) was used to monitor the spray plume and the DESI-sampled spot.

6.3.3. DESI MS Imaging of Artesunate Tablets

DESI MS imaging experiments were performed with Dr. Asiri Galhena, a postdoctoral associate in our group. Image reconstruction was performed using MATLAB software written by Dr. Mitchell Parry, a post doctoral associate in Dr. Wang's group in the Department of Biomedical Engineering, Georgia Institute of Technology. The genuine artesunate tablet evaluated was comprised of a flat surface with somewhat tilted edges and was thus imaged directly without any prior sample manipulation. The counterfeit tablet (Lao 12060) had a more convex shape. This tablet was sanded down to a flat surface using super fine P400 sandpaper (Norton Abrasive, Worcester, Massachusetts) and the particulates released during sanding blown off using N₂ from a gas cylinder. No sample contamination was evident due to sanding. The DESI MS imaging experiment was performed in positive ion mode. Mass spectra were acquired in profile mode with automatic gain control (AGC) turned off. The ion injection time was set at 40 ms. Imaging data were acquired using a "looped"-stage scanning mode. The sample area imaged was 15 mm x 10 mm. The following scan sequence was used for imaging: (i) a forward, and (ii) a reverse scan lines in the x-direction (15 mm) perpendicular to the MS inlet, followed by (iii) a 200 μm step displacement in the y-dimension, away from the MS inlet. The stage scan speed in both dimensions was set to 80 μm s⁻¹. Overlapping forward and reverse scan segments were utilized in order to avoid any image artifacts that might be caused by sample scanning directionality, but only data from the forward scan segments were used to construct the images. Using these settings a lateral resolution of 75 μm was achieved, as determined by scanning a calibrated test image printed on glossy paper. The flow rate of the spray solvent used for the imaging

experiments was $3 \mu\text{L min}^{-1}$. The recorded individual mass spectra scans were finally processed and assembled into an image using an in-house written MATLAB program (version R2008a, MathWorks, Inc. Natick, MA).

6.3.4. DESI MS Analysis of Bromophycolides and Imaging of Alga Tissue Samples

Reagentless DESI MS experiments of bromophycolides were performed using 100 % MeOH. For reactive DESI MS analysis of bromophycolide standards, various additives including NH_4Cl (100 μM), HBr (10 μM) and CF_3COOH (0.001 % v/v = 135 μM) were added to the spray solvent (MeOH) at the concentrations in parenthesis unless stated otherwise. The 100 μM NH_4Cl methanol solution was used for reactive DESI MS profiling and imaging of alga tissues. The spray solvent flowing at a rate of 5 $\mu\text{L}/\text{min}$ was electrically charged externally to -3 kV. Bromophycolide working solutions were prepared in MeOH and 10 μL , 1 mg/mL of each standard were deposited onto PTFE surfaces and air dried prior to analysis. For the reactive DESI MS profiling and imaging analyses of *Callophycus serratus* samples, small pieces of tissue were affixed to glass slides using double sided tape and analyzed by exposing different positions of their surfaces to the DESI spray plume. All experiments were performed on an LCQ DECA XP+ ion trap mass spectrometer (Thermo Finnigan, San Jose CA) operated in negative ion mode. DESI MS analysis of bromophycolide standard and profiling of alga tissue samples were performed with AGC on for an ion trap injection time of 200 ms at 2 μscans per spectrum. For the DESI MS imaging analysis of alga tissue (10 mm x 4 mm), mass spectra were acquired in profile mode with automatic gain control (AGC) turned off and the ion injection time set to 40 ms. The same LabView controlled

motorized stage scan sequence and image assembly protocol described in section 6.3.3 was used.

6.3.5. Estimation of the Concentration of Bromophycolides in Surface Patches of Untreated Alga Tissue by Reactive DESI MS

The concentration of bromophycolides A + B for individual sites on algal surfaces were estimated by comparing integrals from chloride adduct reactive DESI MS signals for these bromophycolides with a standard calibration curve. The calibration curve was developed by depositing known concentrations of bromophycolides A and B in a 2:1 ratio (1 μ L, 1:0.5 mg/mL) on an intact patch-free algal surface (9.4 mm²). The 2:1 ratio of bromophycolides A and B represented a reasonable approximation based on the average 2.2:1 ratio observed by LC-MS for these compounds in extracts.¹⁶⁶ Triplicate analyses of 4 different surface concentrations of this bromophycolides mixture spanning the range 2.4-119.5 pmol mm⁻² were evaluated by reactive DESI MS to give a calibration curve with an r^2 value of 0.97.

6.3.6. Computational Calculations

Computational calculations were performed by Edward Hohenstein, a graduate student in Dr. Sherrill's group in the School of Chemistry and Biochemistry, Georgia Institute of Technology. The geometries of bromophycolides A, B, and E were optimized at the B3LYP-D/6-31+G* level of theory, where the "-D" denotes the inclusion of empirical terms to compensate for the inability of the B3LYP functional to account for dispersion interactions. The empirical dispersion terms developed by Grimme²⁵⁶ were

used in this work. The complexes of bromophycolide A, B, and E with Cl^- , Br^- , and CF_3COO^- were fully optimized at the B3LYP-D/6-31+G* level of theory. Binding energies were computed at the B3LYP-D/6-31+G* level of theory using a Lebedev grid with 302 angular points for each of 100 radial points. This grid was chosen to avoid errors related to numerical integration. Counterpoise correction was applied to all binding energies according to the scheme of Boys and Bernardi.²⁵⁷ Geometries of bromophycolide A, B, and E dimers were optimized at the B3LYP/6-31+G* level of theory. All computations were performed using QChem 3.1²⁵⁹ and Jaguar 5.5.²⁶⁰

6.4. Results and Discussion-Case Study 1: Reagentless DESI MS Imaging of Artesunate Pharmaceutical Tablets

6.4.7. Reagentless DESI MS Imaging of a Genuine Artesunate Tablet

Figure 6.2.a shows a representative DESI spectrum of a genuine artesunate tablet, which shows peaks corresponding to sodiated artesunic acid monomer (m/z 407.2) and dimer (m/z 791.2). Peaks corresponding to sodiated lactose monomer (m/z 365.3) and dimer (m/z 707.2) are also observed in the spectrum. The corresponding DESI MS images of the genuine tablet constructed for four relevant ionic species are shown in Figure 6.2.b. All four images are shown on the same relative intensity false color scale (there is no correlation between the actual color of the formulations and their DESI MS chemical images), thus allowing a qualitative comparison between species. Figures 6.2.b.i and 6.2.b.ii show DESI images generated from the peaks at m/z 407.2 ($[\text{artesunic acid} + \text{Na}]^+$) and 791.2 ($[\text{2 artesunic acid} + \text{Na}]^+$). As indicated by these two images, artesunic acid seemed to be distributed on the surface of the genuine sample

quite homogeneously. The formation of artesunic acid dimer was observed to be favored over the monomer, resulting in a more uniform and intense image (Figure 6.2.b.ii). The preferential formation of artesunic acid dimer is largely dependent on the tablet surface hardness. Lower sample hardness improves the mass transport efficiency between the solid tablet phase and the liquid film formed by the DESI sprayer. This increases the

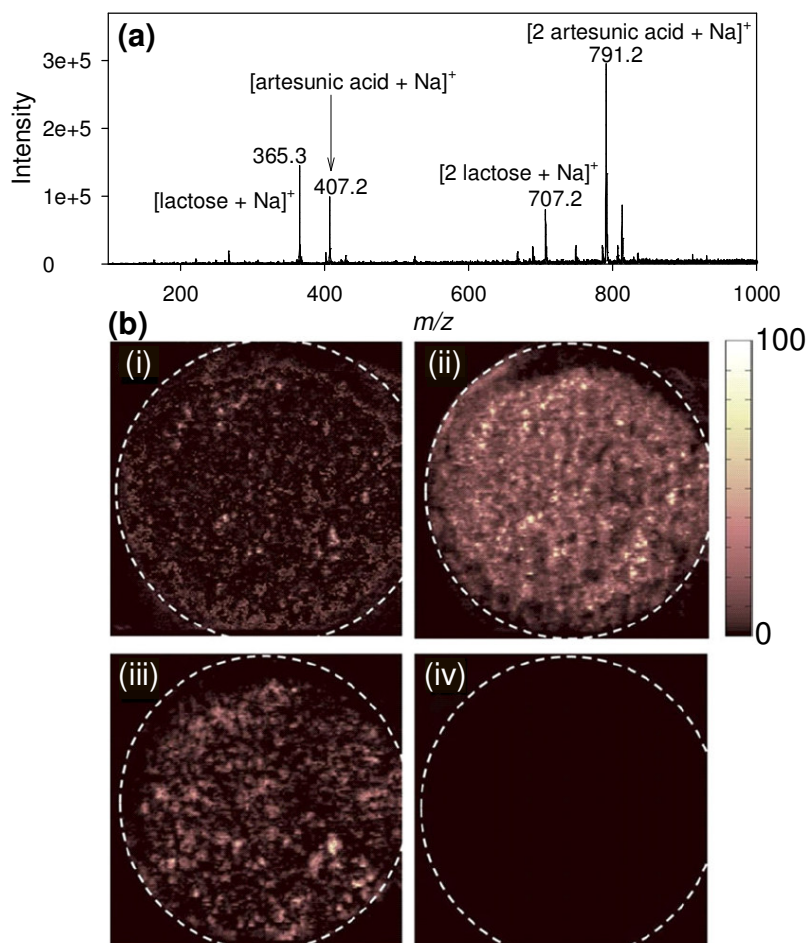


Figure 6.2. (a) Representative DESI spectrum of a genuine artesunate tablet manufactured by Mekophar Pharmaceuticals. (b) DESI MS images of the tablet constructed using the spatial relationship between various spectral features and their intensity, with data acquisition in full-scan MS mode: (i) sodiated artesunic acid (m/z 407.2), (ii) sodiated artesunic acid dimer (m/z 791.2), (iii) sodiated lactose (m/z 365.3) and (iv) sodiated acetaminophen (m/z 174.1). All images are shown in false color scale and pixilated format.

concentration of active ingredients in secondary droplets, favoring dimerization during ion evaporation from charged droplets. The DESI MS image reconstructed from the peak at m/z 365.3 ([lactose + Na⁺]) shows the spatial distribution of lactose in this sample, also revealing a small degree of heterogeneity (Figure 6.2.b.iii). The DESI MS image of a common wrong active pharmaceutical ingredient, m/z 174.1, which corresponds to sodiated acetaminophen is also shown (Figure 6.2.b.iv). The image clearly indicates the absence of acetaminophen in this sample, as expected. In all images (Figure 6.2.b) the tablet edges appear darker. This is an artifact introduced by the somewhat tilted tablet edges, which lead to an increase in the sprayer tip-to-surface distance, reducing sensitivity.

6.4.8. Reagentless DESI MS Imaging of a Counterfeit Artesunate Tablet

Figure 6.3.a shows a representative DESI spectrum of a counterfeit artesunate tablet with collection code, Lao 12060. The spectrum shows peaks at m/z 174.1 and 325.1 corresponding to sodiated acetaminophen monomer and dimer respectively. The spectrum also shows peaks at m/z 363.3 and 707.2 corresponding to sodiated lactose monomer and dimer respectively. The DESI MS images of the counterfeit sample are presented in Figure 6.3.b. Figures 6.3.b.i and 6.3.b.ii show DESI MS images that were reconstructed for the peaks at m/z 174.1 ([acetaminophen + Na]⁺) and 325.1 ([2 acetaminophen + Na]⁺). Both indicated a relatively homogeneous distribution of acetaminophen in the sample. Such findings indicate that counterfeit drug manufacturers are using fairly sophisticated formulation techniques as part of their operations. The spatial distribution of lactose was also homogeneous, as observed in the DESI MS image

that was reconstructed for the species at m/z 365.3 ($[\text{lactose} + \text{Na}]^+$, Figure 6.3.b.iii). Figure 6.3.b.iv shows the DESI MS image that was constructed for the ion signal corresponding to sodiated artesunic acid. DESI MS imaging analysis of such a large area across the sample surface shows unambiguously that artesunic acid is not present in the sample. Trace amounts of artesunic acid has previously been detected on the surface of other types of fakes artesunate samples. A heterogeneous distribution of artesunic acid in such sample would require DESI MS imaging analysis to enable the unambiguous determination of such subtherapeutic counterfeits.

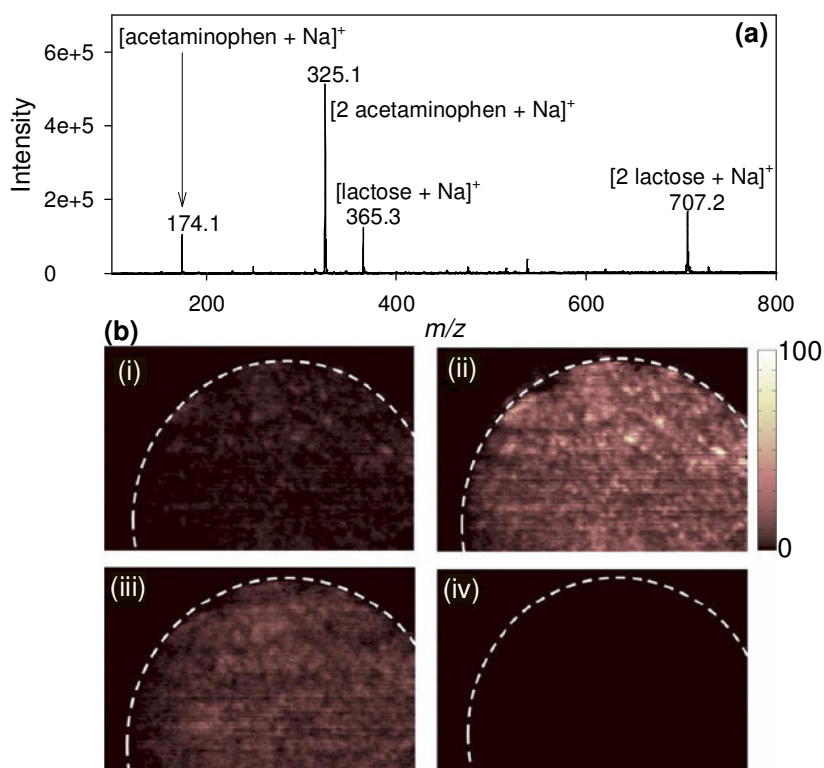


Figure 6.3. Representative DESI spectrum of a fake artesunate tablet (collection code, Lao 12060, type 8 fake). (b) DESI MS images of the tablet constructed based on the spatial relationship between various spectral features and their intensity, with data acquisition in full-scan MS mode: (i) sodiated acetaminophen (m/z 174.1), (ii) sodiated acetaminophen dimer (m/z 325.1), (iii) sodiated lactose (m/z 365.3) and (iv) sodiated artesunic acid (m/z 407.2). All images are shown in false color scale and pixilated format.

6.5. Results and Discussion-Case Study 2: DESI MS Analysis of Bromophycolides and Imaging of Alga Tissue

The higher abundance of bromophycolides A and B relative to other bromophycolides in extracts of the alga *Callophycus serratus*²⁷³ suggested a higher chance for their detection from alga tissue by DESI MS. For this reason, they were chosen for the initial optimization and characterization experiments together with the less abundant bromophycolide E, depicted in Figure 6.4.

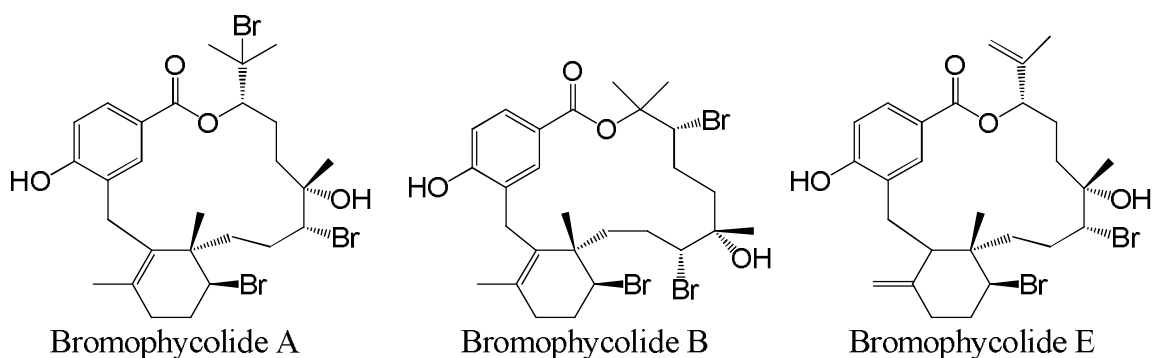


Figure 6.4. Structures of a subset of bromophycolides extracted from the Fijian red alga *Callophycus serratus*.²⁷³

6.5.9. Conventional vs. Reactive DESI MS Analysis of Bromophycolides/Gas Phase Structure of Observed Species

Initial conventional DESI MS analysis of pure bromophycolides was explored in both positive and negative ion modes. However, ionization and detection of bromophycolides was significantly more efficient in the latter, presumably due to the presence of a phenolic acid functionality in their macrolide structure in which the conjugate phenolate anion is electronically stabilized by resonance. No appreciable ionization was observed in positive ion mode even in the presence of various

concentrations of organic acids or various cations such as Na^+ and NH_4^+ which, when added to the spray solution, could potentially enhance ionization efficiency by cationization.¹²¹ As such, all subsequent experiments were performed in negative ion mode.

Figure 6.5 shows the reagentless DESI MS, MS^2 and MS^3 spectra of purified bromophycolides deposited on PTFE substrates, obtained following interrogation with a solution of neat MeOH. Figure 6.5.a shows the DESI spectrum of bromophycolide A.

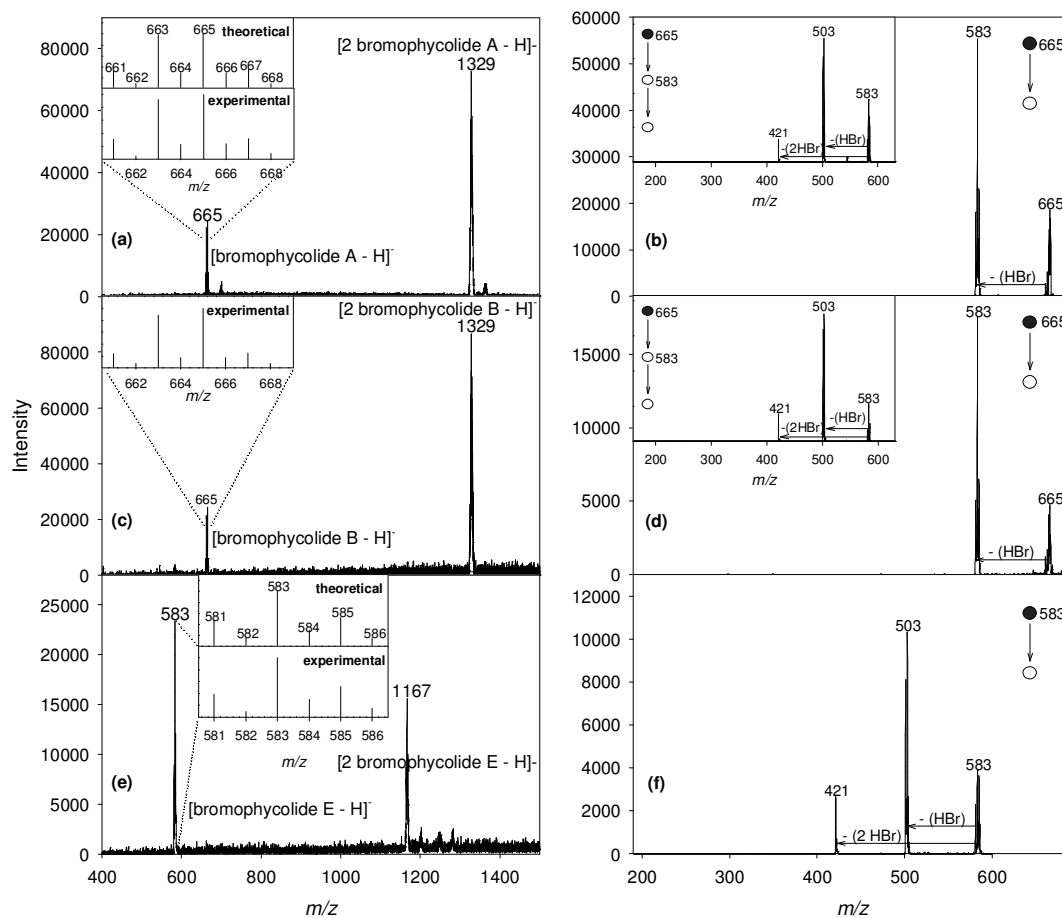


Figure 6.5. Conventional DESI MS, MS^2 , and MS^3 spectra of bromophycolide standards. (a) Full MS of bromophycolide A and (b) corresponding MS^2 of m/z 665 precursor (MS^3 of m/z 583 precursor inserted), (c) full MS of bromophycolide B and (d) corresponding MS^2 of m/z 665 precursor (MS^3 of m/z 583 precursor inserted), (e) full MS of bromophycolide E and (f) corresponding MS^2 of m/z 583 precursor.

The spectrum consists of two major isotopic clusters, with base peaks at m/z 665 and m/z 1329. These clusters correspond to the deprotonated monomeric and dimeric species of bromophycolide A, respectively. The insert in Figure 6.5.a shows the isotopic distribution of the deprotonated bromophycolide A monomer together with the theoretical isotopic pattern based on its elemental formula. As seen in the insert, bromophycolide A shows a unique isotopic distribution consistent with the presence of three bromine atoms in its structure,^{271, 272} matching the theoretical distribution. Deprotonation of bromophycolide A is predicted to preferentially occur on the phenyl hydroxyl group due to the ability of the phenyl ring to stabilize the negative charge (Figure 6.6.a). Deprotonation at this site

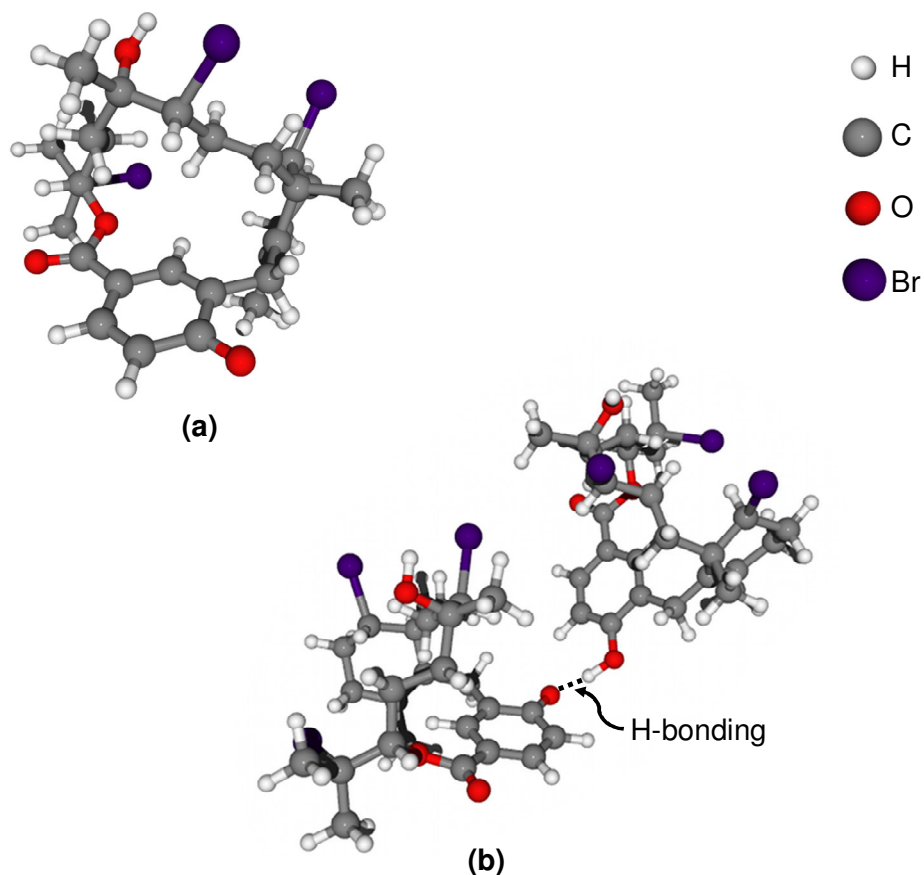


Figure 6.6. Geometries of (a) bromophycolide A (b) deprotonated bromophycolide A dimer, optimized at the B3LYP/6-31+G* level of theory.

was calculated to be about 38 kcal mol⁻¹ more favorable than at the macrolide hydroxyl group resulting in the structure shown in Figure 6.6.a., which was calculated at the B3LYP-D/6-31+G* level of theory.

The structural connectivity of the deprotonated bromophycolide A monomer can be further evaluated by performing sequential ion trap MSⁿ experiments by collision-induced dissociation (CID). Figure 6.5.b shows the MS² spectrum of the deprotonated bromophycolide A monomer, which gives rise to a fragment ion cluster with a base peak at *m/z* 583 corresponding to the elimination of HBr from its precursor. Inserted in Figure 6.5.b is the MS³ spectrum generated from CID analysis of the ion cluster at *m/z* 583, which shows intense fragment ion clusters with base peaks at *m/z* 503 and *m/z* 421, corresponding to the elimination of 1 HBr and 2 HBr molecules respectively. MS⁴ analysis of the cluster at *m/z* 503 generated the ion at *m/z* 421 as the predominant species in the spectrum, corresponding to the elimination of HBr from its precursor ion (data not shown). The sequential elimination of HBr indicates a lability of the C-Br bonds in the precursor ion molecule, presumably due to their relatively longer bond lengths compared to all other bonds in this molecule.²⁷² MS⁵ analysis of the isotopic cluster centered at *m/z* 665 generated ions at *m/z* 377 (loss of CO₂) and *m/z* 359 (loss of H₂O, Figure 6.7.a).

Bromophycolide B is a constitutional isomer of bromophycolide A, containing a 16-membered macrolide within a diterpene-benzoate framework as opposed to a 15-membered macrolide for bromophycolide A.²⁷² Figure 6.5.c shows the DESI MS spectrum for pure bromophycolide B, which shows isotopic clusters with base peaks at *m/z* 665 and 1329 corresponding to the deprotonated monomer and dimer respectively.

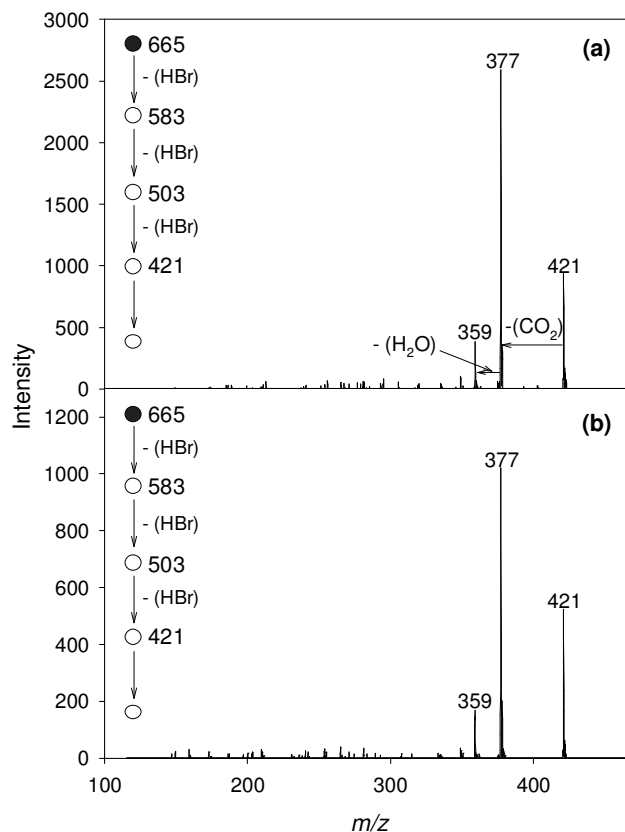


Figure 6.7. DESI MS⁵ spectra of pure bromophycolides, (a) bromophycolide A, (b) bromophycolide B.

Shown as insert in Figure 6.5.c is the isotopic distribution of the deprotonated monomer, which is almost identical to that obtained for bromophycolide A, thus verifying their isomeric relationship. Mass spectrometric distinction between isomeric species can sometimes be accomplished via MSⁿ analysis²⁷⁴ but, as shown in Figure 6.5.d and 6.7.b, stepwise CID analysis (up to MS⁵) of bromophycolide B led to elimination of the same species as for bromophycolide A at each stage, thus eliminating this possibility. Figure 6.5.e shows the DESI MS spectrum of bromophycolide E, which revealed isotopic clusters with base peaks at m/z 583 and 1167, corresponding to the deprotonated bromophycolide E monomer and dimer respectively. MS² analysis of the isotopic ion cluster with a base peak at m/z 583 generated a cluster with a base peak at m/z 503 due to

the elimination of 1 HBr molecule (Figure 6.5.f). Also observed in this spectrum is a peak at m/z 421 corresponding to the completely debrominated species resulting from the elimination of 2 HBr molecules from the precursor ions (Figure 6.5.f).

The potentially low abundance of bromophycolides on the algal tissue surface necessitates an appreciably sensitive detection means. As shown above, the most abundant bromophycolides; A and B, produced the deprotonated dimer as the base peak in their DESI spectra (Figure 6.5). Declustering of such dimers by in-source CID could lead to an increase in the abundance of the deprotonated monomer thus improving the sensitivity for the detection of bromophycolides.^{275, 276} In-source CID experiments were performed by varying the DC voltage offset of the ion source ion transfer octopole between 0-60 V (Figure 6.8). This resulted in an overall decrease in the signal intensity

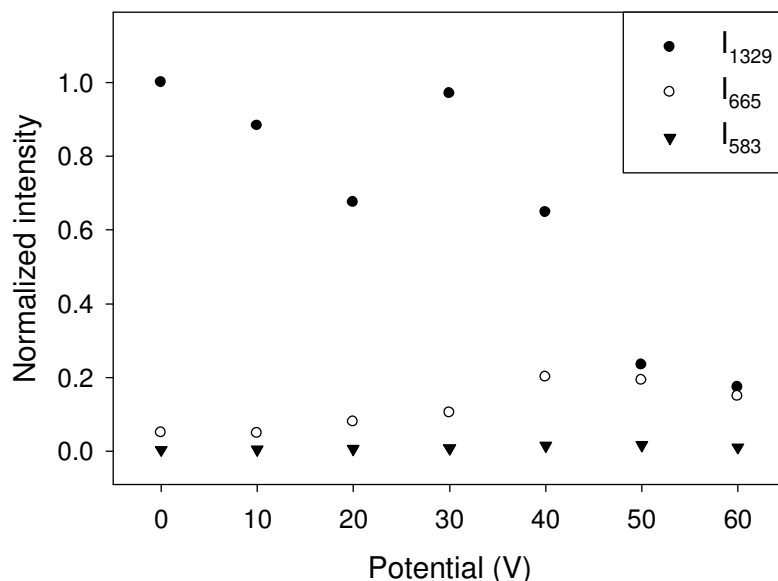


Figure 6.8. Effect of ion source collision induced dissociation energy in the multipole region for various DC offset voltages on the intensity of various bromophycolide A ionic species including: [bromophycolide A - HBr - H]⁻ at m/z 583, [bromophycolide A - H]⁻ at m/z 665 and [2 bromophycolide A - H]⁻ at m/z 1329. The intensity values were normalized to that of the maximum observed.

of the deprotonated bromophycolide A dimer and only in a slight increase in the intensity of the deprotonated monomer ion, with a maximum at 40 V (Figure 6.8). Higher voltages resulted in the concomitant formation of the fragment at m/z 583. Even at the maximum DC offset investigated (60 V) an appreciable signal was still observed for the dimer ion, indicating a significant stability. This stability can be attributed to a strong hydrogen bond between the phenyl hydroxyl group of one bromophycolide molecule and the deprotonated phenyl hydroxyl group of the other, contributing roughly 30 kcal mol^{-1} to the stability as demonstrated by theoretical studies at the B3LYP/6-31+G* level of theory (Figure 6.6.b). Additionally, the stabilization due to dispersion interaction between the two bromophycolide units could be larger than 10 kcal mol^{-1} .

Performing the analysis in the reactive DESI mode provides an alternative approach of improving sensitivity by improving ionization efficiency or increasing ion survival during transport through the atmospheric pressure interface.¹⁰² Addition of halides to the spray solvent has been found beneficial in improving the ionization of target analytes such as explosives.²⁰⁶ In this study, various anions including: Cl^- , Br^- , and CF_3COO^- were explored as additives to investigate their effect on the various bromophycolide signals. Results from the reactive DESI analysis of bromophycolide A standards deposited onto PTFE with various anions are shown in Figure 6.9. When ammonium chloride was added to the DESI spray solvent (Figure 6.9.a), the DESI spectrum showed signals at m/z 701 and 1365, corresponding to $[\text{bromophycolide A} + \text{Cl}]^-$ and $[2 \text{ bromophycolide A} + \text{Cl}]^-$ respectively. A peak at m/z 1329 corresponding to the deprotonated bromophycolide A dimer was also observed. The identity of the peak at m/z 701 was verified by DESI MS^2 (Figure 6.9.b), where the

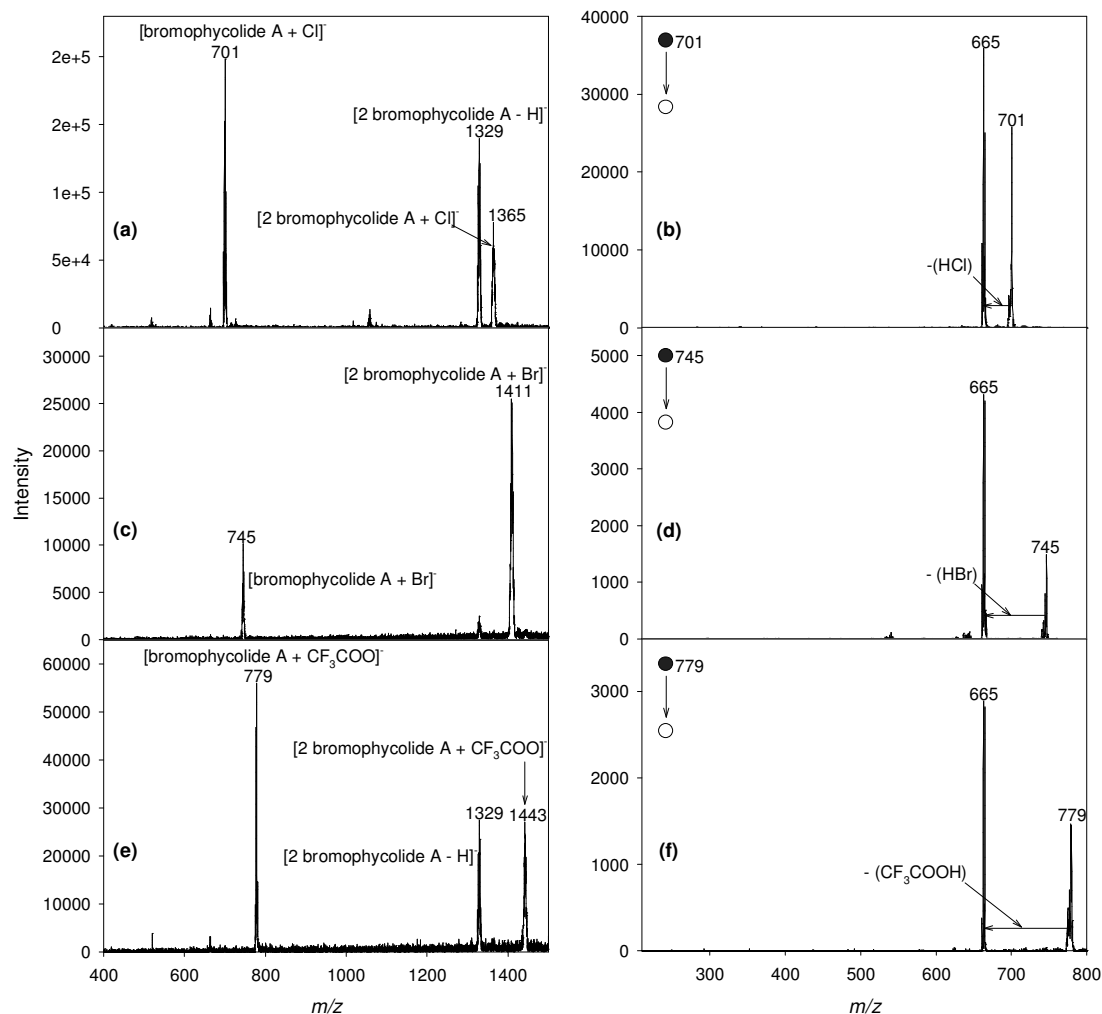


Figure 6.9. Reactive DESI MS and MS² spectra of bromophycolide A standards interrogated with spray solutions of various anions in methanol. (a) 100 μM NH_4Cl , and (b) corresponding MS² spectrum of the m/z 701 precursor, (c) 10 μM HBr , and (d) corresponding MS² spectrum of the m/z 745 precursor, (e) 0.001 %v/v (135 μM) CF_3COOH and (f) corresponding MS² spectrum of the m/z 779 precursor.

non-covalently bound chloride was eliminated as HCl to give the ion at m/z 665 corresponding to deprotonated bromophycolide A. The addition of a low concentration of hydrobromic acid to the DESI spray solvent resulted to peaks at m/z 745 and 1411 assigned to the complexes of bromide with bromophycolide A monomer and dimer respectively (Figure 6.9.c). DESI MS² analysis of the ion at m/z 745 generated

predominantly the ion at m/z 665 corresponding to deprotonated bromophycolide A via loss of HBr (Figure 6.9.d). Peaks at m/z 779 and 1443 corresponding to bromophycolide A monomer and dimer adducts with trifluoroacetate were observed when trifluoroacetic acid was added to the DESI spray solvent (Figure 6.9.e). A peak at m/z 1329 corresponding to the deprotonated bromophycolide A dimer was also observed in the spectrum (Figure 6.9.e). The identity of the peak at m/z 779 was verified by DESI MS² analysis, which gave the deprotonated bromophycolide A monomer by elimination of a trifluoroacetic acid molecule (Figure 6.9.f).

Figure 6.10 shows the B3LYP-D optimized structures of bromophycolide A (Figure 6.10.a), together with its Cl⁻ (Figure 6.10.b), Br⁻ (Figure 6.10.c) and CF₃COO⁻ (Figure 6.10.d) adducts. Density functional optimizations of the bromophycolide

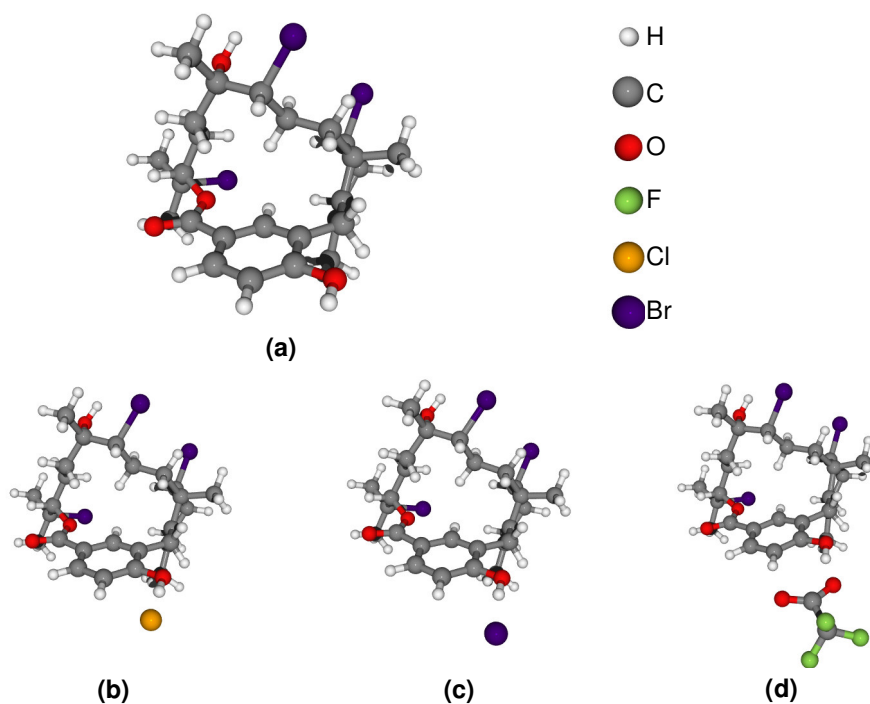


Figure 6.10. Optimized geometries for: (a) bromophycolide A, and its complexes with (b) Cl⁻, (c) Br⁻ and (d) CF₃COO⁻ optimized at the B3LYP-D/6-31+G* level of theory.

complexes with Cl^- , Br^- , and CF_3COO^- showed in all cases a preference for hydrogen bonding between each of these anions with the phenolic hydroxyl over the macrolide ring hydroxyl group. This preference is due in part to the delocalization of the partial negative charge transferred from the anion, over the phenyl ring, as indicated by Mulliken charge analysis. Another reason for the preference for binding to the phenolic hydroxyl is that anion binding to the macrolide ring hydroxyl disrupts the intramolecular hydrogen bonding between this hydroxyl and the neighboring macrolide ring bromine atom. This gives rise to a less stable conformation thereby making anion binding to this site less favorable by roughly 10 kcal mol^{-1} . Also, hydrogen bond lengths resulting from anion binding to the phenyl hydroxyl were about 0.2 \AA shorter for complexes with Cl^- and CF_3COO^- compared to similar complexes where anion binding occurs at the macrolide hydroxyl group. Similarly, for the Br^- complexes, hydrogen bond lengths for the phenyl hydroxyl were shorter by about 0.1 Angstrom . Table 6.1 presents the binding energies for the various bromophycolide-anion complexes together with their corresponding intermolecular hydrogen bond lengths. In general, chloride complexes showed the highest binding energies and bromide complexes the lowest. The former were observed to show greater charge delocalization compared to the bromide complexes, probably accounting

Table 6.1. Binding energies for various bromophycolide-anion complexes obtained from geometry optimizations at the B3LYP-D/6-31+G* level of theory. The intermolecular hydrogen bond lengths are indicated in parenthesis.

Analyte (M)	Binding energy/kcalmol ⁻¹ (H-bond length/Å)		
	[M + Br] ⁻	[M + CF ₃ COO] ⁻	[M + Cl] ⁻
bromophycolide A	32.7 (2.09)	36.2 (1.57)	37.1 (1.92)
bromophycolide B	30.5 (2.10)	34.1 (1.58)	34.9 (1.93)
bromophycolide E	31.9 (2.11)	35.2 (1.58)	36.2 (1.94)

for the higher binding energies. This observation is consistent with the higher sensitivity that was obtained by reactive DESI MS when chloride was added to the spray solvent (*vide infra*). In the case of the CF_3COO^- complex, despite the anion oxygen atoms showing two favorable interactions with the phenolic hydrogen atom of the bromophycolide, the anion tends to retain more of its negative charge, which might account for their slightly lower binding energies compared to the chloride complexes.

Figure 6.11 shows the effect of the DESI spray solvent Cl^- concentrations on the intensity of the corresponding bromophycolide A adduct (m/z 710) and the deprotonated dimer (m/z 1329). The intensity of the Cl^- adduct increases with the concentration of chloride, reaching a maximum at approximately $100 \mu\text{M}$ NH_4Cl . Above $100 \mu\text{M}$ NH_4Cl , the intensity of both species decrease, possibly due to increased analyte suppression effects as the electrolyte concentration increases. When HBr and CF_3COOH were each added to the DESI spray the optimum concentration for the formation of bromide and trifluoroacetate adducts with bromophycolide A were $10 \mu\text{M}$ and $135 \mu\text{M}$ respectively.

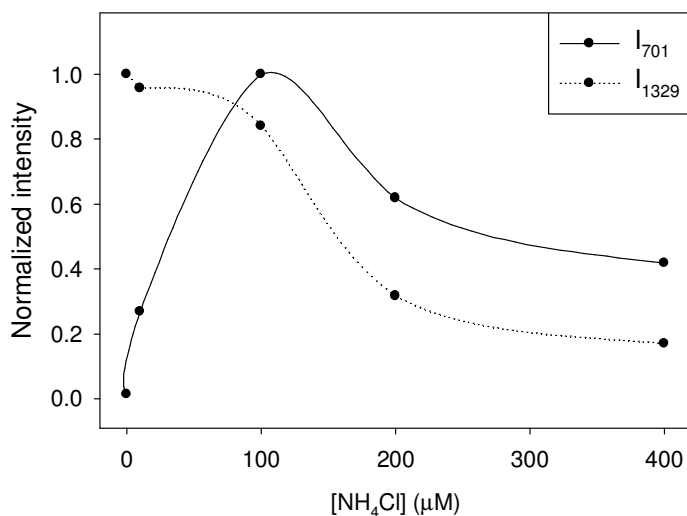


Figure 6.11. Effect of Cl^- concentration on the intensity of the [bromophycolide A + Cl^-] and [2 bromophycolide A - H] $^-$ ions. The intensity values were normalized.

The S/N of all the investigated bromophycolide anion adducts obtained by reactive DESI together with those of their corresponding deprotonated counterparts obtained by reagentless DESI are shown in Figure 6.12. At the optimized concentration of each of the investigated anions the chloride adducts gave the highest S/N. This resulted in S/N gains for the chloride adduct of 10x, 19x and 7x for bromophycolide A, B and E, respectively when compared to the corresponding deprotonated species. The high S/N for the chloride adducts is probably due to the comparably smaller size and high electronegativity of the chloride anion. The presence of chloride in the spray solvent also somewhat inhibits the formation of the deprotonated

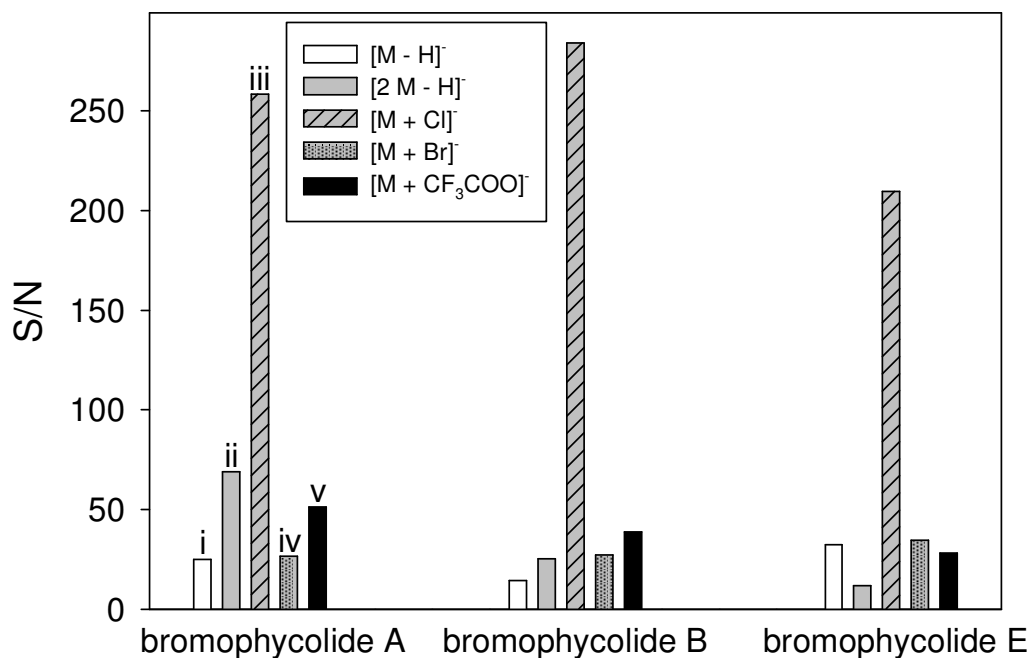


Figure 6.12. Signal-to-noise ratios observed for various bromophycolide species obtained from the DESI MS analysis of pure bromophycolides standards; spraying with a solution of 100 % MeOH, (i and ii) and spraying with a solution of methanol containing various anions including Cl⁻ (100 μM), Br⁻ (10 μM) and CF₃COO⁻ (135 μM) (iii, iv and v) respectively.

dimer species potentially resulting in the improvement of the signal for the monomer adduct. The LOD values ($S/N \geq 3$) for all the investigated species are shown in Table 6.2. The addition of chloride into the DESI spray clearly results in a very sensitive approach potentially allowing the direct and rapid detection for bromophycolides on the alga tissue surface.

Table 6.2. Limits of detection ($S/N \geq 3$) for various bromophycolides obtained by monitoring different species by DESI MS in negative ion mode: [a] reagentless DESI, [b] reactive DESI where various anions including Br^- , CF_3COO^- and Cl^- were added to the spray solution. [a] = reagentless DESI, [b] = reactive DESI.

Analyte (M)	Detection limit (pmolmm^{-2})			
	^[a] [M - H] ⁻	^[b] [M + Br] ⁻	^[b] [M + CF ₃ COO] ⁻	^[b] [M + Cl] ⁻
bromophycolide A	85	80	42	8
bromophycolide B	146	78	55	8
bromophycolide E	66	61	75	10

6.5.10. Direct Reactive DESI MS Profiling of Untreated Alga Tissue Samples

The applicability of the optimized reactive DESI MS protocols was then evaluated for the direct detection of bromophycolides from the surface of untreated *Callophycus serratus* samples. No appreciable bromophycolide signals were observed when analysis was performed by scanning the 400-1500 m/z range. This was probably due to the fact that trapping within such a wide m/z range effectively results in a low number of bromophycolide species trapped in the QiT mass analyzer. Analysis was then performed in the 550–750 m/z range, and signals corresponding to bromophycolide species were unambiguously observed (Figure 6.13). The peak at m/z 701 was assigned as the chloride adduct of bromophycolides A and/or B. This assignment is consistent with the theoretical isotopic distribution of these species. However, there could also be

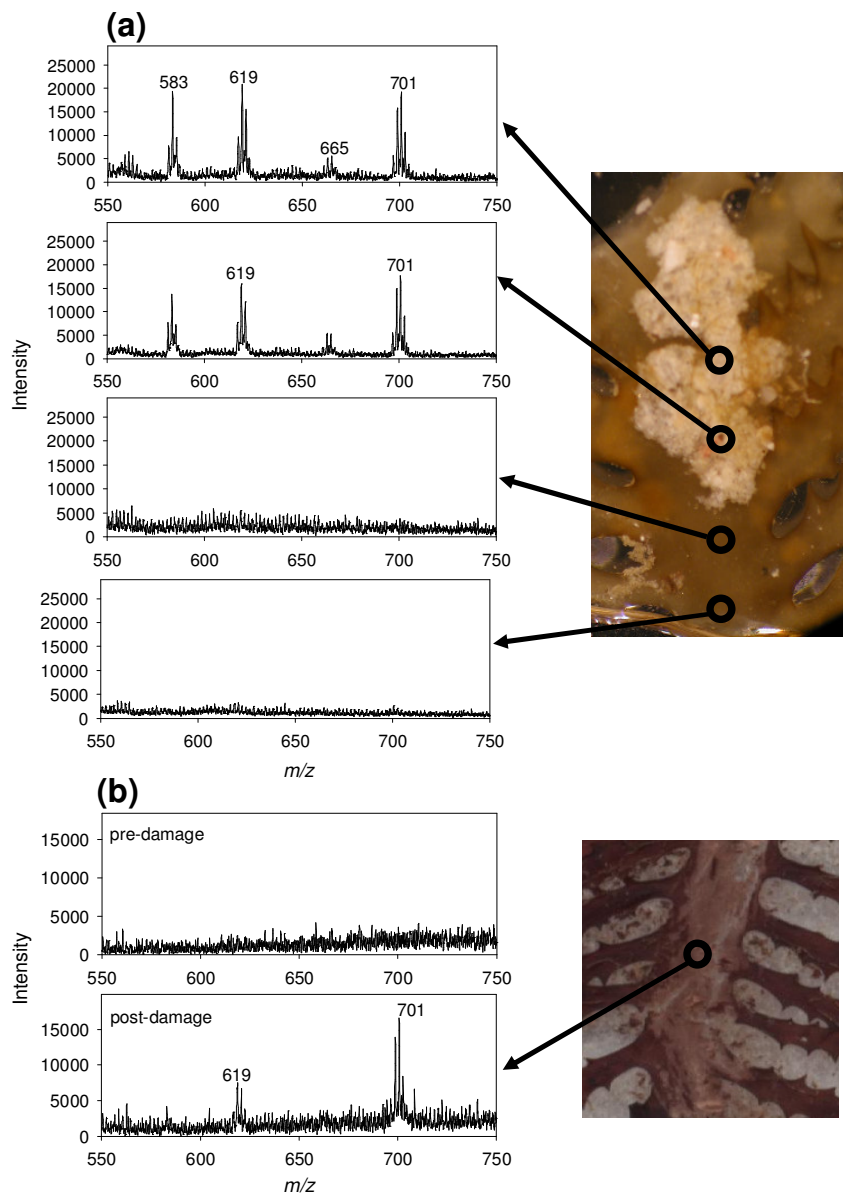


Figure 6.13. (a) Typical spatially-resolved reactive DESI spectra of *C. serratus* surface. (b) Representative reactive DESI spectrum from patch-free algal surface prior to and following mechanical damage. Ion clusters centered at 701, 619 and 583 correspond to [bromophycolide A(B) + Cl]⁻, [bromophycolide E + Cl]⁻ and [bromophycolide E - H]⁻ respectively.

contributions from the less abundant bromophycolides D and H, which have the same elemental formula.^{166, 271} An intense peak was also observed at m/z 619 and this was assigned as the chloride adduct of bromophycolide E, consistent with its theoretical mass

and isotopic distribution. Some minute peaks were also observed at m/z 665 and 583, corresponding to [bromophycolide A(B) - H]⁻ and [bromophycolide E - H]⁻ respectively. The bromophycolide signal intensity was not homogeneous throughout the sample surface, with some regions showing no signal whatsoever (Figure 6.13.a). Reactive DESI MS imaging analysis (*vide infra*) further confirmed this observation. In addition, no bromophycolide signal was observed for samples, which showed no white patches on their surfaces. However, when the surface of such samples was scraped with a razor blade resulting in the exposure of underlying internal tissues, bromophycolide signals were readily observed in all cases (Figure 6.13.b) suggesting an endogenous origin for bromophycolides.

The combined concentration of bromophycolides A and B on patch surfaces was estimated to be 36 ± 23 pmol mm⁻². This was calculated from the integral DESI MS signals of the Cl⁻ adducts of these two bromophycolides measured from 3 independent patches and predicted from a standard curve. The large standard deviation in bromophycolide surface concentrations suggests a high natural variability within the bromophycolide-rich patches. These results are consistent with LC-MS data, which indicates substantial variation of bromophycolide concentrations among extracts of whole algal tissues.¹⁶⁶ An evaluation of the antifungal activity (against *L. thalassiae*) of combined bromophycolides A and B coated onto nutrient agar substrates revealed a mean IC₅₀ value of 17 pmol mm⁻².¹⁶⁶ The IC₅₀ being approximately half the measured concentration of bromophycolides on patches indicates that these compounds are present in surface patches at sufficient levels to inhibit *L. thalassiae* and other susceptible fungi.

6.5.11. Reactive DESI MS Imaging of Untreated Alga Tissue

Figure 6.14.a shows the optical image of a *Callophycus serratus* tissue sample, which shows a heterogeneous distribution of white patches on the tissue surface. Figure 6.14.b shows a representative reactive DESI spectrum obtained from the sample, which shows peaks corresponding to chloride adduct of bromophycolide A and/or B (m/z 701) and bromophycolide E (m/z 619). Figure 6.14.c shows the reactive DESI MS image constructed for the peak at 701, which indicate the distribution of its corresponding species over the tissue sample. As observed in the DESI MS image, the sites corresponding to the highest bromophycolide signal as shown by the color intensity scale matches relatively well with white patches seen in the optical image. This further confirms the presence of bromophycolides on alga tissue in association exclusively within the distinct light-colored patches attached to *Callophycus serratus* surfaces. The

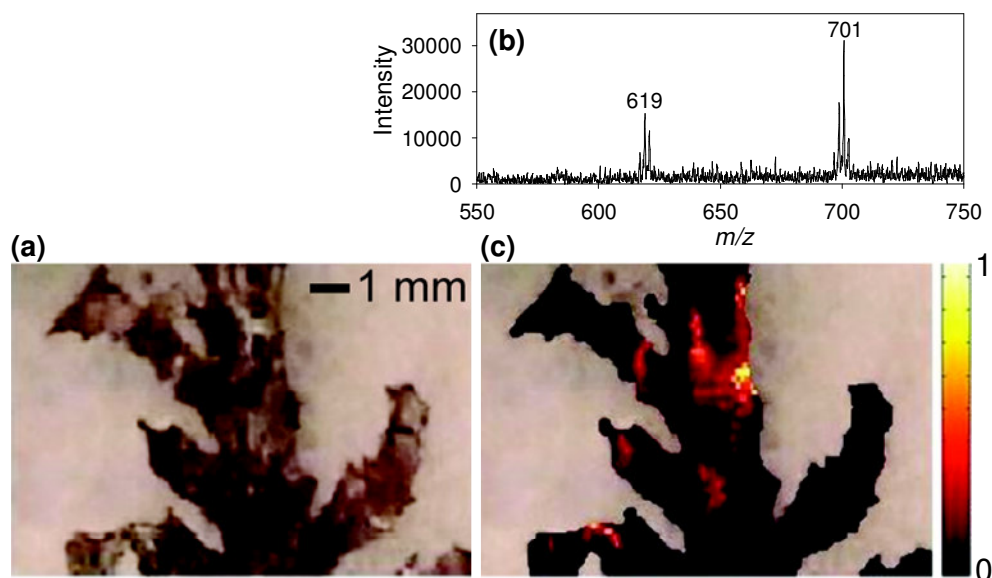


Figure 6.14. (a) *Callophycus serratus* optical image. (b) Representative reactive DESI spectrum of a light-colored patch on the *Callophycus serratus* surface. (b) Reactive DESI MS image reconstructed for the ion at m/z 701. The ion clusters centered at 701 and 619 represent [bromophycolide A(B) + Cl]⁻ and [bromophycolide E + Cl]⁻ respectively.

detection of bromophycolides among heterogeneous patches on algal surfaces and within algal tissues leads to the hypothesis that *Callophycus serratus* maintains these compounds internally and releases them at sparsely distributed surface sites. There are a number of possible explanations for the heterogeneous distribution of bromophycolides across *C. serratus* surfaces. One possibility is that bromophycolide rich sites represent a targeted response to microbial challenge at these sites. Another possibility is that patches are associated with sites of localized algal damage from which bromophycolides have leaked, providing antifungal defenses where tissues are vulnerable to waterborne microbes. Whichever hypothesis prevails, reactive DESI MS imaging presented here provides direct evidence for localization of chemical cues on biological surfaces in concentrations sufficient for targeted antimicrobial defense.

6.6. Conclusions

This study demonstrated the capabilities of chemical imaging by DESI MS as a highly specific and sensitive approach in the determination of the 2-dimensional distribution of various chemical species enabling application in a wide variety of fields. DESI MS imaging of pharmaceutical drug tablets provides information on the homogeneity of active ingredient enabling applications in pharmaceutical drug quality control. The degree of product homogeneity also provides information on the caliber of counterfeit-drug manufacturing practice. The large sample area evaluated during DESI MS imaging analysis is suggested to facilitate the determination of subtherapeutic counterfeit drugs especially those in which the API is inhomogeneous distributed. Sensitivity and selectivity enhancement during DESI MS imaging can be enhanced by

performing the experiment in the reactive mode. Application of reactive DESI MS imaging in the analysis of *Callophycus serratus* provided an unprecedented ability to map secondary metabolites to distinct surface sites. Reactive DESI MS imaging revealed that bromophycolides are not homogeneously distributed across *Callophycus serratus* surfaces but instead are associated within distinct surface patches at concentrations sufficient for targeted antimicrobial defense. This suggests a role of bromophycolides in *Callophycus serratus* in surface mediated antimicrobial chemical defense.

CHAPTER 7. DESORPTION ELECTROSPRAY/METASTABLE-INDUCED IONIZATION (DEMI): A FLEXIBLE MULTIMODE AMBIENT IONIZATION TECHNIQUE

7.1. Abstract

This Chapter presents a new multimode ambient ion source termed Desorption Electrospray/Metastable-Induced Ionization (DEMI), which integrates the benefits and circumvents some of the limitations of Desorption Electrospray Ionization (DESI, polarity range limited) and DART-type Metastable-Induced Chemical Ionization (MICI, molecular weight limited). This ion source allows three unique operation modes, each with unique capabilities, including: spray (DESI-like)-only, MICI-only and DEMI (multimode), and can be thus operated in each of these modes allowing the detection of a wider range of analytes of interest. Ion source operation in the MICI-only mode is particularly well suited for the analysis of low polarity, low molecular weight compounds in powdered, solid or dissolved samples. Operation of the ion source in spray-only mode shows superior performance for the analysis of high molecular weight, high polarity compounds over the MICI-only mode. Heating the nebulizer gas in spray-only mode allows improved analyte solubility in the spray solvent, enabling up to an order of magnitude improvement in sensitivity. Perhaps the most appealing mode of operation of the ion source is the DEMI mode, which allows the simultaneous detection of compounds within a much broader range of polarities and molecular weights than each of the individual modes. For drug quality screening and counterfeit detection applications, operation in the DEMI mode results in the generation of both protonated and sodiated

analytes. The observation of such complementary ionic species facilitates compound identification when investigating unknowns.

7.2. Introduction

In recent years, there has been an increasing demand on analytical technologies to become more universal, enabling the simultaneous detection of a broader range of analyte chemistries. In the realm of mass spectrometric analysis, efforts toward meeting this goal have been directed towards combining more than one ionizer type at the front end of the mass spectrometer.²⁷⁷ Presented in this Chapter is the implementation of a novel multimode ambient ion source; DEMI, which consolidates the complementarity between DESI and DART enabling the simultaneous analysis of a broader range of compound classes.

Multimode ionization sources combining electrospray ionization with atmospheric pressure chemical ionization (ESI/APCI),^{277, 278} electrospray ionization with atmospheric pressure photoionization (ESI/APPI),^{279, 280} for probing high complexity samples by liquid LC-MS²⁸¹ have been reported, and are now commercially available. However, they are still limited by the intrinsic low throughput performance of LC separations, which precede sample ionization/MS analysis. Ambient MS methods on the contrary are particularly attractive because of their rapid throughput capability and their ability to investigate samples of odd shapes and sizes, while preserving their intrinsic chemical information content. DESI is particularly powerful for analyzing thermally labile, non-volatile, polar molecules in a mass range reported to be as high as 45 kDa.¹²⁷ DART, on the other hand, has been shown to be best suited for the analysis of molecules

with a broad range of polarities in a mass range of up to 800 Da,¹⁸³ approximately. The complementarity between DART and DESI mechanisms therefore suggests a potential advantage in combining the two techniques into a hybrid approach.

In this Chapter, a novel ambient multimode ionization technique; DEMI, together with first insights into its associated ion generation mechanisms is presented. This technique combines features of DESI- and DART-type ionization, but with the unique capability of enabling the simultaneous and direct detection of molecules within a broader range of polarities and molecular weights than these techniques alone, without loss of throughput or spatial resolution.

7.3. Experimental Details

7.3.1. Samples and Reagents

All reagents were used without additional purification. HPLC grade methanol (EMD Chemicals, Gibbstown, NJ, USA), ACS grade acetone (Mallinckrodt Baker, Phillipsburg, NJ, USA), and ultrapure water (18.2 M Ω cm⁻¹), obtained from a Nanopure purification unit (Barnstead, San Jose, CA) were used as spray solvent in the spray-only and DEMI experiments. Characterization of capabilities of various ion source operation modes was investigated using the following: Tylenol[®] tablets (500 mg acetaminophen, McNeil-PPC, Inc., Fort Washington, PA, USA), counterfeit artesunate antimalarial tablets collected in Cameroon and Southern China, Halfan[®] tablets (250 mg halofantrine hydrochloride, GlaxoSmithKline, London, UK), multivitamin tablets (Pharmelle Pharmaceutical Company, Gilbert, AZ, USA), trans-10, 11-dibromodibenzosuberone, dibenzosuberone, cholesterol, angiotensin I (Sigma Aldrich, St. Louis, MO, USA) and

spray dried lactose (FMC Corp., Newark, DE, USA). Unless stated otherwise, high-purity He (99.999% Airgas, Atlanta, GA) was used to generate metastables in MICI and DEMI experiments. Industrial grade N₂ (99.998% Airgas, Atlanta, GA) was used as nebulizer gas for the sprayer.

7.3.2. DEMI Ion Source

The experimental setup is shown in Figure 7.1. The DEMI ion source was constructed by interfacing a custom-built glow discharge chamber to produce He metastables¹⁸⁷ to a custom-built DESI-type ion source modified by the addition of a resistive flow-through heater to the nebulizer gas line. The glow-discharge chamber (held at room temperature) was connected to a 3/8 in. Swagelok[®] T-union, fitted with a 10 cm glass capillary (i.d. = 3.8 mm, o.d. = 6.4 mm). The T-union was sealed onto the glass capillary at one end, with the glass capillary extending up to the edge of the opposite, unsealed end. The glass capillary was tapered from the sealed end to a final 1.5 mm i.d., 2.8 mm o.d., creating a concentric clearance for the metastable gas stream flow. This assembly was mounted onto an xyz manual translational stage, with the glass capillary exit aligned with the mass spectrometer capillary inlet. The distance between the glass capillary exit and the MS capillary inlet was 10 mm unless stated otherwise. The spray emitter consisted of an 11.5 cm long inner liquid capillary (83 μm i.d., 190 μm o.d.), surrounded by an outer nebulizer gas capillary (381 μm i.d., 1588 μm o.d.), both made of stainless steel. These were fitted into a 1/4 in. Swagelok[®] T-union (Swagelok Company, Solon, OH, USA) with the inner capillary fixed to its proximal part, and the outer capillary fixed to the distal part, offset by ~0.2 mm from each other. One port of this

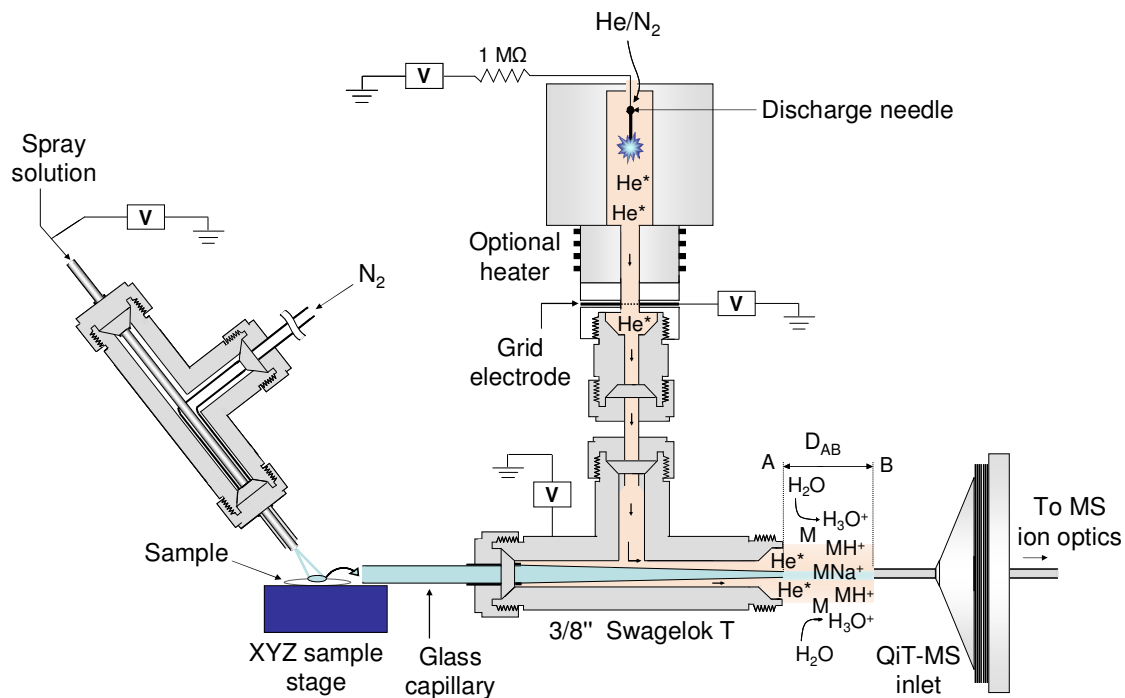


Figure 7.1. Schematic of the DEMI ion source coupled to a quadrupole ion trap mass spectrometer (only inlet shown).

union was connected through an in-line T type air process heater (Omega Engineering, Stamford, CT, USA, not shown in Figure 1) to a N₂ gas cylinder using Teflon[®] tubing to provide heated/unheated nebulizer gas. The temperature of the heated gas was monitored using a 1/8 in. stainless steel K-type thermocouple probe connected to a benchtop model CSC-321-K controller (Omega Engineering, Stamford, CT, USA). The spray solution was delivered to the sprayer through a short piece of 127 μm i.d. PTFE tubing that was connected to one port of a PEEK T-union (Upchurch Scientific, Oak Harbor, WA, USA). The second port of this PEEK union was connected through a longer piece of PTFE tubing to a 250 μL glass syringe (Hamilton Company, Reno, NV, USA) from which the spray solution was delivered. The spray solution was biased to +3000 V via an external high-voltage power supply (SRS PS350, Sunnyvale, CA). This power supply was in

electrical contact with the spray solution through a third port of the PEEK T-union. The sprayer assembly was mounted through posts onto a second xyz manual translational stage. The motorized stage employed in Chapter 6 was used for sample positioning relative to the sprayer. Analytes dissolved by the charged solvent spray, thermally desorbed or aerosolized by the nebulizer gas are transported towards the mass spectrometer inlet through the glass transport capillary. Upon exiting this glass capillary, the dispersed droplets, particulates or sublimated neutrals become entrained with the metastable stream emanating from the glow-discharge source.

7.3.3. Mass Spectrometry

All experiments were performed on a Thermo Finnigan LCQ Deca XP+ quadrupole ion trap mass spectrometer (Thermo Fisher Scientific, San Jose, CA, USA) operated in positive ion mode using *Xcalibur* version 2.0 software. The standard ion transfer capillary was replaced with an extended version (20.5 cm long, 762 μm i.d., 1588 μm o.d., Small Parts Inc., Miramar, FL, USA) that was heated to 300°C. Samples were positioned for analysis so that the glass sampling capillary of the DEMI ion source was ~0.5 mm from the edge of the mounted sample at a collection angle of 0°. The sprayer tip was positioned 4–6 mm from the glass capillary inlet and 1–3 mm away from the surface of the sample at an angle of 55°. Unless stated otherwise, the spray solvent was composed of 90:10 MeOH:H₂O, at a flow rate of 12 $\mu\text{L}/\text{min}$. The nebulizer gas pressure was set to 150 psi and heated to a temperature of 71°C unless stated otherwise. Spectra were collected in full scan mode with automatic gain control turned on for a maximum

injection time of 200 ms, and 2 microscans per spectrum. Data were acquired for a total time of 15 s unless stated otherwise.

7.4. Results and Discussion

7.4.4. DEMI Ion Source Operation Modes

The DEMI ion source allows operation in three different modes (Figure 7.2), including: (i) metastable-induced chemical ionization (MICI)-only, (ii) spray-only (DESI-like) and (iii) DEMI multimode. In MICI-only mode, analyte desorption/ionization can be achieved *via* (a) aerosolization with unheated nebulizer gas (for fine powders) followed by reactions of solid aerosol particles with reactant ions, or (b) thermal desorption using heated nebulizer gas (for non-dispersible solids). In spray-only mode the glow discharge voltage is kept off, while analytes are sampled by micro-extraction into the charged solvent stream produced by the pneumatic sprayer. Operation in this mode can be achieved with the nebulizer gas unheated or heated to modify analyte solubility. In DEMI mode, the shortcomings of MICI (limited in mass range) and spray-only (limited in polarity range) modes are mitigated. Each of these ion source operation modes enable unique capabilities presented in the following sections.

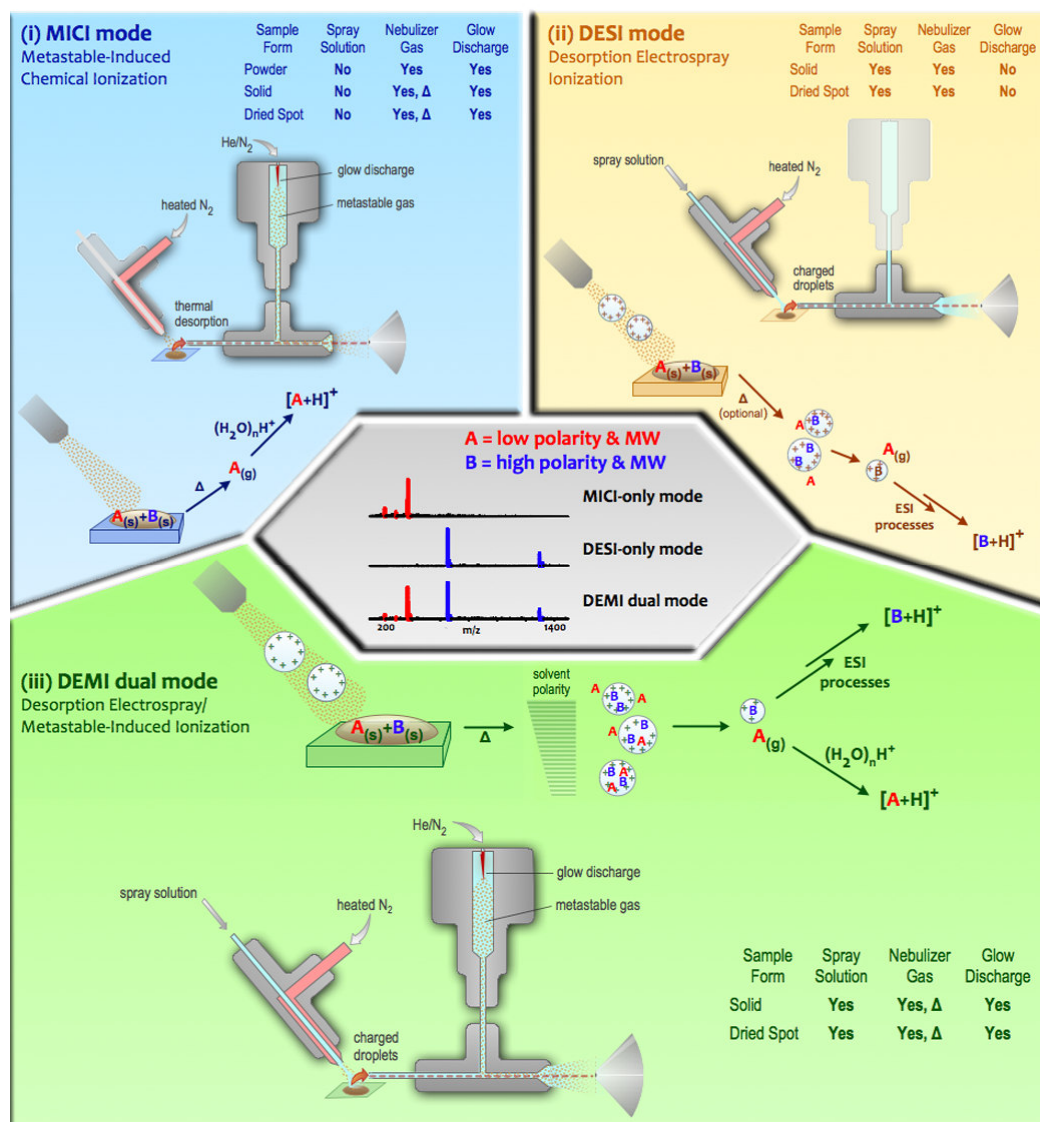


Figure 7.2. Pictorial representation of the different DEMI operation modes, and the corresponding ion generation mechanisms believed to be prevalent in each case.

7.4.5. Reagent Ion Generation/Source Optimization

Figure 7.3 shows a typical background mass spectrum generated by metastable He atoms, when the ion source is operated in positive ion mode. Signals corresponding to protonated water clusters $((H_2O)_nH^+$, $n=2-4$) were observed with $n=2$ dominating the spectrum. These clusters serve as reagent ions for analyte ionization, which occurs by a process whose efficiency depends on the proton affinity of the analyte being greater than

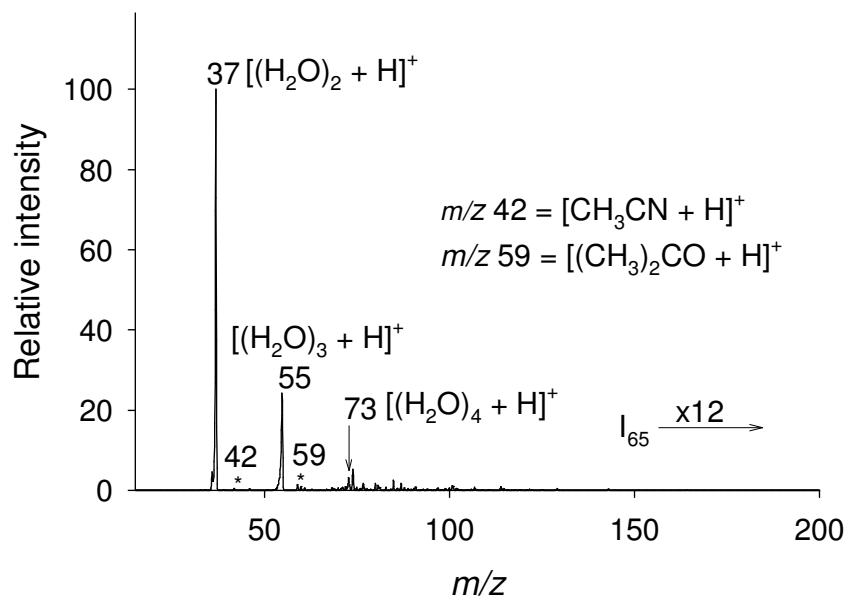


Figure 7.3. Mass spectrum showing typical reagent ions for source operation in the MICI and DEMI modes.

that of the reagents. It has been reported that the proton affinities of $(\text{H}_2\text{O})_n\text{H}^+$ increase with increasing n , and that the cluster with $n=2$ ²⁸² presents the largest reaction cross section.^{282, 283} The predominance of smaller-size clusters in the spectrum ($n=2-3$) should therefore be advantageous for efficient proton transfer. Minute peaks at m/z 42 and 59 (marked with asterisks) corresponding to protonated acetonitrile and acetone were also observed, originating from trace amounts of these chemicals in the laboratory environment. Their relatively low proton affinities^{282, 283} also make them readily available for proton transfer reactions.

In order to maximize dynamic range and minimize ion suppression during direct ionization, the effect of various experimental variables on the total reactant ion intensity was investigated by performing single measurements at each particular setting. Of particular interest was the effect of glow discharge gas flow rate on both the reactant ion signal intensity and the ion trap analyzer pressure. The pressure in the quadrupole ion

trap analyzer region showed a minimum at a gas flow rate of 4 L/min (Figure 7.4.a, right axis), coinciding with the maximum reagent ion cumulative signal, for both He or N₂-supported glow discharges (Figure 7.4.a, left axis). Lower flow rates were detrimental, with the analyzer pressure spiking to values of up to 7.7×10^{-5} Torr. The decrease in analyzer pressure for flows higher than 2 L/min was probably caused by the

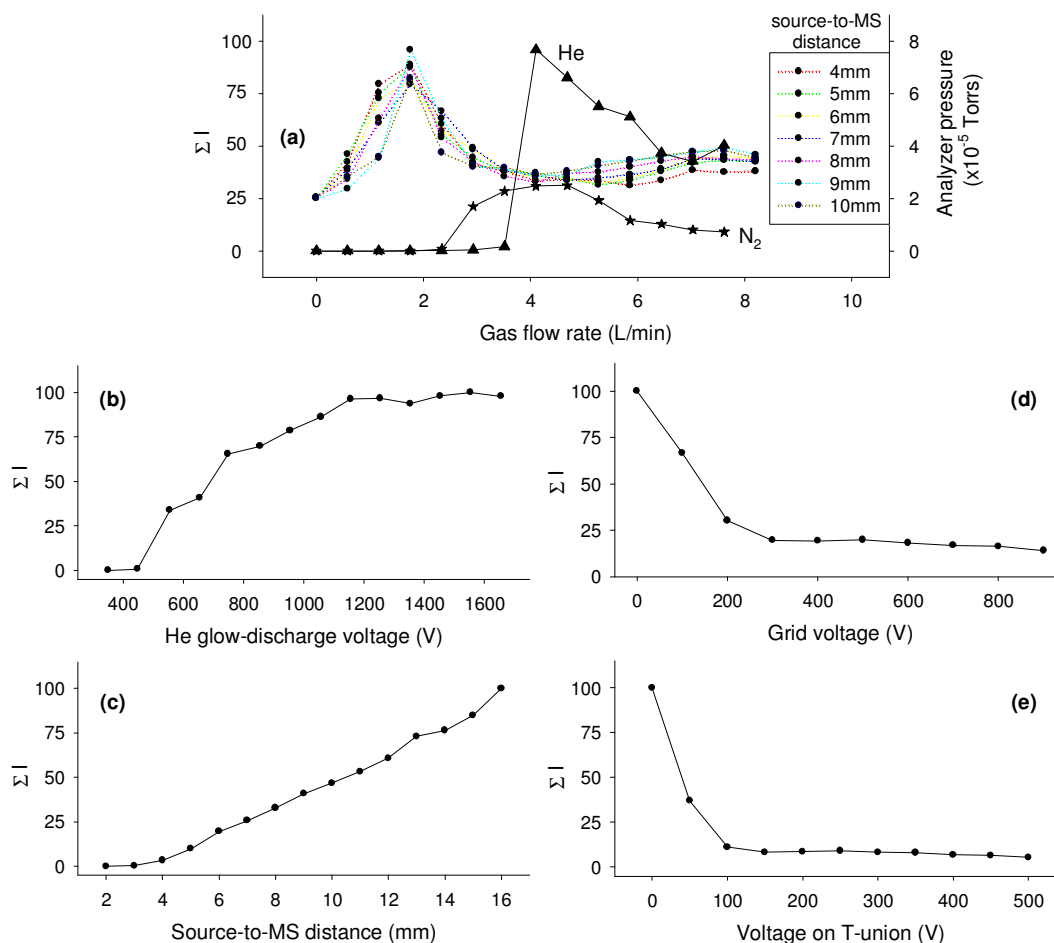


Figure 7.4. Optimization of the total reactant ion signal for the ion source operating in MICI-only mode (a) as a function of He or N₂ discharge gas flow rate (corresponding normalized intensity scale on left ordinate). The dotted lines show the effect of He gas flow rate on the ion trap analyzer pressure (scale on the right ordinate) for different source-to-MS inlet distances (D_{AB}). The effect of (b) the glow-discharge voltage, (c) the source-to-MS distance (D_{AB}), (d) the grid voltage and (e) the voltage bias on T-union on the total reactant ion intensity is shown on the bottom plots. For each plot, the total ion signals were normalized to that of the maximum value.

creation of a low pressure region at the interface with the MS inlet by the glow discharge gas flowing around the periphery of the glass transfer capillary and the MS inlet aligned with it. This effect limited the load on the pumping system, allowing stable operation. Figures 7.4.b-e shows the effect of other experimental variables on the total reagent ion signal. The signal increased with the He glow-discharge voltage up to about +1400 V, the threshold above which a stable glow discharge was achieved (Figure 7.4.b). The total reagent ions signal also increased with the source-to-MS distance (D_{AB}) for the entire range investigated (Figure 7.4.c). This is possibly due to an increasing in reaction time of He or other metastable species with increasing D_{AB} . A fine balance is therefore required to allow generation of sufficient amount of reagent species while minimizes suppression and analyte dispersion effects. It is possible to envision losses in sensitivity due to dispersion effects especially with an increase in D_{AB} . However, sensitivity losses were highly compensated for by the source design due to significantly large cross sectional area of the glass capillary inlet into which droplets and thermally desorbed or aerosolized powdered analytes were sampled. The sampled analytes were focused into a tighter plume before exiting the glass capillary. Efficient sampling of the focused analyte stream emanating from the glass capillary was achieved by aligning its exit with the MS capillary inlet. The flow of the metastable plume around the periphery of the glass capillary also served to focus the analyte plume upon exit, minimizing dispersion. As such no evident losses in sensitivity were observed in this set-up when the source was operated in the DESI-only and/or MICI-only modes, when compared to traditional DESI and DART experiments. The standard capillary inlet has a cross-sectional area which is 25 times smaller than the glass capillary inlet presented here. The total reagent ion signal

was also observed to decrease with increasing grid (Figure 7.4.d) and T-union (Figure 7.4.e) voltages probably due to enhanced neutralization of reagent ions. Based on these studies, the following optimum settings were used for all experiments unless stated otherwise: He glow discharge voltage = +1400 V, voltage on T-union = 0 V, grid voltage = 0 V, $D_{AB} = 10$ mm.

7.4.6. Capabilities of Ion Source Operation in the MICI-only Mode

DEMI operation in the MICI-only modality was observed to be particularly advantageous for the analysis of powders by direct aerosolization. In this approach, sample particles propelled by the nebulizer gas flow are captured by the transfer glass capillary and transported towards the downstream ionization region for reaction with $(H_2O)_nH^+$ ions. Figure 7.5 exemplifies the successful analysis of low polarity compounds in powder form, including dibenzosuberone (Figure 7.5.a), dibromodibenzosuberone (Figure 7.5.b), cholesterol (Figure 7.5.c) and the mixture of all three (Figure 7.5.d) in which the various analytes were detected as either protonated and/or ammoniated species. The detection of all three low polarity compounds in the mixture (Figure 7.5.d) showcases the performance of the MICI-only mode in the analysis of mixtures resulting in minimal suppression effects. Powder analysis in the MICI-only mode was further exemplified by the analysis of some pulverized samples including: spray dried lactose (Figure 7.6.a), a chloroquine containing fake artesunate tablet (Figure 7.6.b), and a Halfan® antimalarial tablet (Figure 7.6.c), in which the main constituents were detected predominantly as protonated species. A small degree of carryover was observed during the analysis of powders in the MICI-only mode. This effect was negligible when small

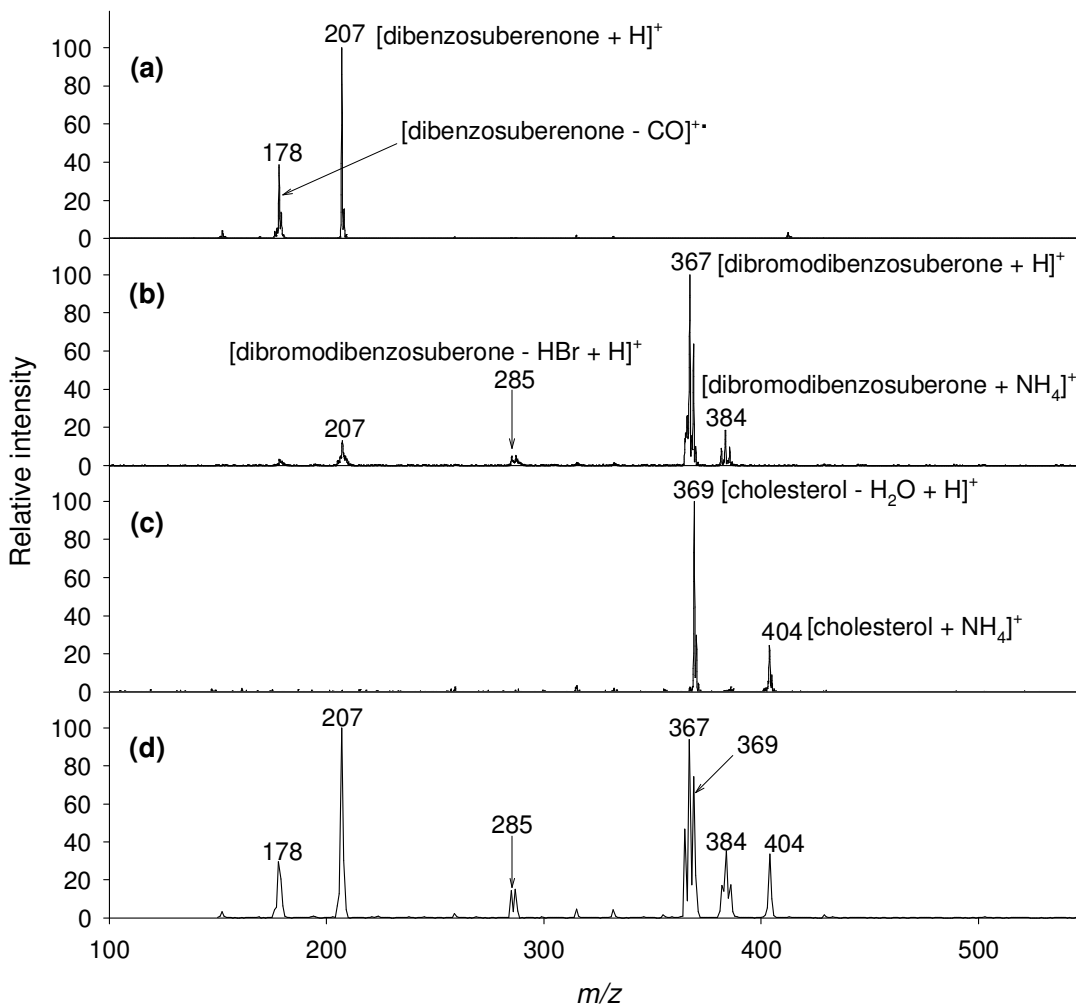


Figure 7.5. Mass spectra of powders of some low polarity compounds and their mixture with the source operating in MICI-only mode. (a) dibenzosuberone, (b) dibromodibenzosuberone, (c) cholesterol (d) mixture of all three. 2 mg powder of each sample deposited onto a glass slide were aerosolized and transported by the N₂ nebulizer gas from the pneumatic sprayer (with spray solvent off) through the glass capillary. 1 mg of each compound was used to prepare the mixture. The N₂ nebulizer gas temperature and pressure were 14°C (unheated) and 150 psi, respectively.

amounts of material were sampled into the glass capillary, but was noticeable when increasing the amount of material sampled. Due to the ease with which the glass capillary assembly is attached to the rest of the source, carryover was prevented by simply unscrewing and rinsing the glass capillary with a solution of 50:50 MeOH/H₂O and reattaching it in-between runs, if necessary.

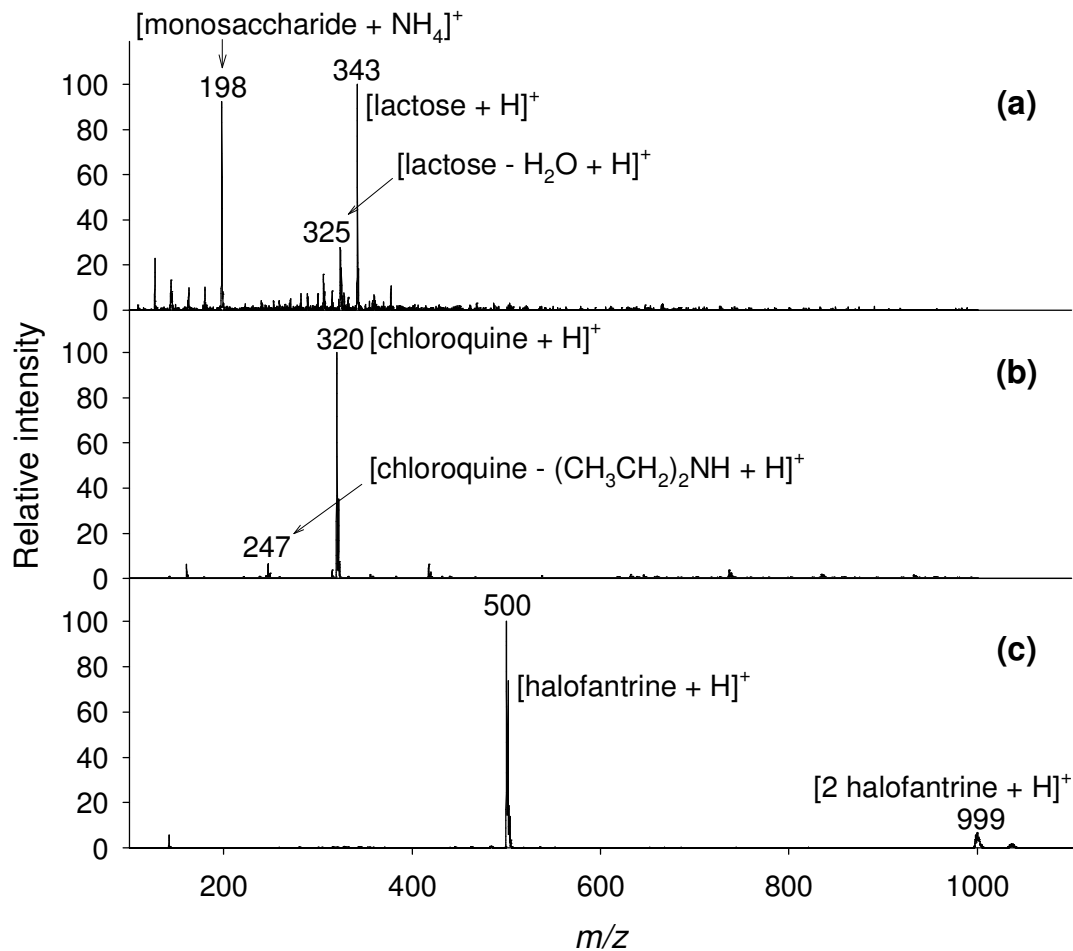


Figure 7.6. Mass spectra of various powdered samples with the source operating in the MICI-only mode. (a) spray dried lactose, (b) powdered chloroquine-containing fake artesunate antimalarial tablet, and (c) powdered Halfan[®] antimalarial tablet containing halofantrine. The pressure of the unheated nebulizer gas was 150 psi.

Figure 7.7 shows a direct comparison of the analysis of an intact (Figure 7.7.a) and powdered (Figure 7.7.b) multivitamin tablet in MICI-only mode. The intact tablet spectrum showed predominantly one peak corresponding to protonated niacinamide, the lightest component in the sample. Powder analysis presented more signals corresponding to niacinamide, ascorbic acid, thiamine, pyridoxine and biotin, the most abundant components in the sample. The observed increase in the number of observable signals can be ascribed to the higher surface area interacting with gaseous reagent ions when the

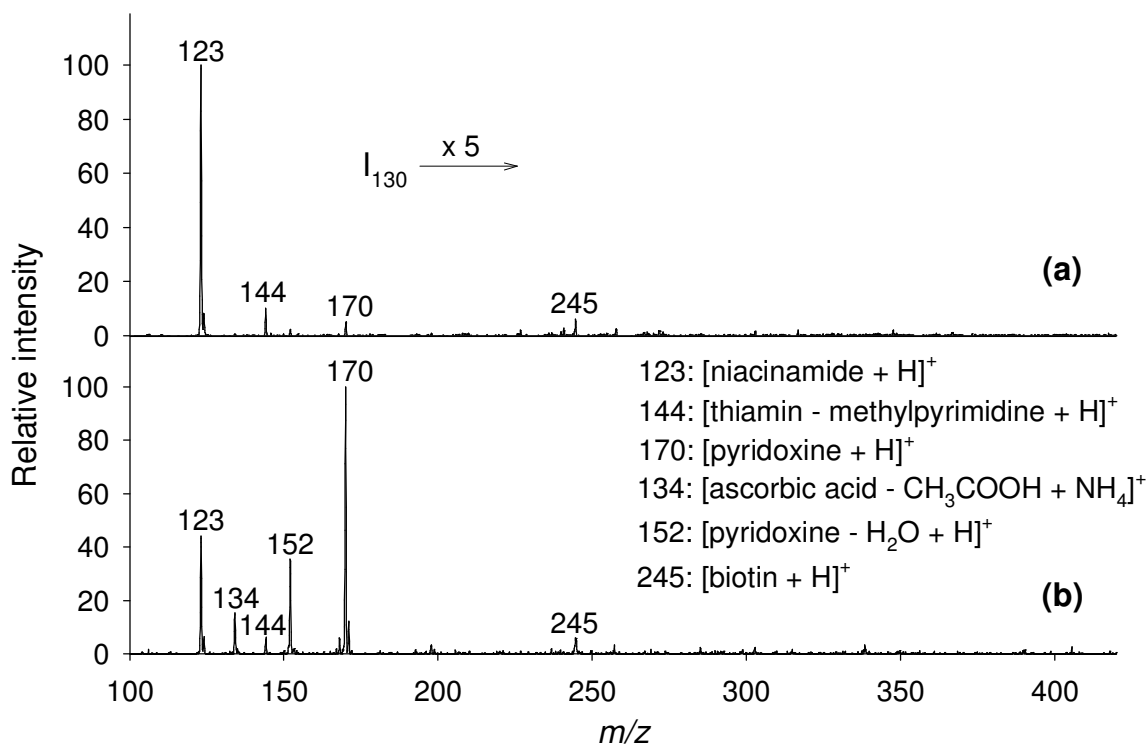


Figure 7.7. Direct ionization mass spectra of a multi-vitamin tablet with the source operating in the MICI-only mode: (a) intact tablet analyzed with the nebulizer gas heated to 83°C, (b) powdered sample deposited on a glass slide and analyzed with the nebulizer gas unheated.

sample was aerosolized. For non-dispersible samples, such as intact tablets, analyte ion yield in the MICI-only mode was found to largely depend on, and increase with the temperature of the nebulizer gas, as shown in Figure 7.8.a for the analysis of an acetaminophen tablet. Figure 7.8.b, c and d show the corresponding mass spectra from this analysis, at three different temperatures, where the protonated analyte monomer (m/z 152) and dimer (m/z 303) were observed as the predominant analyte species in the spectra. Some unidentified background peaks were also observed predominantly at low nebulizer gas temperatures, possibly resulting from contaminating species desorbed from within the gas transfer lines.

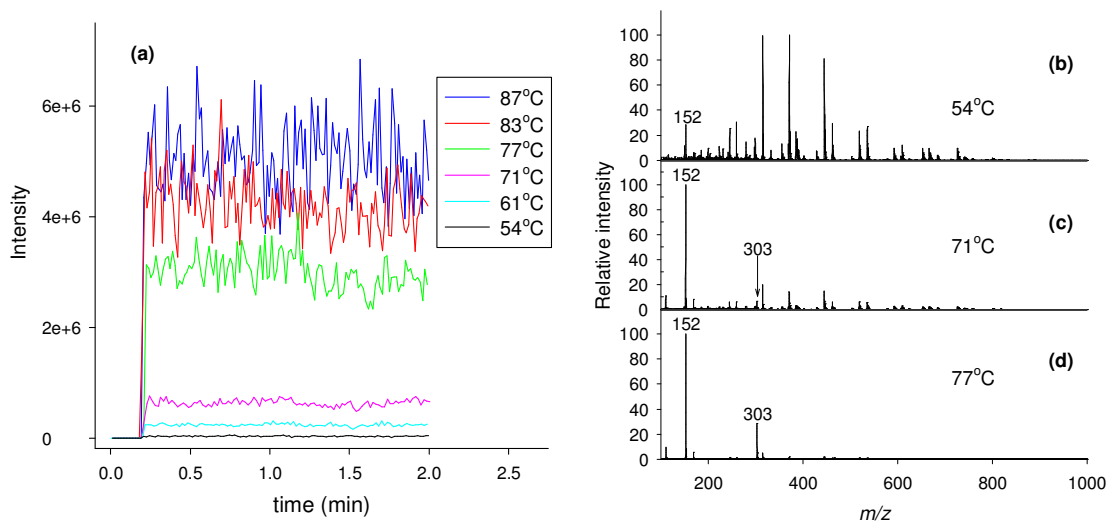


Figure 7.8. Left panel: (a) selected ion intensity ($m/z 152 \pm 0.15$) traces obtained from the analysis of an intact acetaminophen tablet with the source operating in the MICI-only mode. Samples were probed with the nebulizer gas from the sprayer (solvent off) heated to various temperatures with an inline heating element. **Right panel:** corresponding mass spectra obtained for the nebulizer gas heated to (b) 54°C, (c) 71°C, and (d) 77°C.

7.4.7. Capabilities of Ion Source Operation in the Spray-only Mode

DEMI source operation in the spray-only mode, essentially equivalent to DESI, using heated nebulizer gas allows appreciable improvements in the overall analyte signal. This was demonstrated by the analysis of an acetaminophen tablet, which shows peaks corresponding predominantly to sodiated acetaminophen monomer ($m/z 174$) and dimer ($m/z 325$, Figure 7.9.a). The detection of predominantly sodiated species by DESI is presumable due to the presence of sodiated excipient in the tablet matrix. Greater than an order of magnitude improvement in the analytical signal was achieved by heating the nebulizer gas up to 71°C (Figure 7.9.b). This reinforced the idea of a prevailing DESI-like droplet pick-up mechanism where analyte signal largely depends on its solubility in the spray solvent.^{100, 284, 285}

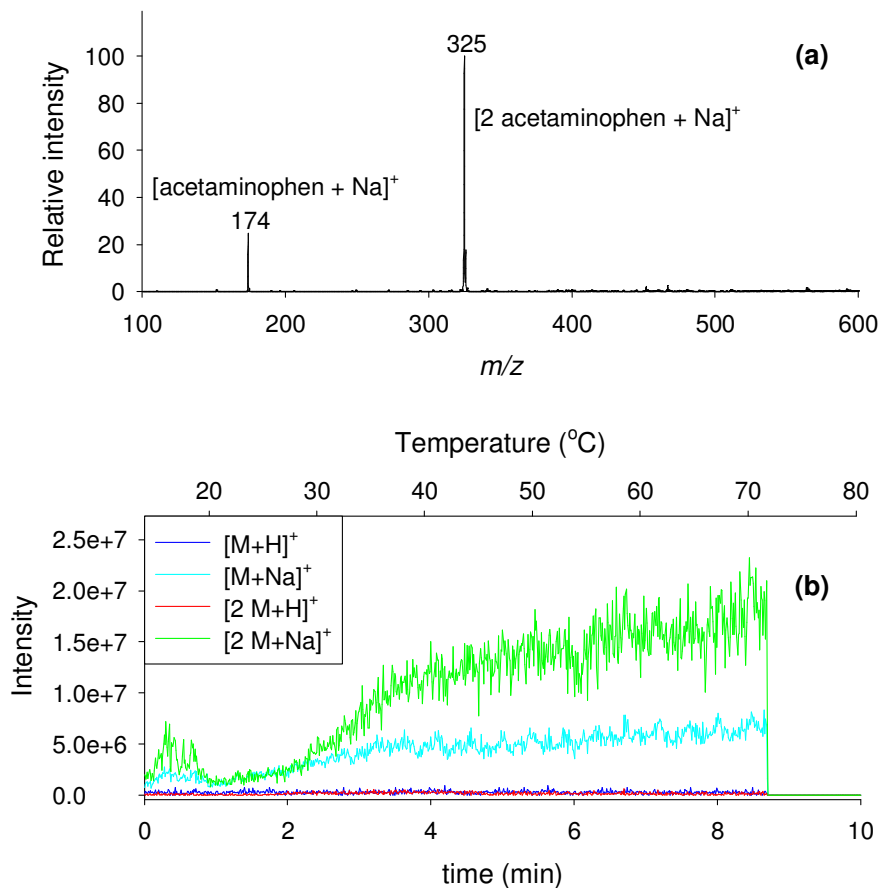


Figure 7.9. (a) Typical mass spectrum obtained from the analysis of an acetaminophen tablet with the source operating in spray-only mode, (b) Selected ion intensity traces (m/z 152, 174, 303 and 325) from the analysis of an acetaminophen tablet with the nebulizer gas set to ramp from 14°C – 83°C at a rate of ~ 6.5°C/min with the source operated in spray-only mode. The window width for all selected ion traces was 0.3 m/z . M = acetaminophen.

7.4.8. Capabilities of Ion Source Operation in the DEMI Mode

Perhaps the most intriguing mode of operation of the ion source is the DEMI mode, which mitigates the limitations of the individual MICI and spray-only modes enabling the simultaneous detection of a broader range of analyte chemistries. This capability was showcased by the analysis of a binary mixture of dibromodibenzosuberone and angiotensin I standards deposited onto glass slides. Figure 7.10 shows the spectra obtained from the analysis of the above mentioned binary mixture with a nebulizer gas

temperature of 71°C, using 90:10 MeOH:H₂O at 15 µl/min as the spray solvent. Only the low polarity, lower molecular weight protonated dibromodibenzosuberone was observed in MICI-only mode (Figure 7.10.a). In the spray-only mode (Figure 7.10.b), only the higher polarity, higher molecular weight, singly and doubly protonated angiotensin I species were observed. In DEMI mode, both dibromodibenzosuberone and angiotensin I

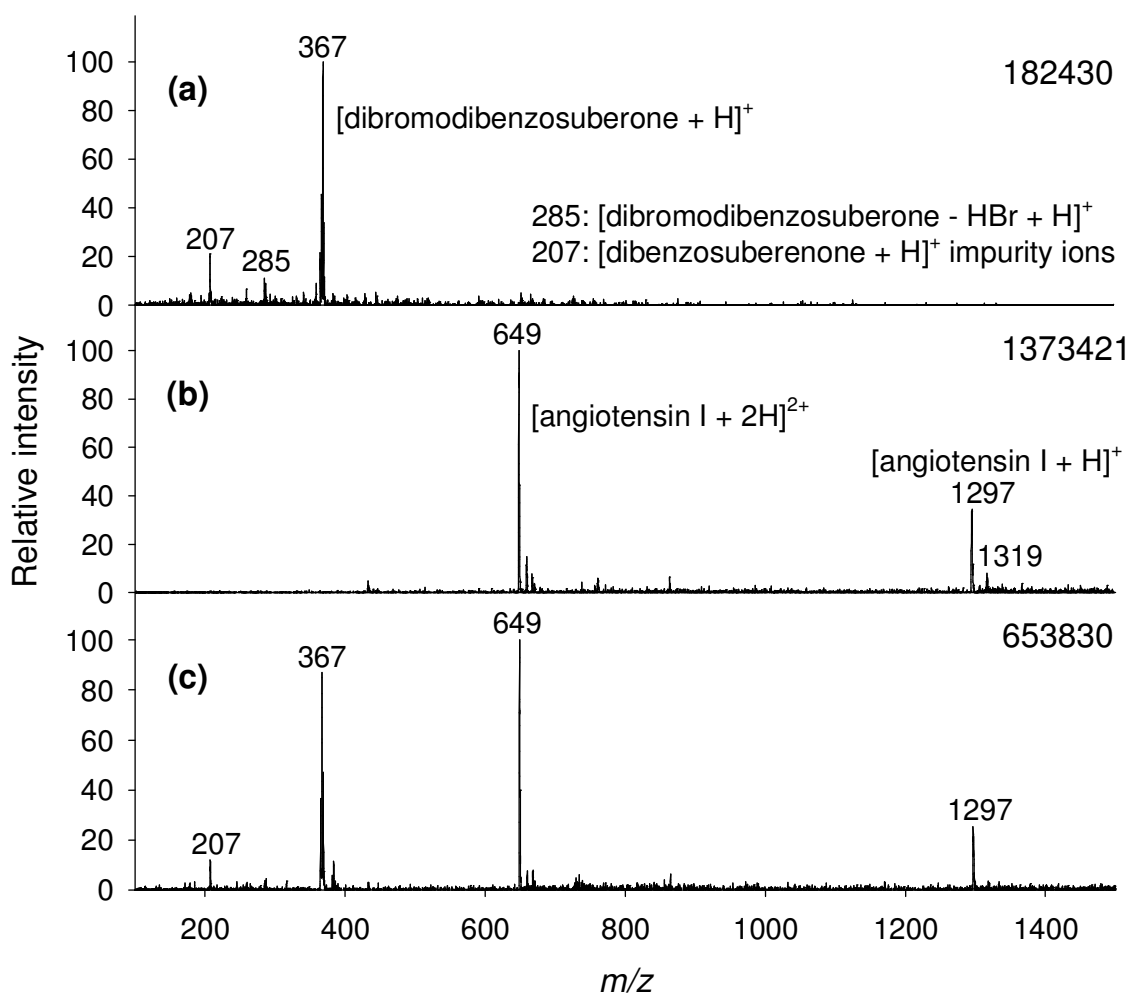


Figure 7.10. Mass spectra of a binary mixture (10 µL, 0.5 mg/mL angiotensin I, 1mg/mL dibromodibenzosuberone, deposited onto a glass slide) analyzed in, (a) MICI-only mode, (b) spray-only mode and (c) DEMI mode. (m/z 1319 = [angiotensin I + Na]⁺). Noted in the upper right corner of each plot is the base peak absolute intensity.

ionic species were observed (Figure 7.10.c). The limits of detection (LOD) for each of the component in this binary mixture for the different operation modes are presented in Table 7.1. When the previous experiment was performed with the nebulizer gas unheated, only peaks corresponding to angiotensin I were observed both in the spray-only and

Table 7.1. Limit of detection ($S/N \geq 3$) for each of the components in a binary mixture of angiotensin I (0.5 mg/mL) and dibromodibenzosuberone (1 mg/mL) spotted onto glass slides (10 μ L) from a solution in 90:10 MeOH:H₂O and analyzed with each of the operation modes after solvent evaporation.

Analyte	LOD (pmol)		
	MICI-only	Spray-only	DEMI
Angiotensin I	-	79	120
Dibromodibenzosuberone	1269	-	760

DEMI modes (data not shown). The poor solubility of dibromodibenzosuberone in the spray solvent is probably the limiting factor preventing efficient analyte pick-up. Similar experiments using a spray solvent mixture of lower polarity (50:50 MeOH:acetone) resulted in peaks corresponding to singly and doubly protonated angiotensin I in spray-only mode (Figure 7.11.a) and peaks for both dibromodibenzosuberone and angiotensin I in DEMI mode (Figure 7.11.b). These findings suggest that the higher polarity angiotensin I presumably undergoes protonation in solution following desorption by ESI-like processes where insufficient basicity of dibromodibenzosuberone precludes its ionization. Dibromodibenzosuberone ions were therefore most likely generated by metastable-induced chemical ionization of gaseous neutrals produced by thermal desorption or following evaporation of the solvent droplets as we further discuss below.

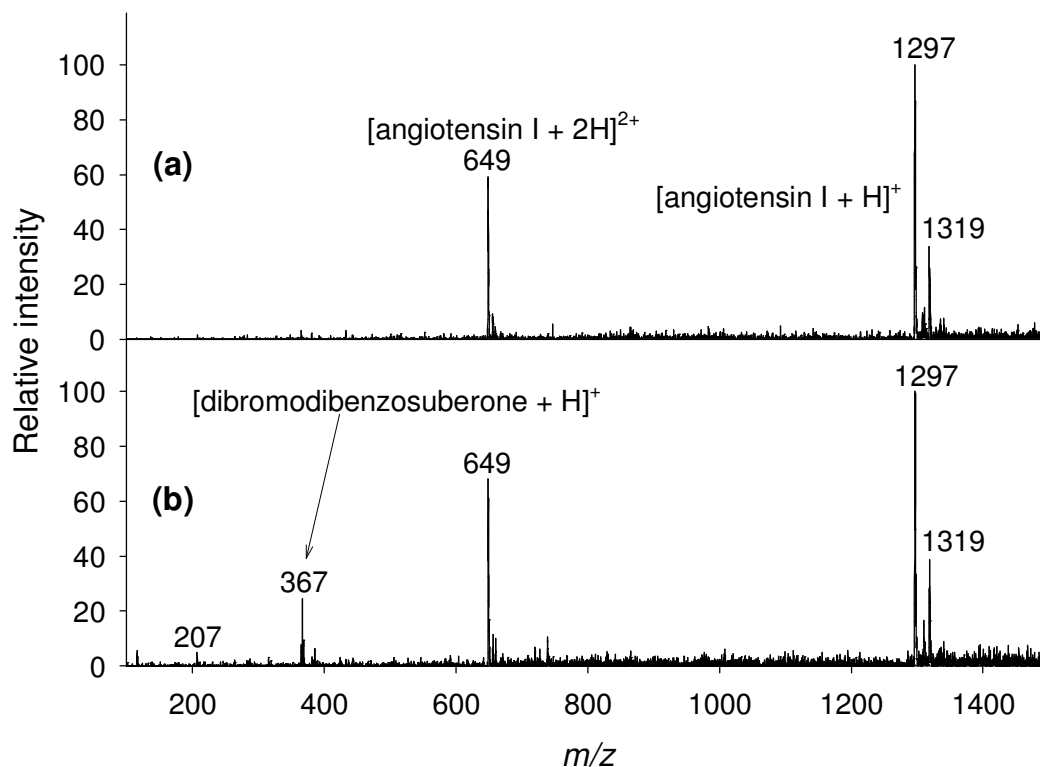


Figure 7.11. Mass spectra of a binary mixture (10 μ L, 0.5 mg/mL angiotensin I, 1mg/mL dibromodibenzosuberone) deposited onto a glass slide and analyzed with a spray solution composed of 50:50 MeOH:acetone, in (a) spray-only and, (b) DEMI modes. The unheated nebulizer gas pressure was 150 psi and the solvent flow rate was 10 μ L/min.

The intensity and types of observed species during DEMI-MS experiments showed a solvent flow rate dependency. This was illustrated by the analysis of an acetaminophen tablet with the nebulizer gas heated to 71°C (Figure 7.12). Protonated acetaminophen species dominate the spectra at lower solvent flow rates while sodiated species predominate at higher flow rates. At an intermediate flow rate, both sodiated and protonated species were observed (Figure 7.12.c). At low flow rates, the spray solvent evaporated quickly before or immediately after impact with the sample surface. This resulted in limited partition into the solvent spray and the generation of gas phase analyte

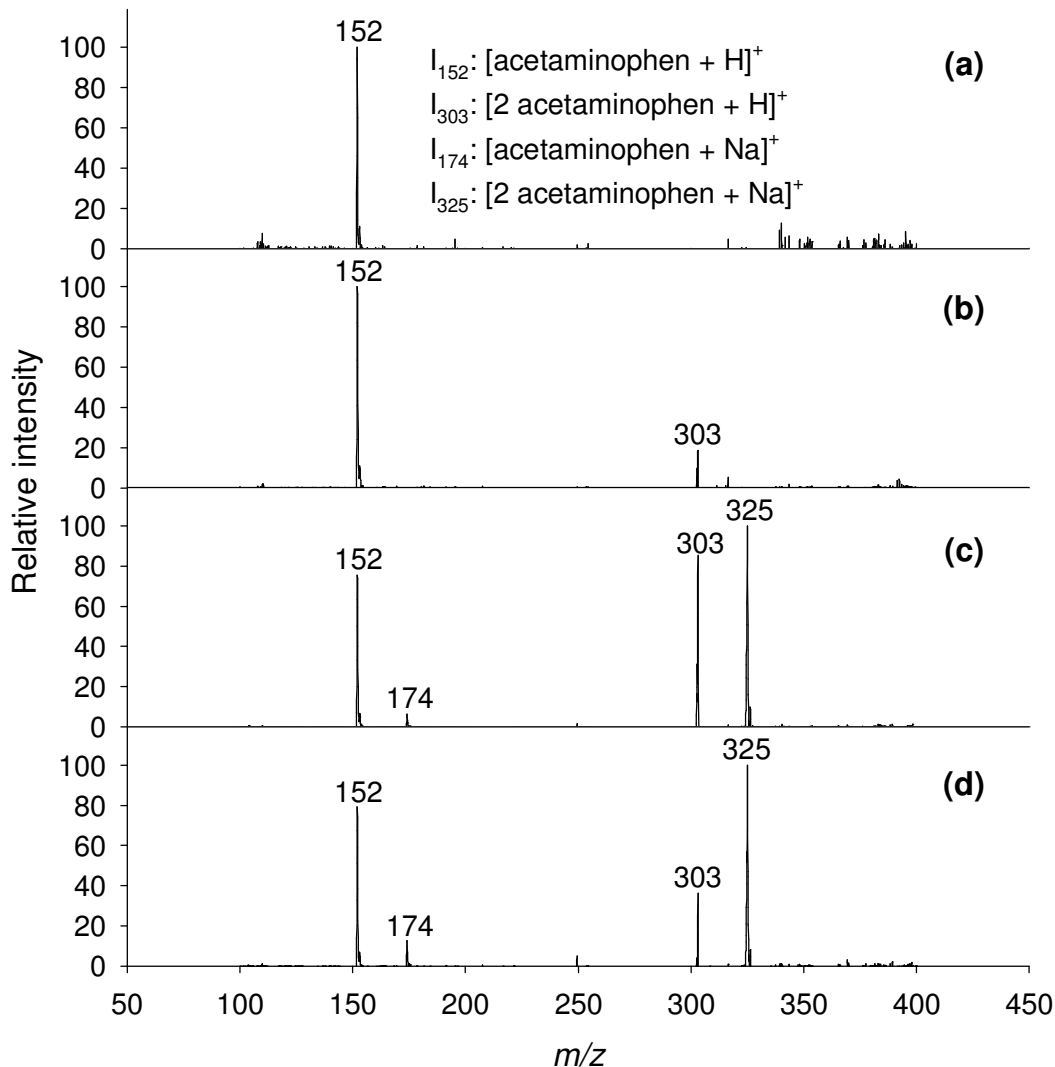


Figure 7.12. Mass spectra of an acetaminophen tablet with the source operated in DEMI mode for different solvent flow rates (a) 5 $\mu\text{L}/\text{min}$, (b) 10 $\mu\text{L}/\text{min}$, (c) 15 $\mu\text{L}/\text{min}$ and (d) 20 $\mu\text{L}/\text{min}$. The temperature of the nebulizer gas was set to 71°C.

species predominantly by thermal desorption with subsequent ionization by proton exchange with reagent ions. Higher solvent flow rates favoured the extraction of analytes molecules into droplets from which sodiation occurs predominantly by adduction with alkali ions dissolved from the excipient matrix.

The effect of different DEMI experimental variables on the appearance of various ionic species was further investigated by sequentially switching on and off various

components of the ion source. No appreciable effect was observed when the spray voltage, or the glow discharge gas flow were sequentially switched on and off while keeping the discharge voltage off (Figure 7.13.a and b, respectively). Sodiated acetaminophen monomer and dimer were the predominant species observed in the spectrum in both cases. However, both sodiated and protonated analyte species were observed when the glow discharge voltage was turned on (Figure 7.13.c). A similar

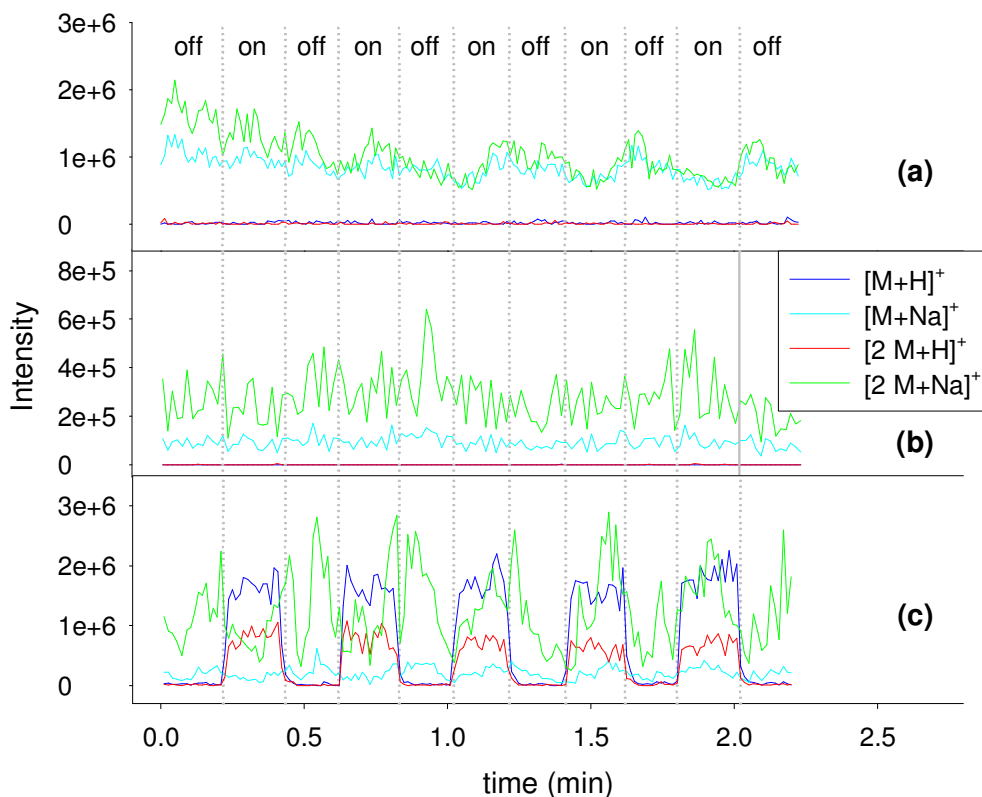


Figure 7.13. Selected ion intensity traces (m/z 152, 174, 303, 325 corresponding to $[M+H]^+$, $[M+Na]^+$, $[2M+H]^+$, $[2M+Na]^+$ respectively, where M = acetaminophen) from the analysis of an acetaminophen tablet under different DEMI ion source operating conditions: (a) spray-only mode, while switching the electro spray voltage off and on repeatedly, (b) spray-only mode while switching the glow discharge gas flow off and on repeatedly while maintaining the glow discharge voltage off, and (c) DEMI mode while switching the glow discharge voltage off and on repeatedly. The nebulizer gas was heated to 71°C and the spray solvent flow rate was $12 \mu\text{l}/\text{min}$. The window width for all selected ion traces was $0.3 m/z$.

response was observed when an acetaminophen standard solution was directly electro sprayed into the glass transfer capillary while alternating the discharge voltage on/off (Figure 7.14). These findings reinforce the previous idea that protonated species observed in DEMI spectra could originate predominantly from the ionization of gaseous neutrals produced by microdroplet desolvation, and not from the competitive displacement of sodium adducts by protonated water clusters. Sodiated species were probably generated by DESI-type mechanisms. Protonated species may be generated in parallel from neutrals thermally desorbed from the sample by the heated nebulizer gas which later undergo metastable-induced chemical ionization within the interface between the glass transfer capillary and the mass spectrometer's inlet. The detection of protonated and sodiated species within the same spectrum by DEMI-MS increases the certainty of

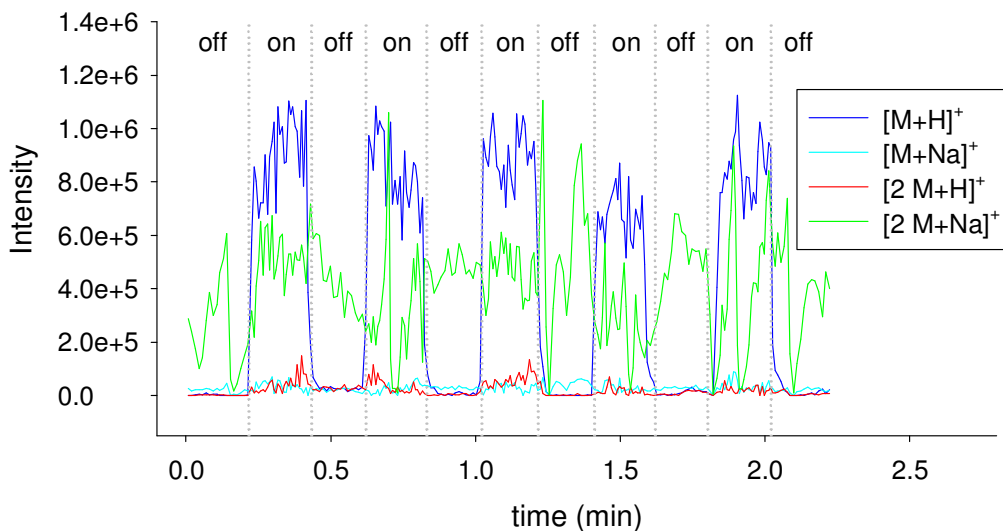


Figure 7.14. Selected ion intensity traces (m/z 152, 174, 303, 325 corresponding to $[M+H]^+$, $[M+Na]^+$, $[2M+H]^+$, $[2M+Na]^+$ respectively, where M = acetaminophen) observed for the infusion of an acetaminophen standard ($5 \mu\text{M}$) operating the ion source in the pneumatically-assisted electrospray/chemical ionization mode while switching the glow discharge voltage off and on repeatedly. The solvent flow rate was $12 \mu\text{L}/\text{min}$ and the nebulizer gas temperature and pressure were 61°C and 150 psi respectively. The window width for all selected ion traces was of $0.3 m/z$.

peak assignments, an important feature in forensic applications such as the identification of unknown pharmaceutical ingredients. This feature was illustrated by analyzing a counterfeit artesunate antimalarial tablet collected in the China/Myanmar border,²⁰⁰ which was found to contain artemisinin. Peaks corresponding to protonated and ammoniated artemisinin species predominated the spectrum for analysis in the MICI-only mode (Figure 7.15.a), while sodiated species predominated in the spray-only mode (Figure 7.15.b). The complementarity between the MICI and spray-only modes was captured for analysis in the DEMI modes where peaks corresponding to protonated, ammoniated and sodiated artemisinin species were observed (Figure 7.15.c).

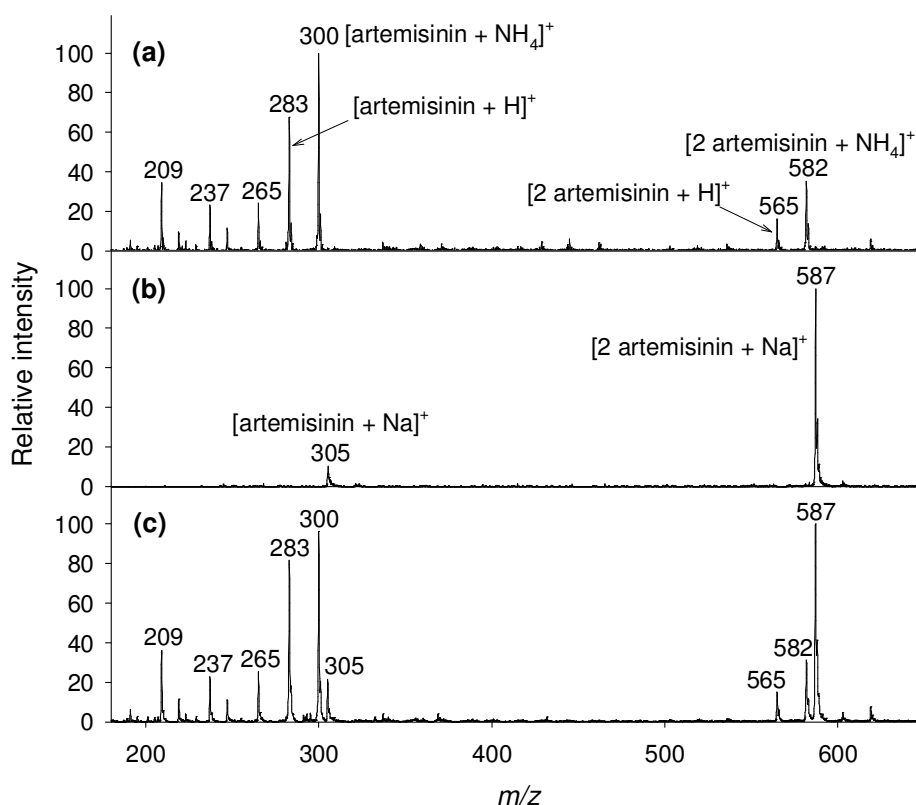


Figure 7.15. Mass spectra of an artemisinin-containing fake artesunate antimalarial tablet with the source operated in the: (a) MICI-only mode, (b) spray-only mode and (C) DEMI mode. (m/z 265 = $[\text{M} - \text{H}_2\text{O} + \text{H}]^+$, m/z 237 = $[\text{M} - \text{H}_2\text{O} - \text{CO} + \text{H}]^+$, m/z 209 = $[\text{M} - \text{H}_2\text{O} - 2\text{CO} + \text{H}]^+$; where M = artemisinin).

7.5. Conclusions

A new ambient multimode ionization technique named Desorption Electrospray/Metastable-induced Ionization (DEMI), which combines DESI and metastable induced chemical ionization mechanisms, is presented. Three unique operation modes are possible (MICI-only, spray-only and DEMI), each with unique features. The data obtained thus far supports a DEMI ionization mechanism where analytes dissolved from the sample are released either as sodiated, protonated and/or neutral species from electrically-charged droplets in positive ion mode. Neutrals undergo further reactions with protonated water clusters, producing protonated species. High polarity analytes are desorbed and ionized following DESI mechanisms, while less polar molecules can be thermally vaporized or dissolved by a low polarity spray mixture, later undergoing metastable-induced chemical ionization.

CHAPTER 8. CONCLUSIONS AND OUTLOOK

8.1. Abstract

This Chapter presents a summary of the results of my investigations on DESI and DART for applications in the analysis of pharmaceutical compounds. The Chapter is concluded with a proposal of potential future directions.

8.2. Accomplishments-Ambient (DESI and DART) MS Investigations

Ambient MS is a new and growing sub-field in mass spectrometry, which has opened new research avenues, particularly for applications relating to the analysis of solid samples. Opportunities in this area increase as new ambient ion sources are introduced and better characterized. The results presented here indicate that ambient ionization techniques such as DESI and DART could serve as complementary tools for the forensic characterization of pharmaceuticals with up to two orders of magnitude improvement in throughput compared to traditional methods such as liquid chromatography mass spectrometry (LC-MS).

The capabilities of DESI MS for the selective and sensitive, qualitative and quantitative analysis and imaging of pharmaceutically important molecules were extensively explored. For the qualitative screening/fingerprinting of pharmaceutical drug tablets, one of the most critical attributes that determined sensitivity/selectivity was solubility in the spray solvent. As such, the chemistry of the spray solvent mixture could be tuned to enable the selective dissolution/detection of specific analytes of interest from the tablet matrix.^{145, 149} Furthermore, the sensitivity of this technique for drug tablet

analysis was also observed to be largely dependent on the nebulizer gas velocity, spray solvent flow rate and sample hardness. These variables determine the efficiency of momentum transfer from the initial primary droplets onto the surface liquid film to generate analyte-containing secondary droplets. These secondary droplets are ejected off the sample surface and sampled at the inlet capillary of the mass spectrometer.^{102, 147} As such, the nebulizer gas velocity and spray solvent flow rate must be appropriately chosen, based on the sample hardness to allow efficient surface sampling. The selectivity of this technique can also be enhanced by performing the experiment in the reactive mode. In this mode, various chemical reagents are added into the spray solvent to enable the selective recognition/reaction with specific moieties in target analytes. These reactions usually result in analyte stabilization, inhibiting fragmentation with a concomitant enhancement in the analyte surface activity, facilitating their evaporation from secondary droplets culminating in an improvement in sensitivity.^{102, 146, 147}

The capability of DESI MS for the direct quantitative analysis of drug tablets by DESI MS was also demonstrated following two different strategies. In the first approach, the analyte signal dependency on DESI geometrical set-up variables was mitigated following the careful and controlled addition of an isotopically labeled internal standard (IS) to the sample resulting to an analyte-to-IS signal ratio, which was largely independent of DESI experimental variables.¹⁴⁸ Thus, monitoring the analyte-to-IS signal ratio as oppose to the absolute signal enabled the direct quantitation of the active pharmaceutical ingredient (API) in drug tablets with up to 94 % accuracy when compared to LC-UV analysis. In the second approach, the analyte signal dependency on set-up variables was mitigated by analyzing samples using a pair of reagents (in the spray

solvent), which had different binding affinities for the analyte to provide an analyte complex ratio, which was independent on the set-up variables. However, the analyte complex ratio was observed to be dependent on the analyte surface concentration, allowing direct quantitative analysis of drug tablets, using this approach, without any requirement for internal standards.¹⁴⁷

Following construction of a DESI MS set-up with imaging capabilities, this technique was also demonstrated as a very powerful tool for determining the 2-D distribution of various pharmaceutically important compounds on tablet and tissue surfaces. The ability to map the distribution of molecules of interest by DESI MS has very great implications in drug tablet quality control¹⁴⁵ and in determining the role of chemical signals presented on tissue surfaces.¹⁶⁶ The mapping of various chemical markers by DESI MS is also showing great prospects in cancer research in determining the spread of malignant tissue.^{162, 286}

DART MS was also explored and observed to be a very powerful tool for the rapid forensic characterization of pharmaceutical drug tablets providing an addition to the analytical toolbox for such applications.^{145, 150, 200, 287} Interfacing the DART ion source to an accurate mass TOF MS instrument demonstrates the utility of this technique in determining the elemental composition of wrong APIs in counterfeit drug samples enabling their identification.

The extensive use of DESI and DART for the various presented applications provided some insights into some of the intrinsic limitations of these techniques. DESI was observed to be limited to ionizing molecules of medium to high polarities without much limitation in terms of mass range, whereas DART is better suited for the analysis of

molecules within a broader range of polarities, but within a more limited mass range (up to 800 Da approximately) due to the desorption mechanisms involved. To circumvent these limitations a novel multimode ambient ion source, desorption electrospray/metastable-induced ionization (DEMI), which combines various aspects of DESI and DART was constructed and tested. Initial experiments with the DEMI ion source have demonstrated its ability to enable the simultaneous analysis of molecules within a broader range of polarities and masses than DESI and DART alone.²⁸⁸

8.3. Proposed Future Directions

Our research on DESI and DART MS was directed towards exploring the capabilities of these techniques, predominantly for the forensic characterization of pharmaceutical drug tablets. The pharmaceutical drug class most extensively evaluated was the artemisinin based antimalarial monotherapies. Ongoing ventures are geared towards extending these efforts to the investigation of antimalarial combination therapies containing artemisinins (ACTs), with the aim of further developing improved approaches for performing rapid mass spectrometric analysis of these drugs and for other applications as follows:

1. Fixed dose ACTs usually contain two or more APIs in the presence of an excipient matrix resulting in a relatively complex sample mixture. The artemisinin constituent in the ACTs usually undergo extensive fragmentation following DART MS analysis resulting in very similar spectra for all the artemisinins. As such, preliminary investigation of such samples by DESI, which is much softer than DART is recommended. DESI MS analysis should in principle, allow the

detection of intact tablet constituents eliminating any unambiguous identification. Analysis of such sample by reactive DART¹⁹⁸ could also be employed to mitigate this limitation. However, the applicability of either DESI or DART MS for the direct analysis of such multi-component samples inevitably suffers from ionization suppression. In the case of DESI, this phenomenon arises from the different proton affinities and surface activities of the various constituents picked up by the DESI spray droplets, resulting in vastly different ionization efficiencies. The APIs however, usually have a higher proton affinity and greater solubility (in commonly used DESI MS compatible sprays solvents) than the excipient constituents resulting in their preferential dissolution/ionization. Nevertheless, the presences of more than one API constituent in ACTs could still result in preferential detection of APIs with higher solubility and ionization efficiencies, precluding the observation of less soluble or ionizable APIs. As such, proposed experiments should be aimed towards determining the sample APIs constituent concentration limits for charge competition and the on-set of ionization suppression effects to allow a determination of the linear dynamic range of DESI MS and its capabilities for the analysis of ACTs. These studies should have important implications in the direct quantitation analysis of APIs in ACTs. Preliminary investigation of the solubility characteristics of the various API in the DESI spray solvent is required in order to decouple, to some degree, the analyte desorption/incorporation into secondary droplets from the subsequent ionization/charge competition effects.

2. For the qualitative analysis of pharmaceutical tablets by DART MS, analyte desorption, which is tightly coupled to ionization occurs predominantly by thermally heating the sample with the heated metastable gas plume. For the analysis of ACTs, sample constituents with greater volatility will be preferentially desorbed. Based on their ionization efficiency, they might greatly suppress the ionization of the less volatile tablet constituents, which are inevitably less abundant in the gaseous phase, precluding their detection. Analysis of the pulverized sample should mitigate this limitation enabling the simultaneous detection of more tablet constituents.
3. DART MS was also observed to show a relatively limited mass range due to the limited molecular weight range of analytes that can be transformed into the gaseous phase following thermal desorption. In addition, DART MS has been observed to show superior performance in the analysis of less polar compounds than DESI MS. As such one strategy for extending the molecular weight range of compounds amenable to DART MS would be to explore spray based desorption approaches for high molecular weight, low polarity species, which might not be easily ionized in an appropriately chosen spray solvent. In such cases, the role of the spray solvent would be to effect analyte pick-up and subsequent transformation into gaseous phase following solvent evaporation. Implementation of this strategy such as in the DEMI set-up would result in the ionization of the gaseous analytes upon interaction with plume from the metastable source.
4. Analyte desorption in DEMI MS occurs by a combination of thermal and spray solvent pick-up, with the subsequent ionization event also occurring following

two different strategies.²⁸⁸ Thus, application of this technique for the analysis of ACTs should mitigate some of the limitation of thermal desorption and ionization discussed above enabling the simultaneous detection of a broader range of sample constituents.

5. An investigation of the size of the analyte-containing solvent droplet emanating from the DEMI source under conditions that allow simultaneous operation of both ionization approaches is required. This investigation should provide insight into the combination of spray solvent, nebulizer gas flow rates and temperatures required for efficient surface sampling to allow optimum sensitivity. Computational simulation modelling of the interaction of the metastable and charge solvent droplet plumes is also required in order to obtain the optimum geometrical setting for efficient sampling of the species generated following both ionization approaches.

**APPENDIXES-SURVEY OF OTHER TECHNIQUES USED IN
COMBINATION WITH AMBIENT MS FOR CHARACTERIZING
COUNTERFEIT ARTEMISININ-BASED ANTIMALARIALS**

**APPENDIX A. ASSESSMENT OF HAND-HELD RAMAN
INSTRUMENTATION FOR IN SITU SCREENING FOR
POTENTIALLY COUNTERFEIT ARTESUNATE ANTIMALARIAL
TABLETS BY FT-RAMAN SPECTROSCOPY AND DIRECT
IONIZATION MS**

A.1. Abstract

This appendix presents an evaluation of the performance of a new portable Raman spectrometer (TruScanTM) as a rapid, user-friendly, reliable and inexpensive method for drug quality screening. The capabilities of this device are illustrated by its application in the chemical characterization of genuine and fake artesunate antimalarial tablets following validation by FT-Raman spectroscopy and direct ionization MS.

A.2. Introduction

An ongoing trend in analytical instrument development has been the deployment of portable technologies that allow robust real-time measurements, particularly attractive for on-site field applications such as in pharmaceutical drug quality control and anticounterfeiting. One key requisite for portable analytical instruments is their operational simplicity, to allow various analyses to be readily accomplished by personnel with minimum training and expertise. This appendix presents an assessment of the capability of a hand-held Raman instrument for the rapid *in situ* determination of counterfeit artesunate antimalarial tablets.

Raman spectroscopy is a very powerful chemical analysis technique for the analysis of condensed phase samples typically requiring no sample preparation. It is based on the Raman effect, which is the inelastic scattering of photons from molecules via interaction with the vibrational modes of the analyte molecules. In this process, a photon typically transfers a fraction of its energy to a vibrational mode within the molecule (Stokes scattering). Consequently, the wavelength of the scattered photon is spectrally red-shifted, with the degree of the shift indicating the amount of energy uptake by the molecule. Since the vibrational modes are quantized and molecule specific, the distribution of observed wavelength shifts is characteristic of that particular molecule. The shift pattern serves, in essence, as a unique fingerprint for the molecule, specific to its structure and conformation.

The general applicability of Raman spectroscopy is limited to samples that do not exhibit strong fluorescence emission in the Raman spectral region, since this can easily overwhelm the relatively weaker Raman signal. However, this problem can be mitigated by using near-infrared excitation away from the electronic absorption bands of most fluorescing species, thus preventing their excitation and consequently the generation of fluorescence emission by these species. Several different portable Raman units are now available from different vendors, and are being subject to performance characterization. For example, the performance of a mobile Raman instruments has been successfully tested for the in situ characterization of art objects.²⁸⁹

The goal of this study was to evaluate the performance of a small hand-held Raman spectrometer to accurately and rapidly screen genuine and fake artesunate antimalarial tablets collected in SE Asia, Ghana and southern China. In order to confirm

the ability of this type of portable Raman spectrometer to detect excipients and active ingredients present in the pharmaceutical tablets evaluated, the results were compared and validated by FT-Raman spectroscopy,²⁹⁰ DESI MS and DART MS. Thirty two representative antimalarial tablets were characterized following this approaches.

A.3. Experimental Details

A.3.1. Samples

Artesunate antimalarial samples, including both genuine artesunate (15) and counterfeit tablets (17) were collected in Vietnam, Lao PDR (Laos), Thai/Burma (Myanmar), China, Ghana and at the Thailand/Burma border are listed in Table A.1. The genuine samples were manufactured by Guilin Pharmaceutical Co. Ltd, (Guilin, PRC), Mekophar Chemical Pharmaceutical Joint Stock Co. (Ho Chi Minh City, Vietnam), Pharbaco (Hanoi, Vietnam), and Traphaco (Hanoi, Vietnam).

A.3.2. Portable Raman Spectroscopy

Portable Raman Spectroscopy measurements on each of the samples were performed by Felicia Yang, a high school student at the time, on a summer internship program in our group. Experiments were performed using a TruScanTM portable spectrometer (Ahura Scientific Inc., Wilmington, MA, USA). This instrument is equipped with a cooled external cavity-stabilized 785 nm laser for excitation, which has a maximum output power of 300 mW, a 2048-element silicon CCD detector, and a resolution of 7.5-10 cm⁻¹ over the Raman shift range of 2875-250 cm⁻¹.

A.3.3. FT-Raman Spectroscopy

FT-Raman spectroscopy experiments were performed by Dr. Camilla Ricci, a postdoctoral associate with Dr. Sergei Kazarian in the Department of Chemical Engineering in Imperial College, London. Laboratory Raman spectra were acquired for each sample in air at room temperature using a Fourier transform Equinox 55 spectrometer (Bruker Optics Inc., Ettlingen, Germany) with an FRA 106 Raman module equipped with a 1064 nm Nd:YAG laser. For these experiments, the laser power was set to 400 mW. A liquid nitrogen cooled Ge detector was used with a resolution of 4 cm⁻¹ and 32 scans in the spectral range 3500-100 cm⁻¹.

A.3.4. Direct Ionization (DESI and DART) MS

DESI MS experiments were performed on each sample in both the reagentless and reactive DESI MS modes using the same ion source and settings described in section 2.3.3. Experiments were performed using the MS conditions described in section 3.3.2. Reagentless DESI MS was performed on each sample in both the positive and negative ion mode to determine the mode that gave unambiguous detection and identification of analytes desorbed from the sample surface. Reactive DESI MS was performed exclusively in the positive ion mode. Several points on the tablet surface and interior were sampled during DESI analysis to obtain an accurate picture of the components present.

DART accurate mass measurements were performed using a JMS-100TLC (AccuTOF™) TOF mass spectrometer (JEOL, Peabody, MA, USA) equipped with a DART ion source (IonSense, Saugus, MA). Experiments were performed in the positive

ion mode, at a temperature of 250 °C. Other settings were as follows: the He flow rate was 4.2 L min⁻¹, the discharge voltage was 2500 V and the exit grid electrode voltage was 200 V. Samples were manually held with a pair of clean metal tweezers in front of the DART ion source for approximately 20 s. The mass spectrometer ion optics settings¹⁹⁸ were as follows: inlet orifice voltage 30 V, ring electrode voltage 5 V, orifice-2 5 V, ion guide bias voltage 29 V, ion guide peaks voltage 300 V. The detector voltage was set to 2,650 V. Mass spectra were acquired in the 100 to 1000 Da range. Unknowns were identified by accurate mass measurements. The spectrometer's mass drift was corrected using neat polyethylene glycol (PEG, average molecular weight 600, Sigma Aldrich, St. Louis, MO, USA). DART mass spectra were exported into MS Excel and searched via a system of macros, against an in-house library of exact masses for protonated molecules derived from the Model List of Essential Drugs published by the WHO.²⁹¹ A match was considered positive if the difference between the experimental accurate monoisotopic mass and the theoretical mass values was less than 5 mmu, and the relative intensity equal or larger than 5 %.

A.4. Results and Discussion

This study was carried out in three stages. First, samples were rapidly analyzed using the portable Raman instrument for the analysis of molecular composition of the tablets. Second, the results were validated through the vibrational characterization of the samples using FT-Raman spectroscopy. Portable Raman and FT-Raman spectroscopy was performed through both the blister packs and after sample removal from the blister packs. The spectra were found to be practically identical due to the transparent nature of

the blister packs, which present little or no spectral features. Also, both sides of the tablets were analyzed and no difference was detected. The principal advantage of using FT-Raman spectroscopy with a near infrared laser is that less fluorescent interference is induced from samples compared to visible excitation. Third, mass spectrometry was used to evaluate the results obtained with spectroscopic techniques and confirm the presence of the active ingredient in the potentially counterfeit tablets.

A.4.1. Analysis of Genuine Artesunate and Artemisinin-containing Tablets

The genuine artesunate tablet and all other samples containing artemisinins resulted in poor efficiency of Raman scattering due to competition with fluorescence phenomenon. This precluded the application of conventional portable Raman spectroscopy for their analysis. The observation of strong fluorescence from such samples by portable Raman spectroscopy however, suggested the presence of an artemisinin, which was identified following FT-Raman and direct ionization MS analysis.

Figure A.1.a shows traces obtained from the FT-Raman spectroscopy analysis of an artesunic acid standard together with those for a genuine artesunate tablet manufactured by Guilin Pharmaceutical Co. Ltd (trace (i)) and Mekophar Chemical Pharmaceutical Joint Stock Co. (trace (ii)). Apparently, these measurements do not suffer from fluorescence and the FT-Raman traces show very similar features for both types of genuine sample clearly indicating the presence of artesunic acid in these samples. Figure A.1.b shows results from the complementary analysis of the genuine Guilin artesunate tablet by DESI MS, which was very similar to that for the Mekophar tablet (data not shown). Reagentless DESI MS analysis of this sample generated peaks

predominantly at m/z 407.2 and 791.3 corresponding to the species $[\text{artesianic acid} + \text{Na}]^+$ and $[2 \text{ artesianic acid} + \text{Na}]^+$ respectively (Figure A.1.b.i). Analysis by reactive DESI MS

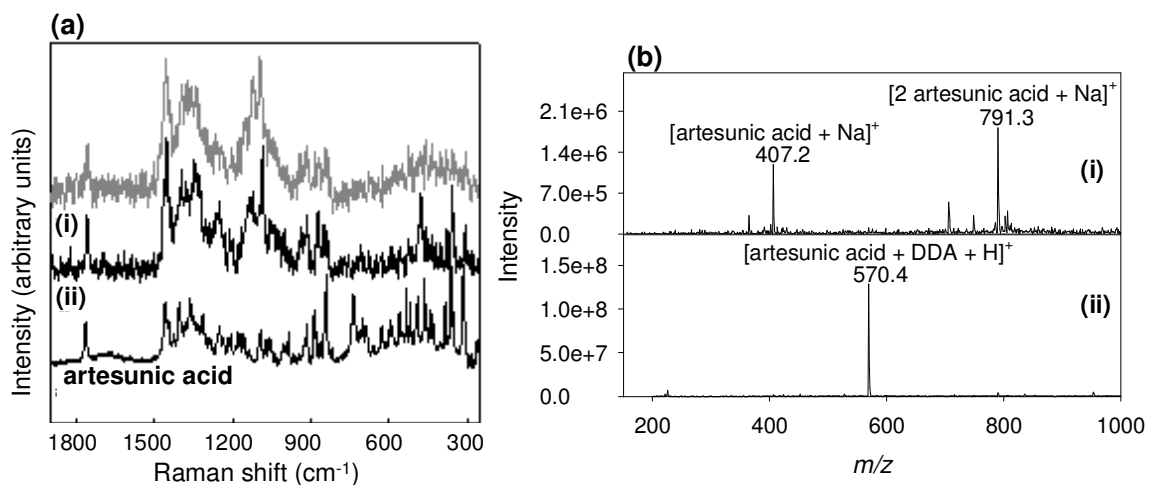


Figure A.1. (a) FT-Raman spectra of genuine (i) Guilin and (ii) Mekophar artesunate tablets, compared with the reference spectrum of artesunic acid. (b) DESI spectra of the genuine Guilin tablet obtained by the (i) reagentless DESI MS and (ii) reactive DESI MS modes.

resulted in the peak at m/z 570.4 corresponding to $[\text{artesianic acid} + \text{DDA} + \text{H}]^+$ as the predominant species in the spectrum (Figure A.1.b.ii). The presence of artesunic acid in these samples was also verified by DART MS analysis (data not shown). The detection of artesunic acid as the only active ingredient in both types of genuine artesunate samples by direct ionization MS was consistent with Raman results.

As with the genuine samples, analysis of the sample S 40-1 by conventional Raman spectroscopy resulted in significant fluorescence, which made it difficult to obtain an unambiguous Raman spectrum for this sample using the portable instrument. This however, suggested the presence of an artemisinin or one of its derivatives in the sample. The sample was determined to contain artemisinin (the artesunic acid precursor)

following FT-Raman spectroscopy analysis (Figure A.2.a). FT-Raman analysis also revealed the presence of starch in this sample. The composition of the sample was

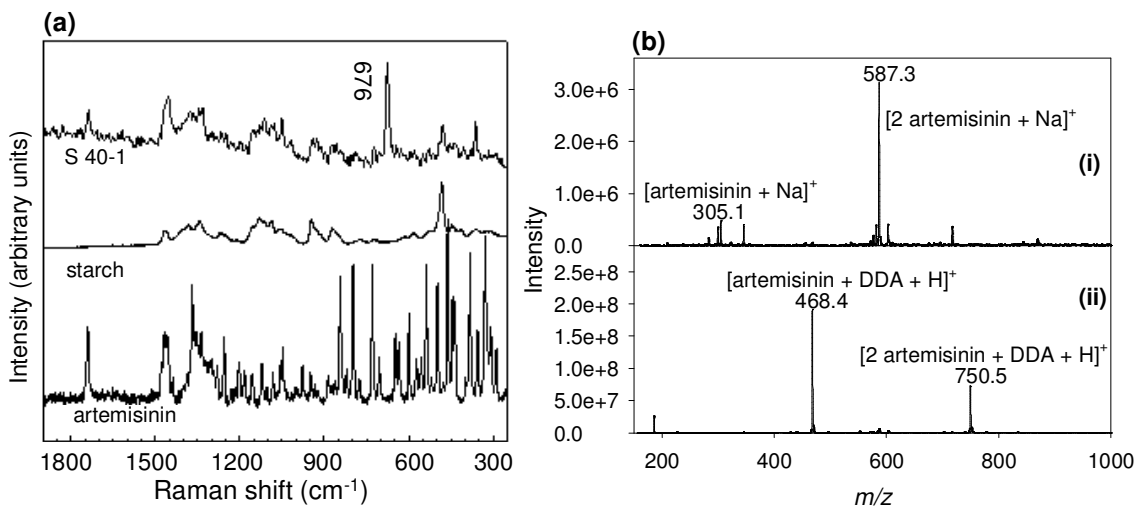


Figure A.2. (a) FT Raman spectra of fake tablet S 40-1 compared with the reference spectra of starch and artemisinin. (b) Corresponding DESI spectra of fake tablet S 40-1: (i) reagentless DESI MS and (ii) reactive DESI MS.

verified by direct ionization MS as follows. Reagentless DESI MS analysis showed peaks at m/z 305.1 and 587.3 corresponding to the species $[\text{artemisinin} + \text{Na}]^+$ and $[2 \text{ artemisinin} + \text{Na}]^+$ respectively (Figure A.2.b.i). These assignments were verified by reactive DESI, which revealed the characteristic protonated artemisinin adduct with dodecylamine at m/z 468.4 (Figure A.2.b.ii). A peak at m/z 750.5 corresponding to the species $[2 \text{ artemisinin} + \text{DDA} + \text{H}]^+$ can also be seen in the reactive DESI spectrum of this sample. Again, the detection of artemisinin in this sample by DESI MS was consistent with the results obtained by Raman spectroscopy.

A.4.2. Analysis of Counterfeit Tablets

Analysis of counterfeit artesunate tablets, most of which do not contain artemisinins, generally resulted in very negligible fluorescence allowing the collection of Raman spectra data using both portable and FT-Raman spectrometers. Results from the analysis of the sample Lao BW8 by both techniques is shown in Figure A.3.a. Both Raman

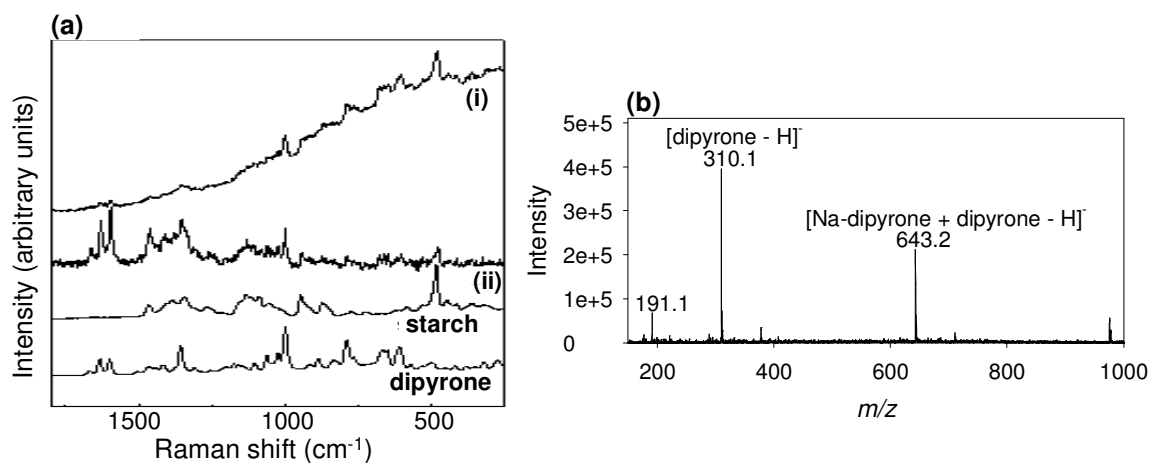


Figure A.3. (a) (i) Portable Raman and (ii) FT-Raman spectra of fake tablet LAO BW8 compared with the reference spectra of starch and dipyron. (b) Corresponding reagentless DESI spectra of fake tablet LAO BW8.

spectroscopic techniques consistently verified the absence of artesunic acid in this sample. However, the Raman spectra show bands predominantly at 1000, 1355, 1598, 1632 and 1666 cm⁻¹ which indicate the presence of dipyron (C₁₃H₁₇N₃O₄S, an analgesic) as wrong active ingredient in this sample. A band at 478 cm⁻¹ attributed to the presence of starch was also observed. Further analysis of this sample by reagentless DESI MS in negative mode (Figure A.3.b) shows peaks at m/z 310.1 and 643.2 corresponding to the species [dipyron - H]⁻ and [Na-dipyron + dipyron - H]⁻ respectively. These peak assignments were verified by DESI MS/MS analysis (data not shown). A peak at m/z

191.1 corresponding to a dipyrone fragment due to the neutral loss of Ph-N=NCH₃ from its precursor was also observed in this reagentless DESI spectrum (Figure A.3.b). The detection of dipyrone in this sample was again consistent with results obtained by Raman spectroscopy using both portable and FT-Raman instruments.

Table A.1. Description of the samples studied.

Sample code	Genuine/fake as determined by packaging inspection and MS (Type) ^a	Results from portable spectrometer	Results from FT-Raman spectrometer	MS results
S 29	Fake (9)	starch, acetaminophen, talc	starch, acetaminophen, calcite, talc	acetaminophen, ^{b, c} artemisinin ^c
S 40-1	Fake (13)	starch, talc	starch, artemisinin, talc	artemisinin ^{b, c}
S 45	Fake (1)	starch, acetaminophen, talc	starch, acetaminophen, talc	acetaminophen, ^{b, c} artemisinin ^c
S 40-2	Fake (13)	starch, calcite, talc	starch, calcite	artemisinin ^c
S 47-2	Fake (14)	starch, talc	starch, calcite, talc	artemisinin ^c
S 47-1	Fake (14)	starch, talc	starch, calcite, talc	artemisinin, ^{c, d} artesunic acid ^{c, d}
S 47-3	Fake (14)	starch, talc	starch, calcite, talc	artesunic acid ^{c, d}
S 50	Genuine	fluorescence	starch, calcite, artesunic acid	artesunic acid ^{b, c}
S 51	Genuine	fluorescence	starch, calcite, artesunic acid	artesunic acid ^{b, c}
S 55	Genuine	fluorescence	starch, calcite, artesunic acid	artesunic acid ^{b, c}
Ghana 0601	Genuine	fluorescence	starch, calcite, artesunic acid	artesunic acid ^{b, c}
China 0604	Fake (10)	starch, talc	artemisinin, starch, talc	artemisinin ^{b, c}
China 0605	Fake (10)	starch, talc	starch, calcite, talc	artemisinin ^{b, c, e}
Lao 0604	Fake (6)	starch, calcite, talc	starch, calcite, talc	artemisinin ^{b, c}
Lao 0503	Fake (11)	starch, acetaminophen, calcite, talc	starch, acetaminophen, calcite, talc	no API detected ^{b, c, e}
Lao BW 8	Fake (10)	starch, dipyrone	starch, dipyrone	dipyrone, ^{b, e} erucamide ^e
Artesunate Vietnam	Genuine	starch, calcite, talc	artesunic acid, calcite, talc	artesunic acid ^{b, c, e}
Artesunate China	Genuine	fluorescence	artesunic acid, calcite	artesunic acid ^{b, c, e}
Lao BW 9	Fake (10)	starch, dipyrone	starch, dipyrone, calcite	dipyrone ^{b, e}
Lao 12060	Fake (8)	calcite, acetaminophen	calcite, acetaminophen	erythromycin A, ^f acetaminophen ^{b, c, f}
Lao 12012	Fake (6)	starch, calcite	starch, calcite, artemisinin	artemisinin ^{b, c}
S 57	Genuine (Mekophar Co.)	starch, calcite	calcite, starch, artesunic acid	artesunic acid ^{b, c, e}
Lao 0704	Genuine (Guilin)	starch, calcite	calcite, starch, artesunic acid	artesunic acid ^{b, c, e}
Lao 0709-5	Genuine (Traphaco Co.)	fluorescence	calcite, starch, artesunic acid	artesunic acid ^{b, c, e}
Lao 0702-1	Fake (1)	calcite, starch, talc	calcite, starch, talc	no API detected ^{b, c, e}
S 65	Genuine (Pharbaco Co.)	fluorescence	calcite, starch, artesunic acid	artesunic acid ^{b, c, e}
Lao 0708	Genuine (Pharbaco)	fluorescence	calcite, starch, artesunic acid	artesunic acid ^{b, c, e}
S 62	Genuine (Guilin)	fluorescence	calcite, starch, artesunic acid	artesunic acid ^{b, c, e}
Lao 0701-1	Fake (16)	calcite, starch	calcite, starch	no API detected ^{b, c, e}
S 60	Genuine (Guilin)	fluorescence	calcite, starch, artesunic acid	artesunic acid ^{b, c, e}
Lao 0705	Genuine (Guilin)	fluorescence	calcite, starch, artesunic acid	artesunic acid ^{b, c, e}
Lao 0703-1	Genuine (Guilin)	starch	calcite, starch, artesunic acid	artesunic acid ^{b, c, e}

^aThe number for types correspond to the type of fake based on the hologram. ^bActive Pharmaceutical ingredient (API) detected by reagentless DESI MS. ^cAPI detected by reactive DESI MS. ^dAPI detected only on the sample surface.

Table A.1 summarizes the results obtained by both vibrational techniques compared with those obtained by direct ionization MS. A total of 30 potentially counterfeit artesunate samples were investigated in this study. Although artesunic acid shows strong fluorescence, making the collection of Raman spectra data using TruScan™ difficult, this shortcoming however serves as an indication of the presence of artesunic acid in the sample. In all of such cases the presence of artesunic acid was verified by both FT-Raman and MS. Also for all the samples for which Raman spectra was obtained using TruScan™, results were consistent with those obtained by FT-Raman spectroscopy. It is worth noting that some samples exhibited a band around 676 cm^{-1} , which can be assigned to the symmetric Si-O-Si stretching mode of talc ($\text{Mg}_3\text{Si}_4\text{O}_{10}(\text{OH})_2$).²⁹² In most cases characteristic features at 363 and 293 cm^{-1} were observed, and these can be related to the deformation modes of the silicate network and the stretching Mg-O vibrations, respectively. This finding is in agreement with the results presented by de Veij *et al.*²⁹³

In summary, except for the samples S 47-1 and S-47-3, which contained very small amounts of artesunic acid on their surface detected only by reactive DESI MS, 18 of 32 of the samples were determined to contain artesunic acid by both Raman and MS methods. Various wrong active ingredients including acetaminophen, artemisinin, dipyrone, erythromycin, erucamide were also detected in various samples by both Raman spectroscopy and MS. No active ingredient was detected in the samples LAO 05017, Lao 0503, Lao 0702-1 and Lao 0701-1 using MS methods.

A.5. Conclusions

This appendix demonstrates the capabilities of a portable Raman spectrometer (TruScan™) as a potentially inexpensive field device for characterizing the composition of counterfeit artesunate antimalarial samples without sample preparation. The strong fluorescence of artesunic acid makes it difficult to obtain Raman spectra using the portable Raman unit. This can however be advantageously exploited as a hint for the absence of artesunic acid in the sample during the determination of counterfeits, which in general do not show any appreciable fluorescence. The use of the more sensitive FT-Raman instrumentation allowed the verification of the absence/presence of artesunic acid in such samples. For samples, which show negligible fluorescence, typically counterfeits with various wrong active ingredients or no active ingredient, the results obtained using the portable Raman unit show consistency with those obtained by FT-Raman. Using the more sensitive direct ionization MS methods including DESI MS and DART MS, the identity of the API present in the various counterfeit artesunate samples was verified. These results suggest the applicability of this portable Raman instrument (TruScan™) as a reliable analytical tool for the routine on-site field analysis of pharmaceutical tablets for drug quality control purposes.

APPENDIX B. COMBINING TWO-DIMENSIONAL DIFFUSION-ORDERED NUCLEAR MAGNETIC RESONANCE SPECTROSCOPY, DESI MS AND DART MS FOR THE INTEGRAL INVESTIGATION OF COUNTERFEIT PHARMACEUTICALS

B.1. Abstract

This appendix presents an investigation of the complementarity between two-dimensional diffusion-ordered ^1H nuclear magnetic resonance spectroscopy (2D DOSY ^1H NMR) and ambient (DART and DESI) MS methods for assessing the quality pharmaceutical tablets for forensic purposes. Fourteen different artesunate tablets, representative of what can be purchased from informal sources in SE Asia, were investigated using these techniques. The correct API was detected in five formulations by both NMR and MS methods. Common organic excipients such as sucrose, lactose, stearate, dextrin and starch were also detected. The graphical representation of DOSY ^1H NMR results proved very useful for establishing similarities among groups of samples, enabling counterfeit drug “chemotyping”. Overall, this study suggests that 2D DOSY ^1H NMR combined with ambient MS composes a powerful suite of instrumental analysis methodologies for the integral characterization of counterfeit antimalarials.

B.2. Introduction

The ever-growing sophistication of counterfeit drugs has placed a requirement for the constant development and deployment of increasingly more in-depth pharmaceutical

analysis approaches for investigating their composition and origin. In this appendix, 2D DOSY ^1H NMR,²⁹⁴ accurate mass DART and DESI MS are compared and combined for the forensic investigation of artesunate antimalarial tablet formulations.

2D DOSY ^1H NMR²⁹⁴ relies on the decrease in diffusion coefficients (D) with increasing molecular mass as a means to virtually separate components in a solution mixture. The separation is based on the differences in the translational diffusion coefficients of individual components in the mixture, which are largely dependent on various physical parameters including temperature, solvent viscosity, size and shape of the molecule. 2D DOSY ^1H NMR spectra therefore show correlations between chemical shifts presented on the horizontal axis and the diffusion coefficients expressed in $\mu\text{m}^2 \text{s}^{-1}$ on the vertical axis. All 2D DOSY ^1H NMR peaks generated from the same component line up at the same diffusion coefficient. As such this technique in a sense provides a localized separation of the components in a mixture solution without the need to for any physical separation such as observed in chromatographic techniques.

Two-dimensional DOSY ^1H NMR has already been shown to provide a highly comprehensive chemical fingerprint of genuine pharmaceutical formulations.^{295, 296} In combination with ambient MS methods, the multipronged approach investigated in this study is likely to produce comprehensive chemical information for determining the similitude between different classes of fake artesunate pharmaceuticals, a critical step in guiding law enforcement and public health agencies towards their most probable origin.

B.3. Experimental Details

B.3.1. Samples

Fourteen tablet formulations (**1-14**) were analyzed in this study by both DOSY and ambient MS methods. Formulations **4, 6, 7, 9, 13** were classified as genuine products based on packaging inspection and were manufactured by Pharbaco (Hanoi, Viet-Nam), Mekophar (Ho Chi Minh City, Viet-Nam), Yangon Pharma (Rangoon, Burma), Mepha (Basel, Switzerland) and Guilin Pharmaceutical (Guangxi, China), respectively. The remaining samples (classified as counterfeit by packaging analysis) were collected on the Thai/Burma border, Burma, Cambodia and the Lao PDR (Laos) and mimicked genuine antimalarial tablets as manufactured by Guilin Pharmaceuticals. A blister pack containing 12 tablets was collected for each suspect sample and one tablet from each blister pack was available for this study. One half of each tablet was processed for NMR experiments whilst the second half was analyzed by DART and DESI MS. The formulations, indicated on their blister packs to all contain 50 mg artesunate per tablet were labeled with the following collection codes with corresponding packaging types²⁰⁰ respectively: **1** (S1/2005, Type 9); **2** (S2/2005, Type 4); **3** (S3/2005, Type 4); **4** (S4/2005, Pharbaco, Hanoi, Viet-Nam); **5** (S5/2005, Type 10); **6** (S8/2005, Mekophar, Ho Chi Minh City, Viet Nam); **7** (S9/2005, Yangon Pharma Industry); **8** (S10/2005, Type 9); **9** (S23/2005, Plasmotrim, Mepha, Switzerland); **10** (Laos 05/03, Type 11); **11** (Burma 2/14029, fake, Type unknown as hologram cut off); **12** (Laos 2/12070, Type 4); **13** (Cambodia 2/13008, genuine, Guilin Pharmaceutical Co. Ltd.); **14** (Laos 05/15, Type 8).

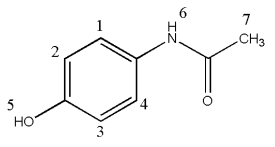
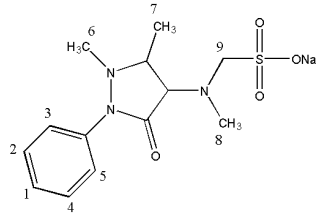
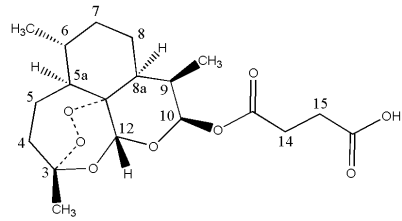
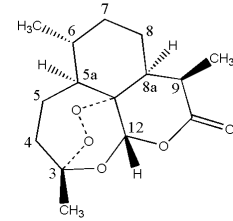
B.3.2. ¹H and 2D DOSY ¹H NMR Analysis

¹H and 2D DOSY ¹H NMR experiments were performed by Stéphane Balayssac, a postdoctoral associate with Dr. Robert Martino in the Groupe de RMN Biomédicale, Université Paul Sabatier, Toulouse, France. For ¹H NMR analyses, a quarter of each tablet was powdered and dissolved in 2 mL of dimethylsulfoxide (DMSO)-d₆ (Eurisotop, Gif-sur-Yvette, France), with magnetic stirring for 15 min and sonication for 5 min. The suspension was centrifuged (10 min, 6000 rpm) and the supernatant poured into a 5 mm NMR tube for analysis. NMR experiments were performed at 298 K on a Bruker Avance 500 spectrometer (Bruker BioSpin, Wissembourg, France) equipped with a triple resonance 5 mm ¹H cryoprobe (TCI) with z-axis gradient. Typical acquisition parameters for ¹H NMR experiments were as follows: 1.02 s acquisition time, 8000 Hz spectral width, 16 K data points, 1 s relaxation delay and 32 scans. The chemical shifts (δ) were referred to an internal trimethylsilylpropane sulfonic acid (TMPS) standard, which gives a singlet for the trimethylsilyl moiety at 0 ppm and three multiplets for the propyl chain at 0.51, 1.58 and 2.40 ppm. In each spectrum, the peaks at 3.17 and 2.53 ppm correspond to the residual signals of HOD and DMSO, respectively.

For 2D DOSY ¹H NMR analyses, stimulated echo bipolar gradient pulse experiments including an eddy-current delay of 10 ms and spoiler gradients of -7.92 and -6.09 G cm⁻¹ with a pulse length of 0.6 s were used. The gradient recovery delay was 3 ms and the relaxation delay was 2 s. Pulse field gradient lengths varied between 2-2.4 ms and the diffusion delay between 100-170 ms. Sequence parameters were adapted in order to decrease the intensity of aromatic NMR signals from the API by at least a factor of 50 at 95% of the full gradient strength. When no API was detected,

signals from excipients were used for sequence optimization. Forty gradient increments (32 scans for each experiment) were recorded with the gradient intensity linearly sampled from 5 to 95%. The gradient system was calibrated to 46.25 G cm^{-1} at maximum intensity prior to all experiments. All data were processed using Gifa 5.2 via the inverse Laplace Transform method together with the Maximum Entropy algorithm (MaxEnt). The processing parameters were 2048 points along the Laplace spectrum diffusion axis and 20,000 MaxEnt iterations. The inverse Laplace Transform was computed only on the columns presenting a signal 32 times greater than the noise level of the experiment. The identification of all APIs and excipients was done by comparing δ values to an in-house 2D DOSY ^1H NMR library, or by spiking the samples with standards. Two-dimensional gCOSY, gHSQC, and gHMBC ^1H NMR experiments were performed to assign the NMR signals of artemisinin and artesunic acid (Table B.1), which matched previous literature data.²⁹⁷ Spectra analysis was done using the NMR notebook software.²⁹⁸

Table B.1. ¹H NMR data of APIs detected in the artesunate antimalarial samples investigated in this study.

Acetaminophen			Dipyron			Artesunic acid			Artemisinin		
											
δ (ppm) ^a	Number of protons, multiplicity ^b (J, Hz)	N°	δ (ppm) ^a	Number of protons, multiplicity ^b (J, Hz)	N°	δ (ppm) ^a	Number of protons, multiplicity ^b (J, Hz)	N°	δ (ppm) ^a	Number of protons, multiplicity ^b (J, HZ)	N°
9.67	1H, s	6	7.48	2H, t (7.9)	2/4	5.69	1H, d (9.6)	10	6.15	1H, s	12
9.16	1H, s	5	7.38	2H, d (7.9)	3/5	5.57	1H, s	12	3.18	1H, m	9
7.35	2H, d (8.6)	1/4	7.28	1H, t (7.9)	1	2.62/2.52	4H, m	14/15	2.29	1H, m	4
6.69	2H, d (8.6)	2/3	3.68	2H, s	9	2.31	1H, m	9	2.08	1H, m	4
2.00	3H, s	7	2.91	3H, s	6	2.21	1H, m	4	1.95	1H, m	5
			2.90	3H, s	8	2.03	1H, m	4	1.81	1H, m	8a
			2.27	3H, s	7	1.84	1H, m	5	1.75	1H, m	8
						1.65	1H, m	8	1.66	1H, m	7
						1.65	1H, m	7	1.56	1H, m	6
						1.58	1H, m	8a	1.38	3H, s	3Me
						1.48	1H, m	8	1.36	1H, m	5a
						1.44	1H, m	6	1.34	1H, m	5
						1.35	1H, m	5	1.17	1H, m	8
						1.31	3H, s	3Me	1.09	3H, d (6.6)	9Me
						1.21	1H, m	5a	1.03	1H, m	7
						0.97	1H, m	7	0.94	3H, d (6.6)	6Me
						0.91	3H, d (6.6)	6Me			
						0.79	1H, d (6.6)	9Me			

^a Spectra were recorded at 298K in DMSO-d₆.

^b s: singlet; d: doublet; t: triplet; m: multiplet.

B.3.3. Ambient Ionization (DART and DESI) MS

DART MS experiments were performed by Glenn Harris, a graduate student in our group. Experiments were performed using a custom-built DART-type ion source¹⁸⁷ interfaced to a JMS-100TLC (AccuTOF™) TOF mass spectrometer (JEOL, Peabody, MA, USA). All experiments were performed in positive ion mode, using similar MS setting described in section A.3.4. The DART-type ion source settings were as follows: high-purity He (99.999% ultrahigh purity helium, Airgas, Atlanta, GA) flow rate 7.2 L min⁻¹, heater temperature 200 °C, corona discharge needle voltage 1000 V, counter electrode voltage 200 V, fixed distance between ion source and MS orifice 3 cm. MS data were acquired and processed using the same procedure described in section A.3.4.

DESI MS experiments were performed using the set-up described in section 6.3.2. Experiments were performed by spraying samples with a solution of 99.9% MeOH, 0.1% HCOOH at a flow rate of 5 µL min⁻¹. The MS experimental parameters were the same as described in section 4.3.4.

B.4. Results and Discussion

All the samples investigated in this study were first analyzed by 2D DOSY ¹H NMR followed by complementary analyses by ambient MS methods including DART and DESI for validation purposes. These analyses resulted in the samples placed into various classes based on the observed chemical signatures, as discussed in the following sections.

B.4.1. Analysis of Genuine Artesunate Tablets

The samples **4**, **6**, **7**, **9** and **13** were all categorized as genuine products based on packaging inspection, and originated from different manufacturers. They were grouped as **Class A** samples (Table B.2). 2D DOSY ^1H NMR and ambient MS analyses revealed two different sub-classes within **Class A** samples, with samples **4**, **6**, **7** and **9** in one sub-class, and sample **13**, manufactured by Guilin Pharmaceutical Co. Ltd, being of a different sub-class. The expected API, artesunic acid, was observed in all the formulations with stearate and starch as excipients, as exemplified by the analysis of formulation **4** (Figure B.1). The major difference between the samples in each sub-class related to the

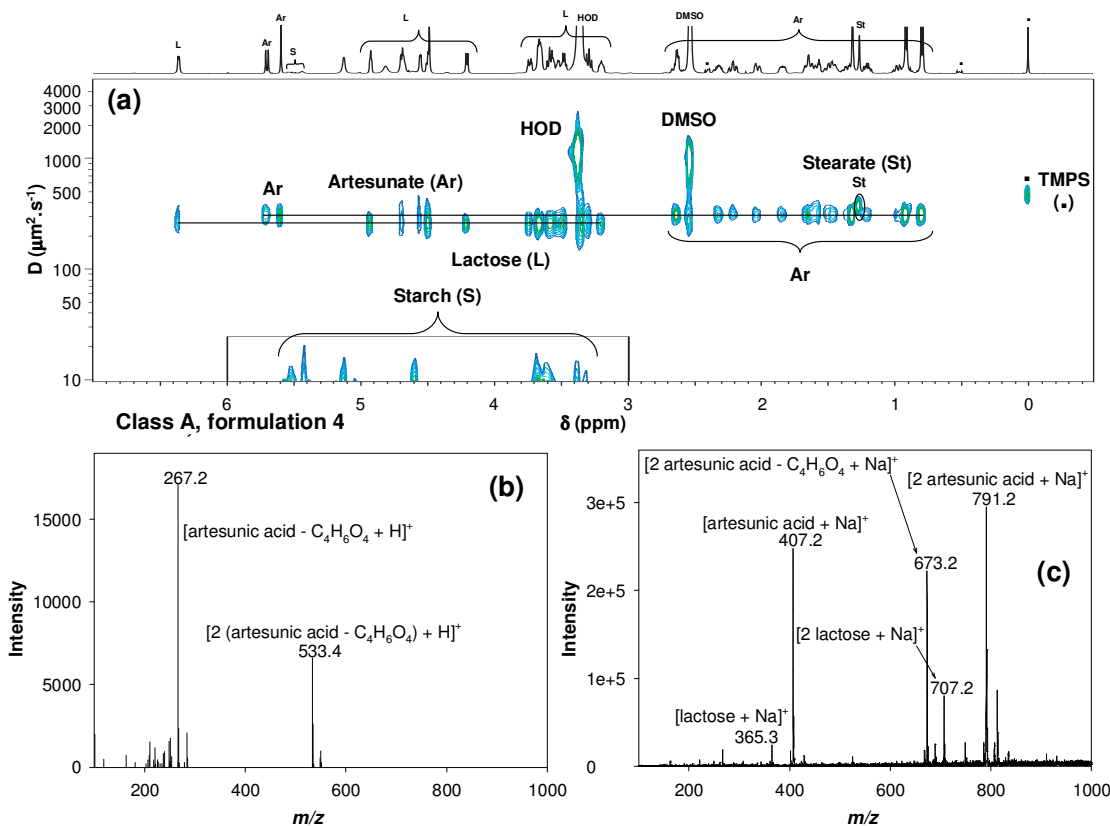


Figure B.1. Analyses of formulation **4** by: (a) 2D DOSY ^1H NMR in DMSO-d_6 with TMPS as internal reference standard, positive ion mode (b) DART MS (c) DESI MS.

identity of the disaccharides present (lactose vs. sucrose). Lactose was identified in the first sub-class (**4, 6, 7, 9**) and sucrose in the second. Results for formulation **4** are a good example of the virtual separation of components, based on their diffusion coefficients, observed in a 2D DOSY ^1H NMR experiment (Figure B.1.a). Differences between self-diffusion coefficients of low M_{W} components, H_2O ($D \approx 1100 \mu\text{m}^2 \text{s}^{-1}$) and DMSO ($D \approx 910 \mu\text{m}^2 \text{s}^{-1}$), intermediate M_{W} components, artesunate ($D \approx 300 \mu\text{m}^2 \text{s}^{-1}$) and lactose ($D \approx 250 \mu\text{m}^2 \text{s}^{-1}$), and starch with a very low diffusion coefficient typical of polysaccharides ($D < 10 \mu\text{m}^2 \text{s}^{-1}$) are readily observed. DART MS analysis of formulation **4** showed peaks at m/z 267.2 and 533.4, assigned as $[\text{artesunic acid-C}_4\text{H}_6\text{O}_4+\text{H}]^+$ and $[2(\text{artesunic acid-C}_4\text{H}_6\text{O}_4)+\text{H}]^+$ respectively (Figure B.1.b). Figure B.1.c shows the complementary DESI spectrum of this sample. The predominant peaks in the spectrum (m/z 407.2, 673.2 and 791.2) were assigned to $[\text{artesunic acid}+\text{Na}]^+$, $[2 \text{ artesunic acid-C}_4\text{H}_6\text{O}_4+\text{Na}]^+$, and $[2 \text{ artesunic acid}+\text{Na}]^+$ respectively. Also in this spectrum, the peaks at m/z 365.3 and 707.2 were identified as $[\text{lactose}+\text{Na}]^+$ and $[2 \text{ lactose}+\text{Na}]^+$ after comparison against DESI MS^2 analyses of standards (*vide infra*).

B.4.2. Analysis of Counterfeit Artesunate Tablets

Figure B.2.a shows the 2D DOSY ^1H NMR spectrum of formulation **2**, which had a unique chemical signature, and was thus placed in a unique sample class (**Class B**, Table B.2). Three compounds were identified in this formulation. The API was artemisinin ($D \approx 620 \mu\text{m}^2 \text{s}^{-1}$), the naturally-occurring precursor for a number of semi-synthetic antimalarial drugs including artesunate, artemether, dihydroartemisinin and artelinic acid. In addition to artemisinin, two other excipients were found in this tablet,

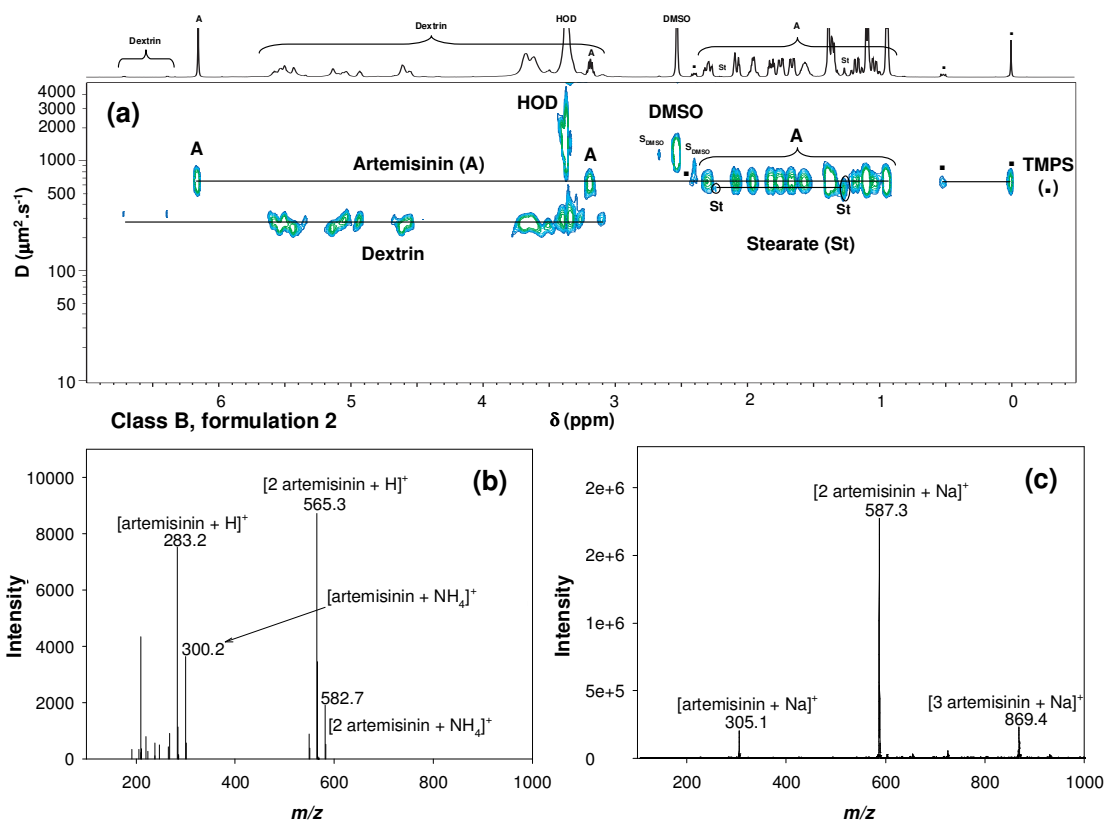


Figure B.2. Analyses of formulation 2 by: (a) 2D DOSY ^1H NMR in DMSO- d_6 with TMPS as internal reference standard (S_{DMSO} represents DMSO satellite signals), positive ion mode (b) DART MS (c) DESI MS.

viz: dextrin, which shows two characteristic doublets at 6.71 and 6.39 ppm, a triplet at 4.93 ppm and two series of broad signals between 5.2-5.8 and 3.8-3.0 ppm in ^1H NMR. The second excipient was a stearate-based lubricant that leads to four signals located at 0.88 (triplet), 1.26 (broad singlet), 1.50 (quintuplet) and 2.14 (triplet) ppm. Results from the complementary analysis of this sample by both DART and DESI MS are illustrated in Figures B.2.b-c. The peaks at m/z 283.2 and 565.3 in the DART spectrum (Figure B.2.b) correspond to the protonated artemisinin monomer and dimer, respectively. Peaks at m/z 300.2 and 582.7 were also observed, corresponding to the respective ammonium adducts. Analysis of this sample by DESI MS in positive ion mode showed peaks at m/z 305.1,

587.3 and 869.4 (Figure B.2.c), which corresponded to sodiated adducts of monomeric, dimeric, and trimeric artemisinin. The excipients detected by 2D DOSY ^1H NMR were not detected by either DART or DESI MS. Although stearate is not expected to ionize well in positive ion mode, dextrin, which could be ionized, was also not observed. This phenomenon could stem from the higher ionization efficiency of artemisinin, which suppresses ionization of other compounds in the sample. Surprisingly, these species were not observed in the negative ion mode probably due to similar effects. The correct API, artesunic acid, was not observed in this sample by any of the assayed methods.

2D DOSY ^1H NMR analysis of formulation **11** (Figure B.3.a) revealed a unique chemical signature, and was assigned as **Class C** (Table 1). The tablet contained no identifiable API, but a stearate-based lubricant along with the tablet diluents starch (five broad signals at 5.53, 5.43, 5.13, 4.61 and 3.61 ppm) and sucrose (two doublets at 5.08 and 4.52 ppm, a triplet at 3.91 ppm and multiplets at 5.21, 4.82, 4.42 and between 3.8 and 3.1 ppm) were found to be present. Minor unknown signals (a singlet at 6.50 ppm and four doublets at 6.08, 7.62, 8.19 and 8.36 ppm) were also detected. DART MS analysis of sample **11** did not yield any identifiable peaks. However, analysis of this sample by DESI MS in positive ion mode showed two prominent peaks at m/z 365.3 and 707.2, identified as sodiated sucrose monomer and dimer respectively (Figure B.3.b). The peak identities were determined by comparing the DESI MS and MS^2 spectra of this sample against sucrose (Figure B.3.c) and lactose (Figure B.3.d) standards. Because these disaccharides are structural isomers, only DESI MS^2 , but not DESI MS, can distinguish between them. Figure B.4 summarizes the various cleavages and fragment ions observed by DESI MS^2 of the precursor ions, m/z 365.3. For both sodiated sugars, cleavages at the glycosidic

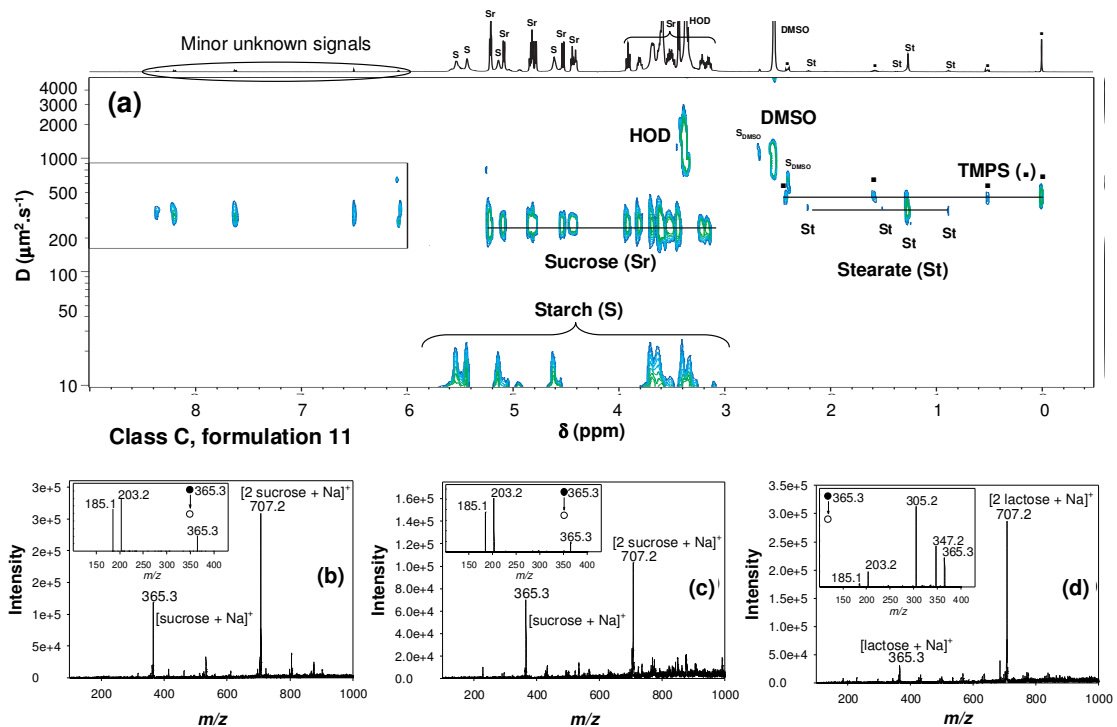


Figure B.3. Analyses of formulation **11** by: (a) 2D DOSY ^1H NMR in DMSO-d_6 with TMPS as internal reference standard (S_{DMSO} represents DMSO satellite signals); and (b) DESI MS in positive ion mode. (C) DESI spectrum of a sucrose standard ($10\ \mu\text{L}$, $1\ \text{mg mL}^{-1}$), (D) DESI spectrum of a lactose standard ($10\ \mu\text{L}$, $1\ \text{mg mL}^{-1}$). Standards were deposited onto PTFE and analyzed after air drying. The inserts in (b), (c) and (d) represent the corresponding DESI MS² spectra generated from the ion at m/z 365.3.

bonds occur with the competitive retention of a sodium ion on each monosaccharide unit, with or without an additional loss of a water molecule to generate $[\text{monosaccharide}+\text{Na}]^+$ and $[\text{monosaccharide}-\text{H}_2\text{O}+\text{Na}]^+$ ions at m/z 203.2 and 185.1, respectively. For sodiated lactose (Figure B.4.a), additional fragment ions corresponding to the loss of a water molecule or two formaldehyde molecules from the precursor ion are observed, generating diagnostic signals at m/z 347.2 and m/z 305.2 for distinguishing between sucrose (Figure B.4.b) and lactose. The detection of sucrose and no APIs in this sample by DESI MS was thus consistent with DOSY NMR results.

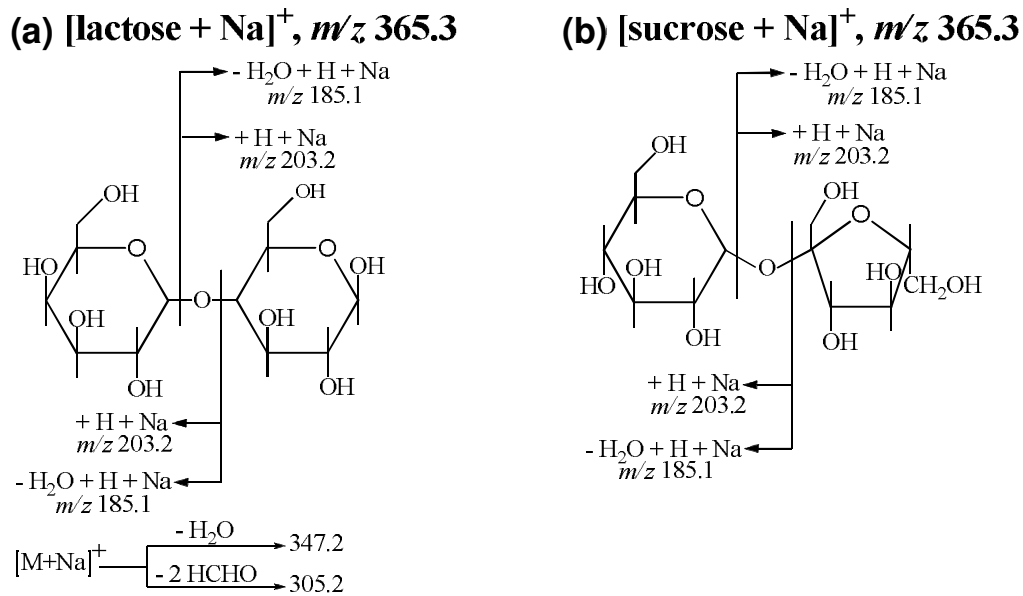


Figure B.4. Fragment ions observed for the isomeric species: (a) [lactose + Na]⁺ and (b) [sucrose + Na]⁺.

Table B.2 presents a summary of the results obtained following 2D DOSY ¹H NMR and ambient MS analyses of all the samples investigated in this study. The analyses of artesunate tablets formulation using these complementary analytical techniques enabled the comprehensive determination of the chemical signatures presented by each sample readily placing them into distinct classes (chemotypes). For a total of 14 formulations evaluated, the correct API was detected in only five formulations. The remaining formulations were observed to contain various “wrong” APIs. DESI and DART did not readily offer information about the presence of stearate and polymeric excipients such as dextrin, which were detected by 2D DOSY ¹H NMR. Interestingly, no disaccharides (lactose, sucrose) were detected by DART. This is possibly due to the different desorption mechanism of this technique, which is believed to be predominantly thermal, compared to DESI, which relies on the solubility of the analyte in the spray solution.

Table B.2. APIs and excipients detected by 2D DOSY ¹H NMR, DESI and DART MS in 14 different antimalarial formulations.

Compound	Technique	Formulations							
		Class A		Class B	Class C	Class D	Class E	Class F	Class G
		4, 6, 7, 9	13	2	11	10, 14	12	1, 8	3, 5
Packaging Type ²⁰⁰		Genuine	Genuine	4	N/A ^c	8, 11	4	9	4, 10
Artesunic acid	DOSY NMR	+	+						
	DESI/DART MS	+/+	+/-						
Artemisinin	DOSY NMR			+					
	DESI/DART MS			+/+					
Acetaminophen	DOSY NMR							+	
	DESI/DART MS							+/+	
Dipyrene	DOSY NMR								+
	DESI/DART MS								+/+
Stearate	DOSY NMR	+	+	+	+	+	+	+	+
	DESI/DART MS								
Sucrose	DOSY NMR		+		+				
	DESI/DART MS		+/-		+/-				
Lactose	DOSY NMR	+				+			
	DESI/DART MS	+/-				+/-			
Dextrin	DOSY NMR			+			+	+	
	DESI/DART MS								
Starch	DOSY NMR	+	+		+	+	+		+
	DESI/DART MS								

^cThe packaging type of **Class C** formulations could not be assigned, because the hologram had been cut off.

B.5. Conclusions

This appendix highlights the use of complementary analytical methods, 2D DOSY ^1H NMR and ambient (DART and DESI) MS to characterize the chemical composition of counterfeit antimalarial drugs. Both methods allowed the detection of various APIs and tablet excipients enabling samples to be readily categorized into seven distinct classes based on their chemical signatures. 2D DOSY ^1H NMR allows a much increased peak capacity compared to classical 1D ^1H NMR, arising from the use of both chemical shifts and diffusion coefficients as analytical dimensions in the former, making it a very appealing analytical technique. The facile chemotyping of samples following 2D DOSY ^1H NMR and ambient MS analyses provides compelling evidence that suggests that samples within each chemotype are most likely manufactured by the same establishment thus alluding to the number of distinct genuine and/or counterfeit artesunate manufacturers.

APPENDIX C. A COLLABORATIVE EPIDEMIOLOGICAL INVESTIGATION INTO THE CRIMINAL FAKE ARTESUNATE TRADE IN SOUTH EAST ASIA

C.1. Abstract

This appendix presents efforts by an international collaboration for the conglomeration of detailed forensic evidence on genuine and counterfeit artesunate tablets, using a plethora of analytical techniques with the goal of determining the source of counterfeits. This collaboration involved our laboratory, a group of police, criminal analysts, palynologists, and health workers, working together under the auspices of the International Criminal Police Organization (INTERPOL) and the Western Pacific World Health Organization Regional Office. The evidence collected following chemical, mineralogical, biological, and packaging analysis suggested that at least some of the counterfeits were manufactured in southeast People's Republic of China. This evidence prompted the Chinese Government to act quickly against the criminal traders with arrests and seizures.

C.2. Introduction

Since the first description of fake artesunate in 2000, very little effort has been invested towards a careful collection of forensic evidence, which could enable a determination of their source to allow possible law enforcement in shutting down operations and prosecution of counterfeiters. Notwithstanding the huge public health consequences of counterfeit artesunate antimalarial, the only actions that were taken

included surveys,^{217, 218, 220, 222, 299, 300} warnings and educational films^{220, 301} resulting in some strengthening of drug regulatory authority (DRA) and malaria program capacity. This appendix presents efforts by a joint multidisciplinary team comprising our lab. (performing ambient MS), the center for disease control (CDC), criminal analysts, palynologists, and health workers under the auspices of the INTERPOL and the Western Pacific World Health Organization Regional Office to collect forensic evidence for the different types of fake and genuine artesunate samples to enable a criminal investigation into the counterfeiting ring.

Following the worsening contamination of the supply of antimalarials in the Greater Mekong Sub-Region by counterfeits, a confidential meeting was held in Manila in May 2005 at the WHO Regional Office for the Western Pacific (WPRO). This meeting brought together WHO officials, physicians, pharmacists and scientists working in the region with the INTERPOL to discuss what could be done. It was decided to join forces to investigate where the counterfeits were being manufactured and develop an intelligence document that could be presented to concerned governments with a request that measures be taken to stop the lethal manufacture and trade in counterfeit artesunate. In the hope that forensic analysis of genuine and counterfeit tablets would provide clues as to the origin of the counterfeits, samples were subjected to high performance liquid chromatography (HPLC), ambient mass spectrometry, X-ray diffraction (XRD), isotope ratio mass spectrometry (IRMS), gas-chromatographic (GC) 'head space' analysis of the gases surrounding tablets in blisterpacks, pollen analysis (palynology) and detailed packaging inspection. This appendix presents a summary of the forensic evidence acquired and the findings relevant to public health.

C.3. Experimental Details

C.3.1. Samples

Data were pulled together from the analyses of a total of 391 samples collected in a wide area of SE Asia encompassing Vietnam (75), Cambodia (48), Lao PDR (115), Myanmar (137) and the Thai/Myanmar border (16), during 2000-2006 period and were kept refrigerated (4° C) until analysis. The samples were collected using convenience sampling,^{217, 218, 299} random sampling (in Laos only)²⁸⁷ and ad hoc at the request of individuals and NGOs in the region. All samples underwent Fast Red Trypaflavine (TR) Dye testing^{227, 302} and/or HPLC, packaging analysis (see section 2.3.2.) and ambient MS. A subset of 27 fakes from this collection and 5 genuines, along with 4 fake (collected in Cambodia) and 2 genuine samples from the United States Pharmacopeia (USP) Drug Quality and Information program, also underwent detailed forensic chemical and palynological examination. 5 samples seized by the Ministry of Public Security (MPS) investigation in China were also evaluated. All laboratories performed the analyses blinded to the results from other laboratories.

C.3.2. Palynology

Palynology is the science that deals with the study of contemporary and fossil palynomorphs, including pollen, spores, dinoflagellate cysts, acritarchs, chitinozoans and scolecodonts, together with particulate organic matter and kerogen found in sedimentary rocks and sediments. Some of these substances have been found trapped in counterfeit drug tablets, and their geographical origin, especially of pollen, have been used to link counterfeit drugs to their source of manufacture. However, results obtained from

palynological analysis must be interpreted with caution as the spore and pollen content could be indicative of either the place of manufacture, the source of the individual ingredients, or both, and could also be influenced by their wind dispersal and seasonality.

Palynological analysis²⁰⁰ was performed by Dallas C. Mildenhall of GNS Science, Lower Hutt, New Zealand. Briefly, tablets were dissolved in hot distilled water or 10% hydrochloric acid yielding two fractions of material in which the top fraction, which contains spores and pollen, was dissolved in 9:1 (v:v) acetic anhydride:sulfuric acid. Mineral material remaining was removed by 50% hydrofluoric acid and was filtered through a 6 µm mesh. All residues were mounted on glass microscope slides and examined at a magnification of x125-250. The taxa of suspected pollen grains were identified by comparison with an internal GNS Science reference library of modern spores and pollen collection.³⁰³⁻³⁰⁶

C.3.3. XRD and IRMS

XRD³⁰⁷ analyses were performed by S. W. Ray Soong from GNS Science, Lower Hutt, New Zealand while stable isotope ratio MS³⁰⁸ was performed by Kevin Faure, also from GNS Science. The basic protocol was as follows: each sample was crushed and mounted as a slurry on a silicon plate and was analyzed by XRD (X'Pert Pro X-ray Diffractometer, Philips, Almelo) and IRMS analysis to determine the mineral composition. Values, in per mil (‰, parts per thousand), are reported in δ¹⁸O

$$\left(1000 \times \left(\left(\frac{^{18}\text{O}}{^{16}\text{O}} \right)_{\text{Samp.}} - \left(\frac{^{18}\text{O}}{^{16}\text{O}} \right)_{\text{Std.}} \right) \div \left(\frac{^{18}\text{O}}{^{16}\text{O}} \right)_{\text{Std.}} \right) \text{ and } \delta^{13}\text{C} \left(1000 \times \left(\left(\frac{^{13}\text{C}}{^{12}\text{C}} \right)_{\text{Samp.}} - \left(\frac{^{13}\text{C}}{^{12}\text{C}} \right)_{\text{Std.}} \right) \div \left(\frac{^{13}\text{C}}{^{12}\text{C}} \right)_{\text{Std.}} \right)$$

notation.³⁰⁹ Samples were analyzed in duplicate and values averaged.

C.3.4. LC Diode Array Analysis

HPLC analysis¹⁹⁸ was performed by Dr. Michael D. Green of the Division of Parasitic Diseases of the CDC, Atlanta, GA. Briefly, a 150 x 4.6 mm octadecylsilica column with a mobile phase consisting of 45% acetonitrile and 55% 0.05 M perchlorate buffer (pH 2.5) was used to effectively separated artemisinin, acetaminophen, and artesunate. For quantitative acetaminophen analysis, the mobile phase was changed to 10% acetonitrile and 90% perchlorate buffer. Components were detected using a diode array detector with wavelengths set at 220 and 254 nm. UV spectra of samples were compared with artesunate, artemisinin and acetaminophen reference standards for validation.

C.3.5. Ambient Ionization (DESI and DART) MS

Ambient MS analyses by DESI and DART MS was performed using the procedure described in section A.3.4. DESI was performed in both the reagentless and reactive mode for validation purposes.

C.4. Results and Discussion

A total of 14 different hologram types were identified in the wide area of SE Asia, up to and including 2006. A further two hologram types were identified in 2006-2007 making a total of 16 hologram types identified in this region (see Figure 2.2, Chapter 2). The aggregated results obtained from the various analyses of the samples constituting all 16 hologram types are summarized in Table S1 of Newton *et al.*²⁰⁰

C.4.1. Determination of API(s) in the Samples

HPLC and/or DART- and DESI-MS confirmed that all specimens speculated to be counterfeit (195/ 391, 49.9%) on the basis of packaging contained no or small quantities of artesunic acid (up to 12 mg per tablet as opposed to the expected 50 mg per genuine tablet). One sample from Cambodia had apparently genuine packaging but contained only 21 mg artesunic acid and was therefore either substandard or had deteriorated in transit and/or storage.²²² Of 321 samples labeled as made by Guilin Pharmaceutical, 195 (61%) were counterfeit. A wide variety of unexpected ‘wrong’ pharmaceuticals were identified in the counterfeit samples, including acetaminophen (n = 24), sulphadoxine (n = 18), pyrimethamine (n = 11), dimethylfumarate (n = 17), erythromycin (n = 8), erucamide (n = 5), safole (n = 6), artemisinin (n = 10) dipyrone (n = 10), 2- mercaptobenzothiazole (n = 5), chloramphenicol (n = 4), metronidazole (n = 2) and chloroquine (n = 2).

C.4.2. Palynological and Mineralogical Investigation

Most of the spores and pollen identified in the samples had a distinct northern Asian temperate signature with evidence for plants such as firs, pines, cypresses, sycamores, alders, wormwood, willows, elms, wattles, and fern spores. Figure C.1 shows photos of some of the debris found in the counterfeit tablets.

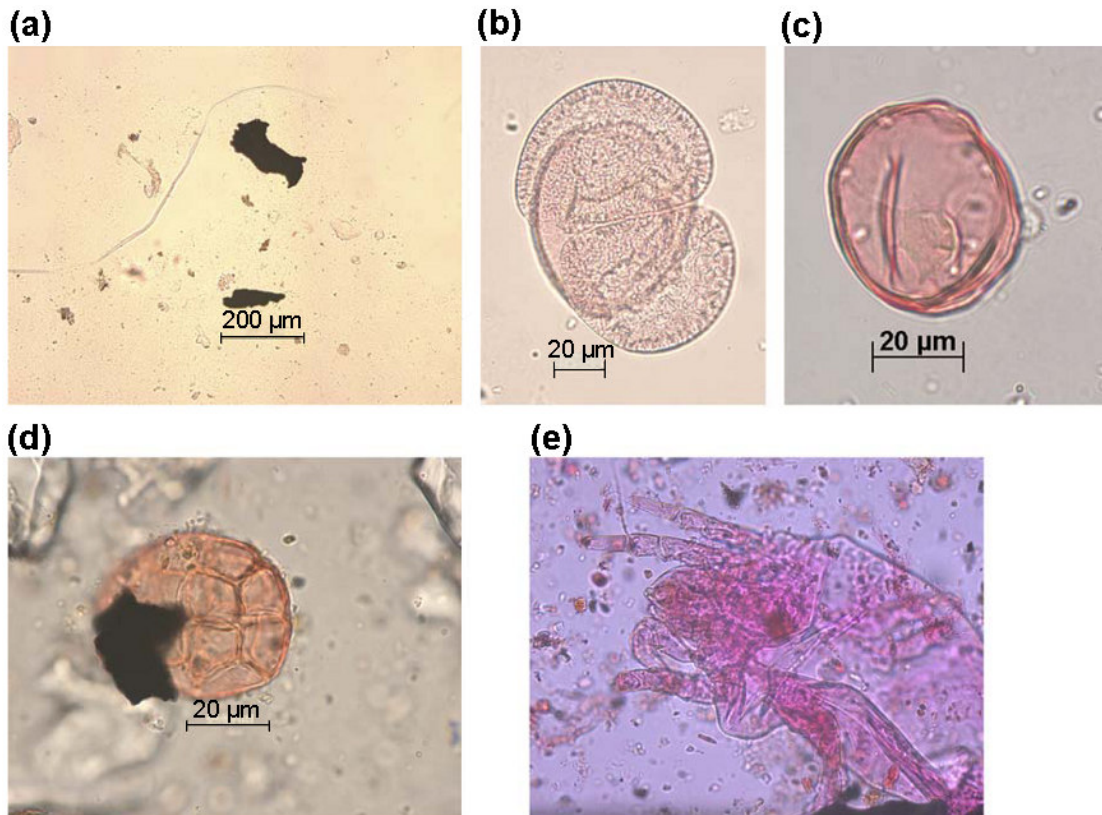


Figure C.1. Photomicrographs of material found in fake artesunate tablets. (a) Debris, including charcoal fragments. (b) *Pinus* pollen grain. (c) *Juglans* pollen grain. (d) *Acacia* pollen grain with charcoal deposit. (e) *Dermatophagoides* mite nymph.

The estimated origin of the samples includes northernmost Vietnam, southern China, and near the mountains, bordering Myanmar and Vietnam (see Figure 2.2). Some of the plant remains, such as *Juglandaceae* pollen (walnut), *Carya* (wing nut), and *Pterocarya* (hickory), suggest manufacture in southern China. In terms of palynological analysis for samples having different types of fake hologram/sticker, Type 2 differs from the others as it lacks fern spores, Type 1 contained little material but appeared similar to Type 3, and Types 10, 11 and 12 had similar pollen signatures. Types 5 and 8 did not contain anything to enable comparisons to be made and Types 4, 6, 7, 9, 13 & 14 were not examined.

In addition to plant remains, five samples contained invertebrates, including a *Dermatophagoides* mite nymph (from Type 11, Vietnam, Figure C.1.e), which is commonly found in house dust and has a global distribution. All fake artesunate tablets contained charcoal fragments and black chips, broken up by the processing for pollen. In some samples, charcoal was so abundant that it suggested the source was an area suffering severe air pollution.

XRD demonstrated great variability in tablet mineralogy. Although, maize starch is the main excipient in the genuine Guilin product, talc (hydrated magnesium silicate), calcite (calcium carbonate) and starch were the main excipients detected in the counterfeit tablets. Trace amounts of aragonite were present in two calcite-dominated fake tablets and traces of chlorite (iron-magnesium hydrosilicate) and quartz (silicon dioxide) were found in another two. Stable isotope analysis of the calcite fraction gave $\delta^{18}\text{O}$ and $\delta^{13}\text{C}$ values between -11 to +2‰ and +2 to + 25 ‰, respectively, as shown in Figure C.2.

Given the similar isotope signatures, the calcite in all (Types 2, 4, 5, 8, and 11) but one sample appears to come from the same source and is either hydrothermal or medical in origin. The one exception is sample 05/17 (Type 12) from southern Laos which, if the calcite is assumed to have been formed by natural geological processes, is typical of marine limestone.

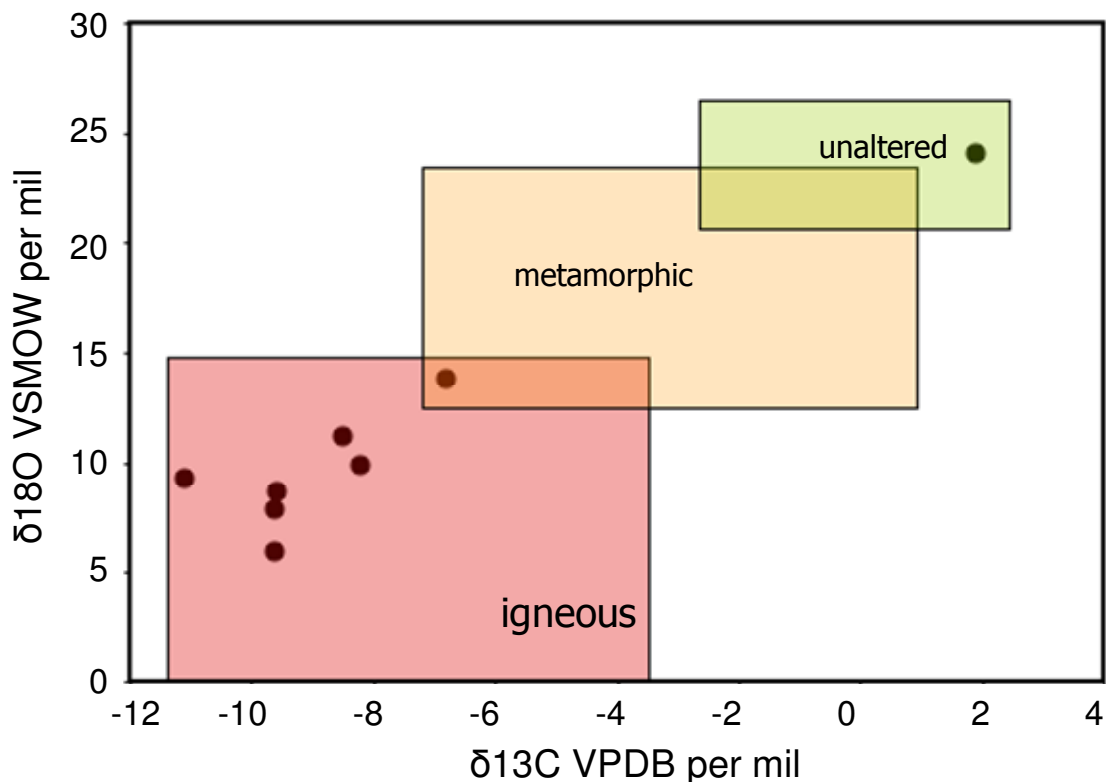


Figure C.2. Plot of $\delta^{13}\text{C}$ and $\delta^{18}\text{O}$ values, in ‰ of carbonate in tablets. Approximate values expected from calcite in different geological environments (pink = igneous; yellow = metamorphosed; green = unaltered) is also plotted. The top right data point represents sample 05/17.

C.4.3. Interpretation of the Evidence

Although at first glance, the pooling of chemical, palynological and packaging evidence suggests a wide diversity of fake artesunate in SE Asia with strikingly different fake holograms and chemical signatures, some generalization can be made. For example, palynological evidence suggests that all counterfeits were produced in temperate areas along the borders between China and neighboring countries in SE Asia. Inspection of maps of the geographical distribution of fake artesunate (see Figure 2.2) suggests that there may be two different origins of counterfeit artesunate, with similarities between the

samples in Myanmar, the Thai-Myanmar border and northern Laos in a westerly group, and similarities between those recovered in southern Laos, Vietnam and Cambodia in a easterly group. Of the 319 samples labeled as made by Guilin Pharmaceutical Co, with a detailed location recorded, there were a significantly higher proportion of counterfeit drugs in the east than in the west (41% (62/151) vs. 79% (133/168), $p < 0001$). In addition, in the west 73% (37/51) of batch numbers used were invalid whereas in the east only 1.5% (2/128) were invalid ($\chi^2 = 107.8$, $p < 0.0001$).

Fakes with stickers were only found in Vietnam and Cambodia while those with holograms were only found in Myanmar and along the Thai-Myanmar border. Both stickers and holograms were found in northern and southern Laos. All of the different fake holograms have mis-registration of the outer ring of the Guilin logo and although the errors differ between all Types, they have been made in the same way, suggesting the use of similar technology and machines. Types 2, 3, 5, 7, 11, and 12 were only found in the east while 6, 9, and 10 were only found in the west. Types 1, 4, and 8 were found in the east and the west but in varying proportions as 82% of Type 1, 17% of Type 4 and 25% of Type 8 were found in the west. With the exception of Type 4, all counterfeits containing calcite bore stickers and not fake holograms. However, the pollen signatures of Types 3, 11 & 12 (easterly) and 9 & 10 (westerly) were similar, suggesting that the manufacturing sites of these two groups may be in the same area of southern China, but that are parts of separate operations having different distribution networks. Types 8, 11, and 12 all contain an error in the upper case font for 'Mfg' and 'Exp' suggesting a link between the producers of these three types. The occurrence of a Type 10 blisterpack in a Type 4 box and a Type 13 blisterpack in a Type 9 box suggests links between the

producers and/or distributors of these fakes. All of this evidence supports the ‘easterly’ and ‘westerly’ distribution hypothesis.

The existence of two main sources is also suggested by DART- and DESI-MS analysis. Metronidazole and artesunate were only found in westerly group samples while sulphadoxine, pyrimethamine, erythromycin and erucamide were found only in the easterly group samples. Dimethylfumarate (88%), 2-mercaptobenzothiazole (80%), metamizole (70%), safrole (67%), acetaminophen (67%) and artemisinin (60%), were found predominantly in the east. Samples containing chloramphenicol, and chloroquine were in equal numbers in each geographical group. Counterfeit artesunate (Type 14) was shown to contain some artesunate on the exterior surface suggesting that the counterfeit tablets may have been contaminated with the genuine ingredient in the tablet press left over from the manufacture of genuine product at an unknown location.¹⁰² The presence of sulphadoxine and pyrimethamine further suggests that the factory had been making, or had access to, sulphadoxine+pyrimethamine, an anti-malarial combination therapy that is no longer effective in SE Asia. The discovery of safrole is of considerable concern and interest as it is a precursor in the synthesis of methylenedioxyamphetamine (MDMA or Ecstasy) and is a banned chemical in the United Nations Convention Against Illicit Traffic in Narcotic Drugs and Psychotropic Substances.³¹⁰ However, MDMA was not detected in or on the counterfeits.

All of the counterfeits purchased from Vietnam, except for Type 12, contained calcite having C and O stable isotope ratios that are consistent with what would be found in an area being volcanic in origin rather than that originating from marine or terrestrial limestone or tap water precipitation. One such area having high temperature

hydrothermal calcite is mined in an area west of Nanning, close to the Vietnam border (see Figure 2.2) and the calcite used in Types 2, 4, 5, 8 and 11 may have originated from these mines.

This combination of excipient composition and palynology results therefore suggested that at least some of the counterfeit artesunate were coming from southern China or close to its border with Vietnam, Thailand and Myanmar. Furthermore, the evidence suggests that there are at least two distribution routes followed for these counterfeit products with westerly origins via Myanmar and easterly origins via Vietnam with Laos in the middle, an area of overlap afflicted by Types of both groups.

The evidence described here was presented by the Secretary General of INTERPOL (Mr. Ronald K Noble) to the Assistant MPS (Mr. Zheng Shaodong) in March 2006 in Beijing, China. In response, a criminal investigation was carried out leading to the arrest of a native of Yunnan Province who, it was alleged, had bought 240,000 blisterpacks of counterfeit artesunate (Figure C.3) from a native of Guangdong Province, China, which is thought to be the origin of these counterfeits. As Guilin Pharmaceutical Co. Ltd. exported 272,000 blisterpacks to Myanmar and Thailand during this time, an estimated 47% of artesunate available in the market was fake which is consistent with previous estimates of the proportion of fake artesunate in mainland SE Asian shops.



Figure C.3. Counterfeit artesunate samples seized during arrests made after reporting of findings of Operation Jupiter to Chinese government officials.

The seized samples appeared to be related to the more sophisticated westerly counterfeits found in Myanmar, Thai-Myanmar border and Laos bearing sophisticated holograms and without the plethora of wrong APIs (other than artemisinin). This assertion was also supported by the absence of calcite in these counterfeits. However, based upon the findings presented here, there is a strong possibility that there is a second trade route involving a different group of criminals distributing and/or manufacturing fake artesunate, with poor quality stickers and a variety of wrong ingredients with calcite, into Vietnam, Cambodia and southern Laos. If this hypothesis is correct, future examination of the prevalence of different types would be expected to demonstrate a reduction in the westerly distribution, but not that being fed by the easterly trade route.

C.5. Conclusions

This appendix showcases the strengths of combining a plethora of analytical techniques including HPLC, ambient MS, XRD, IRMS, GC ‘head space’ analysis, palynology and packaging analysis to allow the collection of detailed forensic evidence to enable a determination of the source of counterfeit artesunate antimalarial tablets. Of 391 tablets investigated using these techniques, 196 (50.1%) were shown to be genuine artesunate samples while the remaining 195 samples were determined to be counterfeit. The counterfeit samples contained various wrong active pharmaceutical ingredients including erythromycin (22.5%), acetaminophen (6.1%), artemisinin (2.6%), saffrole (1.6%), as well as several other compounds. This evidence suggested two different origins of counterfeit artesunate, with similarities between the samples in Myanmar, the Thai-Myanmar border and northern Laos in a westerly group, and similarities between those recovered in southern Laos, Vietnam and Cambodia in a easterly group. The abundant forensic evidence provided by these tools was advantageously exploited to initiate a criminal investigation into the critical fake artesunate trade. This first led to the arrest of a native of Yunnan Province who, it was alleged, had bought 240,000 blister packs of counterfeit artesunate from a native of Guangdong Province, China who was also arrested. All those arrested are currently being prosecuted. The international cross-disciplinary approach presented in this study may be appropriate in the investigation of other serious counterfeit medicine public health problems elsewhere.

REFERENCES

- (1) Takats, Z.; Wiseman, J. M.; Gologan, B.; Cooks, R. G. *Science* **2004**, *306*, 471-473.
- (2) Dempster, A. J. *Physical Review* **1918**, *11*, 316-324.
- (3) Munson, M. S. B.; Field, F. H. *Journal of the American Chemical Society* **1966**, *88*, 2621-2630.
- (4) Vallance, C.; Harris, S. A.; Hudson, J. A.; Harland, P. W. *Journal of Physics B, Atomic, Molecular, and Optical Physics* **1997**, *30*, 2465-2475.
- (5) Benninghoven, A.; Hagenhoff, B.; Niehuis, E. *Analytical Chemistry* **1993**, *65*, 630A-640A.
- (6) Hillenkamp, F.; Karas, M.; Beavis, R. C.; Chait, B. T. *Analytical Chemistry* **1991**, *63*, A1193-A1202.
- (7) Todd, P. J.; Schaaff, T. G.; Chaurand, P.; Caprioli, R. M. *Journal of Mass Spectrometry* **2001**, *36*, 355-369.
- (8) Barber, M.; Bordoli, R. S.; Sedgwick, R. D.; Tyler, A. N.; Whalley, E. T. *Biological Mass Spectrometry* **1981**, *8*, 337-342.
- (9) Bruins, A. P. *Trends in Analytical Chemistry* **1994**, *13*, 37-43.
- (10) Huang, E. C.; Wachs, T.; Conboy, J. J.; Henion, J. D. *Analytical Chemistry* **1990**, *62*, 713A-725A.
- (11) Horning, E. C.; Horning, M. G.; Carroll, D. I.; Dzidic, I.; Stillwell, R. N. *Advances in Biochemical Psychopharmacology* **1973**, *7*, 15-31.
- (12) Horning, E. C.; Horning, M. G.; Carroll, D. I.; Dzidic, I.; Stillwell, R. N. *Analytical Chemistry* **1973**, *45*, 936-943.
- (13) Proctor, C. J.; Todd, J. F. J. *Organic Mass Spectrometry* **1983**, *18*, 509-516.
- (14) Inoue, H.; Hashimoto, H.; Watanabe, S.; Iwata, Y. T.; Kanamori, T.; Miyaguchi, H.; Tsujikawa, K.; Kuwayama, K.; Tachi, N.; Uetake, N. *Journal of Mass Spectrometry* **2009**, *In Press*.
- (15) Sleeman, R.; Burton, I. F. A.; Carter, J. F.; Roberts, D. J. *Analyst* **1999**, *124*, 103-108.

- (16) Horning, E. C.; Carroll, D. I.; Dzidic, I.; Haegele, K. D.; Horning, M. G.; Stillwell, R. N. *Journal of Chromatographic Science* **1974**, *12*, 725-729.
- (17) Horning, E. C.; Carroll, D. I.; Dzidic, I.; Haegele, K. D.; Horning, M. G.; Stillwell, R. N. *Journal of Chromatography* **1974**, *12*, 725-729.
- (18) Thomson, B. A.; Iribarne, J. V. *Journal of Chemical Physics* **1979**, *71*, 4451-4463.
- (19) Thomson, B. A.; Danylewch-May, L. *31st Annual Conference on Mass Spectrometry and Allied Topics: 1983*, Boston.
- (20) Blakley, C. R.; Carmody, J. C.; Vestal, M. L. *Clinical Chemistry* **1980**, *26*, 1467-1473.
- (21) Blakley, C. R.; Carmody, J. J.; Vestal, M. L. *Analytical Chemistry* **1980**, *52*, 1636-1641.
- (22) Fenn, J. B.; Mann, M.; Meng, C. K.; Wong, S. F.; Whitehouse, C. M. *Science* **1989**, *246*, 64-71.
- (23) Fenn, J. B.; Mann, M.; Meng, C. K.; Wong, S. F.; Whitehouse, C. M. *Mass Spectrometry Reviews* **1990**, *9*, 37-70.
- (24) Whitehouse, C. M.; Dreyer, R. N.; Yamashita, M.; Fenn, J. B. *Analytical Chemistry* **1985**, *57*, 675-679.
- (25) Aleksandrov, M. L.; Baram, G. I.; Gall, L. M.; Krasnov, N. V.; Kusner, Y. S.; Mirgorodskaya, O. A.; Nikolaiev, V. I.; Shkurov, V. A. *Bioorganicheskaya Khimiya* **1985**, *11*, 700-704.
- (26) Alexandrov, M. L.; Gall, L. N.; Krasnov, N. V.; Nikolaev, V. I.; Pavlenko, V. A.; Shkurov, V. A. *International Journal of Mass Spectrometry and Ion Processes* **1983**, *54*, 231-235.
- (27) Dole, M.; Mack, L. L.; Hines, R. L.; Mobley, R. C.; Ferguson, L. D.; Alice, M. B. *Journal of Chemical Physics* **1968**, *49*, 2240-2249.
- (28) Meng, C. K.; Mann, M.; Fenn, J. B. *Proceedings of the 36th ASMS Conference on Mass Spectrometry and Allied Topics, 5-10 June 1988, San Francisco, CA*, 771-772.
- (29) Yamashita, M.; Fenn, J. B. *Journal of Physical Chemistry* **1984**, *88*, 4451-4459.
- (30) Bruins, A. P.; Covey, T. R.; Henion, J. D. *Analytical Chemistry* **1987**, *59*, 2642-2646.

- (31) Takats, Z.; Wiseman, J. M.; Gologan, B.; Cooks, R. G. *Analytical Chemistry* **2004**, *76*, 4050-4058.
- (32) Hirabayashi, A.; Sakairi, M.; Koizumi, H. *Analytical Chemistry* **1994**, *66*, 4557-4559.
- (33) Hirabayashi, A.; Sakairi, M.; Koizumi, H. *Analytical Chemistry* **1995**, *67*, 2878-2882.
- (34) Kauppila, T. J.; Bruins, A. P.; Kostianen, R. *Journal of the American Chemical Society for Mass Spectrometry* **2005**, *16*, 1399-1407.
- (35) Kauppila, T. J.; Kotiaho, T.; Bruins, A. P.; Kostianen, R. *Journal of the American Chemical Society for Mass Spectrometry* **2004**, *15*, 203-211.
- (36) Kauppila, T. J.; Kuuranne, T.; Meurer, E. C.; Eberlin, M. N.; Kotiaho, T.; Kostianen, R. *Analytical Chemistry* **2002**, *74*, 5470-5479.
- (37) McEwen, C. N.; McKay, R. G.; Larsen, B. S. *Analytical Chemistry* **2005**, *77*, 7826-7831.
- (38) McEwen, C. N.; Larsen, B. S. *Journal of the American Chemical Society for Mass Spectrometry* **2009**, *20*, 1518-1521.
- (39) Cody, R. B.; Laramée, J. A.; Durst, H. D. *Analytical Chemistry* **2005**, *77*, 2297-2302.
- (40) Haddad, R.; Sparrapan, R.; Eberlin, M. N. *Rapid Communications in Mass Spectrometry* **2006**, *20*, 2901-2905.
- (41) Haddad, R.; Milagre, H. M. S.; Catharino, R. R.; Eberlin, M. N. *Analytical Chemistry* **2008**, *80*, 2744-2750.
- (42) Haddad, R.; Sparrapan, R.; Kotiaho, T.; Eberlin, M. N. *Analytical Chemistry* **2008**, *80*, 898-903.
- (43) Chen, L. C.; Nishidate, K.; Saito, Y.; Mori, K.; Asakawa, D.; Takeda, S.; Kubota, T.; Hori, H.; Hiraoka, K. *Journal of Physical Chemistry B* **2008**, *112*, 11164-11170.
- (44) Chen, L. C.; Nishidate, K.; Saito, Y.; Mori, K.; Asakawa, D.; Takeda, S.; Kubota, T.; Terada, N.; Hashimoto, Y.; Hori, H.; Hiraoka, K. *Rapid Communications in Mass Spectrometry* **2008**, *22*, 2366-2374.
- (45) Yoshimura, K.; Chen, L. C.; Asakawa, D.; Hiraoka, K.; Takeda, S. *Journal of Mass Spectrometry* **2009**, *44*, 978-985.
- (46) Chang, D. Y.; Lee, C. C.; Shiea, J. *Analytical Chemistry* **2002**, *74*, 2465-2469.

- (47) Chen, H. W.; Sun, Y. P.; Wortmann, A.; Gu, H. W.; Zenobi, R. *Analytical Chemistry* **2007**, *79*, 1447-1455.
- (48) Chen, H. W.; Touboul, D.; Jecklin, M. C.; Zheng, J.; Luo, M. B.; Zenobi, R. N. *European Journal of Mass Spectrometry* **2007**, *13*, 273-279.
- (49) Chen, H. W.; Venter, A.; Cooks, R. G. *Chemical Communications* **2006**, 2042-2044.
- (50) Chen, H. W.; Wortmann, A.; Zhang, W. H.; Zenobi, R. *Angewandte Chemie-International Edition* **2007**, *46*, 580-583.
- (51) Jackson, A. U.; Werner, S. R.; Talaty, N.; Song, Y.; Campbell, K.; Cooks, R. G.; Morgan, J. A. *Analytical Biochemistry* **2008**, *375*, 272-281.
- (52) Li, M.; Hu, B.; Li, J.; Chen, R.; Zhang, X.; Huanwen Chen, H. *Analytical Chemistry* **2009**, In Press.
- (53) Chen, H.; Yang, S.; Wortmann, A.; Zenobi, R. *Angewandte Chemie-International Edition* **2007**, *46*, 7591-7594.
- (54) Chen, H. W.; Wortmann, A.; Zenobi, R. *Journal of Mass Spectrometry* **2007**, *42*, 1123-1135.
- (55) Williams, J. P.; Scrivens, J. H. *Rapid Communications in Mass Spectrometry* **2008**, *22*, 187-196.
- (56) Zhu, L.; Gamez, G.; Chen, H. W.; Chingin, K.; Zenobi, R. *Chemical Communication* **2009**, 559-561.
- (57) Dixon, R. B.; Sampson, J. S.; Muddiman, D. C. *Journal of the American Society for Mass Spectrometry* **2009**, *20*, 597-600.
- (58) Cheng, C. Y.; Yuan, C. H.; Cheng, S. C.; Huang, M. Z.; Chang, H. C.; Cheng, T. L.; Yeh, C. S.; Shiea, J. *Analytical Chemistry* **2008**, *80*, 7699-7705.
- (59) Hsu, H. J.; Oung, J. N.; Kuo, T. L.; Wu, S. H.; Shiea, J. *Rapid Communications in Mass Spectrometry* **2007**, *21*, 375-384.
- (60) Huang, M. Z.; Hsu, H. J.; Wu, C. I.; Lin, S. Y.; Ma, Y. L.; Cheng, T. L.; Shiea, J. *Rapid Communications in Mass Spectrometry* **2007**, *21*, 1767-1775.
- (61) Lin, S. Y.; Huang, M. Z.; Chang, H. C.; Shiea, J. *Analytical Chemistry* **2007**, *79*, 8789-8795.
- (62) Shiea, J.; Huang, M. Z.; Hsu, H. J.; Lee, C. Y.; Yuan, C. H.; Beech, I.; Sunner, J. *Rapid Communications in Mass Spectrometry* **2005**, *19*, 3701-3704.

- (63) Shiea, J.; Yuan, C. H.; Huang, M. Z.; Cheng, S. C.; Ma, Y. L.; Tseng, W. L.; Chang, H. C.; Hung, W. C. *Analytical Chemistry* **2008**, *80*, 4845-4852.
- (64) Sampson, J. S.; Hawkridge, A. M.; Muddiman, D. C. *Journal of the American Society for Mass Spectrometry* **2006**, *17*, 1712-1716.
- (65) Sampson, J. S.; Hawkridge, A. M.; Muddiman, D. C. *Rapid Communications in Mass Spectrometry* **2007**, *21*, 1150-1154.
- (66) Sampson, J. S.; Hawkridge, A. M.; Muddiman, D. C. *Journal of the American Society for Mass Spectrometry* **2008**, *19*, 1527-1534.
- (67) Sampson, J. S.; Hawkridge, A. M.; Muddiman, D. C. *Analytical Chemistry* **2008**, *80*, 6773-6778.
- (68) Nemes, P.; Barton, A. A.; Li, Y.; Vertes, A. *Analytical Chemistry* **2008**, *80*, 4575-4582.
- (69) Nemes, P.; Vertes, A. *Analytical Chemistry* **2007**, *79*, 8098-8106.
- (70) Vertes, A.; Nemes, P.; Shrestha, B.; Barton, A. A.; Chen, Z. Y.; Li, Y. *Applied Physics a-Materials Science & Processing* **2008**, *93*, 885-891.
- (71) Rezenom, Y. H.; Dong, J.; Murray, K. K. *Analyst* **2008**, *133*, 226-232.
- (72) Cheng, S. C.; Cheng, T. L.; Chang, H. C.; Shiea, J. *Analytical Chemistry* **2009**, *81*, 868-874.
- (73) Cotte-Rodriguez, I.; Hernandez-Soto, H.; Chen, H.; Cooks, R. G. *Analytical Chemistry* **2008**, *80*, 1512-1519.
- (74) Cotte-Rodriguez, I.; Mulligan, C. C.; Cooks, G. *Analytical Chemistry* **2007**, *79*, 7069-7077.
- (75) Coon, J. J.; Harrison, W. W. *Analytical Chemistry* **2002**, *74*, 5600-5605.
- (76) Coon, J. J.; Steele, H. A.; Laipis, P. J.; Harrison, W. W. *Journal of Mass Spectrometry* **2002**, *37*, 1163-1167.
- (77) Coon, J. J.; Steele, H. A.; Laipis, P. J.; Harrison, W. W. *Journal of Proteome Research* **2003**, *2*, 610-617.
- (78) Na, N.; Zhang, C.; Zhao, M. X.; Zhang, S. C.; Yang, C. D.; Fang, X.; Zhang, X. R. *Journal of Mass Spectrometry* **2007**, *42*, 1079-1085.
- (79) Na, N.; Zhao, M. X.; Zhang, S. C.; Yang, C. D.; Zhang, X. R. *Journal of the American Society for Mass Spectrometry* **2007**, *18*, 1859-1862.

- (80) Harper, J. D.; Charipar, N. A.; Mulligan, C. C.; Zhang, X. R.; Cooks, R. G.; Ouyang, Z. *Analytical Chemistry* **2008**, *80*, 9097-9104.
- (81) Ratcliffe, L. V.; Rutten, F. J. M.; Barrett, D. A.; Whitmore, T.; Seymour, D.; Greenwood, C.; Aranda-Gonzalvo, Y.; Robinson, S.; McCoustra, M. *Analytical Chemistry* **2007**, *79*, 6094-6101.
- (82) Andrade, F. J.; Shelley, J. T.; Wetzel, W. C.; Webb, M. R.; Gamez, G.; Ray, S. J.; Hieftje, G. M. *Analytical Chemistry* **2008**, *80*, 2646-2653.
- (83) Andrade, F. J.; Shelley, J. T.; Wetzel, W. C.; Webb, M. R.; Gamez, G.; Ray, S. J.; Hieftje, G. M. *Analytical Chemistry* **2008**, *80*, 2654-2663.
- (84) Steeb, J.; Galhena, A. S.; Nyadong, L.; Jinata, A. J.; Fernandez, F. M. *Chemical Communication* **2009**, *In Press*.
- (85) Chen, H.; Zheng, O. Y.; Cooks, R. G. *Angewandte Chemie, International Edition* **2006**, *118*, 3638-3742.
- (86) Haapala, M.; Pol, J.; Saarela, V.; Arvola, V.; Kotiaho, T.; Ketola, R. A.; Franssila, S.; Kauppila, T. J.; Kostiainen, R. *Analytical Chemistry* **2007**, *79*, 7867-7872.
- (87) Kauppila, T. J.; Arvola, V.; Haapala, M.; Pol, J.; Aalberg, L.; Saarela, V.; Franssila, S.; Kotiaho, T.; Kostiainen, R. *Rapid Communications in Mass Spectrometry* **2008**, *22*, 979-985.
- (88) Luosujarvi, L.; Arvola, V.; Haapala, M.; Pol, J.; Saarela, V.; Franssila, S.; Kostiainen, R.; Kotiaho, T.; Kauppila, T. J. *European Journal of Pharmaceutical Sciences* **2008**, *34*, S29-S29.
- (89) Luosujarvi, L.; Arvola, V.; Haapala, M.; Pol, J.; Saarela, V.; Franssila, S.; Kotiaho, T.; Kostiainen, R.; Kauppila, T. J. *Analytical Chemistry* **2008**, *80*, 7460-7466.
- (90) Kertesz, V.; van Berkel, G. J. *Analytical Chemistry* **2008**, *80*, 1027-1032.
- (91) Pasilis, S. P.; Kertesz, V.; Van Berkel, G. J. *Analytical Chemistry* **2007**, *79*, 5956-5962.
- (92) Kertesz, V.; Van Berkel, G. J. *Rapid Communications in Mass Spectrometry* **2008**, *22*, 3846-3850.
- (93) Venter, A.; Cooks, R. G. *Analytical Chemistry* **2007**, *79*, 6398-6403.
- (94) Chipuk, J. E.; Brodbelt, J. S. *Journal of the American Society for Mass Spectrometry* **2008**, *19*, 1612-1620.

- (95) Chipuk, J. E.; Brodbelt, J. S. *Journal of the American Society for Mass Spectrometry* **2009**, *20*, 584-592.
- (96) Meng, C. K.; Fenn, J. B. *American Biotechnology Laboratory* **1990**, *8*, 54-60.
- (97) Nefliu, M.; Smith, J. N.; Venter, A.; Cooks, R. G. *Journal of the American Society for Mass Spectrometry* **2008**, *19*, 420-427.
- (98) Takats, Z.; Wiseman, J. M.; Cooks, R. G. *Journal of Mass Spectrometry* **2005**, *40*, 1261-1275.
- (99) Venter, A.; Sojka, P. E.; Cooks, R. G. *Analytical Chemistry* **2006**, *78*, 8549-8555.
- (100) Costa, A. B.; Cooks, R. G. *Chemical Communications* **2007**, 3915-3917.
- (101) Costa, A. B.; Cooks, R. G. *Chemical Physics Letters* **2008**, *464*, 1-8.
- (102) Nyadong, L.; Green, M. D.; De Jesus, V. R.; Newton, P. N.; Fernandez, F. M. *Analytical Chemistry* **2007**, *79*, 2150-2157.
- (103) Yoshimoto, A.; Motoki, S.; Moriwaki, Y.; Kawasaki, K.; Arakawa, Y. *Journal of the Mass Spectrometry Society of Japan* **2009**, *57*, 109-115.
- (104) Hu, Q. Z.; Talaty, N.; Noll, R. J.; Cooks, R. G. *Rapid Communications in Mass Spectrometry* **2006**, *20*, 3403-3408.
- (105) Williams, J. P.; Scrivens, J. H. *Rapid Communications in Mass Spectrometry* **2005**, *19*, 3643-3650.
- (106) Bereman, M. S.; Nyadong, L.; Fernandez, F. M.; Muddiman, D. C. *Rapid Communications in Mass Spectrometry* **2006**, *20*, 3409-3411.
- (107) Leuthold, L. A.; Mandscheff, J. F.; Fathi, M.; Giroud, C.; Augsburger, M.; Varesio, E.; Hopfgartner, G. *Rapid Communications in Mass Spectrometry* **2006**, *20*, 103-110.
- (108) Van Berkel, G. J.; Ford, M. J.; Deibel, M. A. *Analytical Chemistry* **2005**, *77*, 1207-1215.
- (109) Keil, A.; Talaty, N.; Janfelt, C.; Noll, R. J.; Gao, L.; Ouyang, Z.; Cooks, R. G. *Analytical Chemistry* **2007**, *79*, 7734-7739.
- (110) Myung, S.; Wiseman, J. M.; Valentine, S. J.; Takats, Z.; Cooks, R. G.; Clemmer, D. E. *Journal of Physical Chemistry B* **2006**, *110*, 5045-5051.
- (111) Harry, E. L.; Reynolds, J. C.; Bristow, A. W.; Wilson, I. D.; Creaser, C. S. *Rapid Commun Mass Spectrom* **2009**, *23*, 2597-2604.

- (112) Kaur-Atwal, G.; Weston, D. J.; Green, P. S.; Crosland, S.; Bonner, P. L. R.; Creaser, C. S. *Rapid Communications in Mass Spectrometry* **2007**, *21*, 1131-1138.
- (113) Weston, D. J.; Bateman, R.; Wilson, I. D.; Wood, T. R.; Creaser, C. S. *Analytical Chemistry* **2005**, *77*, 7572-7580.
- (114) Zhang, S. F.; Shin, Y. S.; Mayer, R.; Basile, F. *Journal of Analytical and Applied Pyrolysis* **2007**, *80*, 353-359.
- (115) Williams, J. P.; Hilton, G. R.; Thalassinou, K.; Jackson, A. T.; Scrivens, J. H. *Rapid Communications in Mass Spectrometry* **2007**, *21*, 1693-1704.
- (116) Ifa, D. R.; Gumaelius, L. M.; Eberlin, L. S.; Manicke, N. E.; Cooks, R. G. *Analyst* **2007**, *132*, 461-467.
- (117) Bereman, M. S.; Muddiman, D. C. *Journal of the American Society for Mass Spectrometry* **2007**, *18*, 1093-1096.
- (118) Dixon, R. B.; Bereman, M. S.; Muddiman, D. C.; Hawkrigde, A. M. *Journal of the American Society for Mass Spectrometry* **2007**, *18*, 1844-1847.
- (119) Volny, M.; Venter, A.; Smith, S. A.; Pazzi, M.; Cooks, R. G. *Analyst* **2008**, *133*, 525-531.
- (120) Bereman, M. S.; Williams, T. I.; Muddiman, D. C. *Analytical Chemistry* **2007**, *79*, 8812-8815.
- (121) Kauppila, T. J.; Talaty, N.; Jackson, A. U.; Kotiaho, T.; Kostianen, R.; Cooks, R. G. *Chemical Communications* **2008**, 2674-2676.
- (122) Chen, H.; Li, M.; Zhang, Y. P.; Yang, X.; Lian, J. J.; Chen, J. M. *Journal of the American Society for Mass Spectrometry* **2008**, *19*, 450-454.
- (123) D'Agostino, P. A.; Chenier, C. L.; Hancock, J. R.; Lepage, C. R. J. *Rapid Communications in Mass Spectrometry* **2007**, *21*, 543-549.
- (124) Meetani, M. A.; Shin, Y. S.; Zhang, S. F.; Mayer, R.; Basile, F. *Journal of Mass Spectrometry* **2007**, *42*, 1186-1193.
- (125) Song, Y.; Talaty, N.; Datsenko, K.; Wanner, B. L.; Cooks, R. G. *Analyst* **2009**, *134*, 838-841.
- (126) Song, Y. S.; Talaty, N.; Tao, W. A.; Pan, Z. Z.; Cooks, R. G. *Chemical Communications* **2007**, 61-63.
- (127) Shin, Y. S.; Drolet, B.; Mayer, R.; Dolence, K.; Basile, F. *Analytical Chemistry* **2007**, *79*, 3514-3518.

- (128) Takats, Z.; Koblíha, V.; Sevcik, K.; Novak, P.; Kruppa, G.; Lemr, K.; Havlicek, V. *Journal of Mass Spectrometry* **2008**, *43*, 196-203.
- (129) Talaty, N.; Takats, Z.; Cooks, R. G. *Analyst* **2005**, *130*, 1624-1633.
- (130) Jackson, A. U.; Tata, A.; Wu, C. P.; Perry, R. H.; Haas, G.; West, L.; Cooks, R. G. *Analyst* **2009**, *134*, 867-874.
- (131) Dong, J.; Rezenom, Y. H.; Murray, K. K. *Rapid Communications in Mass Spectrometry* **2007**, *21*, 3995-4000.
- (132) Manicke, N. E.; Wiseman, J. M.; Ifa, D. R.; Cooks, R. G. *Journal of the American Society for Mass Spectrometry* **2008**, *19*, 531-543.
- (133) Corso, G.; Paglia, G.; Garofalo, D.; D'Apolito, O. *Rapid Communications in Mass Spectrometry* **2007**, *21*, 3777-3784.
- (134) Kauppila, T. J.; Talaty, N.; Kuuranne, T.; Kotiaho, T.; Kostianen, R.; Cooks, R. G. *Analyst* **2007**, *132*, 868-875.
- (135) Pan, Z. Z.; Gu, H. W.; Talaty, N.; Chen, H. W.; Shanaiyah, N.; Hainline, B. E.; Cooks, R. G.; Raftery, D. *Analytical and Bioanalytical Chemistry* **2007**, *387*, 539-549.
- (136) Song, Y.; Cooks, R. G. *Journal of Mass Spectrometry* **2007**, *42*, 1086-1092.
- (137) Leuthold, L. A.; Mandscheff, J. F.; Fathi, M.; Giroud, C.; Augsburger, M.; Varesio, E.; Hopfgartner, G. *Chimia* **2006**, *60*, 190-194.
- (138) Williams, J. P.; Lock, R.; Patel, V. J.; Scrivens, J. H. *Analytical Chemistry* **2006**, *78*, 7440-7445.
- (139) Williams, J. P.; Patel, V. J.; Holland, R.; Scrivens, J. H. *Rapid Communications in Mass Spectrometry* **2006**, *20*, 1447-1456.
- (140) Chen, H. W.; Talaty, N. N.; Takats, Z.; Cooks, R. G. *Analytical Chemistry* **2005**, *77*, 6915-6927.
- (141) Justes, D. R.; Talaty, N.; Cotte-Rodriguez, I.; Cooks, R. G. *Chemical Communications* **2007**, 2142-2144.
- (142) Mulligan, C. C.; MacMillan, D. K.; Noll, R. J.; Cooks, R. G. *Rapid Communications in Mass Spectrometry* **2007**, *21*, 3729-3736.
- (143) Mulligan, C. C.; Talaty, N.; Cooks, R. G. *Chemical Communications* **2006**, 1709-1711.
- (144) Garcia-Reyes, J. F.; Jackson, A. U.; Molina-Diaz, A.; Cooks, R. G. *Analytical Chemistry* **2009**, *81*, 820-829.

- (145) Nyadong, L.; Harris, G. A.; Balayssac, S.; Galhena, A. S.; Malet-Martino, M.; Martino, R.; Parry, R. M.; Wang, M. D. M.; Fernandez, F. M.; Gilard, V. *Analytical Chemistry* **2009**, *81*, 4803-4812.
- (146) Nyadong, L.; Hohenstein, E. G.; Galhena, A.; Lane, A. L.; Kubanek, J.; Sherrill, C. D.; Fernandez, F. M. *Analytical and Bioanalytical Chemistry* **2009**, *394*, 245-254.
- (147) Nyadong, L.; Hohenstein, E. G.; Johnson, K.; Sherrill, C. D.; Green, M. D.; Fernandez, F. M. *Analyst* **2008**, *133*, 1513-1522.
- (148) Nyadong, L.; Late, S.; Green, M. D.; Banga, A.; Fernandez, F. M. *Journal of the American Society for Mass Spectrometry* **2008**, *19*, 380-388.
- (149) Ricci, C.; Nyadong, L.; Fernandez, F. M.; Newton, P. N.; Kazarian, S. G. *Analytical and Bioanalytical Chemistry* **2007**, *387*, 551-559.
- (150) Ricci, C.; Nyadong, L.; Yang, F.; Fernandez, F. M.; Brown, C. D.; Newton, P. N.; Kazarian, S. G. *Analytica Chimica Acta* **2008**, *623*, 178-186.
- (151) Cotte-Rodriguez, I.; Chen, H.; Cooks, R. G. *Chemical Communications* **2006**, 953-955.
- (152) Zhou, J.; Yao, S.; Qian, R.; Xu, Z.; Wei, Y.; Guo, Y. *Rapid Communications in Mass Spectrometry* **2008**, *22*, 3334-3337.
- (153) Huang, G.; Chen, H.; Zhang, X.; Cooks, R. G.; Ouyang, Z. *Analytical Chemistry* **2007**, *79*, 8327-8332.
- (154) Benassi, M.; Wu, C. P.; Nefliu, M.; Ifa, D. R.; Volny, M.; Cooks, R. G. *International Journal of Mass Spectrometry* **2009**, *280*, 235-240.
- (155) Wu, C.; Ifa, D. I.; Manicke, N. E.; Cooks, R. G. *Analytical Chemistry* **2009**, In Press.
- (156) Ifa, D. R.; Manicke, N. E.; Rusine, A. L.; Cooks, R. G. *Rapid Communications in Mass Spectrometry* **2008**, *22*, 503-510.
- (157) Manicke, N. E.; Kistler, T.; Ifa, D. R.; Cooks, R. G.; Ouyang, Z. *Journal of the American Society for Mass Spectrometry* **2009**, *20*, 321-325.
- (158) Dill, A. L.; Ifa, D. R.; Manicke, N. E.; Ouyang, Z.; Cooks, R. G. *Journal of Chromatography B* **2009**, *877*, 2883-2889.
- (159) Ifa, D. R.; Wiseman, J. M.; Song, Q. Y.; Cooks, R. G. *International Journal of Mass Spectrometry* **2007**, *259*, 8-15.

- (160) Wiseman, J. M.; Ifa, D. R.; Song, Q. Y.; Cooks, R. G. *Angewandte Chemie-International Edition* **2006**, *45*, 7188-7192.
- (161) Wiseman, J. M.; Ifa, D. R.; Venter, A.; Cooks, R. G. *Nature Protocols* **2008**, *3*, 517-524.
- (162) Wiseman, J. M.; Puolitaival, S. M.; Takats, Z.; Cooks, R. G.; Caprioli, R. *Angewandte Chemie, International Edition* **2005**, *55*, 7094–7097.
- (163) Ifa, D. R.; Manicke, N. E.; Dill, A. L.; Cooks, G. *Science* **2008**, *321*, 805-805.
- (164) Van Berkel, G. J.; Kertesz, V. *Analytical Chemistry* **2006**, *78*, 4938-4944.
- (165) Kertesz, V.; Van Berkel, G. J.; Vavrek, M.; Koeplinger, K. A.; Schneider, B. B.; Covey, T. R. *Analytical Chemistry* **2008**, *80*, 5168-5177.
- (166) Lane, A. L.; Nyadong, L.; Galhena, A. S.; Shearer, T. L.; Stout, E. P.; Parry, R. M.; Kwasnik, M.; Wang, M. D.; Hay, M. E.; Fernandez, F. M.; Kubanek, J. *Proceedings of the National Academy of Sciences of the United States of America* **2009**, *106*, 7314-7319.
- (167) Kertesz, V.; Van Berkel, G. J. *Rapid Communications Mass Spectrometry* **2008**, *22*, 2639-2644.
- (168) Abdelnur, P. V.; Eberlin, L. S.; De Sa, G. F.; De Souza, V.; Eberlin, M. N. *Analytical Chemistry* **2008**, *80*, 7882-7886.
- (169) Haddad, R.; Rodrigo, R. C.; Lygia, A. M.; Eberlin, M. N. *Rapid Communications Mass in Spectrometry* **2008**, *22*, 3662-3666.
- (170) Saraiva, S. A.; Abdelnur, P. V.; Catharino, R. R.; Nunes, G.; Eberlin, M. N. *Rapid Communications Mass in Spectrometry* **2009**, *23*, 357-362.
- (171) Wiseman, J. M.; Takats, Z.; Gologan, B.; Davisson, V. J.; Cooks, R. G. *Angewandte Chemie-International Edition* **2005**, *44*, 913-916.
- (172) Yang, P. X.; Cooks, R. G.; Ouyang, Z.; Hawkridge, A. M.; Muddiman, D. C. *Analytical Chemistry* **2005**, *77*, 6174-6183.
- (173) Chen, L. C.; Yoshimura, K.; Yu, Z.; Iwata, R.; Ito, H.; Suzuki, H.; Mori, K.; Ariyada, O.; Takeda, S.; Kubota, T.; Hiraoka, K. *Journal of Mass Spectrometry* **2009**, In Press.
- (174) Shieh, I. F.; Lee, C. Y.; Shiea, J. *Journal of Proteome Research* **2005**, *4* 606-612.
- (175) Chen, H.; Zenobi, R. *Nature Protocols* **2008**, *3*, 1467-1475.
- (176) Chingin, K.; Chen, H.; Gamez, G.; Zhu, L.; Zenobi, R. *Analytical Chemistry* **2009**, *81*, 2414.

- (177) Chingin, K.; Chen, H.; Gamez, G.; Zhu, L.; Zenobi, R. *Analytical Chemistry* **2009**, *81*, 123-129.
- (178) Chingin, K.; Gamez, G.; Chen, H.; Zhu, L.; Zenobi, R. *Rapid Communications in Mass Spectrometry* **2008**, *22*, 2009-2014.
- (179) Peng, I. X.; Shiea, J.; Loo, R. R. O.; Loo, J. A. *Rapid Communications in Mass Spectrometry* **2007**, *21*, 2541-2546.
- (180) Peng, I. X.; Loo, R. R. O.; Shiea, J.; Loo, J. A. *Analytical Chemistry* **2008**, *80*, 6995-7003.
- (181) Sampson, J. S.; Murray, K. K.; Muddiman, D. C. *Journal of the American Chemical Society for Mass Spectrometry* **2009**, *20*, 667-673
- (182) Nemes, P.; Barton, A. A.; Vertes, A. *Analytical Chemistry* **2009**, *81*, 6668-6675.
- (183) Cody, R. B. *Analytical Chemistry* **2009**, *81*, 1101-1107.
- (184) Berkout, V. D. *Analytical Chemistry* **2009**, *81*, 725-731.
- (185) Kpegba, K.; Spadaro, T.; Cody, R. B.; Nesnas, N.; Olson, J. A. *Analytical Chemistry* **2007**, *79*, 5479-5483.
- (186) Song, L.; Dykstra, A. B.; Yao, H.; Bartmess, J. E. *Journal of the American Chemical Society for Mass Spectrometry* **2009**, *20*, 42-45.
- (187) Harris, G. A.; Fernandez, F. M. *Analytical Chemistry* **2009**, *81*, 322-329.
- (188) Yu, S.; Crawford, E.; Tice, J.; Musselman, B.; Wu, J.-T. *Analytical Chemistry* **2009**, *81*, 193-202.
- (189) Pierce, C. Y.; Barr, J. R.; Cody, R. B.; Massung, R. F.; Woolfitt, A. R.; Moura, H.; Thompson, H. A.; Fernandez, F. M. *Chemical Communications* **2007**, 807-809.
- (190) Morlock, G.; Ueda, Y. *Journal of Chromatography A* **2007**, *1143*, 243-251.
- (191) Haefliger, O. P.; Jeckelmann, N. *Rapid Communications in Mass Spectrometry* **2007**, *21*, 1361-1366.
- (192) Dane, A. J.; Cody, R. B. *Lc Gc North America* **2009**, 46-46.
- (193) Petucci, C.; Diffendal, J.; Kaufman, D.; Mekonnen, B.; Terefenko, G.; Musselman, B. *Analytical Chemistry* **2007**, *79*, 5064-5070.
- (194) Vail, T. M.; Jones, P. R.; Sparkman, O. D. *Journal of Analytical Toxicology* **2007**, *31*, 304-312.

- (195) Alpmann, A.; Morlock, G. *Journal of Separation Science* **2008**, *31*, 71-77.
- (196) Jones, R. W.; Cody, R. B.; McClelland, J. F. *Journal of Forensic Sciences* **2006**, *51*, 915-918.
- (197) Yew, J. Y.; Cody, R. B.; Kravitz, E. A. *Proceedings of the National Academy of Sciences of the United States of America* **2008**, *105*, 7135-7140.
- (198) Fernandez, F. M.; Cody, R. B.; Green, M. D.; Hampton, C. Y.; McGready, R.; Sengaloundeth, S.; White, N. J.; Newton, P. N. *Chemmedchem* **2006**, *1*, 702-+.
- (199) Moffat, A. C.; Cody, R. B.; Jee, R. D.; O'Neil, A. J. *Journal of Pharmacy and Pharmacology* **2007**, *59*, A26-A26.
- (200) Newton, P. N.; Fernandez, F. M.; Plancon, A.; Mildenhall, D. C.; Green, M. D.; Ziyong, L.; Christophel, E. M.; Phanouvong, S.; Howells, S.; McIntosh, E.; Laurin, P.; Blum, N.; Hampton, C. Y.; Faure, K.; Nyadong, L.; Soong, C. W. R.; Santoso, B.; Zhiguang, W.; Newton, J.; Palmer, K. *Plos Medicine* **2008**, *5*, 209-219.
- (201) Vaclavika, L.; Cajkaa, T.; Hrbeka, V.; Hajslova, J. *Analytica Chimica Acta* **2009**, *645*, 56-63.
- (202) Jagerdeo, E.; Abdel-Rehim, M. *Journal of the American Society for Mass Spectrometry* **2009**, *20*, 891-899.
- (203) Shelley, J. T.; Wiley, J. S.; Chan, G. C.; Schilling, G. D.; Ray, S. J.; Hieftje, G. M. *Journal of the American Society for Mass Spectrometry* **2009**, *20*, 837-844.
- (204) Schilling, G. D.; Shelley, J. T.; Broekaert, J. A. C.; Perline, R. P.; Bonner, D. M.; Barinaga, C. J.; Koppenaal, D. W.; Hieftje, G. M. *Journal of Analytical Atomic Spectrometry* **2009**, *24*, 34-40.
- (205) Shelley, J. T.; Ray, S. J.; Hieftje, G. M. *Analytical Chemistry* **2008**, *80*, 8308-8313
- (206) Takats, Z.; Cotte-Rodriguez, I.; Talaty, N.; Chen, H. W.; Cooks, R. G. *Chemical Communications* **2005**, 1950-1952.
- (207) Chen, H.; Liang, H.; Ding, J.; Lai, J.; Huan, Y.; Qiao, X. *J Agric Food Chem* **2007**, *55*, 10093-10100.
- (208) Chen, H. W.; Zheng, J.; Zhang, X.; Luo, M. B.; Wang, Z. C.; Qiao, X. L. *Journal of Mass Spectrometry* **2007**, *42*, 1045-1056.
- (209) Coon, J. J.; McHale, K. J.; Harrison, W. W. *Rapid Communications in Mass Spectrometry* **2002**, *16*, 681-685.

- (210) Peng, S.; Edler, M.; Ahlmann, N.; Hoffmann, T.; Franzke, J. *Rapid Communications in Mass Spectrometry* **2005**, *19*, 2789-2793.
- (211) Huang, G.; Ouyang, Z.; Cooks, R. G. *Chemical Communications* **2009**, 556-558.
- (212) World Health Organisation (2006) World Malaria Report - 2005. Available: <http://www.rbm.who.int/wmr2005/html/2001-2002.htm>. Accessed 2022 July **2007**.
- (213) Anon (2007) Malaria. World Health Organisation Media Centre. Available: <http://www.who.int/mediacentre/factsheets/fs2094/en/index.html>. Accessed 2010 August **2007**.
- (214) Fidock, D. A.; Rosenthal, P. J.; Croft, S. L.; Brun, R.; Nwaka, S. *Nature Reviews Drug Discovery* **2004**, *3*, 509-520.
- (215) Greenwood, B. *Nature* **2004**, *430*, 926-927.
- (216) Naik, H.; Murry, D. J.; Kirsch, L. E.; Fleckenstein, L. *Journal of Chromatography B* **2005**, *816*, 233-242.
- (217) Dondorp, A. M.; Newton, P. N.; Mayxay, M.; Van Damme, W.; Smithuis, F. M.; Yeung, S.; Petit, A.; Lynam, A. J.; Johnson, A.; Hien, T. T.; McGready, R.; Farrar, J. J.; Looareesuwan, S.; Day, N. P. J.; Green, M. D.; White, N. J. *Tropical Medicine & International Health* **2004**, *9*, 1241-1246.
- (218) Newton, P.; Proux, S.; Green, M.; Smithuis, F.; Rozendaal, J.; Prakongpan, S.; Chotivanich, K.; Mayxay, M.; Looareesuwan, S.; Farrar, L.; Nosten, F.; White, N. J. *Lancet* **2001**, *357*, 1948-1950.
- (219) Newton, P. N.; Green, M. D.; Fernandez, F. M.; Day, N. P. J.; White, N. J. *Lancet Infectious Diseases* **2006**, *6*, 602-613.
- (220) Newton, P. N.; McGready, R.; Fernandez, F.; Green, M. D.; Sunjio, M.; Bruneton, C.; Phanouvong, S.; Millet, P.; Whitty, C. J. M.; Talisuna, A. O.; Proux, S.; Christophel, E. M.; Malenga, G.; Singhasivanon, P.; Bojang, K.; Kaur, H.; Palmer, K.; Day, N. P. J.; Greenwood, B. M.; Nosten, F.; White, N. J. *Plos Medicine* **2006**, *3*, 752-755.
- (221) Rozendaal, L. *Bull. Mekong Malaria Forum* **2000**, *7*, 62-68.
- (222) Hall, K. A.; Newton, P. N.; Green, M. D.; De Veij, M.; Vandenabeele, P.; Pizzanelli, D.; Mayxay, M.; Dondorp, A.; Fernandez, F. M. *American Journal of Tropical Medicine and Hygiene* **2006**, *75*, 804-811.
- (223) Lon, C. T.; Tsuyuoka, R.; Phanouvong, S.; Nivanna, N.; Socheat, D.; Sokhan, C.; Blum, N.; Christophel, E. M.; Smine, A. *Transactions of the Royal Society of Tropical Medicine and Hygiene* **2006**, *100*, 1019-1024.

- (224) Aldhous, P. *Nature* **2005**, *434*, 132-136.
- (225) Anon. GlaxoSmithKline case study (7 April 2003). Judicial Protection of IPR in China. Available: <http://www.chinaiprlaw.com/english/news/news2014.htm>. Accessed 2005 August **2007**.
- (226) Green, M. D.; Mount, D. L.; Wirtz, R. A. *Tropical Medicine & International Health* **2001**, *6*, 980-982.
- (227) Green, M. D.; Nettey, H.; Rojas, O. V.; Pamanivong, C.; Khounsaknalath, L.; Ortiz, M. G.; Newton, P. N.; Fernandez, F. A.; Vongsack, L.; Manolin, O. *Journal of Pharmaceutical and Biomedical Analysis* **2007**, *43*, 105-110.
- (228) Deisingh, A. K. *Analyst* **2005**, *130*, 271-279.
- (229) Chan, K. L. A.; Elkhider, N.; Kazarian, S. G. *Chemical Engineering Research & Design* **2005**, *83*, 1303-1310.
- (230) Chan, K. L. A.; Hammond, S. V.; Kazarian, S. G. *Analytical Chemistry* **2003**, *75*, 2140-2146.
- (231) Chan, K. L. A.; Kazarian, S. G. *Journal of Combinatorial Chemistry* **2005**, *7*, 185-189.
- (232) Kazarian, S. G.; Chan, K. L. A. *Macromolecules* **2003**, *36*, 9866-9872.
- (233) Kazarian, S. G.; Chan, K. L. A. *Macromolecules* **2004**, *37*, 579-584.
- (234) Ricci, C.; Chan, K. L. A.; Kazarian, S. G. *Applied Spectroscopy* **2006**, *60*, 1013-1021.
- (235) van der Weerd, J.; Kazarian, S. G. *Journal of Controlled Release* **2004**, *98*, 295-305.
- (236) Wellcome Trust Oxford SE Asian Tropical Medicine Research Units (2006) Fake artesunate warning sheet number 2005a. Available: <http://www.tropicalmedicine.ox.ac.uk/FakeArtesunateWarningJan2007.pdf>. Accessed 2023 February **2007**.
- (237) Hoang, T. T.; May, S. W.; Browner, R. F. *Journal of Analytical Atomic Spectrometry* **2002**, *17*, 1575-1581.
- (238) Kalasinsky, V. F.; Jenkins, H. M.; Johnson, F. B. *Vibrational Spectroscopy* **2002**, *28*, 199-207.
- (239) Kapetanaki, S.; Varotsis, C. *Journal of Medicinal Chemistry* **2001**, *44*, 3150-3156.

- (240) Stefansson, M.; Sjoberg, P. J. R.; Markides, K. E. *Analytical Chemistry* **1996**, *68*, 1792-1797.
- (241) White, N. *Philosophical Transactions of the Royal Society B* **1999**, *354* 739-749.
- (242) Chen, H.; Cotte-Rodriguez, I.; Cooks, R. G. *Chemical Communications* **2006**, 597-599.
- (243) Ortelli, D.; Rudaz, S.; Cognard, E.; Veuthey, J. L. *Chromatographia* **2000**, *52*, 445-450.
- (244) Brodbelt, J. S.; Liou, C. C. *Pure and Applied Chemistry* **1993**, *65*, 409-414.
- (245) Wysocki, V. H.; Tsaprailis, G.; Smith, L. L.; Breci, L. A. *Journal of Mass Spectrometry* **2000**, *35*, 1399-1406.
- (246) Safi, B.; Choho, K.; De Proft, F.; Geerlings, P. *Chemical Physics Letters* **1999**, *300*, 85-92.
- (247) Harris, G. A.; Nyadong, L.; Fernandez, F. M. *Analyst* **2008**, *133*, 1297-1301.
- (248) *Quingaosu Antimalaria Coordinating Research Group*, *Journal of Traditional Chinese Medicine* **1982**, *2*, 9-16.
- (249) Singh, B. R.; Prakash, K. A.; Tarun, S.; Singh, K. S. P. *Patent No. PCT/IB2002/005063* **2004**.
- (250) Ward, P.; Small, I.; Smith, J.; Suter, P.; Dutkowski, R. *Journal of Antimicrobial Chemotherapy* **2005**, *55*, 5-21.
- (251) *Customs Agents Seize Fake Tamiflu, Antiviral Drug Stockpiled in Anticipation of Deadly Bird Flu-CBS News*.
<http://www.cbsnews.com/stories/2005/12/18/health/main1134820.shtml>, accessed 07/13/07.
- (252) Lindegardh, N.; Hien, T. T.; Farrar, J.; Singhasivanon, P.; White, N. J.; Day, N. P. J. *Journal of Pharmaceutical and Biomedical Analysis* **2006**, *42*, 430-433.
- (253) *Global Pharma Health Fund*, **2008**,
<http://www.gphf.org/images/downloads/oseltamivir.pdf>.
- (254) Green, M. D.; Nettey, H.; Wirtz, R. A. *Emerging Infectious Diseases* **2008**, *14*, 552-556.
- (255) Stephens, P. J.; Devlin, F. J.; Chabalowski, C. F.; Frisch, M. J. *Journal of Physical Chemistry* **1994**, *98*, 11623-11627.
- (256) Grimme, S. *Journal of Computational Chemistry* **2006**, *27*, 1787-1799.

- (257) Boys, S. F.; Bernardi, F. *Molecular Physics* **1970**, *19*, 553-556.
- (258) Crawford, T. D.; Sherrill, C. D.; Valeev, E. F.; Fermann, J. T.; King, R. A.; Leininger, M. L.; Brown, S. T.; Janssen, C. L.; Seidl, E. T.; Kenny, J. P.; Allen, W. D. *Journal of Computational Chemistry* **2007**, *28*, 1610-1616.
- (259) Shao, Y.; Molnar, L. F.; Jung, Y.; Kussmann, J.; Ochsenfeld, C.; Brown, S. T.; Gilbert, A. T. B.; Slipchenko, L. V.; Levchenko, S. V.; O'Neill, D. P.; DiStasio, R. A.; Lochan, R. C.; Wang, T.; Beran, G. J. O.; Besley, N. A.; Herbert, J. M.; Lin, C. Y.; Van Voorhis, T.; Chien, S. H.; Sodt, A.; Steele, R. P.; Rassolov, V. A.; Maslen, P. E.; Korambath, P. P.; Adamson, R. D.; Austin, B.; Baker, J.; Byrd, E. F. C.; Dachsel, H.; Doerksen, R. J.; Dreuw, A.; Dunietz, B. D.; Dutoi, A. D.; Furlani, T. R.; Gwaltney, S. R.; Heyden, A.; Hirata, S.; Hsu, C. P.; Kedziora, G.; Khalliulin, R. Z.; Klunzinger, P.; Lee, A. M.; Lee, M. S.; Liang, W.; Lotan, I.; Nair, N.; Peters, B.; Proynov, E. I.; Pieniazek, P. A.; Rhee, Y. M.; Ritchie, J.; Rosta, E.; Sherrill, C. D.; Simmonett, A. C.; Subotnik, J. E.; Woodcock, H. L.; Zhang, W.; Bell, A. T.; Chakraborty, A. K.; Chipman, D. M.; Keil, F. J.; Warshel, A.; Hehre, W. J.; Schaefer, H. F.; Kong, J.; Krylov, A. I.; Gill, P. M. W.; Head-Gordon, M. *Physical Chemistry Chemical Physics* **2006**, *8*, 3172-3191.
- (260) *Jaguar 5.5, Schrodinger, LLC, Portland, Oregon, 2003.*
- (261) Brodbelt, J. S. *International Journal of Mass Spectrometry* **2000**, *200*, 57-69.
- (262) Franski, R.; Schroeder, G.; Gierczyk, B.; Niedzialkowski, P.; Ossowski, T. *International Journal of Mass Spectrometry* **2007**, *266*, 180-184.
- (263) W. Henderson; McIndoeand, J. S. *Mass Spectrometry of Inorganic and Organometallic Compounds* **2005**.
- (264) Ventola, E.; Rissanen, K.; Vainiotalo, P. *Chemistry-a European Journal* **2004**, *10*, 6152-6162.
- (265) Goolsby, B. J.; Brodbelt, J. S.; Adou, E.; Blanda, M. *International Journal of Mass Spectrometry* **1999**, *193*, 197-204.
- (266) Dalleska, N. F.; Honma, K.; Armentrout, P. B. *Journal of the American Chemical Society* **1993**, *115*, 12125-12131.
- (267) David, W. M.; Brodbelt, J. S. *Journal of the American Society for Mass Spectrometry* **2003**, *14*, 383-392.
- (268) Vinokur, N.; Ryzhov, V. *Journal of Mass Spectrometry* **2004**, *39*, 1268-1274.
- (269) Sharma, R. B.; Blades, A. T.; Kebarle, P. *Journal of the American Chemical Society* **1984**, *106*, 510-516.

- (270) Wartewig, S.; Neubert, R. H. H. *Advanced Drug Delivery Reviews* **2005**, *57*, 1144-1170.
- (271) Kubanek, J.; Prusak, A. C.; Snell, T. W.; Giese, R. A.; Fairchild, C. R.; Aalbersberg, W.; Hay, M. E. *Journal of Natural Products* **2006**, *69*, 731-735.
- (272) Kubanek, J.; Prusak, A. C.; Snell, T. W.; Giese, R. A.; Hardcastle, K. I.; Fairchild, C. R.; Aalbersberg, W.; Raventos-Suarez, C.; Hay, M. E. *Organic Letters* **2005**, *7*, 5261-5264.
- (273) Lane, A. L.; Stout, E. P.; Hay, M. E.; Prusak, A. C.; Hardcastle, K.; Fairchild, C. R.; Franzblau, S. G.; Le Roch, K.; Prudhomme, J.; Aalbersberg, W.; Kubanek, J. *Journal of Organic Chemistry* **2007**, *72*, 7343-7351.
- (274) Prien, J. M.; Huysentruyt, L. C.; Ashline, D. J.; Lapadula, A. J.; Seyfried, T. N.; Reinhold, V. N. *Glycobiology* **2008**, *18*, 353-366.
- (275) Marotta, E.; Bosa, E.; Scorrano, G.; Paradisi, C. *Rapid Communications in Mass Spectrometry* **2005**, *19*, 391-396.
- (276) Marotta, E.; Paradisi, C. *Journal of Mass Spectrometry* **2005**, *40*, 1583-1589.
- (277) Siegel, M. M.; Tabei, K.; Lambert, F.; Candela, L.; Zoltan, B. *Journal of the American Society for Mass Spectrometry* **1998**, *9*, 1196-1203.
- (278) Yu, K.; Di, L.; Kerns, E.; Li, S. Q.; Alden, P.; Plumb, R. S. *Rapid Communications in Mass Spectrometry* **2007**, *21*, 893-902.
- (279) Short, L. C.; Hanold, K. A.; Cai, S. S.; Syage, J. A. *Rapid Communications in Mass Spectrometry* **2007**, *21*, 1561-1566.
- (280) Short, L. C.; Syage, J. A. *Rapid Communications in Mass Spectrometry* **2008**, *22*, 541-548.
- (281) Schiewek, R.; Lorenz, M.; Giese, R.; Brockmann, K.; Benter, T.; Gab, S.; Schmitz, O. J. *Analytical and Bioanalytical Chemistry* **2008**, *392*, 87-96.
- (282) Kawai, Y.; Yamaguchi, S.; Okada, Y.; Takeuchi, K.; Yamauchi, Y.; Ozawa, S.; Nakai, H. *Chemical Physics Letters* **2003**, *377*, 69-73.
- (283) Kawai, Y.; Yamaguchi, S.; Okada, Y.; Takeuchi, K. *J. Mass Spectrom. Soc. Jpn* **2004**, *52*, 271-276.
- (284) Cooks, R. G.; Ouyang, Z.; Takats, Z.; Wiseman, J. M. *Science* **2006**, *311*, 1566-1570.
- (285) Van Berkel, G. J.; Pasilis, S. P.; Ovchinnikova, O. *Journal of Mass Spectrometry* **2008**, *43*, 1161-1180.

- (286) Dill, A. L.; Ifa, D. R.; Manicke, N. E.; Costa, A. B.; Ramos-Vara, J. A.; Knapp, D. W.; Cooks, R. G. *Analytical Chemistry* **2009**, In Press.
- (287) Sengaloundeth, S.; Green, M. D.; Fernández, F. M.; Manolin, O.; Phommavong, K.; Insixiengmay, V.; Hampton, C. Y.; Nyadong, L.; Mildenhall, D. C.; Hostetler, D.; Khounsaknalath, L.; Vongsack, L.; Phompida, S.; Vanisaveth, V.; Syhakhang, L.; Newton, P. N. *Malaria Journal* **2009**, 8, 1-10.
- (288) Nyadong, L.; Galhena, A. S.; Fernandez, F. M. *Analytical Chemistry* **2009**, In Press.
- (289) Vandenaabeele, P.; Castro, K.; Hargreaves, M.; Moens, L.; Madariaga, J. M.; Edwards, H. G. M. *Analytica Chimica Acta* **2007**, 588, 108-116.
- (290) Ricci, C.; Eliasson, C.; Macleod, N. A.; Newton, P. N.; Matousek, P.; Kazarian, S. G. *Analytical and Bioanalytical Chemistry* **2007**, 389, 1525–1532.
- (291) Gergov, M.; Ojanpera, I.; Vuori, E. *Journal of Chromatography B-Analytical Technologies in the Biomedical and Life Sciences* **2003**, 795, 41-53.
- (292) Sontevska, V.; Jovanovski, G.; Makreski, P. *Journal of Molecular Structure* **2007**, 834, 318-327.
- (293) de Veij, M.; Vandenaabeele, P.; Hall, K. A.; Fernandez, F. M.; Green, M. D.; White, N. J.; Dondorp, A. M.; Newton, P. N.; Moens, L. *Journal of Raman Spectroscopy* **2007**, 38, 181-187.
- (294) Johnson, C. S. *Progress in Nuclear Magnetic Resonance Spectroscopy* **1999**, 34, 203-256.
- (295) Trefi, S.; Gilard, V.; Malet-Martino, M.; Martino, R. *Journal of Pharmaceutical and Biomedical Analysis* **2007**, 44, 743-754.
- (296) Trefi, S.; Routaboul, C.; Hamieh, S.; Gilard, V.; Malet-Martino, M.; Martino, R. *Journal of Pharmaceutical and Biomedical Analysis* **2008**, 47, 103-113.
- (297) Lee, C. H.; Hong, H.; Shin, J.; Jung, M.; Shin, I.; Yoon, J.; Lee, W. *Biochemical and Biophysical Research Communications* **2000**, 274, 359-369.
- (298) NMRtec. Nmrnotebook software; **2007**. Available via the Internet at <http://nmrtec.com>.
- (299) Newton, P. N.; Dondorp, A. M.; Green, M.; Mayxay, M.; White, N. J. *Lancet* **2003**, 362, 169-169.
- (300) Lon, C. T.; Tsuyuoka, R.; Phanouvong, S.; Nivanna, N.; Socheat, D.; Sokhan, C.; Blum, N.; Christophel, E. M.; Smine, A. *Transactions of the Royal Society of Tropical Medicine and Hygiene* **2006**, 100, 1019–1024.

- (301) World Health Organisation Regional Office for the Western Pacific (2005) Dealers in death. Video documentary. A film by Harrikrisna Anenden. A WHO production, Manila. Available:
<http://www.wpro.who.int/sites/mvp/documents/dealersindeath.htm>. Accessed 2002 September **2007**.
- (302) Green, M. D.; Mount, D. L.; Wirtz, R. A.; White, N. J. *Journal of Pharmaceutical and Biomedical Analysis* **2000**, *24*, 65-70.
- (303) Huang, T. C. **1972**, Pollen flora of Taiwan. Tapei: Ching-Hwa Press Co. Ltd. 222 p.
- (304) Huang, T. C. **1981**, Spore flora of Taiwan. Taipei: Tah-Jinn Press Co. Ltd. 111 p.
- (305) Wang, F. S.; Chien, H. F.; Zhang, Y. L.; Yang, H. Q. **1995**, Pollen flora of China, 2nd edition. Beijing: Institute of Botany, Academia Sinica. 461 p.
- (306) Bulalacao, L. J. **1997**, Pollen flora of the Philippines volume 1. Taguig Metro Manila: Department of Science and Technology. 266 p.
- (307) Vitalij, P.; Peter, Z. *Fundamentals of Powder Diffraction and Structural Characterization of Materials (2nd ed.)*. Springer **2008**.
- (308) Paul, D.; Skrzypek, G.; Forizs, I. *Rapid Communications in Mass Spectrometry* **2007**, *21*, 3006–3014.
- (309) Collette, C.; Drahos, L.; De Pauw, E.; Vekey, K. *Rapid Communications in Mass Spectrometry* **1998**, *12*, 1673-1678.
- (310) United Nations (1988) United Nations convention against illicit traffic in narcotic drugs and psychotropic substances. Available:
www.unodc.org/pdf/convention_1988_en.pdf. Accessed 1911 August **2007**.

VITA

LEONARD NYADONG

Leonard Nyadong was born in Bamenda, Cameroon. He attended Government Elementary, Secondary and High School in Bamenda, Cameroon. He pursued his undergraduate studies at the University of Buea, Buea, Cameroon where he earned a B. S. degree in Chemistry with a minor in Materials Science in 2001. In 2003, he moved to USA to pursue graduate studies. In 2005, he earned an M.S degree in Chemistry from the University of Toledo, OH under the supervision of Dr. Bruce Averill. In the same year, he moved to Atlanta to pursue a doctorate in analytical chemistry at the Georgia Institute of Technology.